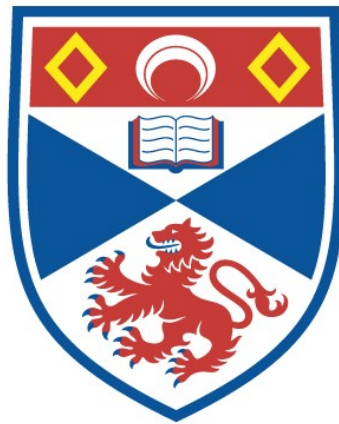


BIOPHYSICAL DAMAGE IN METALLO-ENZYME AND
MAMMALIAN CELLS BY CU-K X-RAYS AND
RADIOISOTOPES

Abdul-Redha Sahib Younis

A Thesis Submitted for the Degree of PhD
at the
University of St Andrews



1989

Full metadata for this item is available in
St Andrews Research Repository
at:

<http://research-repository.st-andrews.ac.uk/>

Please use this identifier to cite or link to this item:

<http://hdl.handle.net/10023/14089>

This item is protected by original copyright

Biophysical Damage in
Metallo-enzyme and Mammalian Cells
by Cu-K X-rays and Radioisotopes



ProQuest Number: 10166457

All rights reserved

INFORMATION TO ALL USERS

The quality of this reproduction is dependent upon the quality of the copy submitted.

In the unlikely event that the author did not send a complete manuscript and there are missing pages, these will be noted. Also, if material had to be removed, a note will indicate the deletion.



ProQuest 10166457

Published by ProQuest LLC (2017). Copyright of the Dissertation is held by the Author.

All rights reserved.

This work is protected against unauthorized copying under Title 17, United States Code
Microform Edition © ProQuest LLC.

ProQuest LLC.
789 East Eisenhower Parkway
P.O. Box 1346
Ann Arbor, MI 48106 – 1346

**Biophysical Damage in
Metallo-enzyme and Mammalian Cells
by Cu-K X-rays and Radioisotopes**

by

Abdul-Redha Sahib Younis

Dip Med Tech (Bagh. Un.), B Sc (Al-Mustansiriyah Un.)
and M Sc (St. Andrews Un.)

A thesis presented to the University of St Andrews,
(St Andrews, Fife, Scotland, United Kingdom),
as requirement for the degree of
Doctor of Philosophy

St. Andrews
1989

Th
A976

Contents of the thesis

Decelaratoin	I
Certificate	II
Copyright Declaration	III
Al-fatiha from the Holy Qur'an	IV
Author's background and publications	V
Acknowledgements	VII
Dedication	VIII
Abstract	IX
Text contents	XI

Declaration

I hereby declare that this thesis has been composed by myself, is a record of my own work and has not previously been presented for a higher degree.

This research was carried out in the J F Allen Research Laboratories, Department of Physics and Astronomy, University of St Andrews, under the supervision of Dr D E Watt.

Abdul-Redha Sahib Younis

25th April 1989

Certificate

I hereby certify that the candidate, Abdul-Redha Sahib Younis, has fulfilled the conditions of the Resolution and Regulations of the University of St Andrews appropriate to the degree of Doctor of Philosophy.

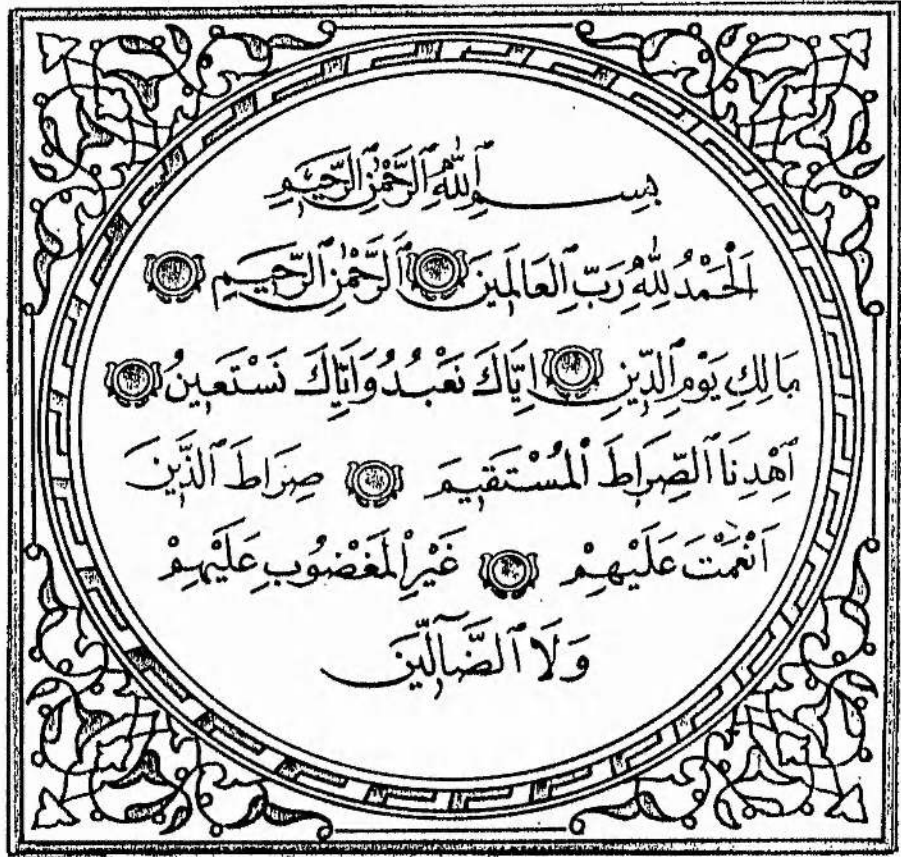
Dr David E Watt
Research Supervisor
25th April 1989

Copyright Declaration

In submitting this thesis to the University of St Andrews I understand that I am giving permission for it to be made available for public use in accordance with the regulations of the University Library for the time being in force, subject to any copyright vested in the work not being affected thereby. I also understand that the title and the abstract will be published, and that a copy of the work may be made and supplied to any *bona fide* library or research worker.

Abdul-Redha Sahib Younis

25th April 1989



In the name of God , Most Gracious, Most Merciful
Praise be to God, The Cherisher and Sustainer of the
Worlds * Most Gracious, Most Merciful * Master of
the Day of Judgment * Thee do we worship, And
Thine aid we seek * Show us the straight way *
The way of those on whom Thou hast bestowed
Thy Grace * Those whose (portion) is not
wrath, and who go not astray.

(The Holy Qur'an :Al- Fatiha)

Author's Background and Publications

I was born in Baghdad and educated at Ebn-Al-Jauzi Primary School from 1956-1961, Al-Kifah Junior Secondary School from 1961-1964, and Al-Nidhal Senior Secondary School from 1964-1966. From 1966-1968 I attended the Higher Institute of Medical Technology (Baghdad University) and obtained the Diploma in Medical Technology. Between 1969 and 1985 I was employed by the Health Ministry as a laboratory assistant in the Institute of Bacteriology and Blood Bank. In 1972, while continuing my occupation, I matriculated at Al-Mustansiriyah University, Baghdad, and graduated in 1977 with the degree of Bachelor of Science in physics. At this point I was promoted to the position of physicist in the Blood Bank. Having been awarded a grant from the Ministry of Higher Education and Scientific Research of the Republic of Iraq, I came to St Andrews University in 1985 to study for the degrees of Master of Science in radiation biophysics, awarded in 1986, and Doctor of Philosophy.

Publications

- Watt D E and Younis, A-R S (1987). Physical mechanism for inactivation of metallo-enzymes : response to correspondence from Goodhead and Nikjoo. *International Journal of Radiation Biology*, **52**, No.4, 657-658.
- Watt D E, Chen C-Z, Kadiri L and Younis, A-R S (1988). Towards a unified system for expression of biological damage by ionizing radiation. 37-41 in British Nuclear Engineering Society. *Conference on health effects of low dose ionizing radiation - recent advances and their implications, 11-14 May 1987*. (London, BNES).
- Younis, A-R S and Watt D E (1989). The Quality of Ionising Radiations Emitted by Radionuclides Incorporated into Mammalian cells. *Physics in Medicine and Biology*. In press.

Watt D E, Sykes C E and Younis A-R S (1988). Model predictions and analysis of enhanced biological effectiveness at low dose rates. Presented at the 4th International Symposium on Radiation physics, Sao Paulo, Brazil. October 3rd-7th, 1988. To be published in Nuclear Instruments and Methods in Physics Research, 1989, In press.

Younis A-R S and Watt D E (1989). Interpretation of damage to mammalian cells, E. Coli and bacteriophages by incorporated radionuclides for prolonged irradiations. To be presented at the 10th Symposium on Microdosimetry, Rome, May 21-26, 1989.

Acknowledgements

I am deeply indebted to many people and it is with great pleasure that I record my thanks to the following:

Dr D E Watt, for his kind and sincere support and many productive discussions throughout the course of this research;

Dr P E Bryant, for his interest in the biological aspects of this work, and for his encouragement during monolayer cell culture studies;

The members of the mechanical workshop especially Ron McCraw, George Radley, Myles Whyte and Jim Clark and the electronic workshop especially Mike Robertson, G. Armstrong and James Wade for their assistance in constructing mechanical apparatus and electronic devices, Miss E W D Bell for her assistance during the course of typing this thesis, Tom McQueen, Derek Bayne and other members of staff; fellow students in the Departments of Physics and Astronomy, and Biology and Preclinical Medicine for offering assistance as appropriate.

The Ministry of Higher Education and Scientific Research of the Republic of Iraq for the provision of a support grant.

I should like to record my gratitude to the people in Scotland for their generous hospitality and sincere "social supervision".

Finally thanks are offered to my colleagues in the field of radiation biophysics, to friends abroad and at home, particularly Mr Naji Hammad and Mr Muhammad Saheh, for their support and encouragement, and to my relatives both those who encouraged me to strive forwards, and those whose discouragement released in me a greater determination to succeed.

**This thesis is dedicated to
my wife; sons and daughters**

الإهداء
إلى زوجتي، أبنائي وبناتي

Abstract

In the fields of radiobiology and nuclear medicine there is considerable interest in the important role played by Auger electron cascades caused by inner-shell ionisation in realistic risk. It is necessary to quantify this risk when radionuclides are used on a routine basis as investigative, diagnostic and radiotherapeutic tools, whether the applications involve incorporated electron capture radionuclides or K-shell ionisation of selected stable nuclides by X-rays, as in "photon activation therapy".

Relevant published survival data on biological damage caused by the internal emitters ^{125}I , ^{77}Br , ^3H , ^{33}P , ^{131}I and ^{32}P which are incorporated into the DNA of mammalian cells, bacteria (*E. Coli*) and bacteriophages have been collected and the results re-analysed in terms of the parameters of a new damage model to determine an inactivation cross-section for each internal emitter. These quality parameters are the absolute specification of radiation quality and are compared with cross-sections similarly determined for the effects of external radiations from heavy charged particles and photons (chapter 2).

The inactivation probabilities obtained for the nuclides ^{125}I , ^{77}Br and ^3H extend over a wide range of values depending on the type of nuclide and its distribution, the type of sensitive target and its shape and distribution, and the environmental temperature during both irradiation and post-irradiation incubation. The higher values approach those determined for heavy charged particles with the same mean free path for primary ionisation, and are an order of magnitude larger than would be expected for external irradiation with photon generated electrons. The results for ^{33}P , ^{131}I and ^{32}P nuclides are appreciably smaller than that expected for external irradiation since the

long range electrons dissipate most of their energy out of the sensitive target.

A theoretical equation for X-ray production by accelerated electrons incident on a thick target has been revised by including factors to compensate for backscattering, direct and indirect ionisation, attenuation in the target and the incident angle of electrons (chapter 3).

An electron accelerator X-ray machine capable of delivering monoenergetic photons up to ~ 4.8 gray/sec exposure dose rate from four different targets has been designed, constructed and tested (chapter 4)

The biophysical mechanisms of direct and indirect radiation action has also been studied using the metallo-enzyme dihydroorotic dehydrogenase. The enzyme was irradiated both in dry state and in solution at different concentrations and at different dose rates using monoenergetic Cu-K photons from our X-ray machine. A technique was developed whereby it was possible to isolate and quantify each type of radiation action (chapter 5).

The inactivation of the enzyme in both solution and in dry state was found to be a single-hit/single-target process. It was also found that in solution the inactivation of the enzyme was dose-rate-and concentration-dependent with efficiency of radical inactivation has an exponential dependence on dose-rate and the inverse of the enzyme concentration. A new model for the inactivation of the enzyme has been suggested and its parameters, namely direct and indirect cross-sections, geometrical cross-section, saturated concentration constant, root mean square diffusion constant, mean free path of radicals absorption, life time and G value of radical production, have been determined. It is expected that this model can be generalised to suit other enzymes (chapter 6).

Contents

Chapter I Biophysical mechanisms of radiation action: inner shell ionisation

1.0	Introduction	1
1.1	Previous work on biophysical damage by soft X-rays	4
1.1.1	Enzymes and chemical molecules	4
1.1.2	Mammalian cells and other organisms	7

Chapter II Specification of Radiation Quality Emitted by Radioisotopes Incorporated into DNA of Living Organisms

2.0	Introduction	12
2.1	Previous work with internal emitters incorporated into DNA	13
2.2	Treatment of data from literature	21
2.2.1	Calculation of average energy of primary electrons from β and electron capture decays	23
2.2.2	Track average LET and mean linear primary ionisation generated by primary electrons	24
2.3	Radiation damage and repair	27
2.3.1	Radiation action and lethal damage	27
2.3.2	Repair mechanisms	29
2.4	Calculation of Inactivation Cross-sections	34
2.5	Description of the Damage Model	46
2.6	Results and Interpretation of Damage	49
2.6.1	Interpretation of damage for mammalian cells.	49
2.6.2	Interpretation of damage for <i>Escherichia Coli</i> and bacteriophages	54

Chapter III
Physical processes in radiation absorption

3.0	Introduction	56
3.1	X- and γ -rays as electromagnetic radiation	56
3.2	Interactions of photons with matter	61
	3.2.1 Fluorescence yield	61
	3.2.2 The Auger effect	62
3.3	Interaction coefficients and cross-sections	64
3.4	Mass attenuation coefficients for mixtures and compounds.	66
3.5	Total interaction coefficients	66
3.6	Restrictions in some interaction coefficients	66
3.7	Mass energy transfer and mass energy absorption coefficients.	68
3.8	Theoretical calculation of characteristic X-ray production.	69
	3.8.1 The total ionisation cross-section	70
	3.8.2 Types of ionisation and back scattering of electrons	72
	3.8.3 Attenuation of K-characteristic x-rays in the target	76

Chapter IV
Production and measurement
of characteristic X-rays

4.0	Introduction	78
4.1	Intensive X-ray production	78
	4.1.1 Electron Gun	79
	4.1.2 Auto-heating circuit of the electron gun	83
	4.1.3 Anode design and cooling	87
	4.1.4 X-ray production chambers and vacuum system	88
	4.1.4.1 The X-ray chambers assembly	88
	4.1.4.2 The vacuum system components and operation	91
4.2	Safety precautions and interlocking	94
	4.2.1 Warning signals	94

4.2.2	Connections and interlocking	94
4.2.3	Monitoring of radiation	98
4.2.4	Personal monitoring	98
4.3	Physical specification of the output beam: X-ray spectroscopy.	98
4.3.1	Construction of the proportional counter	99
4.3.2	Purity testing of the photon beam	105
4.3.3	Energy calibration curve and the determination of unknown photon energy	109
4.4	Attenuation of the photon beam	111
4.5	Calorimetry	112
4.5.1	Principles and design of the calorimeter	114
4.5.1.1	Heat transfer	114
4.5.1.2	Methods of calorimetry and temperature change control	118
4.5.1.3	Calorimeter design	124
4.5.1.4	The electronic measurement of temperature differences	127
4.5.1.5	The absorbed dose and energy leakage.	129
4.6	Measurement of the dose from characteristic X-rays using an ion chamber	130

Chapter V
Experimental aspects and techniques used
to study the Metallo-enzyme
(Dihydroorotate Dehydrogenase)

5.1	Characteristic of the enzyme	136
5.2	Preparation of chemical solutions	137
5.3	Enzymatic assay procedure	140
5.4	Reaction rate and calibration curves of enzyme.	141
5.5	Irradiation procedure and survival fraction determination for the enzyme	143

Chapter VI
**Inactivation of Enzyme in Solid and in
solution by Cu-K X - rays**

6.1	Radiation dosimetry of enzyme	144
6.2	Dose response curves	146
6.3	Inactivation cross-sections of enzyme	150
6.4	Model for inactivation of enzyme in solution and in solid state	151
6.5	Interpretation of damage in metallo-enzyme.	158
 Chapter VII: Conclusions and Recommendations		165
 Appendix A: Spectra from Soft X-rays and other Radiation sources obtained by Using a Na(Tl) Scintillation Detector and a Proportional Counter		170
 Appendix B: Experimental data for the Metallo-enzyme irradiated by Cu-K X-rays in solution and in dry state		178
 References		190
 Selective bibliography.		202

List of Tables

2.1	Summary of data for experiments with ^{125}I incorporated into nuclear DNA of mammalian cells.	16
2.2	Summary of data for experiments with ^3H incorporated into nuclear DNA of mammalian cells.	17
2.3	Summary of data for experiments with ^{77}Br and ^{131}I radionuclides incorporated into nuclear DNA	18
2.4	Summary of data for experiments with ^{32}P , ^{33}P and ^3H radionuclides incorporated into DNA of bacteriophages T-1 and T-4	18-9
2.5-2.6	Summary of data for experiments with ^{32}P , ^{33}P and ^{125}I radionuclides incorporated into DNA of bacterial strains (E. Coli) at storage temperature -196°C .	20-1
2.7	Track average LETs and average linear primary ionisation for equilibrium electron spectrum generated by Auger electrons from decaying of ^{125}I and ^{77}Br	25
2.8	Average energy of primary electrons and the projected ranges for the decay of ^{125}I , ^3H , ^{77}Br , ^{131}I , ^{33}P and ^{32}P	26
2.9-2.15:	Concentration of source electrons (C) and fluence of electrons Φ_0 or Φ_{37} for the radionuclides ^{125}I , ^3H , ^{77}Br , ^{131}I , ^{33}P and ^{32}P incorporated into DNA	36-41
2.16-2.18	Effect cross-sections and intrinsic efficiencies of ^{125}I , ^3H , ^{77}Br and ^{131}I radionuclides incorporated into DNA of mammalian cells	42-3
2.19-2.22	Effect cross-sections and intrinsic efficiencies of ^{125}I , ^{33}P , ^{32}P and ^3H radio-nuclides incorporated into bacterial strains and phages.	43-45
4.1	Attenuation of K-X-rays through different thicknesses of aluminium absorber	107-8
4.2	Attenuation correction for K-X-rays from copper target	112
4.3	Calorimetric determinations of energy fluence with different absorbers and temperature detectors	114
4.4	Relationship between resistance and temperature of the thermistor	120
4.5	Relationship between resistance, temperature and the	

	power dissipated in the thermistor	123
4.6	The relation between the applied power, the applied accelerated voltage and the exposure dose rates	133-5
6.1	Elemental composition of the catalase enzyme	145
6.2	Mass energy absorption coefficients for enzyme D. De nase at different concentrations	146
6.3	The dose rates for enzyme in different concentrations	146
6.4	Doses at 37% survival of enzyme in solution at different concentrations and in dry state	147
6.5	Electron spectrum generated by the interaction of 8.04 keV photons with water	150
6.6	Effect cross-sections and intrinsic efficiencies of the interactions of electrons in the slowing down spectrum for enzyme in solution and in solid state	151
6.7	Metallo-enzymes irradiated in dry state with different mono-energetic photons	160

List of Figures

1.1	Schematic diagrams of DNA segments and its probabilities of radiation action	8
2.1	The intrinsic efficiencies of damage of different radionuclides incorporated to the nuclear DNA of mammalian cells against their linear primary ionisations	50
2.2	Probabilities for inactivation, as a function of the mean free path for primary ionisation for fast heavy particles, X-rays and radionuclides ^{125}I , ^3H , ^{77}Br and ^{131}I	51
2.3	Survival fractions calculated from equation 2.10 are compared with experimental data for radionuclides ^{125}I , ^3H , ^{77}Br and ^{131}I	55
2.4	The intrinsic efficiencies of damage of different radionuclides incorporated to the nuclear DNA of E. Coli cells against their linear primary ionisations	56
2.5	The intrinsic efficiencies of damage of different radionuclides incorporated to the DNA of T-1 and T-4 bacteriophages against their linear primary ionisations	57
2.6	The intrinsic efficiencies of damage for different radionuclides incorporated to DNA of mammalian cells, E. Coli and bacteriophages	58
3.1	The fluorescence yield from different elements calculated from equations 3.2 and 3.3	63-4
3.2	Theoretical and experimental back scattering coefficients for electrons at different incident energies on a copper target	75
3.3	Back scattering coefficients for incident electrons of energy 20 keV at differing angles of incidence	76
3.4	Schematic diagram for a beam of electrons incident on a target at an angle θ and X-rays collected at an angle ϕ	77
4.1	A schematic diagram of the electron gun	80
4.2	The characteristic curve of the filament	81
4.3	Stabilised DC power source of 26 volts floated up to 100 kV with respect to earth by stand-off insulator	82
4.4	The calibration curve of the high voltage supply against an electrostatic meter reading	84
4.5	Preheating timer circuit for the electron gun filament	85-6
4.6	Schematic diagram of the anode	87

4.7	The mechanical construction of the production chambers and the vacuum components	89-90
4.8	Schematic diagram of the production chambers and the vacuum system	93
4.9	The arrangement of the safety interlock system and its connections	96-7
4.10	The component parts of the proportional counter . . .	103
4.11	Photon transmission curve through aluminium absorber.	106
4.12	Fraction of transmitted photons through aluminium absorber	109
4.13	The electronic equipment configuration for radiation source spectroscopy using a scintillation detector (NaI(Tl))	110
4.14	Calibration curve for the determination of unknown sources using a scintillation detector (NaI(Tl))	110
4.15	Characteristic temperature constant of the thermistor	121
4.16	Relation between temperature rising and power dissipated in the thermistor	122
4.17	The component parts of the calorimeter	125
4.18	Conventional Wheatstone bridge circuit for measuring the temperature changes in the thermistor	128
4.19	The most common circuitry for the ionisation chamber	132
5.1	Curves of reaction rate for enzyme at different concentrations	142
5.2	Calibration curve of enzyme's reaction	142
6.1-6.4	Dose survival curves of enzyme solutions 0.5 - 5.0 unit/ml irradiated by photons of energy 8.04 keV at different dose rates	147-9
6.5	Dose survival curve of dry enzyme irradiated by photons of energy 8.04 keV at dose rate 1.99 gray/sec.	149
6.6	Survival curve of dry enzyme drawn against the applied fluence of electrons	155
6.7	Calibration curve drawn from equation 6.13 by using experimental data of enzyme solution irradiated at different concentration.	156
6.8	Dose of 37% survival of dry metallo-enzyme irradiated with different mono-energetic photons.	161

6.9	Enzyme in solution of different concentration inactivated by Cu-K-photons at different dose rate.	162
6.10	Effect cross-section for dry enzyme and in solution of different concentration irradiated by Cu-K photons at 1.99 gray/sec.	163
6.11	The intrinsic efficiency of damage by Cu-K x-rays for for the metallo-enzyme in solution and in solid state. .	164

Chapter I

Biophysical Mechanisms of Radiation Action: Inner Shell Ionisation

1.0 Introduction

In the field of nuclear medicine, investigators have long been acquainted with the drastic damaging consequences of inner-shell ionisation (Emmons 1959, Addink 1965, Halpern and Stocklin 1974, etc). This problem is also of significant importance in radiobiology and nuclear chemistry (Feinendegen, Ertle and Bond 1970, Feinendegen 1977 and Fujiwara and Mayazaki 1987). If a radionuclide undergoing a nuclear process associated with inner-shell ionisation, eg K-capture, belongs to an atom bound in a molecule, the latter has a small chance of surviving.

This encouraged the greater use of naturally decaying isotopes in these fields, as described in Chapter II in which survival data for Iodine-125, Bromine-77, Tritium-3, Phosphorus-33, Iodine-131 and phosphorus-32 have been collected from the literature and reanalysed to extract cross-sections for inactivation caused by the slowing down charged particle fluence. Such cross-sections are absolute specifications of the radiation quality.

The biophysical implications are greatly increased by the fact that selected inner-shell vacancies can also be formed when monoenergetic low energy X-rays interact with matter via the photoelectric effect (Ohara, Shinohara, Kabayashi and Ito (1987), Humm and Charlton (1987 a). Whatever the mode of primary inner-shell ionisation, the electronic readjustment that inevitably follows is essentially the same, resulting in

one or more Auger vacancy cascade(s) and multiple charging of the affected atom.

Studies of the atomic readjustment to inner-shell vacancies and its chemical consequences were first carried out by Carlson and White (1966). In experimentation on simple isolated gaseous molecules decomposition was observed. Charlton, Booz, Fidorra, Smit and Feinendegen (1978), Charlton and Booz (1981), Humm *et al* (1982) and Humm and Charlton (1987 b) studied the condensed phases and reported multiple charging, resulting in charge migration. The biological and biochemical effects of such multiple charging together with the direct and indirect actions of liberated radiation particles in the biomolecules are of particular interest because of the obvious implications for radiation therapy.

Direct interactions can take two forms. The absorption of energy in, and hence possible damage to, a molecule is effected either through direct ionisation by the primary interactions, or through secondary products of these primary interactions. An indirect action is one in which the ionising radiation produces ions and radicals in the solvent. These in turn interact with the solute molecules resulting in biological damage.

In both direct and indirect cases the spectrum of damage is usually considered to be relatively dependent on the mode of radiation absorption in the matter of interest because these interactions depend on the type of secondaries produced in the sensitive entities, as explained in section 3.2.

Previous studies considered the combined effects of radiation without attempting to quantify each action separately.

It is proposed to develop a technique by which it will be possible to isolate the indirect action of radiation and to quantify the direct action. This is accomplished by choosing a simple biochemical molecule (see section 5.1) and irradiating it in the dry state and in solution. The result of this study might be used to extend the area of the investigation to determine the biophysical parameters responsible for radiation damage in more complex molecules which have repair mechanisms. By so doing it should be possible to isolate the effect of these repair mechanisms.

Soft X-rays have been used by many investigators to study the biophysical effect of photons in living organisms. (Diehn *et al* 1976, Al-Wajidi 1984, Goodhead and Thacker 1977, Cox *et al* 1977, Goodhead *et al* 1979.) Significant biomolecular action is observed.

In our research programme it has been decided to study the effects of K-characteristic X-rays from copper (photon energy = 8.04 keV). This energy is of considerable importance as it exceeds the K-absorption edges of the constituent atoms of most living systems (Gomberg 1964, Humm *et al* 1982).

In order to accomplish this, it has been necessary to design and construct an intensive K-characteristic X-ray machine (see section 4.1, 4.2), which is capable of producing sufficiently large doses to study enzymes in the dry state, and devices which are necessary to quantify and qualify its output (see section 4.3, 4.6 for details of the design and construction of these devices: a calorimeter and a proportional counter).

1.1 Previous Work on Biophysical Damage by Soft X-rays

1.1.1 Enzymes and Chemical Molecules

A series of experiments have been performed by Hussey and Thomson (1923, 1924, 1925 a, b, and c) on the effects of X-rays on the enzymes Trypsin, Pepsin, and Invertase. They found that all these enzymes are easily inactivated in solution form.

In 1942 Lea and Salman described direct and indirect actions of radiation on Viruses and enzymes. They irradiated dry preparation of Myosin and Ribonuclease and they found that they required a dose (D) of 3.4×10^7 roentgens to reduce the activity of Ribonuclease to 37 per cent. The D_{37} for Myosin is 5.5×10^6 roentgens. The shape of the survival curves for both Ribonuclease and Myosin are typical of "one hit" interaction.

Dale (1942) irradiated enzyme in aqueous solution at different concentrations. He found that he needed 50 roentgens to inactivate 30 per cent of a very dilute solution and 100 roentgens to inactivate the same percentage for 345 times more concentrated solution. He concluded that this dilution phenomena can be understood by one assumption, namely that the radiation acts primarily on the water which in turn produces the effects on the enzyme.

Emmons (1959) has irradiated dry catalase with fluorescent emission lines. The response is demonstrated for characteristic K-X-rays whose energies are 6.4 keV (iron) and 5.89 keV (manganese). It was found that dry catalase subjected to the emission line required an induction dose before damage was evident. When it was irradiated by K_{α} X-rays from nickel (7.471 keV) and chromium (5.411 keV), a single hit exponential decrease in the catalytic effectiveness of the catalase was

demonstrated. Emmons' study of catalase was geared to determining whether there was an effect for K_{α} characteristic photons, in addition to direct and indirect action on biomolecules which contained heavy metals. This additional effect he called a "resonance interaction" which might have significant damage power across the K-edge of these metals.

Gomberg (1964) studied the effect upon biological systems of ionising radiation in the 5-20 keV X-ray energy range. Results obtained with zinc carboxypeptidase A indicate that inactivation is energy dependent, as well as dependent on the K-edge effect.

Addink (1965) irradiated a solution of carbonic anhydrase in water with a continuum of X-rays, regulating only the maximum wavelength by changing the tube voltage. He has shown that polychromatic X-rays whose maximum energy lies at 9 keV are significantly less effective in releasing zinc from carbonic anhydrase than X-rays with $E_{\max} = 10.5$ keV given equal radiation time. He provided neither dosimetry data nor absorption calculations.

Radical concentration in TdR and BUdR, expressed per unit dose absorbed, has been investigated by Halpern and Stocklin (1974). They reported that, when BUdR was irradiated in solution, a three-fold increase in radical concentration per unit energy absorbed at the K edge of bromine was observed, showing the efficiency of radiation in producing radicals in solution. This efficiency was shown to depend directly on the photon energy across the K edge of the heavy atom in the biomolecule.

Muller and Kohnlein (1964) reported G values of 0.8 and 0.4 for radical formation in BUdR and TdR respectively when irradiated by Cobalt-60 gamma rays.

Diefallah *et al* (1970) irradiated Thyroxine compounds in the solid state. They reported that chemical effects in solution are generally determined by the interaction of radicals from radiolysis of the solvent. The study was designed to show whether there was any chemical effect due to resonance absorption of X-rays in the iodine. The authors neglected to consider the energy absorption due to other elements in the molecule.

Diehn *et al* (1976) studied the inactivation of Bovine carbonic anhydrase (BCA) irradiated in the solid phase with monoenergetic low-energy X-rays of copper, zinc, germanium and arsenic, of photon energies 8.04, 8.74, 10.01 and 10.69 keV respectively. The inactivation, normalised to an equal dose absorbed, was shown to depend on the X-ray energy. For photon energies slightly above the zinc edge, they reported that the inactivation significantly exceeded that expected on the basis of energy absorption.

This amplification effect was interpreted in terms of Auger charging resulting from inner shell vacancies in the zinc atoms. Al-Wajidi (1984) studied the inactivation of the enzyme Ribonuclease in aqueous solution resulting from low energy X-rays (10-100 keV). It was deduced that the enzyme was inactivated by a simple single hit process. The study aimed to find the effect of low energy photons on aqueous solution of the enzyme R-Nase in the production of free radicals, and hence the interaction of these radicals with the functional groups of the amino acids of the enzyme leading to production of organic radicals followed by inactivation. The survival fraction decreased exponentially with the increase in the applied dose. The radiosensitivity of the enzyme proved large at the lowest concentration and decreased with the increase in concentration and with the increase in the applied X-ray energy.

1.1.2 Mammalian Cells and Other Organisms

Biological studies using X-rays to evaluate the effect of very short tracks were performed by Neary *et al* (1964), Neary *et al* (1967) and Neary *et al* (1970). They used X-rays of energies down to 1.3 keV to repeat and extend the pioneering experiments of Catchside and Lea (1943). They deduced that chromatid aberrations in *tradesantia* resulted from the interaction of two damaged structures of "site radius" about 0.2 μm . They also concluded that one energy-loss event of ~ 60 eV was sufficient to cause a primary lesion, while Lea and Catchside (1942) concluded that ~ 17 energy-loss events were required.

Ultrasoft X-rays of 1.5-3 keV were shown to inactivate viruses (Lea and Salman, 1942). Neary *et al* (1970) found that 1.5 keV X-rays produced single- and double-strand breaks in DNA with an efficiency comparable to that of protons of similar linear energy transfer (LET).

Some of the many models proposed to explain the mode of action of radiation on mammalian cells *in vitro* are based principally on the spatial distribution of the primary radiation energy deposition within the cells (Kellerer and Rossi, 1972, Katz *et al* , 1971,1972 and Roth *et al* , 1976). Kellerer and Rossi (1972) explained radiation damage in terms of the deposition of energy within a "sensitive site" of relatively large dimension ($\sim 1\mu\text{m}$). However Chadwick and Leenhouts (1973) and Leenhouts and Chadwick (1975) assumed that the site for damage was of the order of 1-10 nm diameter, and they derived the expression from simple assumptions based on the molecular nature of the lethal event. They proposed that double-strand breaks (Figure 1.1) in cellular DNA could result in cell lethality. Such breaks were considered to result from a single track as well as from double track. This model predicted that the rate of induction of double-strand breaks in cellular DNA

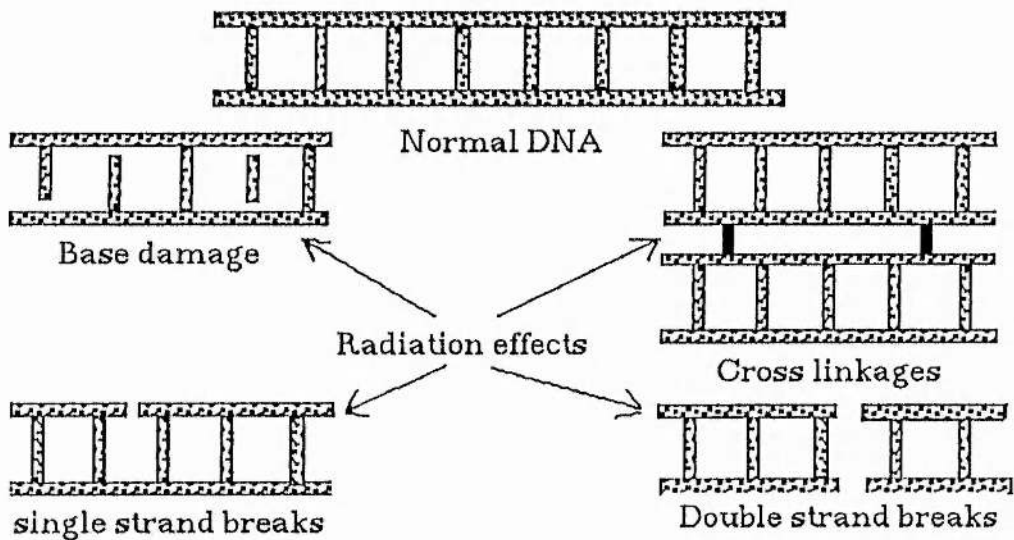
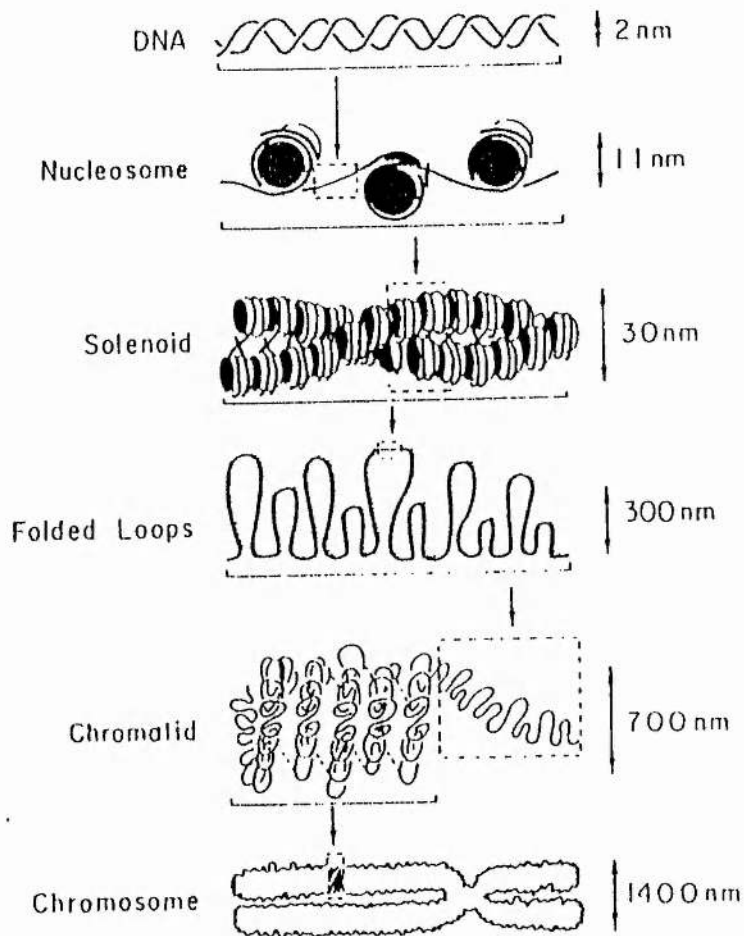


Figure 1.1: A schematic diagrams of DNA segments and its probabilities of radiation action.

should be related to the rate of cellular inactivation. However the frequency of induction of single-strand breaks (eg. Bryant and Blocher 1980) would be insufficient for this interaction to occur at doses used in cellular radiobiology.

These assumptions encouraged workers in radiobiology and radiotherapy to test photoelectrons of ranges $\leq 1\mu\text{m}$ which were produced by the absorption of X-rays of quantum energy less than 10 keV. So they suggested that X-rays of appreciably low energy might discriminate between the biophysical models. (Biophysical models of radiation action have been reviewed by Goodhead, 1987).

Goodhead and Thacker (1977) used ultrasoft X-rays which produce tracks of short lengths for the determination of the size of the cellular events involved in radiobiological effects. It was shown that Aluminium K-X-rays with track length less than $0.07\mu\text{m}$ could be used for quantitative radiation experiments, and that these X-rays were considerably more effective per unit dose, than gamma rays in the inactivation of Chinese hamster, V79, cells. These results have been confirmed, and a similar result obtained for Human diploid fibroblast cells in culture by Cox *et al* (1977). Cultured cells of both types (V79 and Human diploid) have been irradiated with Helium ions of unrestricted ranges, but of similar linear energy transfer (LET) to Aluminium K-X-rays of limited track lengths. The aim of this experiment was to establish the patterns of response of these cells to radiation of the same and different LET (Helium ions of LET 20-50 $\text{keV}\mu\text{m}^{-1}$, Neutrons, and hard X- or γ -rays).

Thacker *et al* (1977) have described the quantitative estimation of X- and γ -ray induced mutation of the enzyme hypoxanthine guanine phosphoribosyl transferase (HGPRT) in V79 hamster cells. For human

diploid fibroblast cells the same experiment has been done by Cox and Masson (1976). A comparative study of mutagenesis by low LET radiation in V79 and Human diploid fibroblasts has been undertaken by Thacker and Cox (1975) to estimate the mutagenic effects in these cells.

Experiments introduced the track length parameter which reflects the site diameter, or the interaction distance, dependent on the limited range of both the photo-electrons and the resultant Auger electrons (Goodhead and Thacker 1977 and Goodhead *et al* 1979). Such experiments concluded that K-X-rays from Aluminium were incapable of producing intra-track effects over distances greater than $0.07\mu\text{m}$ if the site diameters or interaction distances were greater than $0.07\mu\text{m}$. The effectiveness of Aluminium K-X-rays would be expected to be similar to that of low LET radiation, with considerable inter-track action, but different from irradiation with ion track intersections for which the intra-track action dominates even at the moderate LET of $\sim 20 \text{ keV}\mu\text{m}^{-1}$.

In another experiment, Goodhead *et al* (1979) used Carbon K-characteristic X-rays of photon energy 0.278 keV to produce electrons of range $<7 \text{ nm}$, which is an order of magnitude smaller than those from Aluminium K-X-rays, and is only about three times the diameter of the DNA double helix. It was shown that despite their very low energy and short track lengths, Carbon K-X-rays do cause inactivation and mutation of cultured Chinese hamster and Human diploid fibroblast cells. It was clear that such photons were more effective per unit dose than γ -rays or 250 kVp X-rays, and were probably as effective as long-tracks of Helium ions of similar LET. This implied that the sensitive sites were $\leq 7 \text{ nm}$ in size, and that less than fifteen ionisations within a site were sufficient to produce a biological effect. The importance of low energy photon interaction with DNA to induce Auger electron cascades of bound atoms has been studied by Booz *et al* (1982) and Humm *et al*

(1982). Photons interact with matter mainly by the photoelectric effect, whereby one photoelectron and one or more Auger electrons of low energy are emitted. Auger electrons from DNA-bound atoms may have energies less than 270 eV (Carbon), 509 eV (Oxygen) or 1.89 keV (Phosphorus). Within this range of energies, soft X-rays play an important role. Photo-interactions with Phosphorus are important for photons between the K-absorption edge of Oxygen (537 eV) and the L-absorption edge of Phosphorus (131 eV). The mean number of electrons emitted per photoelectric interaction is 2.2, 2.2, and 4.1 for C, O and P respectively.

Each electron emitted carries away one negative charge leaving one positive charge on the atom. These changes are neutralized whereby the energy is transformed into other forms of energy, kinetic energy of low energy electrons, ionization potentials of singly ionized states of neighbouring atoms, excited states of the neutralized atoms, etc. The dose contribution from direct photon interactions in DNA is small. Most of the absorbed dose in DNA is from the electrons at the very end of their ranges when they reach the most damaging energy which is absorbed completely to induce multiple Auger cascades.

Booz *et al* (1982) concluded that it is possible to evaluate the energy locally deposited around the site of a photoelectric interaction followed by an Auger-electron cascade. In this evaluation, not only the energy loss of the emitted electrons is to be considered, but also other forms of energy resulting from neutralization during and after the Auger-electron cascade. This second form of energy deposition may even be significant in magnitude for low-Z atoms such as C, N, O, and P, ie for those atoms which have the dominant photoelectric cross-section in biological tissue.

Chapter II

Specification of Radiation Quality Emitted by Radioisotopes Incorporated into DNA of Living Organisms

2.0 Introduction

In nuclear medicine, radioactive nuclides are used extensively on a routine basis for investigative, therapeutic and diagnostic purposes. As in all other applications of technology, the benefits obtained must be balanced against possible hazards. For radiological protection purposes, it is important to be able to assess these hazards with reasonable accuracy.

There are two main reasons why conventional dosimetry [based on absorbed dose (ICRU 1979)] may not be suitable for appraising the hazard from incorporated radionuclides. Firstly, many of the radioisotopes used have complex decay schemes in which an inner shell vacancy is produced resulting in characteristic X-ray emission accompanied by Auger electron cascades. For example, a single decay of ^{125}I can result in the emission of up to 56 low energy Auger electrons which have ranges localised in cellular or subcellular dimensions thereby possibly producing an anomalously large degree of damage (Charlton *et al* 1978, Cottrall 1985, Mole 1986 and Humm and Charlton 1987). Secondly, if the radionuclide is incorporated into an especially sensitive site within the cell structure, eg in the DNA molecule, excessive damage may be expected beyond that predicted from conventional dosimetry.

In this chapter relevant published survival data on biological damage caused by internal emitters ^{125}I , ^{77}Br , ^3H , ^{131}I , ^{33}P and ^{32}P which are incorporated into the DNA of mammalian cells, bacteria and

bacteriophages have been collected and the results re-analysed in terms of the parameters of a new radiation damage model to determine an inactivation cross-section for each internal emitter. These quality parameters (inactivation cross-sections) are the absolute specification of radiation quality which can be compared with cross-sections similarly determined for the effects of external radiations with heavy charged particles and photons. Also, the survival curves can be studied by applying a proposed semi-theoretical description of radiation damage, and salient features of the basic damage mechanisms can be deduced.

2.1 Previous work with internal emitters incorporated into DNA

Most previous studies on the radiobiological effects of internal emitters have concentrated on the use of survival curves of various organisms and mammalian cells to interpret the effectiveness of the highly localised dose distribution characteristics, and to identify the primary sub-cellular radiosensitive targets responsible for radiation-induced cell death. It is generally concluded that the biological effects of radioactive nuclei, randomly distributed in the cell, are due almost entirely to the ionogenic action of the secondary electrons, (Charlton *et al* 1978). Therefore, the action of such radionuclides is analogous to that of external radiations and involves the usual problems with absorbed dose, fluctuations in specific energy, and radiation quality. However the localisation of the energy deposition within the sensitive structure apparently increases the radiation risk. (Ackery and Baverstock 1987, Howell, Sastry, Hill and Rao 1985, Sastry, Haydock, Basha and Rao 1985, Rao, Govelitz and Sastry 1983, Commerford, Bond and Cronkite 1980.)

It has been suggested that non-ionogenic effects due to radioactive transmutation (ie. local events accompanying the decay) of internal emitters incorporated in the DNA could be important if the disintegration takes place within the DNA molecule, in which case the relative importance of various local events of killing (transmutation, atomic de-excitation, charge cascades, recoil energy, etc) will be related to the specific activity and not to the absorbed dose (Krisch 1970, 1972, Charlton *et al* 1978, Kassis, Howell, Sastry and Adelstein 1987).

As the electrons in the electron cascades can have very short ranges, the severity of the biological effect must depend upon the distribution of the radionuclides within the various parts of organs, cells and sub-cellular structures (Hofer, Harris and Smith 1975, Commerford *et al* 1980, Kassis, Adelstein, Haydock and Sastry 1980, Gaulden 1983, Yasui, Hofer and Warters 1985, Rao, Sastry, Govelitz, Grimmond and Hill 1985 a and b and Yasui and Hofer 1986).

Cell survival studies confirm the cytotoxicity of ^{125}I decay. For example it was found by Yasui, Paschoa, Warters and Hofer 1987 that, when ^{125}I nuclides are incorporated randomly inside the nuclei, $D_0 = 96$ decays / cell, but the cytotoxicity is increased three fold when only 5% of the nuclear DNA is labelled with the same nuclides ($D_0 = 30$ decays / cell).

Kassis, Fayed, Kinsey, Sastry, Taube and Adelstein 1987 tested the radiotoxicity of ^{125}I in Chinese hamster V-79 lung fibroblast under three conditions (localization of ^{125}I nuclides) of irradiation viz. extracellular (Na^{125}I), cytoplasmic (Iododi-hydrorhdamine, ^{125}I DR) and when incorporated directly into the nuclear DNA (^{125}I UdR). For the same exposure circumstances, Na^{125}I produced no observable damage. ^{125}I DR produced a survival curve with a distinct shoulder but in contrast the survival curve obtained with DNA-bound ^{125}I UdR was pure exponential and with lethal dose, D_{37} of 1/6 of that observed for the cytoplasmic

distribution. Furthermore the survival fraction for ^{125}I UdR was determined as a function of ^{125}I atoms contained in the DNA. It was found to be inversely proportional to the number of ^{125}I labelled atoms.

Cytotoxicity of ^3H decay in bacteriophages T-1 and T-4 has been also studied by Funk, Person and Bockrath 1968, after labelling DNA by ^3H -thymidine and protein by ^3H -amino acids. It was found that the ratio of killing efficiencies for decays originating in phage DNA to those originating in phage protein is 2.6. Information from this study is collected in table 2.4c. Such experiments suggest that the main target responsible for cell killing is the nuclear DNA, but not all the nuclear genome is equally sensitive to radiation therefore there must be an important gene(s) which must be inactivated to kill the cell (Yasui *et al* 1987).

Lethal effects in different organisms of ^{125}I , ^3H , ^{32}P and ^{33}P radioisotopes have been also under investigation. ^{32}P and ^{33}P , β emitters of average energy 695 and 77 keV respectively, have been incorporated into DNA of T-1 and T-4 bacteriophages and sensitive and resistant strains of Escherichia Coli, (E. Coli). It was clear that for different storage temperatures with these radionuclides the efficiency of damage at $+4^\circ\text{C}$ is higher than that at -196°C . This reflects the enhanced relative importance of repair mechanisms and the indirect actions of long range β rays due to radical species which are free to move and act within a specified time period. Irradiation in freezing temperatures will eliminate almost all of the 80 - 90 % indirect effect produced by radical interactions.

A summary of information on experiments using various mammalian cell lines irradiated by incorporation of the electron capture nuclide ^{125}I is given in table 2.1, and by incorporation of the β emitter, ^3H , in table 2.2, for electron capture ^{77}Br and β emitter ^{131}I in table 2.3; bacteriophages T-1 and T-4 irradiated by ^{32}P , ^{33}P and ^3H in table 2.4; E.

Coli strains irradiated by ^{32}P and ^{33}P in table 2.5; and for E. Coli strains and bacteriophage T-1 irradiated by ^{125}I in table 2.6.

Reference	Cell Line	Temp (°C)	Label Type (1)	Irradiation time (hours)	D_0 Decay/cell
Burki <i>et al</i> (1973)	CH.H.V ₇₉	-196	Randomly	15	39*
Koch & Burki (1975)	CH.H.V ₇₉	-196	Randomly	16-18	39*
Koch & Burki (1975)	CH.H.V ₇₉	+4	Randomly	16-18	35
Miyazuki & Fujiwara (1981)	CH.H.V ₇₉	-49	Unifilar	14	40
Burki <i>et al</i> (1973)	Leukaemic cells L _{5178Y}	-196	Randomly	10-11	46
Hofer & Hughes (1971)	Leukaemic cells L ₁₂₁₀	37 <i>vivo</i>	Randomly	9	45
Hofer <i>et al</i> (1975)	Leukaemic cells L ₁₂₁₀	37 <i>vivo</i>	Randomly	9	45
Liber, Lemotte and Little 1983	Human diploid TK6	37	Randomly	22	28
Liber, Lemotte and Little 1983	Human diploid TK6	-70	Randomly	22	28

1 Location of labeled nuclides on the DNA and * Shouldered survival curves

Table 2.1: Summary of data for experiments with ^{125}I incorporated into nuclear DNA of mammalian cells.

References	Cell Line	Temp (°C)	Label Type (1)	Irradiation Time (hours)	D ₀ Decay/cell
Burki <i>et al</i> (1973)	CH H V ₇₉	-196	Randomly	15	970 *
Koch & Burki (1975)	CH H V ₇₉	-196	Randomly	16-18	970 *
Koch & Burki (1975)	CH H V ₇₉	+ 4	Randomly	16-18	262 *
Burki & Okada (1970)	Leukaemic cells L _{5178Y}	-196	Unifilar	10	175
Burki & Okada (1970)	Leukaemic cells L _{5178Y}	-196	Reverse Unifilar	40	167
Bedford <i>et al</i> (1975)	Leukaemic cells L _{5178Y}	-196	Unifilar	11-12	222
			Bifilar	44-48	226
Hofer & Hughes (1971)	Leukaemic cells L ₁₂₁₀	37 <i>vivo</i>	Randomly	9	360 *
Hofer <i>et al</i> (1975)	Leukaemic cells L ₁₂₁₀	37 <i>vivo</i>	Randomly	9	360 *
Liber <i>et al</i> (1983)	Human diploid TK6	37	Randomly	22	385
Liber <i>et al</i> (1983)	Human diploid TK6	- 70	Randomly	22	385

1 Location of labeled nuclides on the DNA and * Shouldered survival curves

Table 2.2: Summary of data for experiments with ³H incorporated into nuclear DNA of mammalian cells.

Isotope and reference	Cell line	temp. of incubation oC	Type of label DNA	Irradiat. time (h.)	Radiation dose decay/cell
⁷⁷ Br (Kassis et al, 1982)	Ch. hamster V-79	37	Bifilar	18	311
¹³¹ I (Hofer & Hughes, 1971)	Leukaemic cells L1210	37(vivo)	Random.	9	342

Table 2.3 : Summary of data for experiments with ⁷⁷Br and ¹³¹I radionuclides incorporated into nuclear DNA

Bacteriophage	Storage temperature °C	Individual dose decay/phage	Average dose D ₀ in decay/phage
T-1	-196	18.18 15.38	16.78
T-1	+4	7.35 6.58 7.46	7.11
T-4	-196	9.80 11.76	10.72
T-4	+4	6.94 7.04	6.99

(Irradiation times are not specified but are prolonged ≥ 9 hrs.)

Table 2.4 a: Summary of data for experiments with ³²P radionuclide incorporated into DNA of bacteriophages T-1 and T-4 (after Krisch 1970)

Bacteriophage	Storage temperature °C	Individual dose decay/phage	Average dose D ₀ in decay/phage
T-1	-196	29.41 32.26	30.84
T-1	+4	9.52 6.90	8.21
T-4	-196	21.28 27.78	24.53
T-4	+4	10.00 10.42	10.21

(Irradiation times are not specified but are prolonged ≥ 9 hrs.)

Table 2.4 b: Summary of data for experiments with ^{33}P radionuclide incorporated into DNA of bacteriophages T-1 and T-4 (after Krisch 1970)

Bacteriophage & exp. temper.	^3H -thymidine DNA dose decay/DNA	Av. dose to DNA decay/DNA	^3H -amino acids protein dose decay/phage	Av. dose to protein decay/phage
T-1 +5 °C	12.66	-	17.54	-
	8.33	-	17.86	-
	6.67	-	23.26	-
	7.14	-	30.30	-
	7.14	8.39	25.64	22.92
T-4 +5 °C	18.18	-		
	21.74	-		
	23.25	-		
	16.39	19.89		

(Irradiation times are not specified but are prolonged ≥ 9 hrs.)

Table 2.4 c: Summary of data for experiments with ^3H radionuclide incorporated into DNA (^3H -thymidine) and to nuclear protein (^3H -amino acids) of bacteriophages T-1 and T-4 (after Funk *et al* 1968)

Bacterial strain	Individual dose (decay/phage)	Average dose, D_0 (decay/phage)
E. Coli Bs-1	20.83 23.81	22.32
E. Coli AB2463	20.41 19.61	20.01
E. Coli AB1157	83.33 125.00	104.17
E. Coli 15THU	38.46 41.67	40.01

(Irradiation times are not specified but are prolonged ≥ 9 hrs.)

Table 2.5 a: Summary of data for experiments with ^{32}P radionuclide incorporated into DNA of bacterial strains (E. Coli) at storage temperature -196°C . (after Krisch 1970)

Bacterial strain	Individual dose (decay/cell)	Average dose, D_0 (decay/cell)
E. Coli Bs-1	17.54 31.25	24.39
E. Coli AB2463	15.87 23.26	19.57
E. Coli AB1157	45.45 83.33	64.39
E. Coli 15THU	50.00 33.33 52.63	45.32

(Irradiation times are not specified but are prolonged ≥ 9 hrs.)

Table 2.5 b: Summary of data for experiments with ^{33}P radionuclide incorporated into DNA of bacterial strains (E. Coli) at storage temperature -196°C . (after Krisch 1970).

Bacterial strain or phage	^{125}I atoms per genome	^{125}I atoms per cell	Slope of surv. curve	Individual dose decay/genome
E. Coli Bs-1	13.2	349.00	5.92±0.99	1.92 - 2.69
	62.2	142.00	28.00±1.5	2.10 - 2.35
	63.2	523.00	28.20±1.5	2.13 - 2.37
	114.4	1300.00	49.00±4.6	2.14 - 2.58
	157.3	1410.00	70.20±4.0	2.12 - 2.38
E. Coli B/r	27.9	265.00	6.03±0.47	4.29 - 5.03
	39.1	88.00	11.10±0.40	3.40 - 3.65
	49.3	231.00	12.00±0.8	3.86 - 4.41
	118.6	629.00	19.70±1.0	5.75 - 6.33
	137.7	595.00	29.50±1.6	4.42 - 4.95
E. Coli k-12 AB2463	23.30	27.00	18.81±0.52	2.50 - 2.81
	2.08	22.00	1.39±0.49	1.11 - 2.31
E. Coli 15THU	85.5	161.00	12.70±0.4	6.49 - 6.94
	22.4	90.00	3.30±0.32	6.21 - 7.52
Bacteriophage T-1	7.13	-	3.06±0.85	1.82 - 3.22
	12.50	-	6.73±0.43	1.75 - 1.98
	21.90	-	10.14±0.57	2.04 - 2.29

(Irradiation times are not specified but are prolonged ≥ 9 hrs.)

Table 2.6: Summary of data for experiments with ^{125}I radionuclide incorporated into DNA of bacterial strains (E. Coli) and bacteriophage (T-1) at storage temperature -196°C . (after Krisch 1972).

2.2 Treatment of data from literature

D_0 values (the gradient of the final slope of the survival curve at high doses measured in decays/cell) for inactivation of mammalian cells (Chinese hamster (V-79), human diploid (TK6), and leukaemic cells L1210 and L5178Y from mice), E. Coli strains (Bs-1, B/r, k-12 AB2463, k-12 AB1157 and 15THU) and bacteriophages (T-1 and T-4) by the internal emitters ^{125}I , ^3H , ^{32}P , ^{33}P incorporated directly into the DNA of the cell nucleus, were extracted from the exponential portion of survival curves, lethal efficiencies of decay, α , or directly from the published values in the literature and expressed in terms of number of decays per cell as indicated in tables 2.1, 2.2, 2.4, 2.5 and 2.6.

In addition to this information, Kassis, Adelstein, Haydock, Sastry, McElvany and Welch (1982) have published results for ^{77}Br in which V-79 cells were subjected to chronic irradiation (18 hours) at a dose rate of 4.8×10^{-3} Bq (0.13 pCi) per cell, the corresponding D_0 was 311.7 disintegrations per cell. Results are also available for ^{131}I -labelled leukaemic cells, L1210, irradiated for 9 hours, (Hofer and Hughes 1971). For these, D_0 was found to be equal to 342 decays per cell (Table 2.3).

Cells were irradiated either *in vivo* or *in vitro* and grown in plastic petri dishes in normal culture media. No modifying drugs as protectors or sensitizers were added. Experiments were performed at different temperatures ranging from 37°C to -196°C . There was no dose-rate effect (Burki and Okada 1970, Burki, Roots, Feinendegen and Bond 1973) and no significant difference in cell killing efficiency was observed between unifilar and bifilar modes (Bedford, Mitchell, Griggs and Bender 1975, Panter 1981).

Bacteria strains were grown on H medium which contains a mixture of amino acids and for bacteriophages, wild type T-1 and T-4 were used and generally grown and assayed on E. Coli k-12 AB1157 or E. Coli 15THU. No sensitizers or protectors were added. Storage of labelled bacteria or phages during the irradiation time involved 1:100 dilution of radioactive growth medium to minimise the external action of long range radiation on nuclear DNA. Irradiation was carried out either in $+4^\circ\text{C}$ electric refrigerator or in a liquid nitrogen refrigerator (-196°C). For viable assays, the frozen samples were thawed rapidly in a water bath of 37°C . Assay of both bacteria and phages was carried out on nutrient agar petri-dishes using standard techniques for dilution and plating (Krisch 1970 and 1972).

2.2.1 Calculation of Average Energy of primary electrons from β and electron capture decays

The average kinetic energy, $E_{av.}$, of the β rays from radioisotopes under consideration has been calculated from the relation

$$E_{av.} = \frac{\int_0^{E_{max}} E N(E) dE}{\int_0^{E_{max}} N(E) dE} \quad 2.1$$

where E_{max} is the maximum β particle energy for which there is emission in the composite spectrum (E_{max} values for the β particles of the radioisotopes were taken from Lederer and Shirley 1978) and $N(E)$ is the number of particles of energy E in the composite spectrum which is given by

$$N(E) = \sum_{i=1}^k P_i N_i(E) \quad 2.2$$

where k is the number of β spectra emitted by the isotope under consideration, P_i is the frequency of emission for the spectrum i and $N_i(E)$ is the number of particles of energy E in the spectrum i which can be calculated as follows

$$N_i(E) = f(Z,E) S_c S_n (E_i - E)^2 (E + 1) (E^2 + 2E)^{1/2} \quad 2.3$$

Where $f(Z,E)$ is the Fermi function which is a factor giving the effect of the atomic field in general on the spectrum (Fano 1952), S_c is the screening effect correction factor due to the Coulomb field from atomic electrons (Reitz 1950), S_n is the shape factor (Wapstra, Nijgh and von Lieshout 1959) and E_i is the maximum β particle energy of the spectrum i . E_i and E are in units of m_0c^2

The numbers and energies of primary electrons ejected in the decay of ^{125}I and ^{77}Br by electron capture were obtained from known spectral data, table 2.7 a and b (Charlton *et al* 1978, Charlton and Booz 1981, Kassis *et al* 1982).

2.2.2 Track average LET and mean linear primary ionisation generated by primary electrons

Physical quantities necessary for interpretation of the biological results are the track average LET and the linear primary ionisation representative of the secondary charged particle equilibrium spectrum generated in the cell nuclei by the primary electrons. To determine the latter, first the numbers and energies of primary electrons ejected in the decay were obtained either from known spectral data or calculated as in section 2.2.1. Then the secondary charged particle equilibrium spectrum in liquid water was calculated for each primary electron energy band of the emitted spectrum (Watt, Al-Affan, Chen and Thomas, 1985). The track average LET and the mean linear ionisation per unit track for the equilibrium spectrum generated by each primary electron band were weighted appropriately for their frequency in the original spectrum to yield single average values for each radionuclide.

Ranges, weighted for the slowing down distribution of electrons, were deduced from Iskef 1981, Iskef, Cunningham and Watt 1983, and Al-Ahmad and Watt 1984. The basic physical data used in the calculations are given in Tables 2.7 and 2.8.

No. of electrons in group (Charlton and, Booz 1981)	Average energy of electron (keV)	(\bar{L}_T) (keV/ μm)	(\bar{I}_i) (μm^{-1})
28	2.382	11.7	214
30	1.310	15.3	300
23	0.526	20.0	426
14	0.608	19.5	407
12	0.368	21.3	462
6	0.123	23.2	443

Table 2.7(a): Track average LETs (\bar{L}_T) and average linear primary ionisation (\bar{I}_i) for equilibrium electron spectrum generated by Auger electrons from decaying of ^{125}I

Yield of electrons per 100 decays (Kassis <i>et al</i> ,1982)	Average energy of electron (keV)	(\bar{L}_T) (keV/ μm)	(\bar{I}_i) (μm^{-1})
35.3	10.08	5.1	81
113.0	1.251	15.7	309
2.8	0.146	23.1	475
173.0	0.081	23.2	319
174.0	0.042*	-	-
34.0	0.019*	-	-

* Electrons of energy less than 50eV are neglected

Table 2.7(b): Track average LETs (\bar{L}_T) and average linear primary ionisation (\bar{I}_i) for equilibrium electron spectrum generated by Auger electrons from decaying of ^{77}Br

Isotope (decay mode)	Av. energy of primary electron (keV)	Range (μm)	\bar{L}_T (keV/ μm)	\bar{I}_i (μm^{-1})
^{125}I (electron capture)	1.17	0.03	17.0	342
^{77}Br (electron capture)	1.58	0.05	18.7	291
^3H (β emitter)	5.97	0.42	8.4	149
^{131}I (β emitter)	179.5	176.1	0.7	10
^{33}P (β emitter)	78.92	118.63	2.04	31.44
^{32}P (β emitter)	695.6	2845.8	0.47	6.5

Table 2.8: Average energy of primary electrons and the projected ranges for the decay of ^{125}I , ^{77}Br , ^3H , ^{131}I , ^{33}P and ^{32}P . The track average LET (\bar{L}_T) and the average linear primary ionisation (\bar{I}_i) are for the electron equilibrium spectra.

2.3 Radiation damage and Repair

The damage caused by ionising radiation can be classified into three types; lethal damage, LD, which is irreparable, irreversible, leading to cell death, and measured by loss of reproductive integrity; sublethal damage, SLD, which under certain circumstances can be repaired within a matter of hours unless additional SLD is added (e.g. from a second radiation dose which can cause interaction with the first SLD to form lethal damage); and potentially lethal damage, PLD, that component of radiation damage which is predominantly damage influenced by post-irradiation environmental conditions and which, if left unrepaired, leads to cell death (Hall 1978).

No one is really sure of the nature of any of these forms of damage, whether or not they involve the same structures within the cell, and how they are related. In radiotherapy it is important to understand these types of damage and their repair mechanisms.

2.3.1 Radiation action and lethal damage

Macromolecules of biological interest such as enzymes and DNA, have unique biological activities. The loss of such biological functions as a result of the irradiation of these molecules is of major importance for some radio-biological effects.

Information on the interaction of radiation with molecules helps us to understand molecular mechanisms of radiobiological phenomena. Radiation is found to interact either directly or indirectly. Direct action is the interaction of radiation with molecules resulting in damage to molecules. The concept of direct action came about as a result of the development of target theory. The indirect action is the reaction between

the solute molecules (targets) and the radical species which are the activated solvent molecules formed as a result of the direct action of radiation with the solvent molecules (i.e. water). The concept of indirect action resulted from studies of radiation-induced chemical reactions in aqueous solutions.

The relative comparison between these two types of radiation action depends on the state of the biological molecule (whether it is in solid or in liquid state) and the radiation's quality parameters (Linear energy transfer, LET, mean free path for primary ionisation, inactivating cross-section etc.).

From these it was found that the mean free path for primary ionisation along the tracks of radiation particles within the cell nucleus is identified as the most important physical parameter determining the biological action of radiation. This is common to the induction of mutation, chromosome aberrations and inactivation (Watt 1989 a & b).

In mammalian cells, the DNA double strand breaks, dsb, were considered to be the main type of molecular lesions induced by ionising radiations which lead to cell death, but Bloecher and Pohlit (1982) showed that this was limited to cases of extremely high dose in which repair might be restricted. For the low doses used for cell survival studies ($D \leq 8$ grays), all dsb might be repaired in which case other types of DNA damage could not be excluded, e.g misrepair or mutations arising possibly from the repair of dsb themselves, might be responsible for cell killing. There is evidence to suggest that for a cell of dsb repair deficient yeast (rad 52) one unrepaired dsb is lethal (Frankenberg, Frankenberg-Schwager, Blocher and Harbich 1981).

Double strand breaks of DNA are presumed to be induced by three mechanisms : (i) pure direct primary interactions with two

neighbouring strands (ii) pure indirect effects on both strands due to diffusing of radical species from a track in close proximity to the sensitive targets (iii) combined action (mixed) caused by direct action on one strand and indirect action on the other strand. Direct radiation action is interpreted as being governed by the statistical probability that two interactions occur two nanometers apart. These interactions may be caused by either a single charged particle track which matches with similarly spaced sensitive sites on the DNA double-stranded segments, or by two charged particles acting separately, each on one strand. (These types of actions are called intratrack and intertrack action respectively).

Quantification of damage by direct action depends on the number of direct interactions, via the interaction cross-section, and not on the amount of energy transferred which is relatively unimportant. It follows that absorbed dose and energy related parameters such as LET, RBE etc. cannot be generally satisfactory quantitative parameters (Cannell and Watt 1985, Watt *et al* 1985). The observed differences in quality between photons (electrons) and heavy charged particles can be determined by the number of DNA segments at risk per track penetration of the cell nucleus (≤ 1 for photons (electrons) and ~ 10 for heavy charged particles) and by the efficiency with which the radiation produces double strand breaks.

2.3.2 Repair Mechanisms

Mammalian cells can repair radiation-induced damage and their response to radiation and recovery from damage depend strongly on many physicochemical repair processes associated with the sensitization by oxygen and electron affinity chemicals and protection by SH compounds occurring in characteristic times of the order of milliseconds, minutes and hours. Repair mechanisms may also

depend on other factors which might be affected directly or indirectly, such as the environmental treatment during and after irradiation.

Shoulders which are observed in some survival curves might indicate; the need for damage to be accumulated to effect lethality; waste of energy outside the sensitive targets; lack of matching of interactions to produce double strand breaks; over saturation of energy on the same sensitive sites and/or dose saturation of the capabilities of the repair system.

In the case of the capabilities of the repair system for instance, the shoulder region of a survival curve is indicative of SLD accumulation resulting from the repair during and after irradiation. SLD repair is important for radiotherapy since, if the radiation dose is split into two or more doses then the net survival is increased when the interval between these doses is increased until it reaches the peak at about 6 hours (Utsumi and Elkind 1979).

PLD repair leads to an increase in survival when appropriate post-irradiation conditions, such as those suboptimal for growth, are imposed after a single dose. The increase in survival due to the repair of PLD apparently results because the rate of fixation of damage is inhibited, thus permitting more repair to be effected, but if post-irradiation conditions amplify the damage or differentially inhibit the rate of its repair, more damage may be expressed leading to a decrease in survival. PLD repair is difficult to demonstrate in some cell lines of actively growing cells when an increase in survival is used as an indication of repair (Hall 1978).

The extent of cellular repair depend: on the type of irradiated cell and the physical parameters of the radiation. For Chinese hamster V-79 cell line it was found by Koch and Burki (1975) that the D_0 value at 37

$^{\circ}\text{C}$ is 970 decays/cell while, when the same cells are irradiated at -196°C , the D_0 value is 262 decays/cell. For Chinese hamster Don cells, which were tested by Panter (1981), the D_0 for cells irradiated at 37°C is appreciably more than the D_0 value for the same cells irradiated at -196°C . Survival of Chinese hamster Don cells irradiated by X-rays at 37°C and -196°C was also studied (Ibid) and D_0 values of 1.55 Gy and 6.73 Gy were obtained respectively.

From these results we can see that the effectiveness of X-rays for cell killing was reduced by a factor of about 4 when the temperature was reduced from 37°C to -196°C . Here we can distinguish the importance of indirect radiation action by X-rays. Miyazaki and Fujiwara (1981) found that when Chinese hamster V-79 cells as IdU/dT and dT/dT were irradiated by external X-rays at room temperature and at -79°C , the rate of mutation induction frequency per gray was 6 times greater in IdU/dT cells than in the dT/dT cells at room temperature and only 1.7 times at -79°C .

This may explain the importance of the indirect action which is more effective at room temperature than at -196°C , since in freezing temperature the mobility of free radicals which are produced by ionising radiations will be reduced and the probability that radical species recompense is increased. Also it is explained that IdU/dT cells irradiated by X-rays will liberate more electrons (Auger cascades) than in dT/dT cells and so the first will generate more free radicals in the medium. We know that in the repair mechanism there might be one or more enzymic processes involved.

It has been reported by Blocher and Pohlit (1982) that for Ehrlich ascites tumour cells, EATC, irradiated by X-rays, it seems likely that the enzyme system for repair is not damaged at doses ≤ 2000 Gy, and that in yeast dsb repair was found to be unaffected at doses ≤ 3000 Gy. The

number of dsb was found also to be a function of absorbed dose for EATC up to 2000 Gy and the induction was linear with dose and equalled 41 dsb per cell per gray. The repair mechanism was found to vary with the state of both the cell and the repair conditions, and the repair rate decreased with age in the stationary phase.

The number of dsb was found also to reach a minimum at about 24 hours of incubation after irradiation; the number of ssb reached its minimum at 0.5 hours (Bryant and Blocher 1980, Blocher and Pohlit 1982). The fraction of residual dsb increased with dose, and the behaviour of the induction curve for doses $30 \leq D \leq 500$ was quadratic and for doses >500 was linear.

Irradiation of cells under freezing temperatures may also affect the repair mechanisms which take place during the irradiation period, especially in the case of irradiation by internal emitters, nuclides, for which the time of irradiation may be hours (9 - 18 hours). It was also found that incubation directly after irradiation, ie delayed plating of cells in the same medium in which the cells were irradiated, gives better survival as compared with survival for cells under the same conditions but plated directly after irradiation. The difference between the two shouldered survival curves has been attributed to the repair of PLD occurring after irradiation (Frankenberg-Schwager *et al* 1988).

From this we might say that if cells are incubated directly after irradiation some of the damaged ends or molecules change their positions by disruption through handling or differences in temperature and tonicity of media which may cause shrinkage or expansion of sensitive sites. For all the above reasons repair mechanisms might be ineffective either by mis-repair of DNA or loss of some of the repair system's capacity.

Incubation of cells before irradiation is also found to affect the survival. When asynchronous Chinese hamster V-79 cells are irradiated by X-rays 17 - 20 hours after plating, the survival curve differs from the survival curve seen for cells irradiated at a short time after plating, and the ratio of $D_{17-20\text{ h}}/D_{\text{short time}}$ is 1.9. This difference is probably related to the partial synchronization induced by trypsinization which leads to a progressive increase in S-phase cells which develop with increasing time after plating (Lehnert 1975).

Changes of radiosensitivity and repair of damage accompanying growth and cell division are also important in physicochemical processes which are taking place during and after irradiation. Radiation was found to make changes in the cell cycle distribution after irradiation, e.g. changes in the histogram shape, the number of G_2 cells (increasing and reaching the maximum after 10.5 hours), the frequencies of G_1 and G_2 (returning to normal about 18 hours after irradiation), and the mitotic index (dropping to zero about 3-4 hours after irradiation and returning to normal after 9 hours, followed by an overshoot between 10-14 hours) (Roti Roti, Kristy and Higashikubo 1986). Another study showed that after cells were irradiated by tritium thymidine incorporated in the DNA, it was found that there was an increase of G_2 cells since there is a block which inhibits the cells from entering the mitotic-phase and the protein content of these cells is increased.

Survival of cells after irradiation can be influenced by exposure to anisotonic shock before or after X-rays (Raaphorst and Dewey 1979). Hypertonic solution treatment during and after irradiation was found to enhance the survival by increasing the potentially lethal damage repair, while hypotonic treatment was found to fix the damage if both treatments were at the same temperature (20 °C). Thus hypertonic and

hypotonic solutions affect the cellular sensitivity very differently and this effect might be related to the changes in the shape, the volume and the state of the sensitive cellular targets in which the radiations and radical species become more or less effective and the repair mechanisms become more active or inhibited.

From the above it can be concluded that the action of radiation on the sensitive targets and repair mechanism precursors depend on many physical, chemical and biological factors in which there is strong interrelation either to fix the radiation action or recovery from it by increasing the probability of repair mechanisms.

2.4 Calculation of Inactivation Cross-sections

To facilitate comparison of damage from incorporated radionuclides with other similar analyses for external radiations (Cannell and Watt 1985, Chen and Watt 1986, Watt, Chen, Kadiri and Younis 1987, and Watt 1988 (a)) it is convenient to convert the observed 37% survival fractions to effect cross-sections given by

$$\sigma = \frac{1}{R \cdot C_0} \quad 2.4$$

where R is the range of the frequency-weighted average energy of electron representative of the decay spectrum and C_0 is the concentration of source electrons emitted by the incorporated radionuclide. If D_0 is the gradient of the final slope of the survival curve at high doses measured in decays per cell, N_e is the average yield of electrons per decay and V is the volume of the cell nucleus then

$$C_0 = \frac{D_0 N_e}{V} \quad 2.5$$

From slowing down theory (eg McGinnies 1959), the range, R , represents the secondary charged particle fluence, Φ_s , generated per unit source strength (C_0) and equation (2.4) is seen to be equivalent to the well-known relation

$$\sigma (\text{cm}^2) = \frac{1}{\Phi_s (\text{cm}^{-2})} \quad 2.6$$

which, from equations (2.4) and (2.5), can be written as

$$\sigma (\text{cm}^2) = \frac{V(\text{cm}^2 \cdot \mu\text{m})}{R (\mu\text{m}) \cdot D_0 \cdot N_e} \quad 2.7$$

To obtain the total secondary charged particle fluence, the continuous slowing down approximation (csda), range R in equation 2.7 should be used. However in the present application, for reasons to be discussed later, it is only that portion of the secondary fluence generated at the end of the primary tracks that contributes significantly to the damage and so R was taken as the range of the mean energy of the slowing down spectrum to yield an estimate of the fluence in the critical region.

Concentration of source electrons, C , and fluence of electrons, Φ_0 , (corresponding to D_0 decay/cell) or Φ_{37} (corresponding to D_{37} decay/cell) using equations 2.5 and 2.6 and the inactivation cross-sections, σ_{eff} , using equation 2.7 were calculated for the reported survival data listed in tables 2.1 to 2.6 and using the physical, information given in tables 2.7 and 2.8. Information of these calculations is arranged in tables 2.9 - 2.22. The volume of a typical mammalian cell nucleus was taken as $270 \mu\text{m}^3$ (on the basis of a spherical nucleus with mean nuclear diameter of $8 \mu\text{m}$, Kassis et al 1980, Bedford et al 1975). *E. Coli* were treated as a sphere of radius $0.65 \mu\text{m}$ with a nucleus of radius $0.222 \mu\text{m}$ which contains 5.8×10^{-15} gm of DNA, then the volume of *E. Coli* cell nucleus is $4.58 \times 10^{-2} \mu\text{m}^3$ and the bacteriophage also was treated as a sphere of

radius $0.031 \mu\text{m}$ and a volume of $1.25 \times 10^{-4} \mu\text{m}^3$. The effect cross-sections so obtained were normalised by the geometrical cross-sectional area of the sensitive sites, σ_g , selected arbitrarily as $30 \mu\text{m}^2$ for mammalian cells, $0.155 \mu\text{m}^2$ for E. Coli and $3.02 \times 10^{-3} \mu\text{m}^2$ for bacteriophages, for comparison with the earlier results for external irradiations. These geometrical areas are approximately the saturation cross-sections which, in the theoretical model to be described, represent the product of the projected area of the sensitive targets (assumed to be the DNA) and the number of sites (presumably segments of the DNA) at risk per particle track traversal of the nucleus (~ 10 for heavy particles and near 1 for electrons in an equilibrium spectrum). For the present purpose the geometrical area of $30 \mu\text{m}^2$ for mammalian cells, $0.155 \mu\text{m}^2$ for E. Coli and $3.02 \times 10^{-3} \mu\text{m}^2$ for bacteriophages are used simply as a scaling factor to make the intrinsic efficiencies of action, σ_R , approximately unity at saturation.

Cell line	Dose, D_0 (D_{37}) * decay/cell	Concentration of source electrons C_0 (C_{37}) (μm^{-3})	Fluence electron Φ_0 (Φ_{37}) (elec./ μm^2)
CH. H. V79	39	3.06	0.10
	35	2.75	0.09
	40	3.14	0.10
Leukaemic cells L5178Y	46	3.61	0.12
Leukaemic cells L1210	45	3.54	0.01
Human diploid TK6	28	2.20	0.07

* Data from table 2.1

Table 2.9: Concentration of source electrons (C) and fluence of electrons Φ_0 (corresponding to D_0 decay/cell) or Φ_{37} (corresponding to D_{37} decay/cell) for the radionuclide ^{125}I incorporated into nuclear DNA

Cell line	Dose, D_0 (D_{37}) * decay/cell	Concentration of source electrons C_0 (C_{37}) (μm^{-3})	Fluence electron Φ_0 (Φ_{37}) (elec./ μm^2)
CH. H. V79	970	3.59	1.49
	262	0.97	0.40
Leukaemic cells L5178Y	175	0.65	0.27
	167	0.62	0.26
	222	0.82	0.34
	226	0.84	0.35
Leukaemic cells L1210	360	1.33	0.56
Human diploid TK6	385	1.43	0.59

* Data from table 2.2

Table 2.10: Concentration of source electrons (C) and fluence of electrons Φ_0 (corresponding to D_0 decay/cell) or Φ_{37} (corresponding to D_{37} decay/cell) for the radionuclide ^3H incorporated into nuclear DNA

(a) ^{77}Br

Cell line	Dose, D_0 (D_{37}) * decay/cell	Concentration of source electrons C_0 (C_{37}) (μm^{-3})	Fluence electron Φ_0 (Φ_{37}) (elec./ μm^2)
CH. H. V79	311.7	3.74	0.19

(b) ^{131}I

Cell line	Dose, D_0 (D_{37}) * decay/cell	Concentration of source electrons C_0 (C_{37}) (μm^{-3})	Fluence electron Φ_0 (Φ_{37}) (elec./ μm^2)
Leukaemic cells L1210	342	1.27	2.23×10^2

* Data from table 2.3

Table 2.11: Concentration of source electrons (C) and fluence of electrons Φ_0 (corresponding to D_0 decay/cell) or Φ_{37} (corresponding to D_{37} decay/cell) for the radionuclides (a) ^{77}Br (b) ^{131}I incorporated into nuclear DNA

Bacterial strain or phage	Dose, D_0 (D_{37}) * decay/cell	Concentration of source electrons C_0 (C_{37}) (μm^{-3})	Fluence electron Φ_0 (Φ_{37}) (elec./ μm^2)
E. Coli Bs-1	2.28	1.05×10^3	33.74
E. Coli B/r	4.61	2.11×10^3	67.66
E. Coli K12 AB2463	2.19	1.00×10^3	32.06
E. Coli 15 THU	6.79	3.11×10^3	99.60
Phage T-1	2.19	3.68×10^6	1.18×10^5

* Data from table 2.6

Table 2.12: Concentration of source electrons (C) and fluence of electrons Φ_0 (corresponding to D_0 decay/cell) or Φ_{37} (corresponding to D_{37} decay/cell) for the radionuclide ^{125}I incorporated into DNA of E. Coli and bacteriophage.

Bacterial strain or phage	Dose, D_0 (D_{37}) *	Concentration of source electrons C_0 (C_{37}) (μm^{-3})	Fluence electron Φ_0 (Φ_{37}) (elec./ μm^2)
T-1	12.66	1.01×10^5	4.22×10^4
	8.33	6.66×10^4	2.77×10^4
	6.67	5.34×10^4	2.22×10^4
	7.14	5.71×10^4	2.38×10^4
T-4	18.18	1.46×10^5	6.06×10^4
	21.74	1.74×10^5	7.25×10^4
	23.25	1.86×10^5	7.75×10^4
	16.39	1.31×10^5	5.46×10^4

* Data from table 2.4 c

Table 2.13: Concentration of source electrons (C) and fluence of electrons Φ_0 (corresponding to D_0 decay/cell) or Φ_{37} (corresponding to D_{37} decay/cell) for the radionuclide ^3H incorporated into DNA

Bacterial strain or phage	Dose, D_0 (D_{37}) * decay/cell	Concentration of source electrons C_0 (C_{37}) (μm^{-3})	Fluence electron Φ_0 (Φ_{37}) (elec./ μm^2)
E. Coli Bs-1	24.39	5.33×10^2	6.32×10^4
E. Coli AB 2463	19.57	4.27×10^2	5.07×10^4
E. Coli AB 1157	64.39	1.41×10^3	1.67×10^5
E. Coli 15 THU	45.32	9.89×10^2	1.17×10^5
phage T-1	30.84	2.97×10^5	2.93×10^7
	8.21	6.57×10^4	7.79×10^6
phage T-4	24.53	1.96×10^5	2.33×10^7
	10.21	8.17×10^4	9.69×10^6

* Data from tables 2.4 b and 2.5 b

Table 2.14 : Concentration of source electrons (C) and fluence of electrons Φ_0 (corresponding to D_0 decay/cell) or Φ_{37} (corresponding to D_{37} decay/cell) and the effect cross-section for the radionuclide ^{33}P incorporated into nuclear DNA

Bacterial strain or phage	Dose, D_0 (D_{37}) *	Concentration of source electrons C_0 (C_{37}) (μm^{-3})	Fluence electron Φ_0 (Φ_{37}) (elec./ μm^2)
E. Coli Bs-1	22.32	4.87×10^2	1.39×10^6
E. Coli AB 2463	20.01	4.37×10^2	1.24×10^6
E. Coli AB 1157	104.17	2.28×10^3	6.49×10^6
E. Coli 15 THU	40.01	8.74×10^2	2.49×10^6
phage T-1	16.78	1.34×10^5	3.82×10^8
	7.11	5.69×10^4	1.62×10^8
phage T-4	10.72	8.59×10^4	2.44×10^8
	6.99	5.59×10^4	1.59×10^8

* Data from tables 2.4 a and 2.5 a

Table 2.15 : Concentration of source electrons (C) and fluence of electrons Φ_0 (corresponding to D_0 decay/cell) or Φ_{37} (corresponding to D_{37} decay/cell) for the radionuclide ^{32}P incorporated into nuclear DNA

Cell line	Temperature (°C)	D ₀ (decay/cell)	Effect cross section, σ_{eff} (μm^2)	Intrinsic efficiency σ_{R}
CH. H. V79	-196	39	10.30	0.34
	+4	35	11.48	0.38
	-49	40	10.04	0.34
Leukaemic cell L5178Y	-196	46	8.73	0.29
Leukaemic cell L1210	37	45	8.93	0.30
Human diplo. TK6	37	28	14.35	0.48
	-70	28		

Table 2.16: Effect cross-sections and intrinsic efficiencies of ¹²⁵I radionuclide incorporated into DNA of mammalian cells

Cell line	Temperature (°C)	D ₀ (decay/cell)	Effect cross section, σ_{eff} (μm^2)	Intrinsic efficiency σ_{R}
CH. H. V79	-196	970	0.67	0.02
	+4	262	2.48	0.08
Leukaemic cells L5178Y	-196	175	3.71	0.12
		167	3.89	0.13
		222	2.92	0.10
		226	2.87	0.10
Leukaemic cells L1210	37	360	1.80	0.06
Human diplo. TK6	37	385	1.69	0.06
	-70	385		

Table 2.17 :Effect cross-sections and intrinsic efficiencies of ³H radionuclide incorporated into DNA of mammalian cells

^{77}Br (electron capture)				
Cell line	Temperature (°C)	D_0 (decay/cell)	Effect cross section, σ_{eff} (μm^2)	Intrinsic efficiency σ_R
CH. H V79	37	312	5.37	0.18
^{131}I (electron capture)				
Leukaemic cells L1210	37	342	4.48×10^{-3}	1.49×10^{-4}

Table 2.18: Effect cross-sections and intrinsic efficiencies of ^{77}Br and ^{131}I radio-nuclides incorporated into DNA of mammalian cells

Bacterial strain or phage	Temperature (°C)	D_0 (decay/cell)	Effect cross section, σ_{eff} (μm^2)	Intrinsic efficiency σ_R
E. Coli Bs-1	-196	2.30	2.99×10^{-2}	0.19
		2.23		
		2.25		
		2.36		
		2.25		
E. Coli B/r	-196	4.66	1.48×10^{-2}	0.10
		3.53		
		4.14		
		6.04		
		4.69		
E. Coli K-12 AB2463	-196	2.66	3.12×10^{-2}	0.20
		1.71		
E. Coli 15 THU	-196	6.72	1.00×10^{-2}	0.07
		6.87		
Bacterio- phage T-1	-196	2.52	0.85×10^{-4}	0.03
		1.87		

Table 2.19: Effect cross-sections and intrinsic efficiencies of ^{125}I radio-nuclide incorporated into DNA of bacterial strains and phages

Bacterial strain or phage	Temperature (°C)	D_0 (decay/cell)	Effect cross section, σ_{eff} (μm^2)	Intrinsic efficiency σ_R
E. Coli Bs-1	-196	24.39	1.58×10^{-5}	1.02×10^{-4}
E. Coli AB2463	-196	19.57	1.97×10^{-5}	1.27×10^{-4}
E. Coli AB1157	-196	64.39	0.60×10^{-5}	0.39×10^{-4}
E. Coli 15 THU	-196	45.32	0.85×10^{-5}	0.55×10^{-4}
Phage T-1	-196	30.84	3.42×10^{-8}	1.13×10^{-5}
	+4	8.21	12.83×10^{-8}	4.25×10^{-5}
Phage T-4	-196	24.53	4.30×10^{-8}	1.42×10^{-5}
	+4	10.21	10.32×10^{-8}	3.42×10^{-5}

Table 2.20: Effect cross-sections and intrinsic efficiencies of ^{33}P radio-nuclide incorporated into DNA of bacterial strains and phages

Bacterial strain or phage	Temperature (°C)	D ₀ (decay/cell)	Effect cross section, σ_{eff} (μm^2)	Intrinsic efficiency σ_R
E. Coli Bs-1	-196	22.32	0.72×10^{-6}	4.65×10^{-6}
E. Coli AB 2463	-196	20.01	0.80×10^{-6}	5.19×10^{-6}
E. Coli AB 1157	-196	104.17	0.15×10^{-6}	0.99×10^{-6}
E. Coli 15 THU	-196	40.01	0.40×10^{-6}	2.60×10^{-6}
Phage T-1	-196	16.78	0.26×10^{-8}	0.87×10^{-6}
	+4	7.11	0.62×10^{-8}	2.04×10^{-6}
Phage T-4	-196	10.72	0.41×10^{-8}	1.36×10^{-6}
	+4	6.99	0.63×10^{-8}	2.08×10^{-6}

Table 2.21: Effect cross-sections and intrinsic efficiencies of ³²P radio-nuclide incorporated into DNA of bacterial strains and phages

Bacterio-phage	Temperature (°C)	D ₀ (decay/cell)	Effect cross section, σ_{eff} (μm^2)	Intrinsic efficiency σ_R
T-1	+5	12.66	0.24×10^{-4}	0.79×10^{-2}
		8.33	0.36×10^{-4}	1.19×10^{-2}
		6.67	0.45×10^{-4}	1.49×10^{-2}
		7.14	0.42×10^{-4}	1.39×10^{-2}
T-4	+5	18.18	0.17×10^{-4}	0.55×10^{-2}
		21.74	0.14×10^{-4}	0.46×10^{-2}
		23.25	0.13×10^{-4}	0.43×10^{-2}
		16.39	0.18×10^{-4}	0.61×10^{-2}

Table 2.22: Effect cross-sections and intrinsic efficiencies of ³H radionuclide incorporated into DNA of bacteriophages

2.5 Description of the Damage Model

Despite the excessive damage observed for ^{125}I , ^{77}Br and ^3H when concentrated within the cell nucleus compared with that observed for a homogeneous distribution of electrons throughout the cellular material there seems to be no 'ad hoc' reason why there should be difference except in two possible ways: (i) If the radionuclide is incorporated into the DNA then it is presumably localised in the immediate vicinity of a sensitive site. In this case there is also the probability that the dissipation of the recoil energy (and/or coulomb charge) arising from the decay could produce irreparable lethal or sublethal damage; (ii) The emission of several cascade electrons simultaneously could lead to the instantaneous production of multiple lesions which would have smaller probability of total repair than a single lesion produce within a finite time period.

In an attempt to interpret the mechanism responsible for the experimental results a model has been adopted which attributes the dominant cause of biological damage to three processes viz. direct action by a single track on two sites spaced at 2nm on the same DNA segment to produce a lesion; the 'mixed action' of a direct effect on one site and indirect effect by diffusing chemical species on the other site and by indirect effect on both sites. Provision is made for the repair of lesions and for dynamical aspects of the cell cycle. All lesions must be repaired for the cell to survive. The survival fraction is related by Poisson statistics to the mean number of lesions (probably a type of double-strand break in the DNA) which remain unrepaired by the time in the cell cycle at which damage may be considered fixed. Thus in terms of specified physical and biological parameters the survival fraction, F , is given by (Watt, 1989(b))

$$\ln(F) = -K(t_j) \cdot \{ \sigma_g \cdot n_0 \cdot \mathcal{E} \cdot \Phi_s + [k_0 \cdot \bar{L}_T \cdot \dot{\phi}_s \cdot t_c (1 - e^{-t_j/t_c})$$

$$(\sigma_g \cdot n_o \cdot \mathcal{E} \cdot \Phi_s) + [k_o \cdot \bar{L}_T \cdot \dot{\phi}_s \cdot t_c (1 - e^{-t_i/t_c})]^2 \quad 2.8$$

where the terms in the curled brackets represent respectively the direct, mixed and indirect components of radiation action and the symbols are defined as follows.

σ_g = the geometrical cross-sectional area of the intra-nuclear DNA $\sim 3.0 \mu\text{m}^2$

n_o = the initial number of DNA segments at risk along a mean chord traversal of the cell nucleus

\mathcal{E} = the efficiency of production of double strand breaks (dsb's)

= $(1 - e^{-\lambda_o/\lambda})$ for $\lambda_o > \lambda$
and = 1 for $\lambda < \lambda_o$

λ = mean free path for primary ionisation of the secondary charged particles

$\lambda_o = 1.8 \text{ nm}$, the critical spacing of the DNA sites

t_r = the mean recovery time for dsb's

t_t = the time in the cell cycle at which damage may be considered fixed.

t_s = the time of the start of the irradiation of duration t_i

t_i = the duration time of irradiation

t_c = the mean life time of radicals capable of indirect action

$\dot{\phi}_s$ = the fluence rate of charged particles in the equilibrium spectrum

Φ_s = the total integral equilibrium fluence = $\dot{\phi}_s \cdot t_i$

k_o = the radical reaction parameter in units of $\text{cm}^2 \cdot \mu\text{m}/\text{keV}$

Note The value of σ_g , the projected area of the nuclear DNA in the mammalian cell, is taken to be $3.0 \mu\text{m}^2$. This can be calculated from the known mass of nuclear DNA (Approximately 6 pgm; Charlton,

Goodhead, Wilson and Paretzke, 1985), assuming that the DNA occupies a spherical volume.

$$K(t_i) = \frac{1}{t_i} \int_0^{t_i} \exp(- (t_i - t) / t_r) \cdot dt \quad 2.9$$

is a factor which modifies the growth of damage by the repair of lesions produced during the irradiation time, t_i . In the present application the irradiation time is the same within each data set analysed and so $K(t_i)$ is a constant factor which cannot be determined separately from the other constants in equation 2.8. A similar problem arises with the chemical reaction term and so equation 2.8 reduces to the special form

$$\begin{aligned} \ln(F) = - \{ a_1 \cdot \sigma_g \cdot n_0 \cdot \mathcal{E} \cdot \Phi_s + (a_2 \cdot \bar{L}_T \cdot \Phi_s \cdot a_1 \cdot \sigma_g \cdot n_0 \cdot \mathcal{E} \cdot \Phi_s) \\ + (a_2 \cdot \bar{L}_T \cdot \Phi_s)^2 \} \\ = - \{ a_1 \cdot \sigma_g \cdot n_0 \cdot \mathcal{E} \cdot \Phi_s + a_2 \cdot \bar{L}_T (a_1 \cdot \sigma_g \cdot n_0 \cdot \mathcal{E} + a_2 \cdot \bar{L}_T) \Phi_s^2 \} \quad 2.10 \end{aligned}$$

where a_1 and a_2 are constants. If there is no repair then a_1 is unity for cell inactivation and a_2 equals k_0 .

Equation 2.8 has yet to be established in final form as it has been tested for only a few data sets (Watt, 1988(b)) and some of the parameters are yet to be determined. Nevertheless a particular virtue of this form is that it enables survival curves to be interpreted in terms of the three proposed modes of action. As equation (2.8) contains only well defined physical and biological parameters there should be a unique solution for any specified biological end-point and cell type. However in practice the magnitudes of some of the parameters are not known and one must resort to carrying out a non-linear least squares fit (NAG routine E04 FCF) to observed data. In this way details can be extracted concerning the magnitudes of fixation times, recovery times, chemical reaction times, the number of lesions induced by the radiation and which can be

compared with values determined by alternative methods as a test of validity. However to determine meaningful magnitudes for the various parameters involved, accurate survival curves measured for different radiation types and for widely varying time intervals at different dose rates are required. The following results are obtained within the limitations of available data.

2.6 Results and Interpretation of Damage

2.6.1 Interpretation of damage for mammalian cells.

Figure 2.1 shows explicitly that the inactivation probabilities obtained for the nuclides ^{125}I , ^{77}Br and ^3H extend over a wide range of values, depending on temperature and cell type. The higher values approach those determined for heavy particles having the same mean free path for primary ionisation and that they are an order of magnitude larger than would be expected for external irradiation with photon-generated electrons. The result for ^{131}I is appreciably smaller than that expected for external irradiations. Interpretation of these findings is attempted below.

Observation of the apparently excessive damage for the low energy electron emitters when incorporated into the cell nucleus has been remarked upon by others (Commerford *et al* 1980 Kassis *et al* 1987a&b) and has stimulated investigation of the underlying mechanisms involved.

The results, shown in figure 2.1, confirm that the microscopic effect cross-sections for electrons in the respective slowing down charged particle spectra represent realistically the radiation quality of the incorporated radio-nuclides.

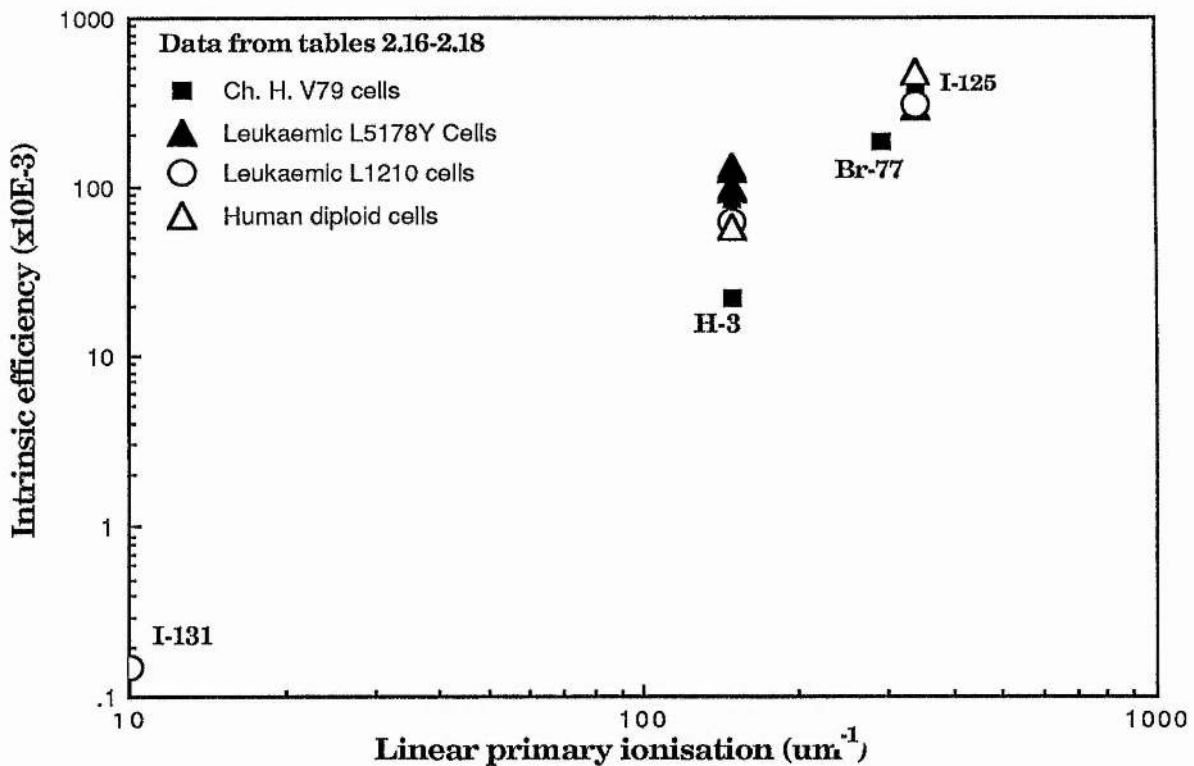


Figure 2.1: The intrinsic efficiencies of damage of different radionuclides incorporated to the nuclear DNA of mammalian cells against their linear primary ionisations

From study of the action of delta-rays and of electrons produced by external photon irradiation (figure 2.2), it was deduced that electrons cause damage with maximum efficiency when their tracks stop within the cell nucleus because then their mean free path for ionisation reaches an optimum of 2nm which matches the critical spacing required to produce a lesion (Chen and Watt 1986). As the DNA in the cell nucleus occupies only about one percent of the nuclear volume, it is to be expected that most of the energy expended by electron emitting radionuclides incorporated into the DNA will be expended beyond the DNA and the maximum damage will be caused when the end of the tracks interact with a DNA segment. Therefore no significant difference is to be expected in the damage caused by unifilar or bifilar labelled DNA compared with that from the same radionuclides dispersed at random in the nucleus except in the special case where the electron ranges are very short - less than a few tens of nanometers i.e.

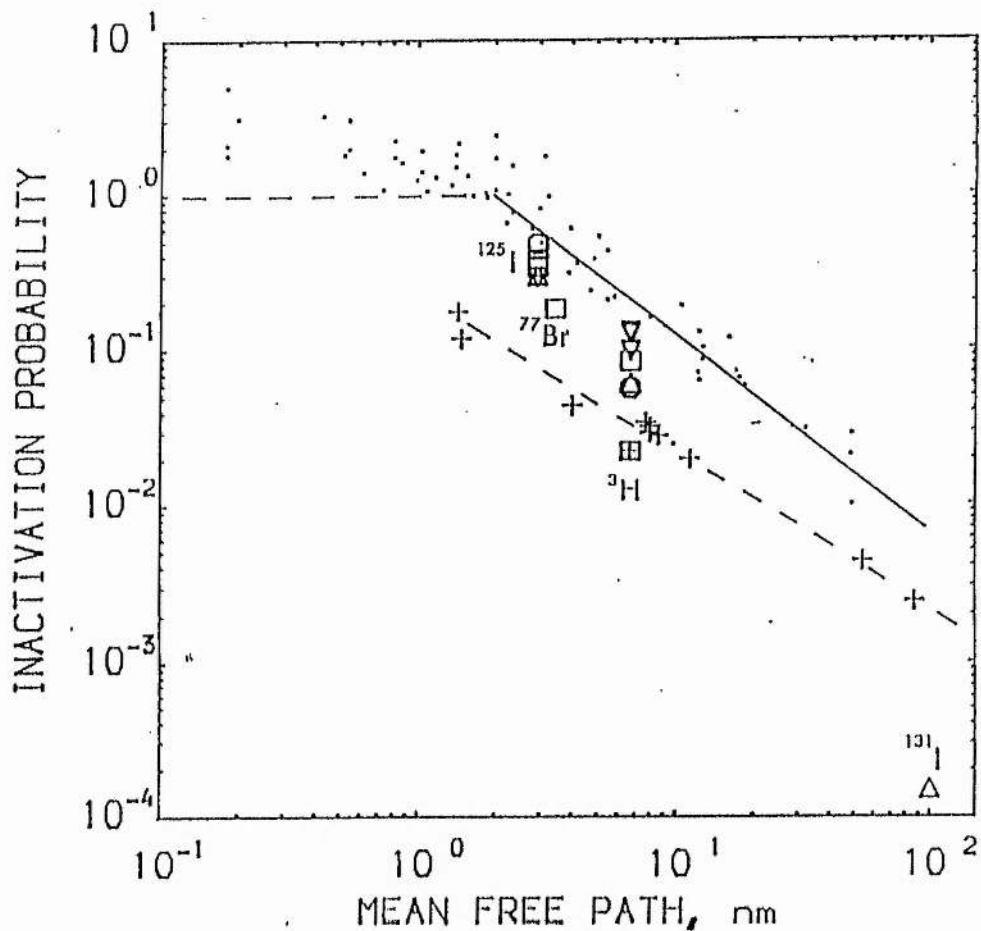


Figure 2.2: Probabilities for inactivation, as a function of the mean free path for primary ionisation for fast heavy particles (.) (Todd 1967, 1975, Barendsen *et al* 1977, Skarsgard *et al* 1967 and Cox *et al* 1977) and for X and γ rays (+) [references are given in Chen and Watt 1986] in external irradiations are compared with the results using equation 2.7 for incorporated ^{125}I , ^{77}Br , ^3H and ^{131}I . Other symbols: V-79 ; human diploid cells ©; leukaemic cells L1210 Δ and leukaemic cells L5178 ∇ . The dashed horizontal line indicates a probability of unity. Values in excess of unity are attributed to secondary particle action on secondary cellular targets.

for primary electron energies ≤ 700 eV. The results obtained here are consistent with the notion that damage occurs predominantly at the ends of the electron tracks.

For the nuclides ^{125}I and ^{77}Br the dose-response curves are linear. Only the first term in equation 2.10 applies which when fitted to the observed data as shown in figure 2.3 a and b yields values of $18.23\mu\text{m}^2$ and $13.21\mu\text{m}^2$ respectively for the cross-sectional area of the sensitive sites at risk (σn_0). If the action efficiency (\mathcal{E}) of the radiation is taken into account the net cross-sections are $8.56\mu\text{m}^2$ and $5.36\mu\text{m}^2$. As discussed earlier, it is not possible to determine directly if any repair factor is present because of the constant exposure time used in the experiments.

Difference in temperature of the cells during irradiation is not expected to cause a significant change in the effectiveness of the radiation from both ^{125}I and ^{77}Br because the induced damage is predominantly by direct single track action. For both of these nuclides the emitted radiations are absorbed completely within the nucleus and there are many short-ranged electrons less than a few hundred eV. Consequently the damage is highly localised in the vicinity of the disintegrating nuclide and one would expect a distinct increase in sensitivity if the nuclide is localised in the DNA compared with random dispersal elsewhere in the nucleus (Commerford *et al* 1980, Kassis *et al* 1987 b).

Tritium emits β rays with an end point energy of 18 keV and an average energy of about 6 keV. Most of the β spectrum will be stopped within the cell nucleus if the nuclide is incorporated. The damage mechanism for tritium was found to be quite different from that of ^{125}I and ^{77}Br as only the indirect component of action appears to be significant (figure 2.3c). No evidence was found for either direct or

mixed action although the analysis was limited by the large spread and paucity of the experimental points.

The survival fraction is given by

$$\ln(F) = - [0.998 L_T \bar{\phi}_s]^2 \quad 2.11$$

These results can be understood on the basis that the primary electrons emitted from tritium incorporated in the DNA have long ionisation mean free paths and are therefore very unlikely to induce a direct break in a neighbouring site on the same segment of origin. Having left that segment the β rays generate a slowing down fluence of secondary electrons which are most likely to be dispersed in the vast volumes of interstitial material around the remaining DNA. A large concentration of different chemical products will be built up some of which will react with the DNA to produce lesions. Direct effects will occur but simple geometrical considerations suggest that these will be small. As indirect action dominates, temperature effects should be considerable and may have been observed (figure 2.3c and table 2.2).

A small amount of mixed action could be accommodated but was an order of magnitude smaller than the indirect action. As the tritium β rays act mainly at a distance of a few tenths of microns no difference is expected in the survival curves observed for DNA incorporated, and for randomly distributed, nuclides in the cell nucleus.

^{131}I emits β rays with maximum energy of 0.81 MeV. The range of the average energy β -ray (180 keV) is about 380 μm and consequently the action of ^{131}I is expected to be typical of that for a full equilibrium spectrum of electrons generated throughout the medium. However the concentration of ^{131}I is too small to give full equilibrium and so the intrinsic efficiency of damage should be appreciably less than that for

external irradiations with photons and electron beams having the same effective mean free paths for ionisation. The minimum least squares fit of equation 2.10 to the ^{131}I survival data yielded

$$\ln(F) = 0.0589 \epsilon \Phi_s + 1.257 \times 10^{-3} \epsilon L_T^- \Phi_s \dot{\phi}_s + [4.559 \times 10^{-4} L_T^- \dot{\phi}_s]^2 \quad 2.12$$

which corresponds to an effect cross-section of $4.48 \times 10^{-3} \mu\text{m}^2$ at 37% survival. Because of the presence of both the dose rate dependent terms associated with the indirect action, the cross-section will be a function of time and rate. As shown in figures 2.1 and 2.2, the cross-section of ^{131}I lies below the group of cross-sections observed for external photon irradiations. The relative contributions of the direct, mixed and indirect actions are approximately equal within the survival and dose ranges studied. At survival levels greater than 95% direct single track action is 5 to 10 times more probable than mixed and indirect action.

2.6.2 Interpretation of damage for E Coli and Bacteriophage

From tables 2.19 -2.21 and figure 2.4 the inactivation effect cross-sections and the intrinsic efficiencies of radiation action for E. Coli cells irradiated by electron capture ^{125}I and β emitters ^{33}P and ^{32}P nuclides show a range of values depending on the incorporated nuclide to the nuclear DNA and on the type of E.Coli cell and its DNA distribution; shape; and volume. Although temperature dependence of irradiation and incubation environment is very important, as we have seen in section 2.6.1, especially for high energy β emitters, but it does not appear in these experiments since all experiments were done at -196°C .

The ranges of the inactivation probability (intrinsic efficiency) for ^{125}I , ^{33}P , and ^{32}P nuclides are 0.07 - 0.19, 0.39×10^{-4} - 1.27×10^{-4} and 0.87×10^{-6} - 5.19×10^{-6} respectively. These ranges of data can be compared with the results for radionuclides incorporated into nuclear DNA

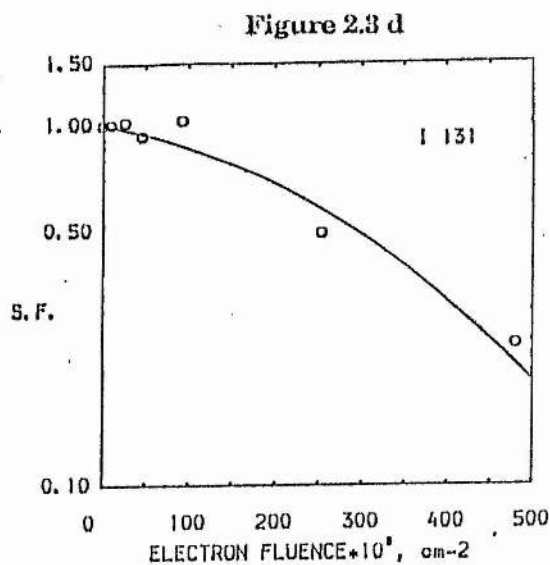
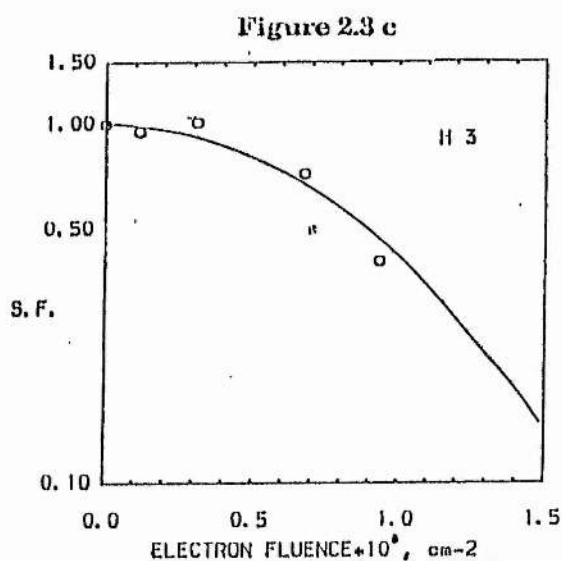
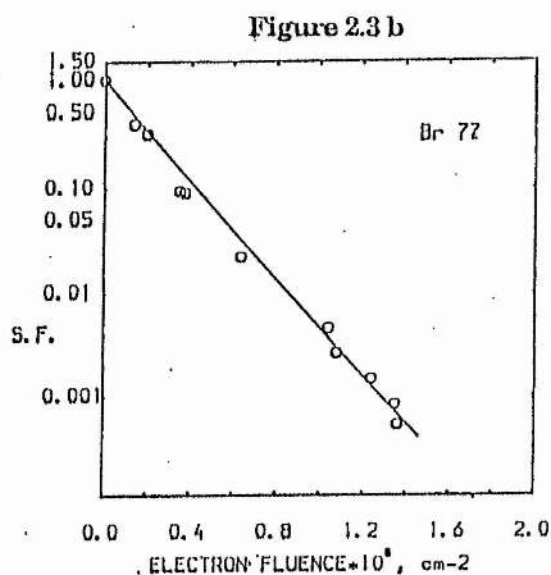
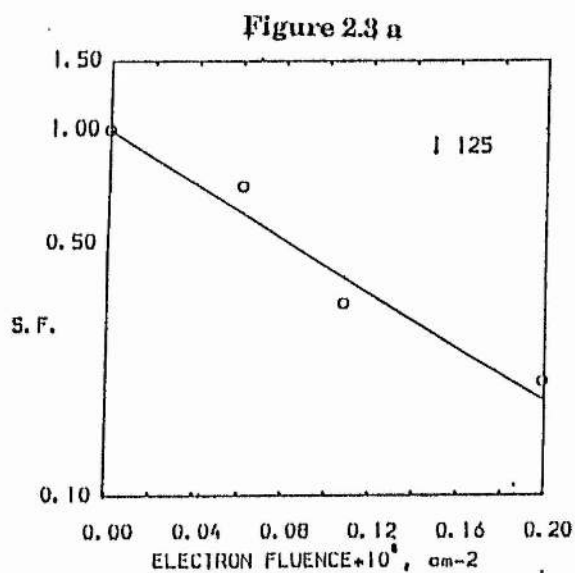


Figure 2.3: Survival fractions calculated from equation 2.10 (solid lines) are compared with the experimental data from Table 2.1 for ^{125}I (figure 2.3 a). Only direct action is identifiable and $\sigma_{\text{p}}n_0 = 18.23 \mu\text{m}^2$. Figure 2.3 (b) shows similar results for ^{77}Br (Table 2.3) with $\sigma_{\text{p}}n_0 = 13.21 \mu\text{m}^2$. For incorporated ^3H (figure 2.3 c and Table 2.2 data) there appears to be predominantly indirect action. ^{131}I (figure 2.3 d) has components of direct, mixed and indirect action and has all the characteristics of external β or photon irradiation due to the high β -ray energy.

(section 2.6.1) in which the probability of direct radiation action is increased by increasing the linear primary ionisation of these nuclides. On the other hand, the component of indirect radiation action becomes more dominant, figure 2.4. The ratios of the intrinsic efficiency for ^{125}I to that of each of ^{33}P and ^{32}P are 1.7×10^3 and 4.1×10^4 respectively since the long range electrons dissipate their energy out of the sensitive target.

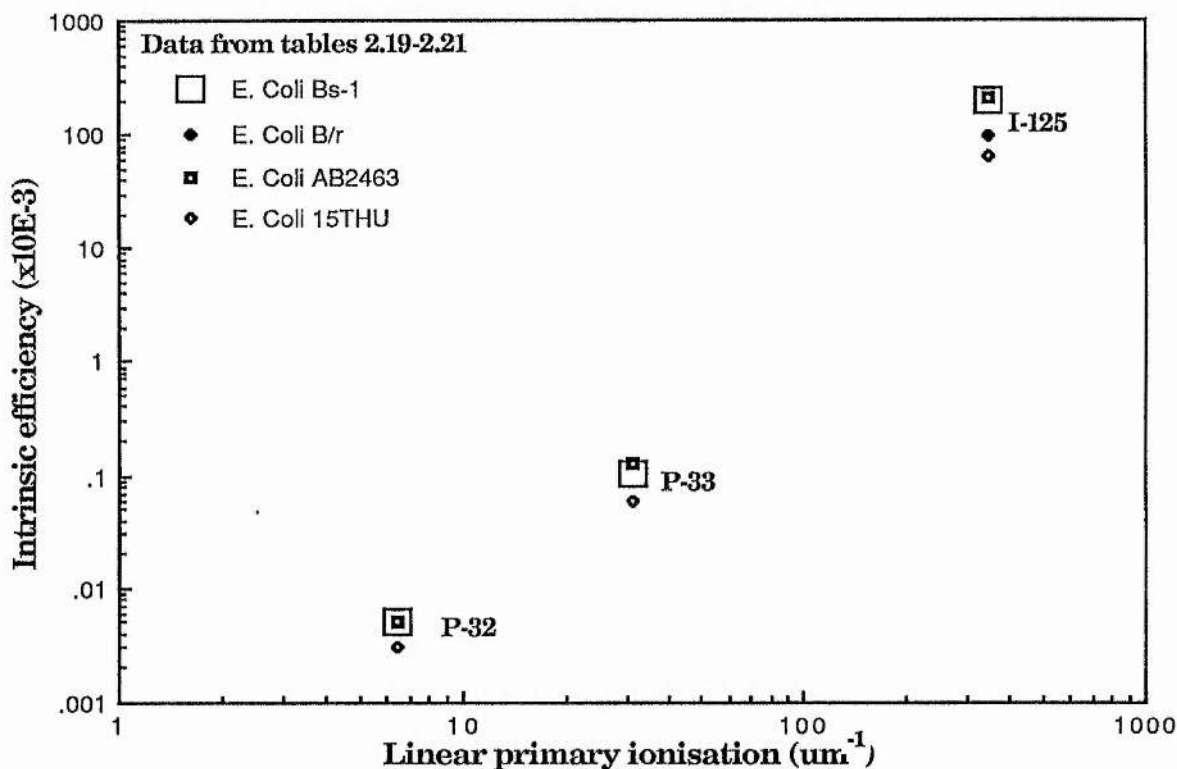


Figure 2.4: The intrinsic efficiencies of damage of different radionuclides incorporated to the nuclear DNA of E. Coli cells against their linear primary ionisations.

Results of T-1 and T-4 bacteriophages irradiated with ^{125}I , ^3H , ^{33}P and ^{32}P incorporated to their DNA show that there is a clear temperature dependence for phages irradiated with long range nuclides and this dependence increases as the range of these nuclides increases (tables 2.20 - 2.22 and figure 2.5). Also there is a difference in the radiation action with T-1 and T-4 phages for the nuclides ^3H , ^{33}P and ^{32}P where the ratios of intrinsic efficiency with T-1 to that with T-4 are 2.4,

1.24 and 0.98 respectively for phages irradiated at 4 - 5 °C. Ratios for ^{33}P and ^{32}P nuclides drop to 0.79 and 0.64 respectively when the same phages are irradiated at -196 °C. This means that inactivation of T-4 phage for long range β emitters is less dependent on the temperature difference than T-1 phage and inactivation of T-1 phage is more dependent on indirect radiation action which becomes very small at freezing temperature where radicals are indiffusable

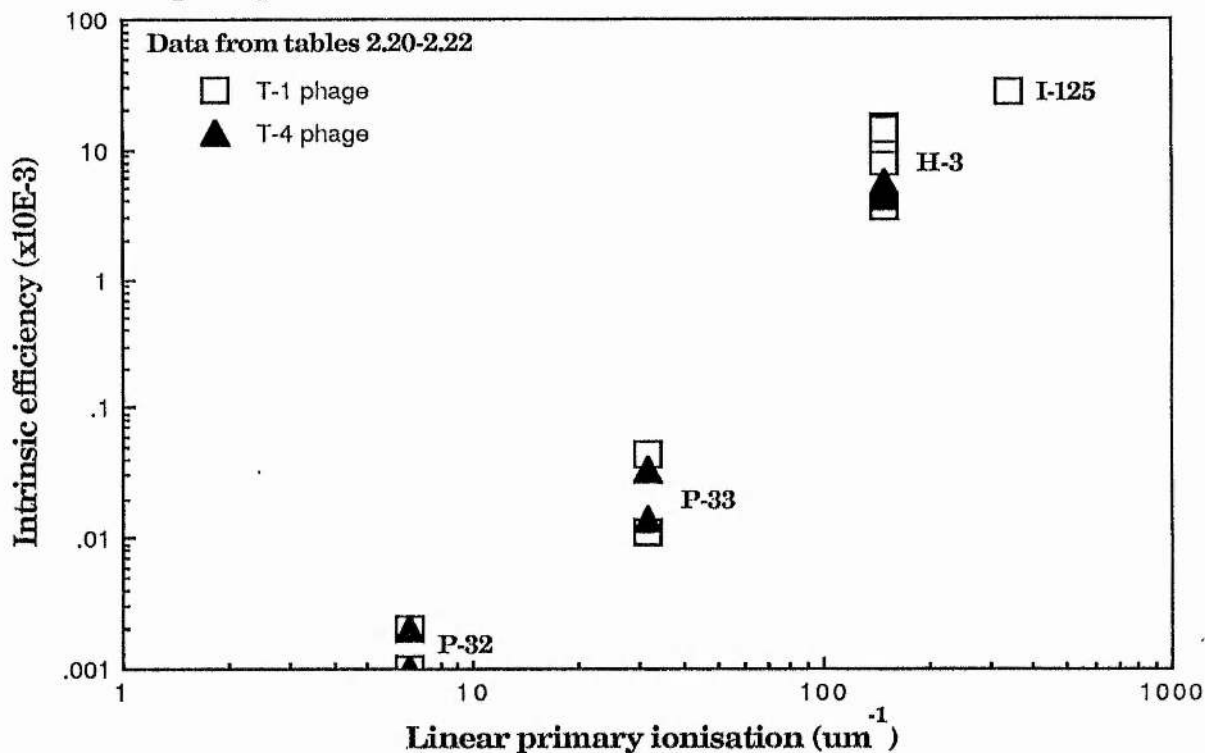


Figure 2.5: The intrinsic efficiencies of damage of different radionuclides incorporated to the DNA of T-1 and T-4 bacteriophages against their linear primary ionisations

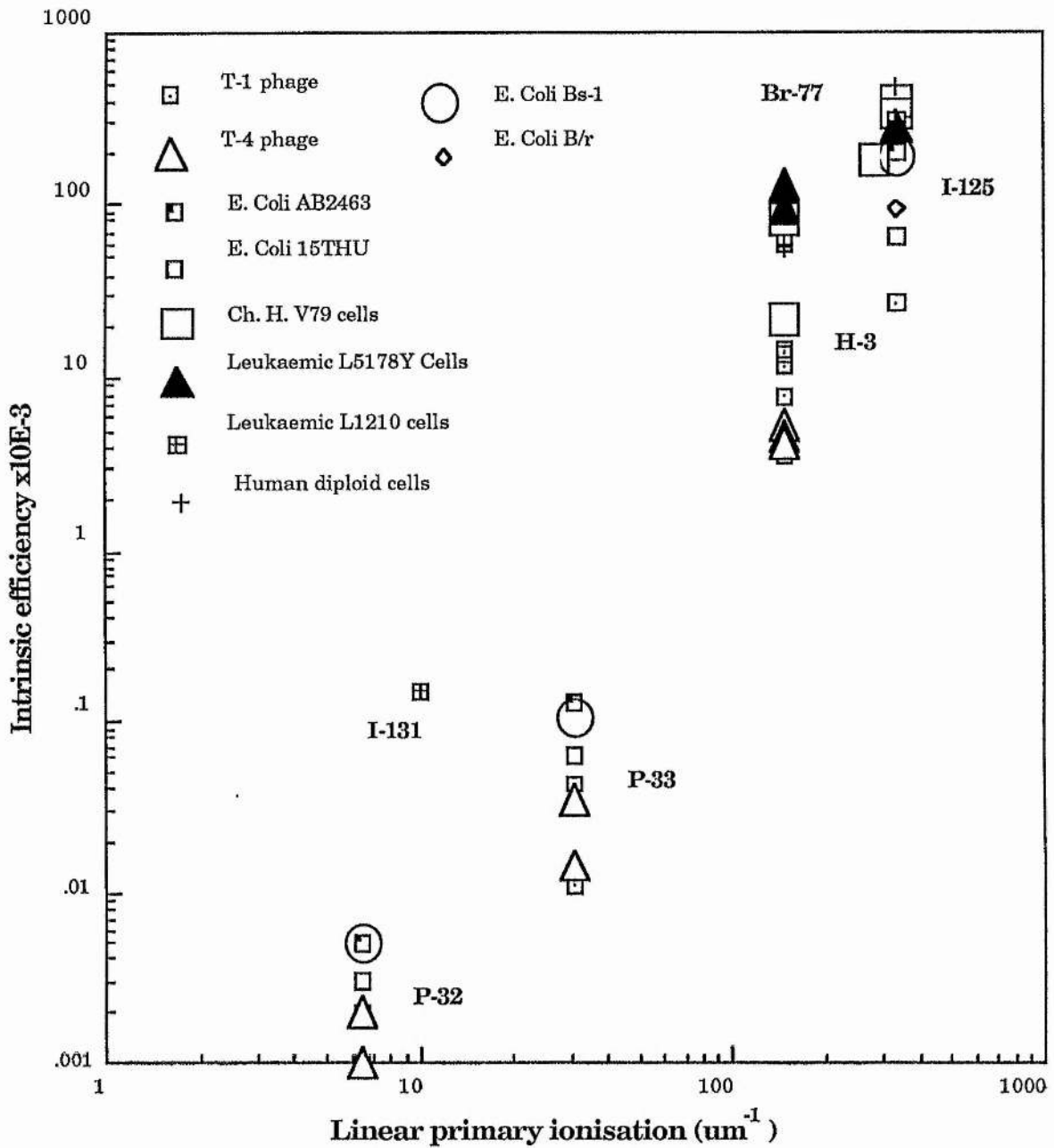


Figure 2.6: The intrinsic efficiencies of damage for different radionuclides incorporated to the DNA of mammalian cells, bacterial strains (E. Coli) and bacteriophages

Chapter III

Physical Processes in Radiation Absorption

3.0 Introduction

The absorption of energy from radiation by biological materials may lead to excitation or to ionisation. The raising of an electron in an atom or molecule to a higher energy level, without actual ejection of the electron from that atom or molecule, is called excitation. If the radiation has sufficient energy to eject one or more orbital electrons from the atom or molecule, this process is referred to as ionisation, and irradiation is said to be an ionising radiation.

Ionising radiation may be classified as direct or indirect ionising radiation. All of the charged particles (electrons, protons, alpha particles, negative Π mesons and heavy charged ions) are directly ionising. Provided that these individual particles have sufficient kinetic energy, they can directly destruct the atomic structure of the absorber through which they pass, and produce chemical and biological changes. Electromagnetic radiation and neutrons are indirectly ionising radiation, as they produce ionisation via the secondary charged particles released in the primary collisions.

3.1 X- and γ -rays as Electromagnetic Radiation

X- and γ -rays are the most commonly used type of electromagnetic radiation in both therapy and diagnosis, and because most experiments with biological systems have involved X- or γ -rays either as original radiation to study their effects on matter, or use them for comparison studies with other types of radiations.

X- and γ -rays do not differ from one another in nature or in properties; the designation X- or γ - reflects the way in which they are produced. X-rays are produced extra-nuclearly, while γ -rays are produced intranuclearly. In the practical terms this means that X-rays are produced in a device which accelerates charge particles, electrons for example to high energy. As the electrons decelerate in the target, part of the kinetic energy is radiated as bremsstrahlung or continuous X-rays. γ -rays, on the other hand, are emitted by radioactive isotopes. They represent excess energy which is given off as the unstable nucleus de-excites to a lower, more stable state. For the rest of this work, all that is said of X-rays will apply equally well to γ -rays.

Both X- and γ -rays may be thought of as a stream of photons, or "packets" of energy. Each energy packet contains an amount of energy equal to $h\nu$, where h is Planck's constant (6.63×10^{-34} joules sec), and ν is the frequency to which reference has already been made. If a radiation has a long wavelength it will have a small frequency and *vice versa*.

There is a simple numerical relationship between the photon energy, E , (in keV) and the wavelength, λ (in Angstroms which is a unit of length equal to 10^{-8} cm).

$$\lambda = \frac{h \cdot c}{E}$$

$$\text{ie } \lambda = \frac{1.2375}{E(\text{keV})} \text{ nm} \qquad 3.1$$

When X-rays are absorbed in material, energy is deposited in the tissues and cells; this energy is not spread out evenly but is deposited stochastically in discrete packets.

3.2 Interactions of Photons with Matter

The processes by which the photons interact depend upon the energy of the photons concerned, and upon the chemical composition of the absorbing material. The details of the energy absorption are important in radiobiology (including diagnostic radiology and radiotherapy). Photons usually interact with planetary electrons and more rarely with atomic nuclei via the electric field associated with these electrons or nuclei. In so doing, they may lose all, part, or none of their energy.

There are nine possible interaction processes. Two of these are of dominant importance in medical applications (photoelectric and Compton effects), a third becomes important at photon energies above 1.02 MeV (pair production), and two others need to be taken into account in limited circumstances (Releigh scattering, or coherent scattering, and nuclear photoeffect).

Photoelectric absorption is very strongly dependent on the atomic number of the absorber, increasing as a function of $\sim Z^5$, and reducing with increasing photon energy in approximate proportion to $(h\nu)^{-7/2}$ at low energies and to $(h\nu)^{-1}$ at high energies. It is always accompanied either by characteristic radiation which is called fluorescent radiation, or by Auger electron emission.

3.2.1 Fluorescence Yield

The fluorescence yield of an atomic shell or subshell is defined as the probability that a vacancy in that shell or subshell is filled through a radiative transition (ie the emission of characteristic radiation). The probability of such transitions is approximately proportional to Z^4 while that of radiationless transitions (ie the emission of Auger

electrons) is almost independent of Z . Thus, the fluorescence yield of the K-shell, ω_k , is given approximately by

$$\omega_k = \frac{Z^4}{(a_k + Z^4)} \quad 3.2$$

(Burhop 1952) where $a_k = 1.12 \times 10^6$, and Z is the atomic number of the material.

There is another semi-empirical equation for ω_k , given by Laberrigue-Frolow and Radvanyi, (1956), which is

$$\omega_k = \frac{(A + BZ + CZ^3)^4}{1 + (A + BZ + CZ^3)^4} \quad 3.3$$

where $A = -0.0217$, $B = 0.03318$, $C = -1.14 \times 10^{-6}$.

Some values of ω_k are recommended in an extensive review by Bambynek et al (1972). From this review it can be seen that low atomic number materials give rise to very little characteristic radiation, and high Auger electron probability (ICRU 1979 b). The fluorescence yields, ω_k , have been calculated from equations 3.2 and 3.3 for elements of atomic number $Z = 5-100$, and illustrated in figure 3.1.

3.2.2 The Auger Effect

All electron transitions to vacancies in inner shells are not necessarily accompanied by characteristic radiation. Radiationless transitions can occur in which the available energy is used to eject an electron from an outer shell. This process is called the Auger Effect, and the ejected electron is called an Auger electron.

The atom now has two vacancies, which may be filled by the emission of further Auger electrons (an Auger cascade) leading to multiple ionisation of the atom. The possible transitions are often numerous and the spectra of Auger electrons can be very complex. Radiationless

transitions can also take place between subshells of a shell such as the L or M. These are called Coster-Kronig transitions (for more details see Chattarji 1976).

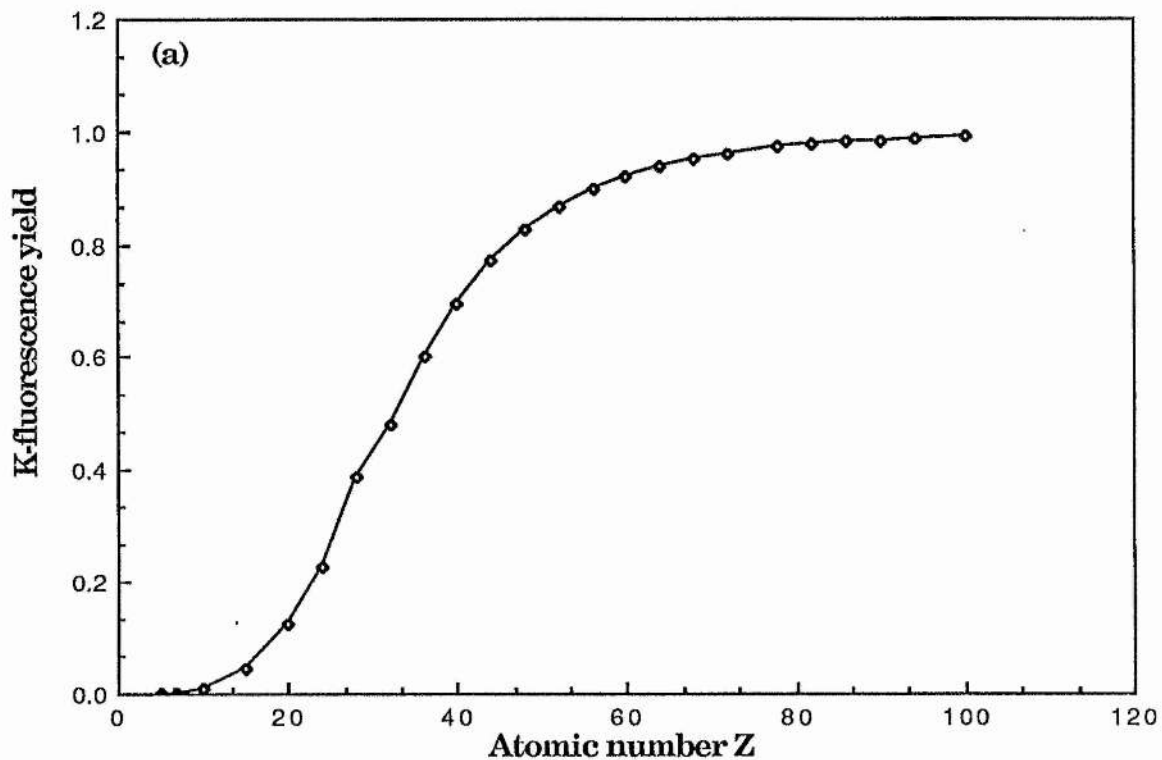


Figure 3.1(a): The K- fluorescence for different elements calculated from equations 3.2 .

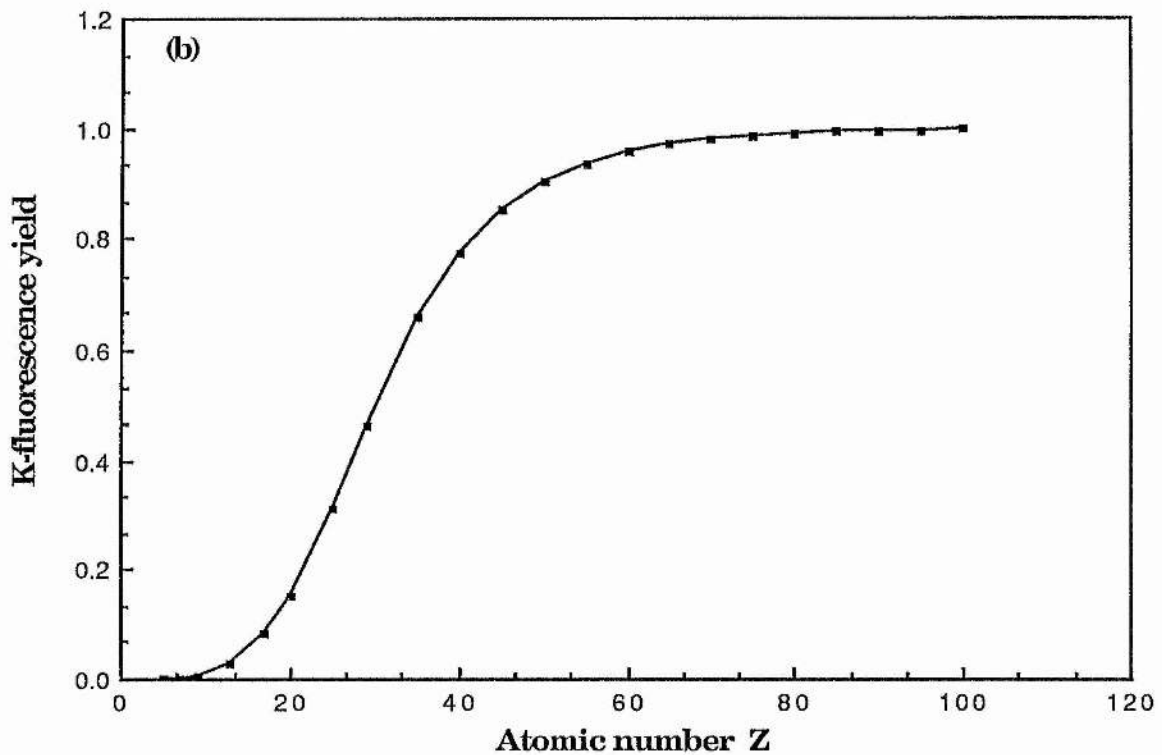


Figure 3.1(b): The K- fluorescence for different elements calculated from equations 3.3.

3.3 Interaction Coefficients and Cross-sections

The indirectly ionising radiation interacts with matter in processes which take place randomly, therefore it can be only possible to speak of the probability of interactions (photoelectric, Compton, pair production, etc). This probability can be expressed in terms of a cross-section or various interaction coefficients.

Thus the concept can be introduced of a cross-section, or apparent projected area, that an interaction centre (electron, nucleus, atom, etc) presents to the radiation which, if traversed by the radiation, gives rise to an interaction. More precisely in terms of probability

$$\text{cross-section, } \sigma = \frac{\text{probability of interaction}}{\text{unit particle fluence}}$$

The SI unit is in m^2 but a special unit, the barn, b, equal to 10^{-28}m^2 is also used.

If we have, for example, a material of density, N , or number of interaction centres per unit volume, and Φ is the mono-directional fluence, then there will be $N\sigma\Phi$ interactions per unit path length, or $N\sigma\Phi dl$ in path length dl . The fractional change in fluence $d\Phi/\Phi$ in path dl is then $-N\sigma dl$. $N\sigma$ is called the linear attenuation coefficient. It is usually represented by the symbol μ , and has dimension l^{-1} . The SI unit is m^{-1} . Thus

$$\frac{d\Phi}{\Phi} = -\mu dl$$

$$\text{ie } \Phi_1 = \Phi_0 \exp(-\mu l) \quad 3.4$$

where Φ_0 and Φ_1 are the unidirectional fluence of radiation particles before and after it passes through directional length, l , in the same direction as the fluence.

If the number of atoms per unit volume, N , of a substance of density, ρ , and molar mass, M , is $N_A \rho / M$, where N_A is the Avogadro number, then $\mu = N_A \rho \sigma / M$, where σ is the atomic cross-section.

Linear attenuation coefficients are proportional to the density, ρ , (in Kg m^{-3}) of the material (through the atomic density) and does not, therefore, have a unique value because it will be influenced by the physical state of the medium. Therefore, for tabulation purposes, it is convenient to remove this density-dependence by using the mass attenuation coefficient, μ / ρ ($\text{m}^2 \text{kg}^{-1}$) = $N_A \sigma / M$

3.4 Mass Attenuation Coefficients for Mixtures or Compounds

The interaction coefficients of a mixture or compound is calculated from the interaction coefficients of the constituent elements, assuming independence of the elementary interactions. Thus

$$\frac{\mu}{\rho} = \sum w_i \frac{\mu_i}{\rho_i} \quad 3.5$$

where w_i is the proportion by weight of the i th component and μ_i / ρ_i is the mass attenuation coefficient of the same element.

The assumption of independence of elementary interactions is true for mixtures, and in compounds only breaks down in the vicinity of absorption edges.

3.5 Total Interaction Coefficients

The probabilities of interactions of photons with matter by photoelectric, Compton, pair production, etc effects can be discussed independently of one another, and in consequence, the total interaction probability is the sum of the individual probabilities. If we take, for example, the total mass attenuation coefficient, μ/ρ , which is the sum of the mass attenuation coefficients, of the individual interactions

$$\mu/\rho = T/\rho + \sigma_c/\rho + \kappa/\rho \quad 3.6$$

where T/ρ , σ_c/ρ , κ/ρ are the mass attenuation coefficients for photoelectric, Compton, and pair production effects respectively.

3.6 Restrictions in Some Interaction Coefficients

In radiation dosimetry it is important to distinguish between those parts of an interaction process which merely scatter photons and

those which result in an actual transfer of photon energy to kinetic energy of charged particles.

In the photo-electric process, characteristic radiation will be emitted. This will carry away a fraction of energy $h\nu$ of the incident photon given by

$$\frac{\delta}{h\nu} = \frac{T_K}{T} \frac{E_K}{h\nu} \omega_K + \frac{T_L}{T} \frac{E_L}{h\nu} \omega_L \quad 3.7$$

where T_K and T_L are the photo-electric effects in the K and L shells respectively, T is the total photo-effect, ω_K and ω_L are the fluorescence yields in K and L shells, E_K and E_L are the energies of fluorescence photons arising from transitions to the K and L shells, δ is the average energy emitted as fluorescence radiation per photon absorbed. For biological materials this emitted fraction $(\delta / h\nu)$ is quite negligible as the fluorescence yields are small and E_K is only about 0.5 keV.

On the other hand, in the Compton effect, the photons which are scattered can carry away a very considerable fraction of the incident photon's energy, particularly at low energies. Thus the part of the total Compton mass attenuation coefficient that actually transfers energy to electrons is σ_a / ρ .

In the pair production process, an energy $2mc^2$ is emitted in the form of two annihilation photons, and the fraction converted to kinetic energy of charged particles is $(1 - 2mc^2 / h\nu)$.

3.7 Mass Energy Transfer and Mass Energy Absorption Coefficients

The physical parameter which is often used in the specification of radiation effect in radiobiology and radiotherapy etc is the absorbed energy (or dose). The accurate measurement of this parameter is the concern of the field of radiation dosimetry. For the theoretical calculation of absorbed dose, the mass energy transfer coefficient and the mass absorption coefficient are important.

(i) Mass energy transfer coefficient, μ_{tr} / ρ , of a material for photons is based on the kinetic energy released in a small volume such that all the scattered photons are assumed to escape. It is defined as the ratio $\frac{dE_{tr}}{E_{hv}} / \rho dl$, where $\frac{dE_{tr}}{E_{hv}}$ is the fraction of the incident photon energy that is transferred to kinetic energy of electrons by interactions in transversing a distance dl in a medium of density ρ (ICRU 1971).

It is convenient to derive from the total mass attenuation coefficient, a coefficient that relates to the photon energy actually transferred to kinetic energy of charged particles. Such a coefficient is the mass energy transfer coefficient, μ_{tr} / ρ .

$$\frac{\mu_{tr}}{\rho} = \frac{T}{\rho} \left(1 - \frac{\delta}{hv} \right) + \frac{\sigma_a}{\rho} + \frac{\kappa}{\rho} \left(1 - \frac{2mc^2}{hv} \right) \quad 3.8$$

where δ is the average energy emitted as fluorescent radiation per photon absorbed (ie equal to ΦE_b , where Φ is the fluence of photons and E_b is the binding energy of the electron), and

$\frac{\sigma_a}{\rho} = \frac{\sigma_c}{\rho} \frac{E_{el}}{hv}$ where E_{el} is the average energy of the Compton electron per scattered photon of energy hv .

(ii) The mass energy absorption coefficient, $\frac{\mu_{en}}{\rho}$, is simply the mass energy transfer coefficient modified by a factor (1-g) to correct for the energy expended outwith the localised region of interest, since the energy transferred to kinetic energy of charged particles is not necessarily absorbed completely by the irradiated material, where g is the fraction of the energy of the secondary charged particle which is transferred from the local region in the form of Bremstrahlung

$$\frac{\mu_{en}}{\rho} = \frac{\mu_{tr}}{\rho} (1 - g) \quad 3.9$$

$\frac{\mu_{en}}{\rho}$ and $\frac{\mu_{tr}}{\rho}$ may differ appreciably when Bremstrahlung production is large, ie when the kinetic energy of the secondaries is comparable to, or larger than, their rest energies, specially in media of high atomic number. Bremstrahlung emission is usually small in biological materials as these have low atomic numbers. For example, in tissue-like media, the two coefficients are always about equal.

3.8 Theoretical Calculation of Characteristic X-ray Production

The creation of a vacancy in an inner electron shell is an essential process for the production of characteristic X-radiation. The vacancy is created either naturally (the decay of radioactive nucleides by electron capture) or artificially by bombarding a certain target with accelerated particles (electrons, protons or other heavy particles). The vacancy so created is subsequently filled by a less tightly-bound electron. The rearrangement of orbital electrons may involve several stages as the vacancy moves outwards through the atom. Ionization by electron bombardment shows that a progressive increase in the

energy of the incident electrons causes ejection of more tightly bound electrons (K or L shell electrons).

K quanta may be produced by an atom when an electron from the L, M, or N shells falls into a vacancy in the K shell caused by ionisation. The alternative to the emission of a K quantum is an internal conversion process resulting in Auger electron emission. The relative probability of these two processes is described by the fluorescence yield of the K shell, ω_K , the fraction of K ionisation resulting in K quantum emission.

3.8.1 The Total Ionization Cross-section

Bethe's (1930) non-relativistic formula for the total ionization cross-section per atom for the Xth shell or subshell (where X = K, L, M, ...), σ_X , was the starting point for Mott and Massey (1949) who modified his expression to

$$\sigma_X = \frac{2\pi e^4}{E_0 E_X} \frac{Z_X}{2} b_X \ln \left(\frac{4E}{B_X} \right) \quad 3.10$$

where e is the electronic charge, E_0 is the kinetic energy of the incident electron, E_X is the binding energy of the Xth shell, Z_X is the number of electrons in that shell, b_X is a constant, and B_X is a function of E_X , all values being in electrostatic units.

After comparison with Burhop's (1940) detailed calculations, Mott and Massey concluded that for K shell ionization

$$B = 1.65 E_K \text{ and } b = 0.35 \quad (a)$$

This would not be satisfactory when E_0 is not much greater than E_K because the cross-section would not approach zero as E_0 approached E_K .

Worthington and Tomlin (1956) pointed out that this is only true for large U ($U = E_0 / E_K$) and for their numerical integrations they used

$$B = (1.65 + 2.35 e^{1-U}) E_K \text{ and } b = 0.35 \quad (b)$$

The limiting value of B in (b) as $U \rightarrow 1$ with b modified to fit the experimental results at $U = 3$ was

$$B = 4 E_K \text{ and } b = 0.35 \times 1.73 \quad (c)$$

Therefore the total ionization cross-section per atom by one incident accelerated electron for the K shell can be written from equations 3.10 and (c) as

$$\sigma_K = \frac{2\pi e^4}{U E_K^2} b_K \ln U \quad 3.10 a$$

where $b_K = 0.35 \times 1.73$.

Equation 3.10 a has been found to be a good approximation for elements with $Z < 50$ (Dyson 1973). In the present study we are interested in the yield of characteristic X-rays from thick targets. In this case the total number of ionizations along the electron path in the target, n_K , is given by

$$n_K = \int_0^x \sigma_K N dx$$

$$\text{ie } n_K = \int_{E_K}^{E_0} \sigma_K N \left(\frac{dE}{dx}\right)^{-1} dE \quad 3.11$$

where N is the number of atoms per unit volume of the target, x is the distance measured along the incident electron path in the target, and $\frac{dE}{dx}$ is the energy transferred per unit track at continuous slowing down approximation, csda.

Not all the ionization atoms will give rise to characteristic X-rays. Only a fraction, ω_K , of them will yield fluorescent X-rays. Thus the total number of K quanta, N_K , emitted by the bombarded element per incident electron of energy E_0 will be

$$N_K = \omega_K n_K \quad 3.12$$

3.8.2 Types of Ionization and Back Scattering of Electrons

If a thick target is bombarded by electrons ionization of the Xth shell of that target atoms is caused in two ways. The first process of ionization, caused by the primary incident electrons, is called direct ionization and the number of resultant ionizations is $n_K(\text{direct})$. The second process of atomic ionization is caused by the continuous Bremsstrahlung radiations which have energies greater than the binding energy, E_X , of the Xth electron of the target atom. These quanta are produced through the deceleration of the incident electrons in the target. This type of ionization is called indirect ionization, and the number of ionizations is $n_K(\text{indirect})$. Thus for the Kth shell

$$n_K = n_K(\text{direct}) + n_K(\text{indirect})$$

The above equation assumed that the incident electrons remained in the target until they reached a point where their energy was equal to E_K . The path of the electrons beyond this point gives rise to no K ionization since $E < E_K$. So the relation is valid for all electrons which complete their paths in the target material, irrespective of the particular shape of the trajectory. For paths of the form where the electron leaves the target as a result of back scattering before its energy has fallen to E_K , the equation of ionization production must be modified by introducing a back scattering correction factor, R , where

$R = 1 - \eta$, and η is the back scattering coefficient. Hence equation 3.12 will become

$$N_K = \omega_K (1 - \eta) n_K \quad 3.13$$

Originally two different theories were put forward to explain the back scattering of electrons. These were single large angle scattering (Everhart 1960 and Nakhodkin *et al* 1962) or multiple small angles scattering (Archard 1961 and Jacob 1974).

The theory of single large angle scattering considers only one deflection and ignores the possibility that electrons are deflected for a second time through another large angle and thus their paths remain within the target. Therefore this theory can not give satisfactory agreement with the experimental results.

The multiple theory says incident electrons penetrate in straight lines into the target up to a certain specified distance, after which they will disperse randomly in all directions. This theory depends on the belief that multiple collisions occur only after the electrons reach the dispersal point, and it neglects the probability of large single angle elastic collisions within the depth of target between its surface and the dispersal point.

To formulate a complete theory it was necessary to consider all the processes which might happen to deflect the electrons from their paths. So a combined theory was suggested by Archard and Mulvey (1963). This combined the diffusion and large single angle scattering theories and was called the theory of back scattering. It assumed that for targets of low atomic number, the ratio of diffusion depth, x_d , to the maximum range of the incident electron, R_{max} , would increase in such a way that back scattering could not take place since the electrons which penetrate to a diffusion distance, x_d , can not reach the surface

again until they pass another projected depth equal to x_d . Therefore if $\frac{x_d}{R_{\max}} > 0.5$ no electrons will reach the surface by a diffusion mechanism. As the atomic number of the target increases, the ratio will decrease because the electrons will reach the diffusion depth immediately (ie penetrate for a very short distance). In this case the probability of large angle scattering is very small whereas it is very high for low Z targets. The diffusion depths and the maximum range of electrons have been calculated by Archard and Mulvey (1963) and Fitting (1974) respectively.

From the combined theories, target materials can be classified into three groups; (a) high atomic number elements ($Z \geq 50$) where the diffusion processes are dominant since the diffusion depth is very small; (b) low atomic number elements ($Z \leq 30$) which have large diffusion depths and to which the Everhart theory of large single angle scattering is applicable; (c) medium atomic number elements ($30 < Z < 50$) where both single and multiple scattering are expected to occur.

According to the above conclusions, Werner (1979) has given us a successful formula which allows us to obtain the back scattering coefficients for solids over the energy range of incident electrons, 5 - 100 keV, at normal incidence. The experimental data of Hunger and Kuchler (1979) and Neubert and Rogaschewski (1980) agree with Werner's results for low Z materials ($Z \leq 30$) with errors of less than a few per cent, while for elements with high atomic numbers ($Z \geq 50$) the error rises to about 10%, and for elements of medium atomic number ($30 < Z < 50$) to about 15%. Hunger and Kuchler's (1979) expression has been used in our study since it covers different theoretical and experimental data and also it was derived for thick targets. Their equation is

$$\eta = E^{M(Z)} \exp[C(Z)] \quad 3.14$$

where η is the back scattering coefficient, E is the energy of the incident electron in keV, $M(Z)$ is a function of Z (given by $M(Z) = 0.1382 - 0.9211Z^{-0.5}$), and $C(Z)$ is also a function of Z (given by $C(Z) = 0.1904 - 0.2236 \ln Z + 0.1292 \ln^2 Z - 0.01491 \ln^3 Z$). The back scattering coefficients, η , have been calculated from equation 3.14 for a copper target, and comparison made with the measured coefficients of Hunger and Kuchler (1979) as illustrated in figure 3.2.

The electron back scattering coefficient, η , has also been studied by Neubert and Rogaschewski (1980). They measured it as a function of incident electron energy, angle of incidence, and target atomic number. Their results show that the coefficient decreases as the energy of the incident electron increases and as the angle of incidence with the normal increases. The back scattering coefficient of copper is drawn as a function of the incident angle of electrons in figure 3.3.

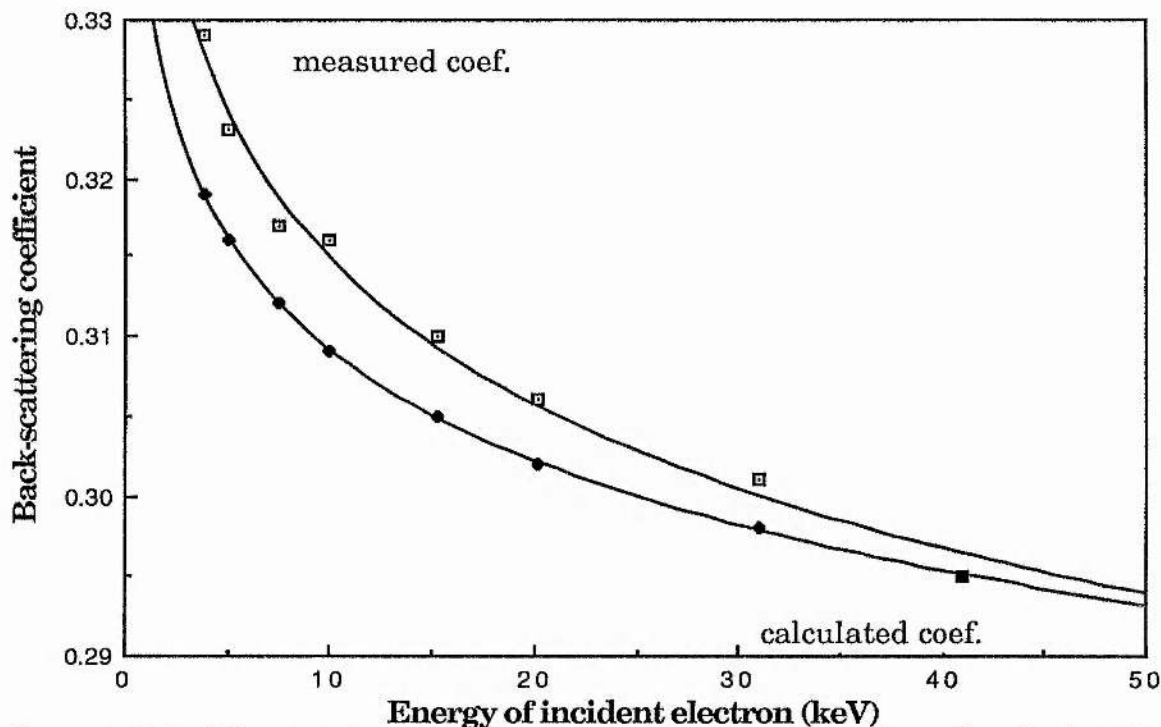


Figure 3.2: The measured (Hunger & Kuchler (1979)) and calculated (Equation 3.14) back scattering coefficients (of copper is drawn as a function of incident electron energy.

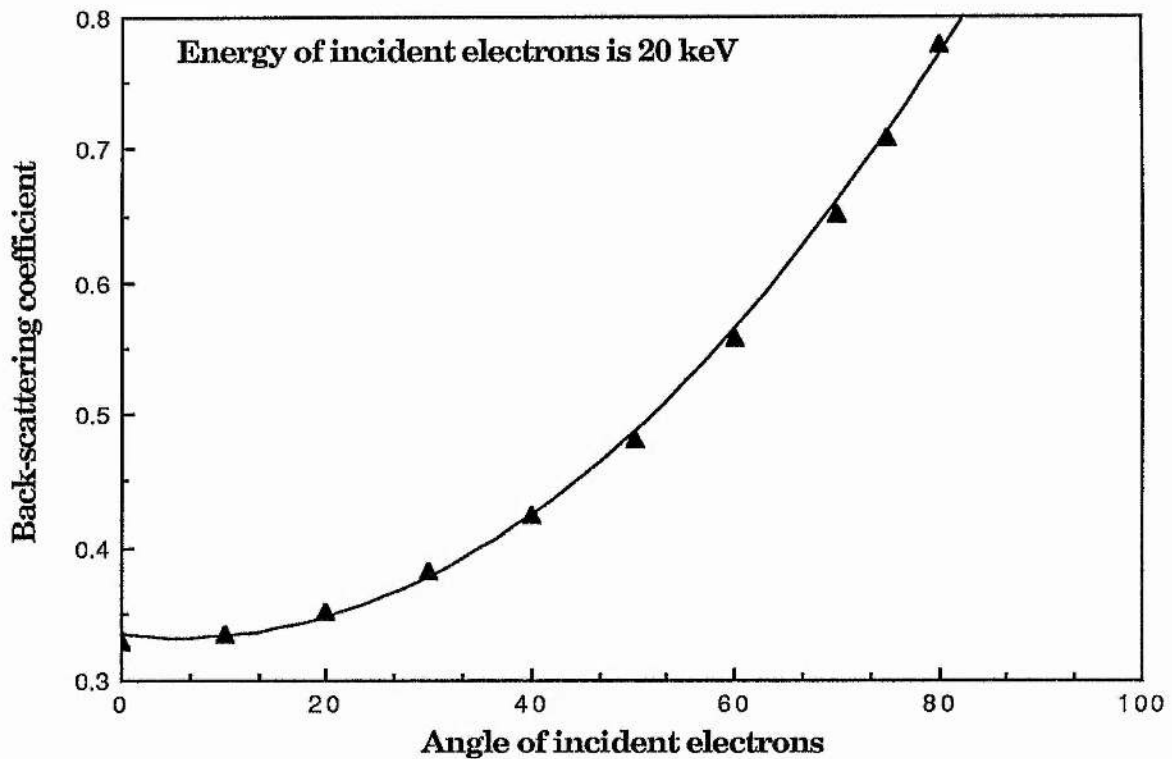


Figure 3.3: The back scattering coefficients of copper drawn as a function of the incident angle of electrons

3.8.3 Attenuation of K-characteristic X-rays in the Target

The number of K quanta is subject to attenuation while passing through the target. Hence it becomes necessary to introduce an attenuation correction into equation 3.13. Thus, assuming that only K_{α} and K_{β} quanta are emitted, the number of quanta per unit solid angle per electron at an angle Φ will be

$$N_K = \frac{\omega_K (1-\eta) n_K}{4\pi} [\alpha e^{(-\mu_{\alpha} x \csc \Phi)} + \beta e^{(-\mu_{\beta} x \csc \Phi)}] \quad 3.14$$

where α and β are the fraction of K_{α} and K_{β} quanta, and μ_{α} and μ_{β} are the K_{α} and K_{β} linear absorption coefficients respectively.

Equation 3.14 holds true provided that the electron beam is normal to the target surface. Generalising this equation for different incident angles θ with the normal (figure 3.4) gives

$$N_K = \frac{\omega_K(1-\eta) n_K}{4\pi} [\alpha e^{(-\mu_\alpha R \cos\theta \operatorname{cosec}\Phi)} + \beta e^{(-\mu_\beta R \cos\theta \operatorname{cosec}\Phi)}] dx \dots\dots\dots 3.15$$

where R is the projected range of the electron in the target.

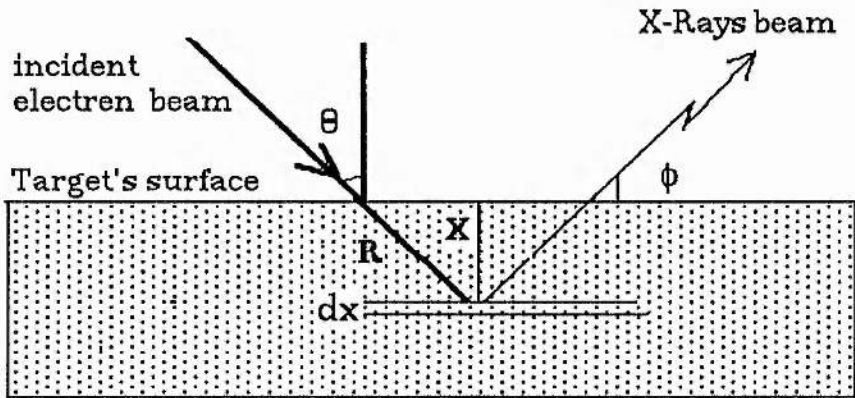


Figure 3.4: Schematic diagram for a beam of electrons incident on a target at an angle θ with the vertical and X-Ray beam collected in an angle Φ with the target surface

Chapter IV

Production and Measurement of Characteristic X-rays

4.0 Introduction

In the present experimental research it was decided to study a chemical molecule (enzyme) in the dry state and in solution in an attempt to isolate the indirect action of photons, and to quantify the direct action of electrons at secondary charged particle equilibrium. The result of this study will be applied to more complex biological samples which have a repair mechanism. Thus, the final aim of this project will be to irradiate mammalian cells *in vitro* in order to test the biophysical model of damage.

This type of study needs an intensive source of photons (high fluence rate) of characteristic X-rays of selective energy. Towards this end a high intensity source of X-rays has been designed and constructed. Relevant methods of dosimetry were also developed and used.

4.1 Intensive X-ray Production

In recent years the subject of X-ray physics has become important to a much wider scientific circle than hitherto. The greatest expansion of the subject has probably been in the field of elemental analysis, for which several methods of X-ray production are currently in extensive use. These methods include the electron microprobe, tube-excited X-ray fluorescence, isotope-excited X-ray fluorescence, and particle-induced X-ray emission. The latter technique may be subdivided into proton-induced, α -particle-induced, and heavy-ion-induced X-ray

production (Dyson 1959, 1973, 1987). From these methods, inner shell ionisation of specific target atoms by electron bombardment has been chosen because of its efficient production of low energy photons. (See chapter III)

The construction of a complete and intensive X-ray machine and its ancillary equipment required consideration to be given to many physical as well as mechanical aspects.

A machine was required which would operate at low vacuum ($\sim 10^{-7}$ torr), and have the capability of bombarding four different targets to permit energy selection. A facility was also required to irradiate samples both upwards and downwards. The machine was designed to operate automatically via an auto-heated filament which controlled the accelerating high voltage supply and hence maintained a constant source of radiation. Detailed descriptions of the machine components are given below.

4.1.1 Electron Gun

Figure 4.1 shows a cross-section of the electron gun assembly, which is mounted on a disc and connected to the ends of the two insulated lead-throughs which are used to feed both the high voltage to the cathode and the current to the filament. The lead-throughs were designed by the manufacturer (Ferranti Electronics Ltd) to withstand up to 250 kV and carry up to 10 Amps. The ceramic tubes which covered the leads near the flange were replaced by PTFE tubes to improve the unwanted leakage current at high voltages.

As the required current is up to 4 Amps, a 0.2mm diameter, 12cm length of pure (99.95%) tungsten wire (of resistivity, ρ , $5.6 \times 10^{-8} \Omega \cdot m$ at $20^\circ C$) is used as the filament material. Tungsten is particularly suitable for this application because it has a high melting point, low

vapour pressure, relatively high electrical and thermal conductivity, and high mechanical strength. The total resistance, R , of the filament wire which is wound into a tight spiral is given by :-

$$R = \rho l / A \text{ Ohms}$$

where l is the length in metres, A is the cross-sectional area in square metres, and ρ is the resistivity of the wire in $\Omega\cdot\text{m}$.

The characteristic curve of the filament can be seen in figure 4.2.

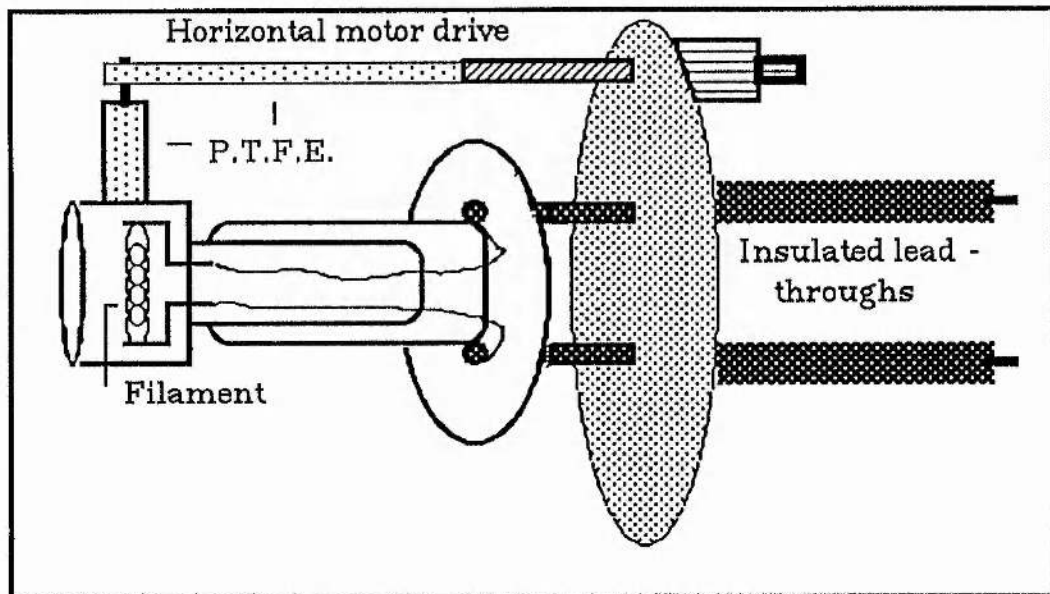


Figure 4.1: A schematic diagram of the electron gun

The filament current is supplied by a stabilised DC power source of 26 Volts output (Kingshill, type NS3020). The high power was floated up to 100 kV with respect to earth, by using a very good stand-off insulator (Figure 4.3) and a mains isolation transformer of the same high voltage isolation (Goodyear Transformers Ltd, serial number 80/51847).

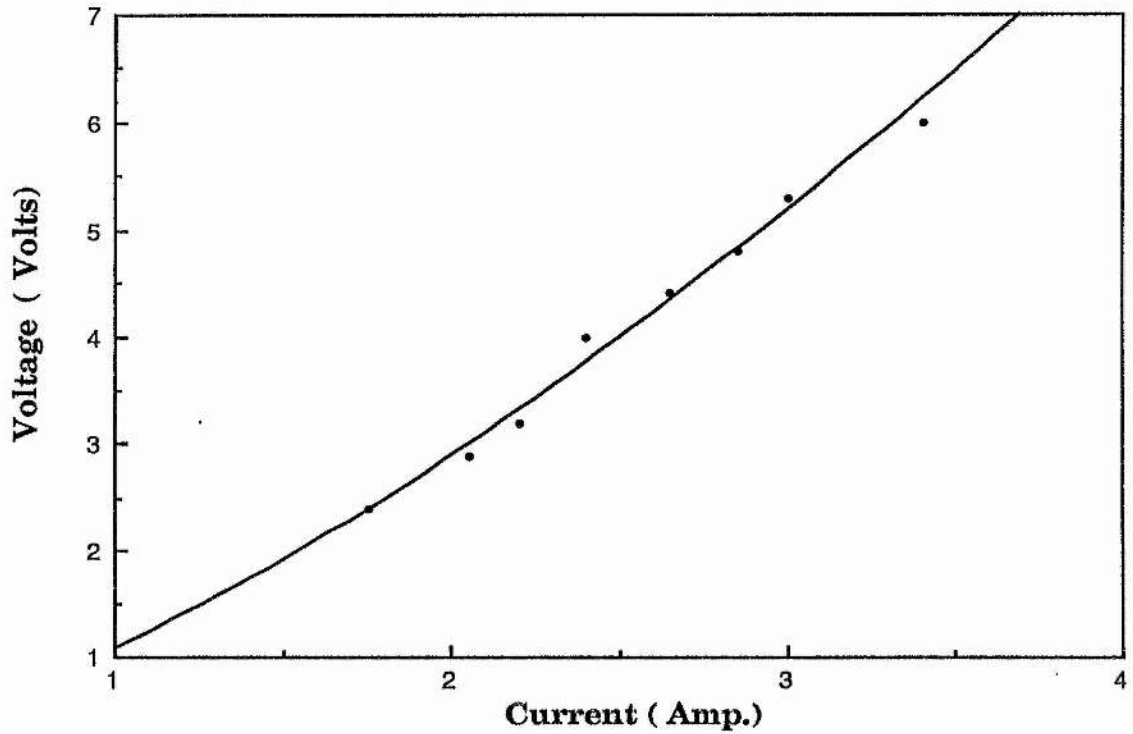


Figure 4.2: Characteristic curve of the filament

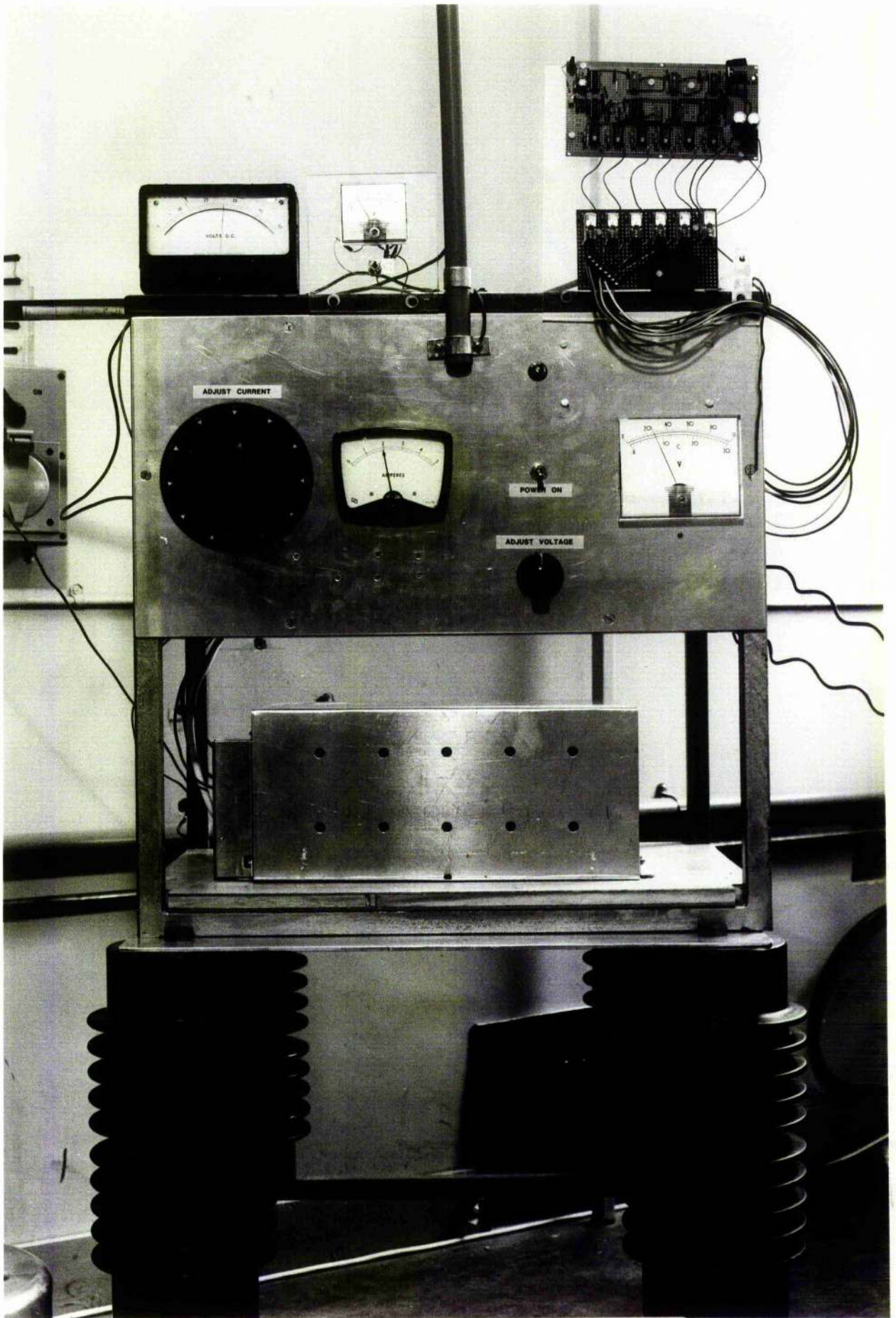


Figure 4.3: Stabilised D.C.
Power Source

The filament is fitted inside a cup-like stainless steel cathode which opens horizontally forwards, and faces a tube of stainless steel of 1.6 cm inner diameter, and 16 cm length. This tube collects the electrons which are accelerated by the high negative voltage of the cathode and focused by the 16 cm tube into a narrow beam to hit the target which is connected to the earth. The negative high voltage is supplied by a stabilised high power source (Hunting Hi-volt Ltd type 1400 series). The output of this power source has been calibrated against a Universal Kilovolt meter type RX 100/C/AC number 428 (Henry A Patterson & Partners Ltd). The calibration curve (Figure 4.4) shows the relationship between the system's reading and the actual output voltage. Because of the importance of the gap between the cathode (high negative voltage) and the stainless steel tube in optimising the collection and the acceleration of the electrons inside the tube, the cathode has been connected to a horizontal drive mechanism to enable it to move slightly forwards and backwards, thus controlling the size of the gap. This drive mechanism is controlled externally without affecting the vacuum system.

4.1.2 Auto-heating Circuit of the Electron Gun

The filament power capacity is quite low compared with the maximum output of the power supply used. The power source is operated at the stabilising voltage. Nevertheless, with either current or voltage stabilisation, the filament needs to warm up slowly. This requires at least one hour. Thus it was decided to design a timer which was controlled by an auto-preheating circuit. Chen's circuit (1987) has been improved to meet the requirement of the present work with the assistance of R D Zhang. This circuit increases the output of the power supply to the filament slowly as a function of time, in pre-set steps at five

minute intervals. (Total time taken is 35 minutes.) The timing control circuit which operates the process is given in figures 4.3 and 4.5.

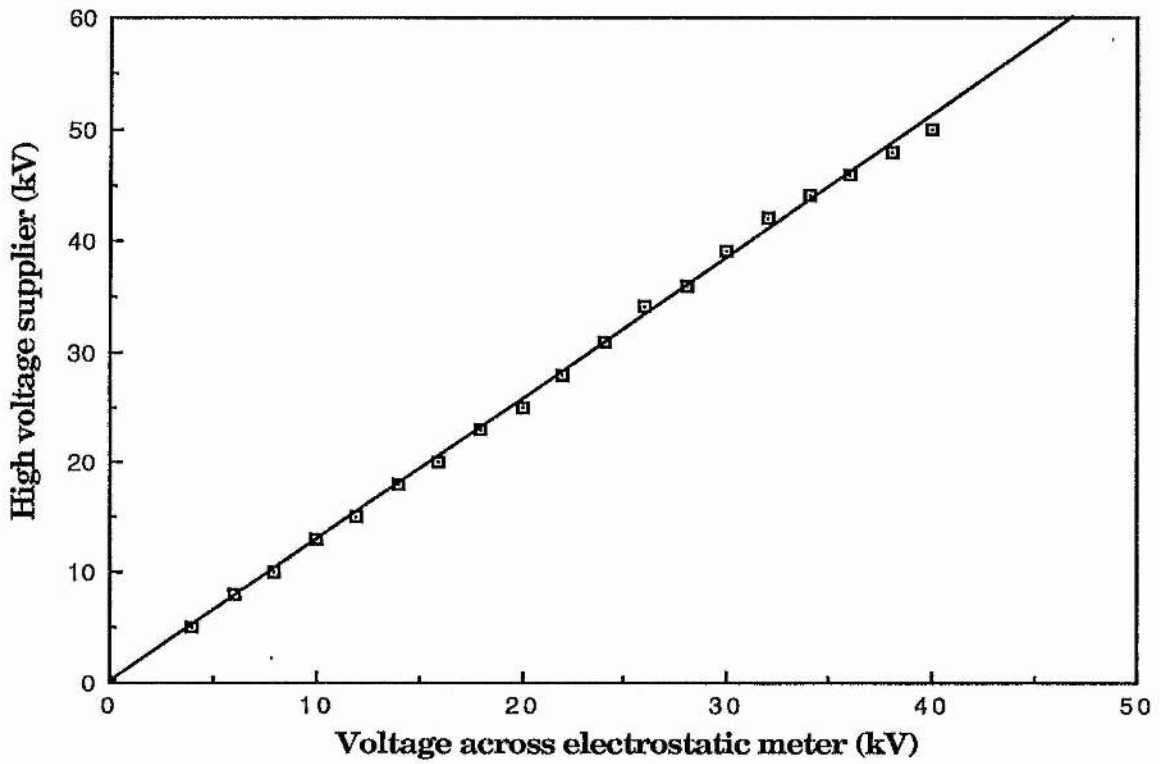


Figure 4.4: Calibration curve of the high voltage supplier against an electrostatic meter

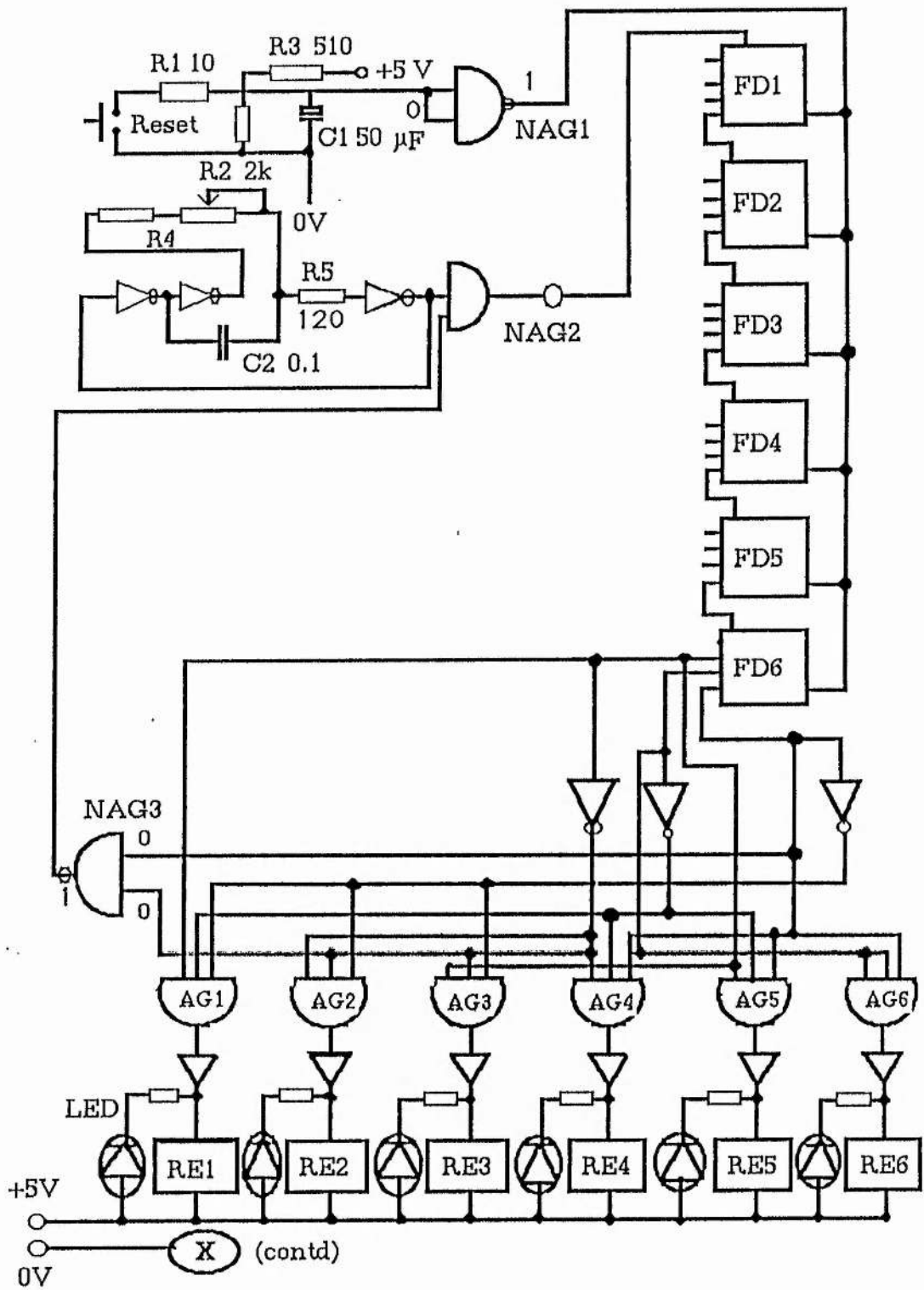


Figure 4.5 a : Preheating timer circuit for electron gun filament.

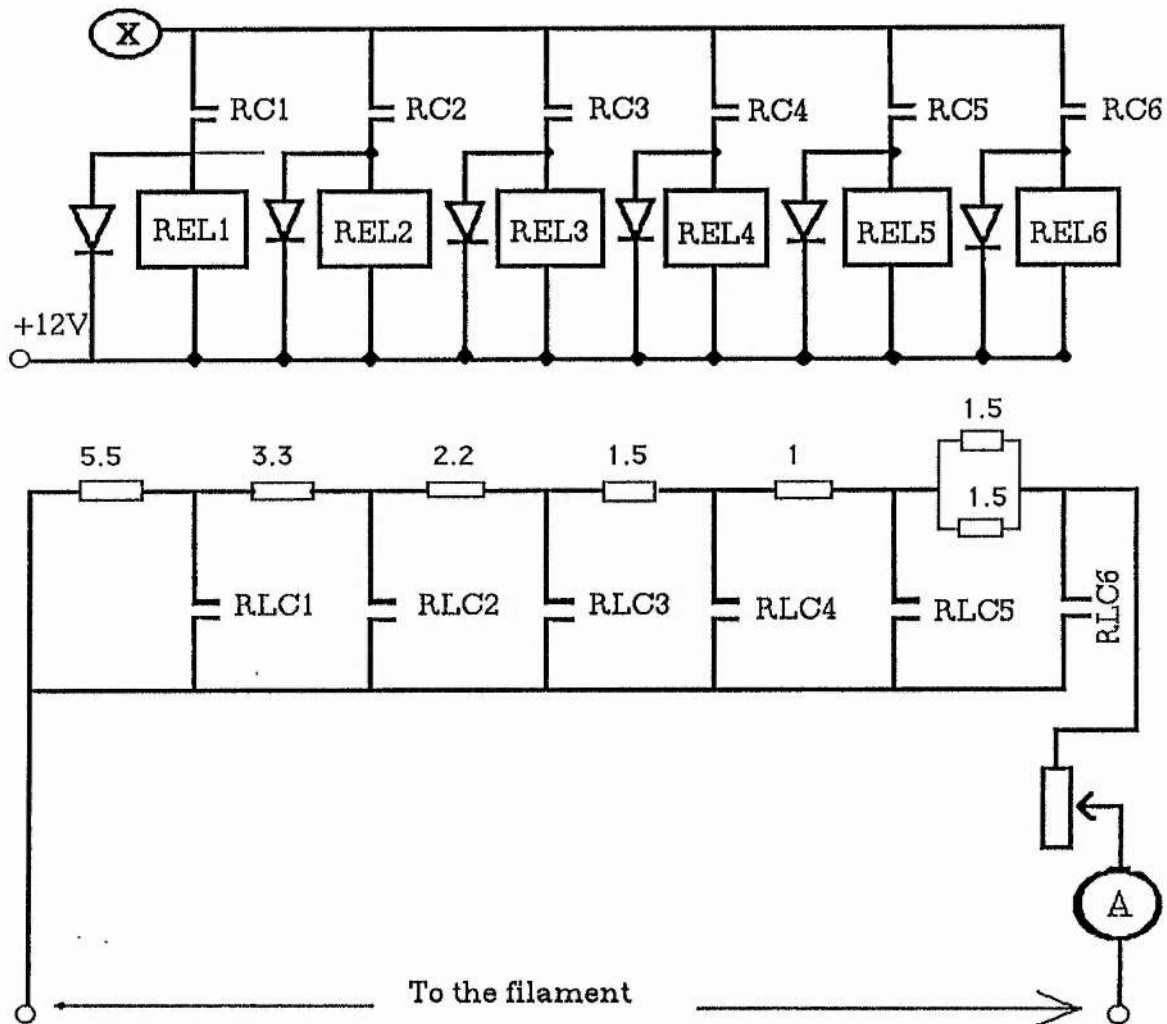


Figure 4.5b : Preheating timer circuit for the electron gun filament.

There has also been constructed a series of timers which control sequentially the processes of the high vacuum system, filament power supply, and the auto-preheating circuit.

4.1.3 Anode Design and Cooling

Figure 4.6 shows a schematic diagram of the anode which is a block of copper of a truncated pyramid shape. The four sides of the pyramid are inclined at an angle of 25° from the normal. These surfaces can be plated with four different metals to be used as targets for the accelerated electrons to produce the characteristic radiation of these metals.

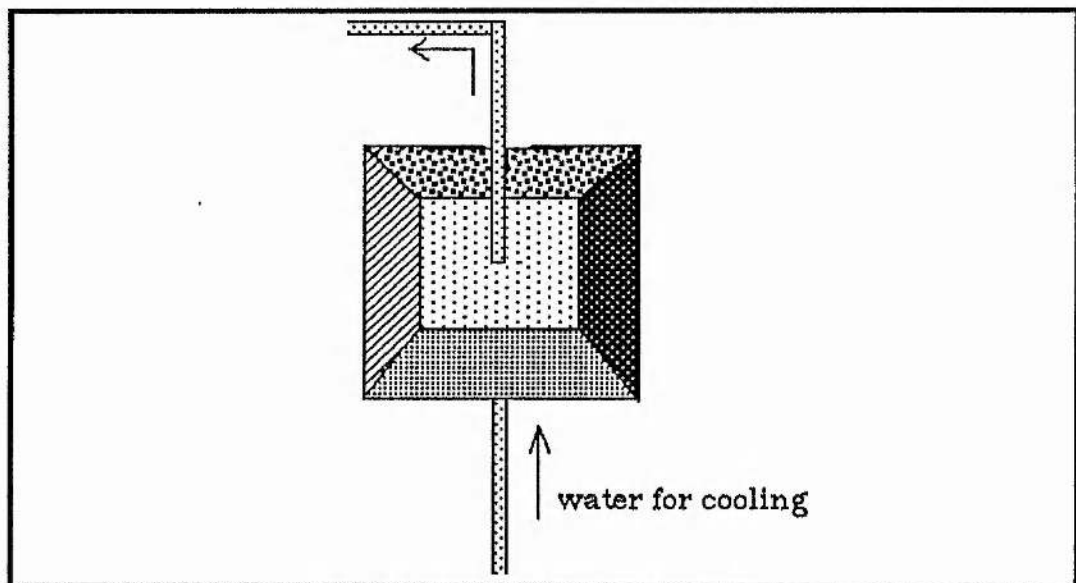


Figure 4.6: Schematic diagram of the anode which is a block of copper of a truncated pyramid shape.

In the present research a copper target will be used. This can be provided by polishing any one of the four bare faces of the pyramid, and orientating it towards the accelerated electron beam.

Because of the high percentage of accelerated electrons, power ($\leq 10\text{kW}$) is dissipated as heat energy. The temperature of the anode target

will be raised very quickly to a high level which may damage the target. Thus, an efficient cooling system is required. This has been effected by making a chamber of 4 x 4 x 2 cm inside the pyramid. Two tubes of stainless steel have been sealed to the top and the base of the pyramid, the upper and lower faces of the chamber. Water enters through the lower tube and exits through the upper one, regardless of the orientation of the chamber, thus ensuring that the chamber remains full of water. The cooling efficiency depends on the rate of water flow inside the chamber. A plate of copper is fixed at the centre to baffle the straight flow, and to make the water rotate, hence absorbing most of the heat generated in the target.

4.1.4 X-ray Production Chambers and Vacuum System

The mechanical construction of the production chambers as well as the vacuum system component is shown in figure 4.7.

4.1.4.1 The X-ray Chambers Assembly

Figure 4.7 shows that this assembly consists of two chambers, the electron gun chamber, and the anode chamber (the target chamber).

The electron gun chamber is a horizontally mounted cylinder made of stainless steel of 30 cm diameter and 25.5 cm length. The whole assembly of the electron gun (section 4.1.1) is fitted onto a stainless steel flange of 35 cm diameter which covers one side of the chamber. The other side is covered by another flange of the same size through which is inserted the 16 cm tube (section 4.1.1) to join the electron gun chamber to the anode chamber. The chamber also has two view ports (anterior and posterior windows) through which processes of sparking discharge, filament feeding conditions, and the movement of the horizontal drive mechanism can be monitored. The upper side of the chamber is connected by a stainless steel tube, 35 cm in length and 3.5 cm in

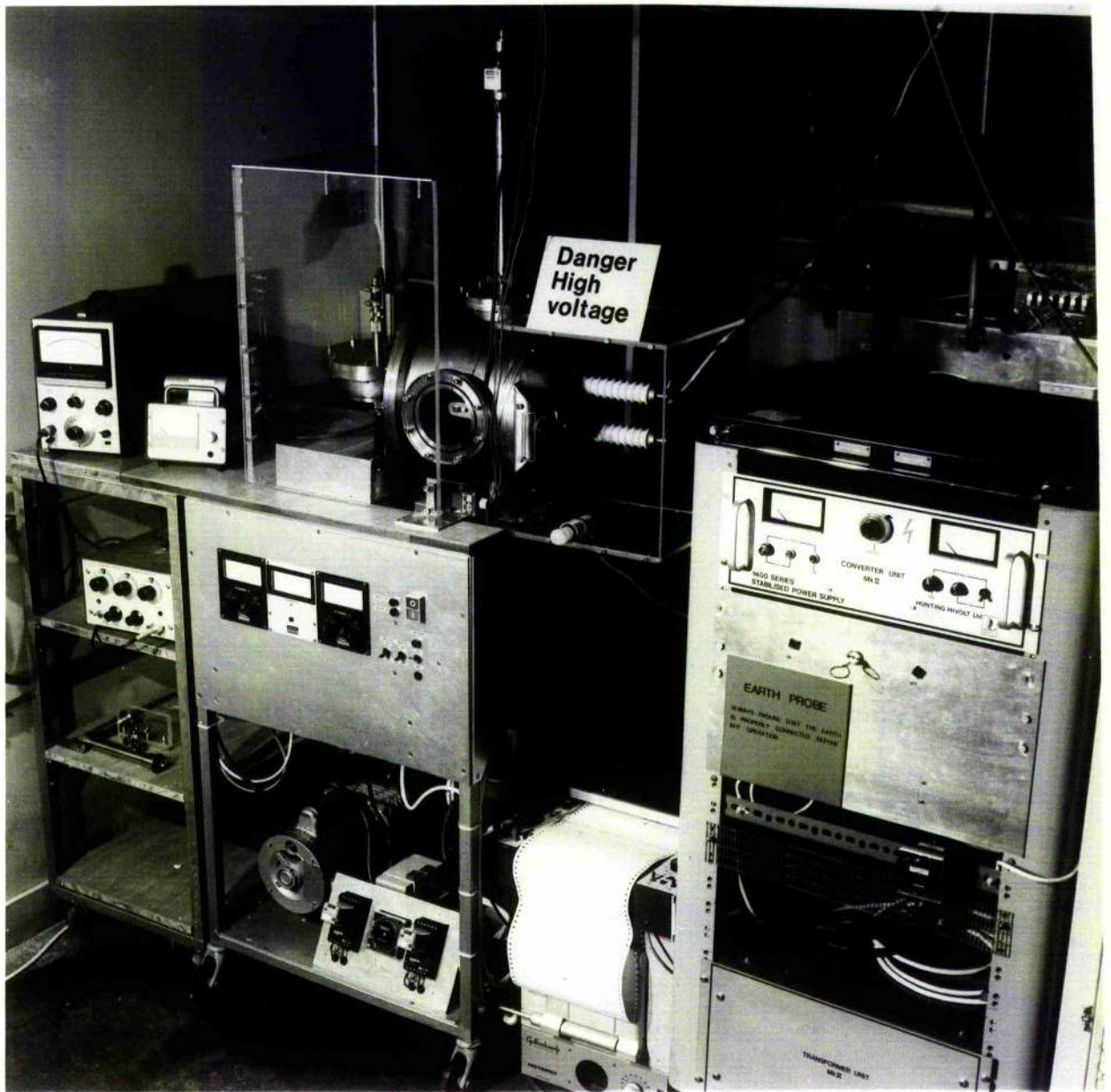


Figure 4.7a: Mechanical construction of the X-ray machine

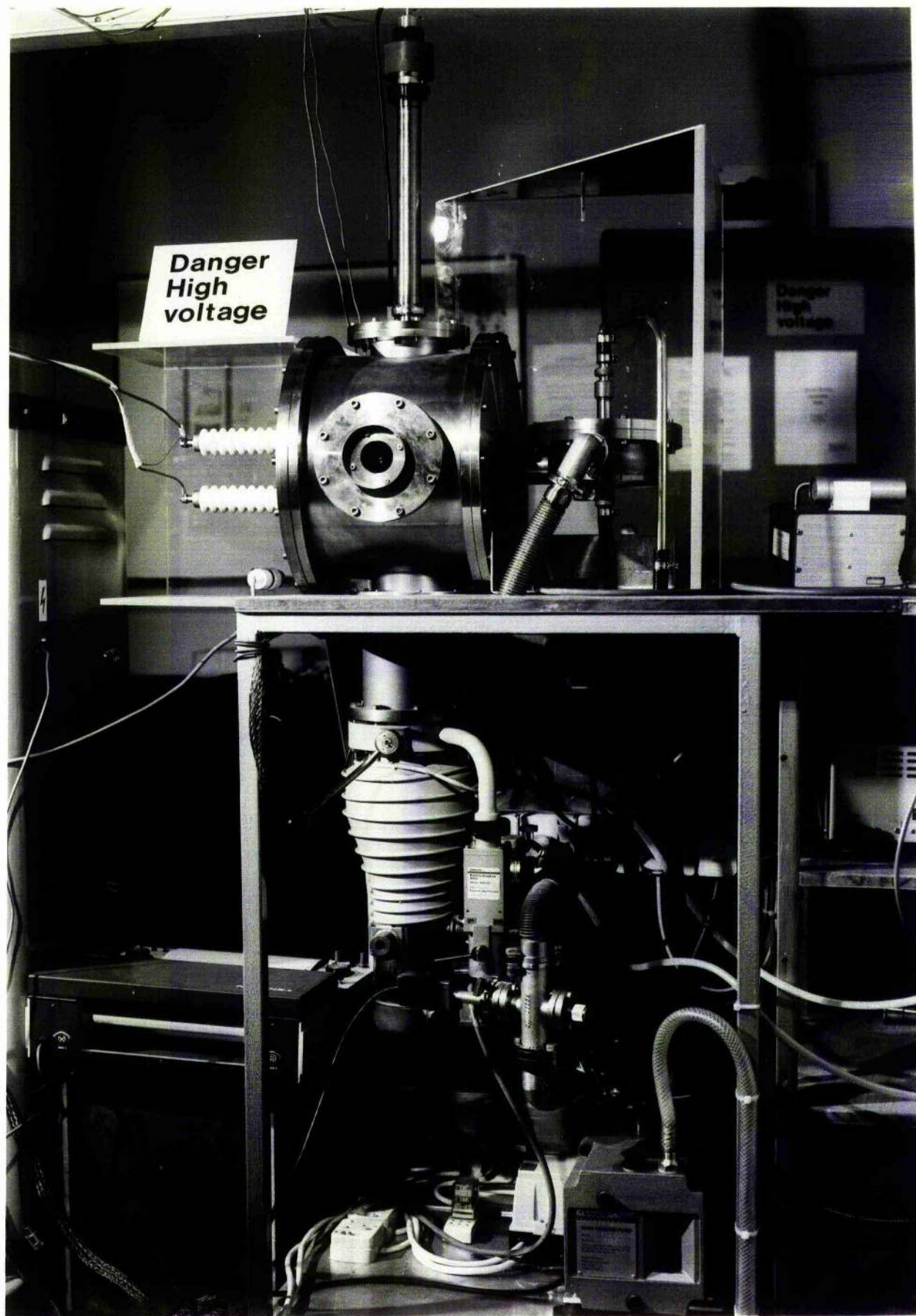


Figure 4.7b: Mechanical construction of the X-ray machine including the vacuum system

diameter, to the head of a Penning gauge, and the lower side is connected by another tube, 29 cm in length and 13 cm in diameter, to the diffusion pump.

The anode chamber (target chamber) is a vertically mounted cylinder of stainless steel, 14 cm in diameter and 7 cm in length, connected through the side wall to the electron gun chamber by the 16 cm tube. Also entering the chamber through the side wall is a tube connecting it to the vacuum system. The connections for the water cooling system are located in the top and bottom faces. The exit window (of 13 mm diameter, and 1.33 cm^2 in cross-section) for the radiation, is covered by a disc of pure (99.8%) Beryllium foil of thickness 0.125 mm, and diameter 19 mm.

4.1.4.2 The Vacuum System - Components and Operation

The vacuum system consists of a rotary pump (RP), a diffusion pump (DP), a magnetic vacuum valve (MV), and two types of pressure gauge. A Pirani gauge is used to monitor the roughing pump, and Penning gauges for the backing pump. The high standard of construction, and the high efficiency of pumping enable the system to maintain a vacuum of the order of $\sim 10^{-7}$ torr under running conditions. A schematic diagram of the vacuum system is given in figure 4.8. The system is operated in the following manner:

- 1 Switch on the mains supply to provide the power for the rotary pump timer, Pirani gauge, and the main circuit board of the machine.

- 2 Ensure that valve 1, valve 2 (small air admittance valve) and the butterfly valve on the diffusion pump are all closed, and that valve 3 or roughing/packing valve (two-way valve) is on the roughing side.

3 Switch on the rotary pump which also operates (opens) the magnetic vacuum valve. To allow the rotary pump to operate efficiently, it is wise to leave it running for ten minutes in this state to warm up and avoid the possibility of automatic cut-off due to overloading when it is required to evacuate a large volume of gas from the chambers. After heating, open valve 1.

4 Leave the system running in this manner until the pressure reaches 10^{-2} to 10^{-3} torr.

5 Set the two-way valve to packing, and when the Pirani gauge reads 10^{-2} torr, switch on the diffusion pump, ensuring that the water supply for cooling is turned on.

6 When the diffusion pump has warmed up for about ten minutes, open the butterfly valve and select the Penning gauge scale according to the pressure in the system.

To close down the vacuum system it is advised to carry out the following procedure:

1 Switch off the Penning gauges, close the butterfly valve on the diffusion pump, and then switch off the diffusion pump.

2 When the diffusion pump has become cold, switch off the cooling water.

3 Turn the two-way valve to roughing, close valve 1 and switch off the rotary pump.

It is very important to follow the described procedures (figure 4.8), in order to retain the efficient function of, and to limit any possible damage to the system.

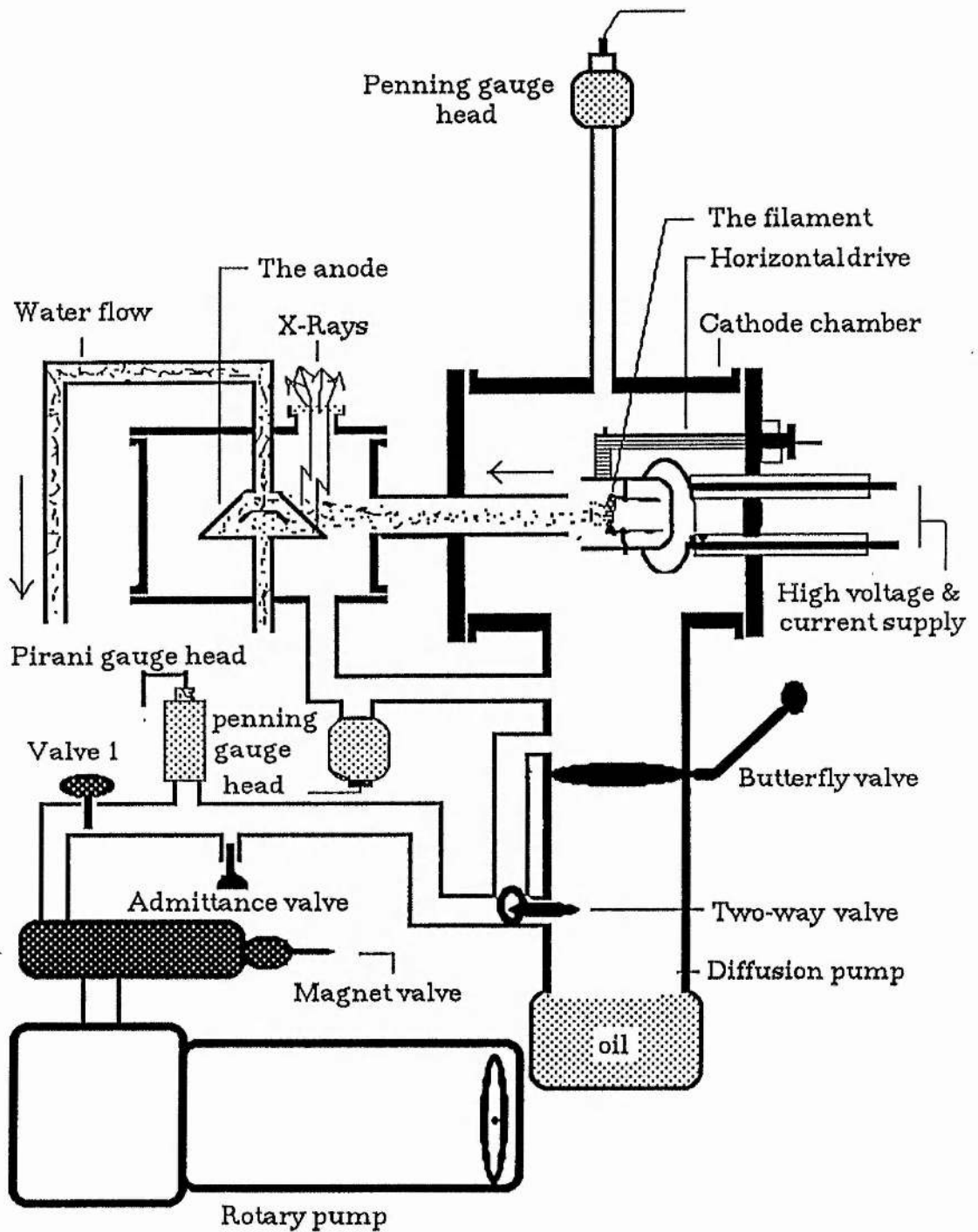


Figure 4.8 : Schematic diagram of the mechanical construction of the production chambers and the vacuum system of the X-ray machine.

4.2 Safety Precautions and Interlocking

To avoid the potential hazards from the high voltage and to restrict the exposure to the radiation from the X-ray machine (which is capable of delivering up to 4 Gy/sec) in the work area, some precautions and reasonable practical measures are required.

4.2.1 Warning signals

A warning signal indicating that X-rays are being generated (X-RAYS ON) has been fixed at the main door to the room, and is clearly visible from many angles. It is illuminated by two red bulbs fitted inside the signal box, and connected in parallel to the operation circuit. There is also an automatic warning lamp which operates while the machine is energised, and is positioned immediately adjacent to the tube. Failure of either both bulbs in the signal box or the bulb in the warning lamp automatically cuts off the operation circuit.

The operator is protected from the radiation by a shield of steel, 4 mm thick, which encloses the complete assembly, and is linked to the control panel by an interlock.

4.2.2 Connections and Interlocking

These may be considered in three groups.

(a) All high voltage connections must be completely insulated and tightly fixed to the reference points. The operator must ensure that the anode of the machine and other components are well earthed, with the obvious exception of the electron gun assembly.

(b) Operation of the high voltage supply can be commenced only when the master key is used. Thus this key must be kept in a safe place when the machine is not in use. The high voltage may be switched off

by using either the OFF button, or the master key, both of which are found on the front board of the control panel.

(c) Interlocks have been provided to ensure that any opening of the access door, or removal of the tube shield will result in automatic shutdown of the high voltage system. The high voltage can only be switched on again when the controlling circuit is completed, ie when the access door is closed, the shielding in position, and the circuit controlling the warning signals is complete.

The safety interlock switches are of the 'fail-safe' type and are designed to operate in a positive mode, ie only when action is taken to force the switches closed. The arrangement of the safety interlock connections is shown in figure 4.9.

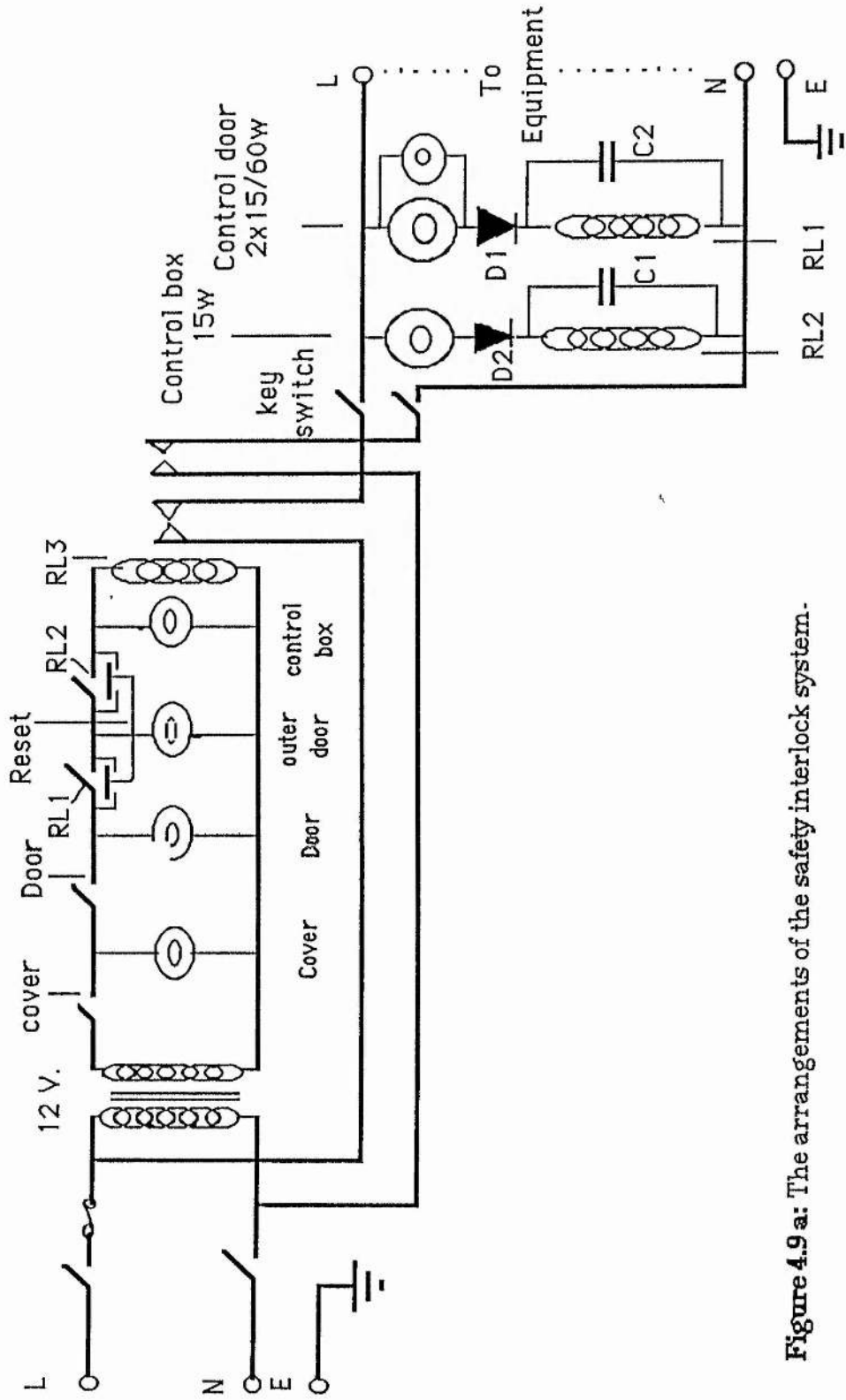


Figure 4.9 a: The arrangements of the safety interlock system.

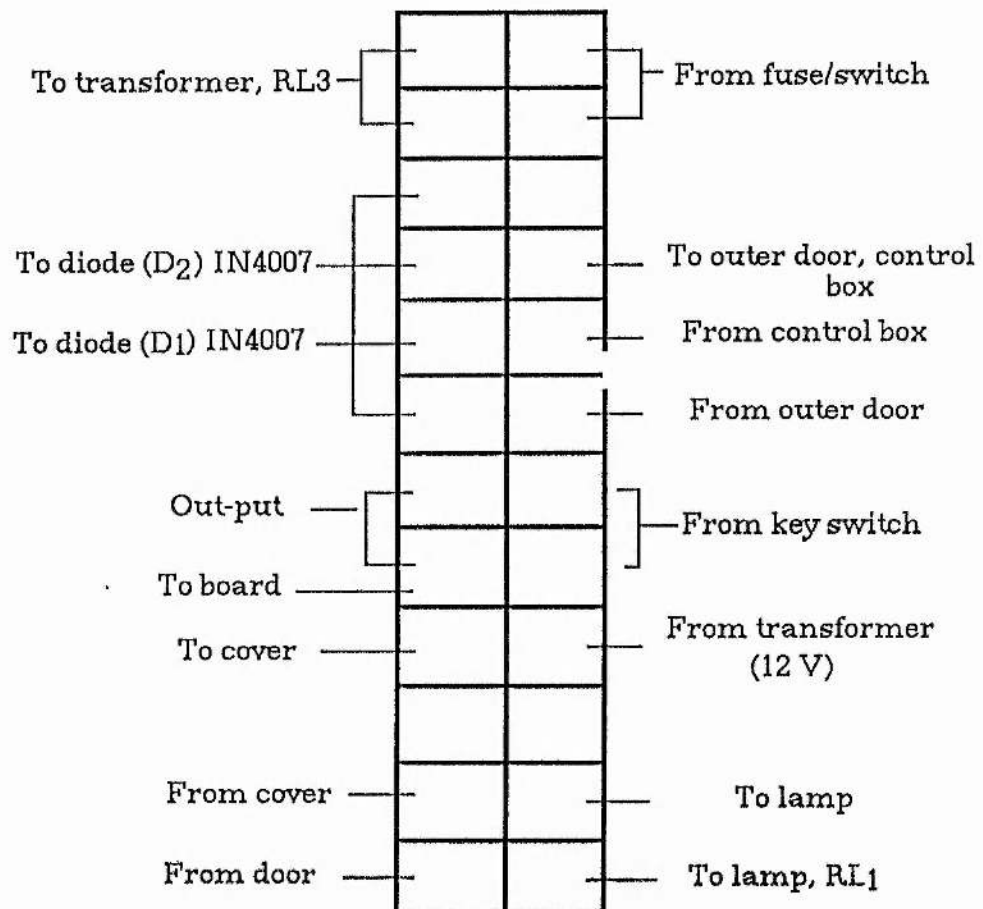


Figure 4.9b: The arrangement of the safety interlock system connections

4.2.3 Monitoring of Radiation

In order to ensure that the shielding is efficient enough to reduce the ambient dose-levels to acceptable levels for the operator appropriate radiation monitoring must be carried out. The nature and frequency of such monitoring is compatible with the degree of hazard associated with the normal operation of the machine, and checking should be carried out after repair, maintenance or modification of the machine prior to returning the generator into service.

4.2.4 Personal Monitoring

This type of monitoring is carried out with personal dosimeters which are issued to all persons who may be exposed to the ionising radiation from the X-ray machine. The dosimeters issued are normally of the thermo-luminescent type commonly referred to as TLD.

4.3 Physical Specification of the Output Beam:

X-ray Spectroscopy

Spectroscopy is the method of studying radiation beam distribution by analysing it qualitatively and quantitatively to find the energy distribution of the spectrum (energy fluence, fluence rate etc). This can be done by studying the pattern of the interactions which take place between the particles of the beam and the matter of the detector (spectrometer) which is used. X-ray spectroscopy using solid-state detectors is continually developing.

X-ray photons of energies in the range below 30 keV can be measured with a silicon(lithium) [Si(Li)] X-ray detector system, while sodium iodide(thallium) [NaI(Tl)] systems are useful for photons of

higher energies. Comparative study shows that the spectrum response of the radiation beam is of higher resolution with Si(Li) than with either a proportional counter or NaI(Tl), and that the resolution of NaI(Tl) is less than that of a proportional counter (EG & G Ortec Co. Ltd, 1984). A similar comparison has been undertaken using commercially available NaI-(Tl), and a proportional counter which has been specially constructed to analyse the spectra of the X-ray machine at differing applied voltages. (See Appendix A).

4.3.1 Construction of the Proportional Counter

A proportional counter is in effect an ionisation chamber with gas amplification. It delivers a pulse proportional in height to the number of primary ions formed in the gas, and hence, as the average energy per ion pair is constant and known for the given gas mixture, the pulse height is also proportional to the energy dissipated in the gas.

A proportional counter can be used as a spectrometer, by determining the distribution of pulse height by means of a multichannel analyser (MCA), by scanning with a single-channel analyser, or by differentiating the curve obtained by plotting the pulse rate against the discriminator setting. There are now various computer software packages for MCA. If the gas gain is the same at all parts of the counter, the result gives the distribution of the number of primary ions formed within the sensitive medium by individual particles. This in turn corresponds to the spectrum of energy dissipation.

The design of a proportional counter is limited by some important practical features: high voltage insulation, gas amplification consistent with proportionality, and the requirements of gas pressure and volume. These factors determine the choice of dimensions, and such applied parameters as the anode and cathode radii, r_a and r_c , the applied

voltage, V , the gas pressure, p , and, to a lesser degree, the length of the counter, l .

Our proportional counter has been designed to have a cylindrical geometry, a stainless steel anode wire of radius, $r_a = 0.005$ cm, a coaxial brass cathode of internal radius $r_c = 6.25$ cm and length, $l = 28$ cm. And has two field tubes each of 1.22 cm in diameter. The effective length is 20.4 cm (Figure 4.10).

If a high negative voltage, V , is applied to the anode, the electric field, E_r , at any radial distance, r , from the centre of the counter is given by

$$E_r = \frac{V}{r \ln(r_c / r_a)} \quad 4.1$$

The voltage, V_r , at any radial distance, r , from the centre of the counter will be

$$V_r = \frac{V \ln(r / r_a)}{\ln(r_c / r_a)} \quad 4.2$$

Equation 4.2 is important in the calculation of the field tube voltage.

There is greater latitude in the choice of filling gas. In order to operate the proportional counter faster, and to enable it to differentiate between individual ionising particles according to the number of primary ions formed within the sensitive volume, any gas which does not attach electrons is suitable. The pressure may vary from 1 or 2 cm Hg, to several atmospheres. It is not essential to include a quenching agent since the probabilities of the various processes responsible for the initiation of secondary discharges are so small that spurious pulses are rare, provided that the initial pulse is not too large (Emery 1966). However, its addition does improve the performance of the counter.

Despite careful consideration of the design factors, good counting characteristics, stability of gas gain, long flat plateaux, and 100% efficiency of particle detection may not be attained, simply because the electric field per unit pressure, E/p , at the collecting electrode is not sufficient to ensure saturation collection of the ions. Therefore, Watt (1967) has published some approximate saturation values (E/p in $V\text{ cm}^{-1}\text{ Torr}^{-1}$). These values play a very important role in minimising the attachment and recombination losses, improving the resolution and the counting plateaux, and making the counter less susceptible to the presence of small amounts of electron-attaching impurities (eg O_2 and H_2O vapour).

To satisfy all these requirements, a gas mixture of 90% Argon and 10% Methane (as the quenching agent) has been selected.

The gas gain, (the proportional factor of gas multiplication), can be defined as the ratio of the number of charges collected at the anode to the actual number of primary charge particles formed by the ionising radiation in the counter's volume. The number of ion pairs, N_e , initially formed can be given by

$$N_e = \epsilon / w \quad 4.3$$

where ϵ is the total energy dissipated in the counter, and w is the mean energy required to produce an ion pair. This mean energy, w , may be taken as constant for the whole spectrum distribution.

If it is assumed that the counter is operated within the proportionality region, the total number of charged particles collected, N_T , is equal to GN_e , where G is the gain factor.

The gas gain for a proportional counter (cylindrical type) has been given by Campion (1971) as

$$\ln(G) = AV/B \ln\left(\frac{r_c}{r_a}\right) \left[\exp(-r_a BP \ln\left(\frac{r_c}{r_a}\right) / V) - \exp(-r_c BP \ln\left(\frac{r_c}{r_a}\right) / V) \right] \quad 4.4$$

where A and B are constants which have been determined by Campion and Kingham (1971 a, b) as $9.9 \text{ cm}^{-1} \text{ torr}^{-1}$ and $212 \text{ V cm}^{-1} \text{ torr}^{-1}$ respectively.

The electrons which are produced induce a pulse smaller than that induced by the positive ions. Thus the major contribution in the voltage drop is due to the positive ions, which is a function of time. The pulse voltage, V_t , can be expressed by

$$V_t = \frac{N_e G e \ln(1 + t/t_0)}{2 C \ln(r_c/r_a)} \quad 4.5 a$$

where V_t is the pulse voltage height at time t , e is the electronic charge, and C is the capacitance of the counter.

$$t_0 = \frac{p r_a^2 \ln\left(\frac{r_c}{r_a}\right)}{2 V M}$$

where M is the positive ion mobility at gas pressure, p .

Equation 4.5a suggests that the counter amplification time constant, t_0 , should be equal to or greater than the collecting time, t , of the positive ions (ie $t = [(r_c/r_a)^2 - 1] t_0$). Thus equation 4.5a will be reduced to

$$V_t = N_e G e / C \quad 4.5 b$$

From equations 4.1 and 4.5 b, the final pulse height of the counter is proportional to the energy deposited, which can be given as

$$V_t = G e \epsilon / C w \quad 4.6$$

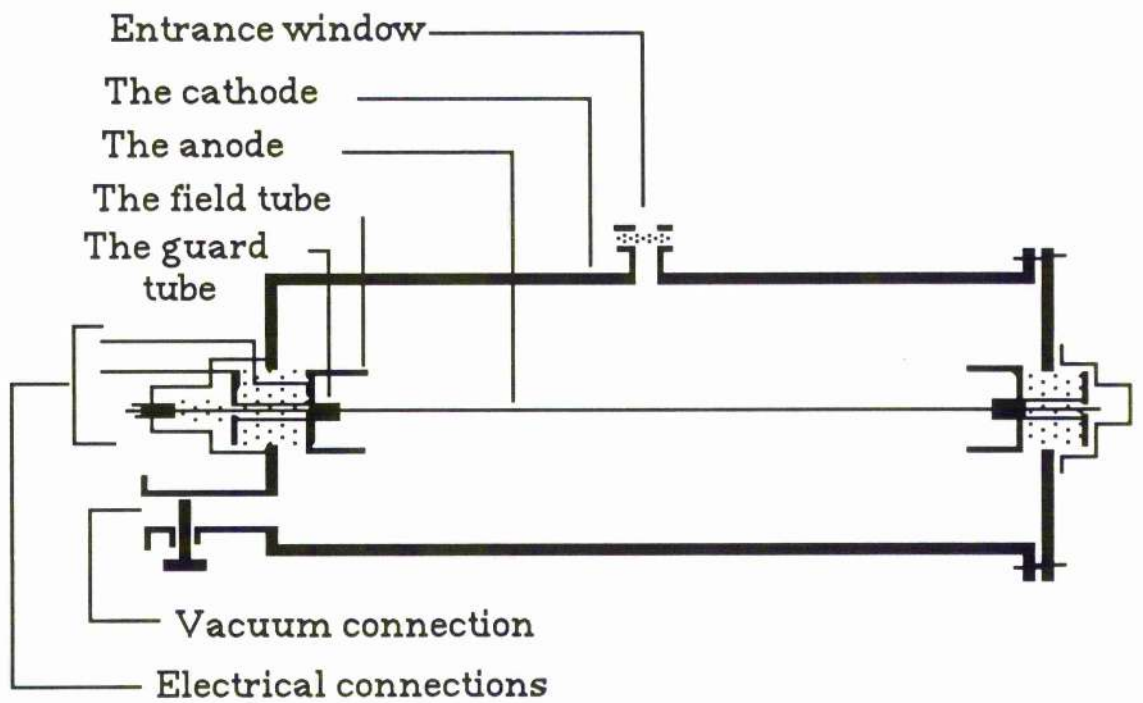


Figure 4.10 : The component parts of the proportional counter

The resolution power of the counter is dependent on a number of instrumental and statistical factors.

The instrumental factors include:

(a) The counter and amplifier gain must remain constant, and the gas gain constant over the whole of the counter's volume.

(b) The high voltage supplier and the amplifier must be very stable.

(c) The gas density must be as closely controlled. (In the flow type of counter it will be necessary to control the temperature and the barometric pressure of the gas.)

(d) The volume occupied by an avalanche is so small that the possibility of an ionisation taking place near the anode can be neglected. It is important that the multiplication in the avalanche should be the same at all points on the wire. This is most simply achieved by having a very uniform wire accurately centred on the axis of the cylindrical cathode.

(e) The electric field at the two ends of the anode might be distorted. This can be reduced by introducing a conductor of greater radius than the anode. Cockroft and Curran (1951) solved this problem by introducing a "field tube" concentric with the anode and extending slightly beyond its extremities. (Figure 4.10). To this tube a potential, V_r , which can be calculated from equation 4.2, is applied, where r is the radius of the "field tube".

(f) Leakage current problems can be overcome by introducing guard tubes into both sides of the anode. These may serve two different purposes, to prevent current leaking from the high voltage electrode to the collector, (screening of the anode), and to define the volume within the counter from which the electrons can reach the collecting electrode.

The guard tube must surround the collecting electrode, and be maintained at the same applied voltage.

The statistical factors include statistical fluctuation, both in the size of the individual avalanches, and in the number of primary ions formed in the counter. (See Emery, 1966).

4.3.2 Purity Testing of the Photon Beam

The photon beam was tested to determine the range of the energy distribution. A characteristic X-ray machine is more efficient when producing photons in a narrow range of energies. Since photons are attenuated primarily by photo-electric, Compton, and pair production interactions (see section 3.2) the intensity of the radiation decreases exponentially with the depth of penetration into the absorbing material.

Photon attenuation was tested with aluminium, (table 4.1) and the transmission curve drawn (figure 4.11).

The homogeneity of an X-ray beam can also be derived from the intensity equation (equation 4.7).

$$I = I_0 e^{-\mu x} \quad 4.7$$

where I_0 is the initial beam intensity, I is the beam intensity after transmission through an absorbing medium, x is the thickness of the medium and μ is its linear attenuation coefficient.

When $I = 1/2 I_0$, x is known as the half value layer (HVL) of the absorbing medium. From equation 4.7 we get, $\ln(I/I_0) = \mu x$, hence

$$\ln(0.5) = \mu x_{1/2} \quad 4.8$$

The homogeneity factor, H , is defined by, $H = (HVL_1)/(HVL_2)$, where HVL_1 is as defined above, and HVL_2 is the additional depth of

material required for a further reduction of 50% in the beam intensity. The homogeneity factor has been determined for the X-ray beam (table 4.1, figure 4.12)

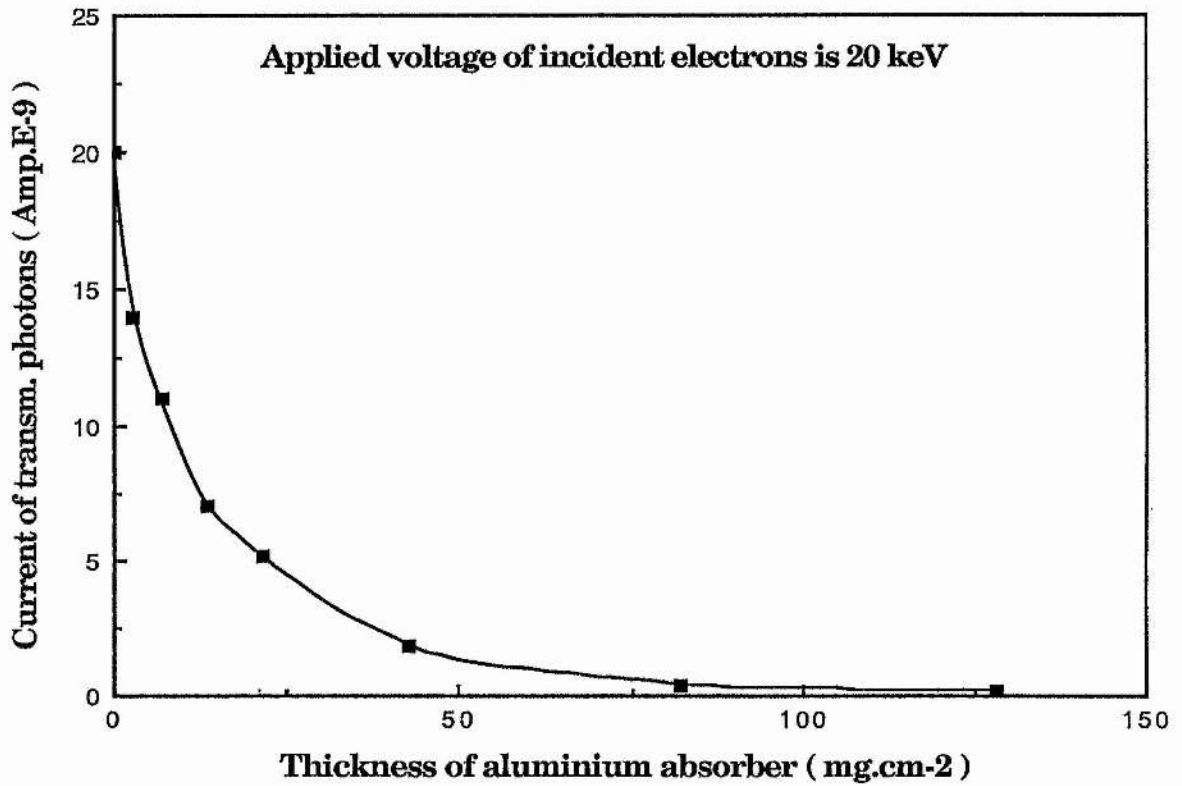


Figure 4.11: Photon transmission curve attenuated through an aluminium absorber.

Applied Voltage (keV)	Transmitted Ionisation Current through Aluminium absor. of Different Thicknesses in mg.cm^{-2} (Amps $\times 10^{-9}$)			
	0.0 mg.cm^{-2}	2.75 mg.cm^{-2}	6.75 mg.cm^{-2}	13.5 mg.cm^{-2}
10.0	4.4	1.90	1.10	0.47
11.0	5.30	2.50	1.45	0.72
12.0	6.20	3.20	2.00	1.10
12.5	7.20	3.90	2.50	1.45
13.0	8.30	4.70	3.15	1.85
14.0	9.40	5.50	3.80	2.40
15.0	11.00	6.40	4.60	2.90
15.7	13.00	7.50	5.35	3.50
16.0	14.00	8.60	6.25	4.10
17.0	15.00	10.00	7.20	4.75
18.0	16.50	11.50	8.10	5.45
19.0	18.00	13.00	9.20	6.30
20.0	20.00	14.00	11.00	7.05
20.5	21.50	15.00	12.00	7.80
21.0	23.00	16.50	13.00	8.90
22.0	24.50	18.00	14.20	9.80
22.5	26.00	20.00	15.80	11.00
23.0	28.50	21.50	17.00	12.00

Table 4.1 : Photon attenuation through different thicknesses of aluminium absorber with 20.4W applied to the filament

Applied Voltage (keV)	Transmitted Ionisation Current through Aluminium absorber of Different Thicknesses in mg.cm^{-2} (Amps $\times 10^{-9}$)			
	21.6 mg.cm^{-2}	42.7 mg.cm^{-2}	82 mg.cm^{-2}	128 mg.cm^{-2}
10.0	0.30	0.069	0.009	0.0025
11.0	0.48	0.13	0.019	0.005
12.0	0.72	0.21	0.034	0.011
12.5	1.00	0.31	0.053	0.018
13.0	1.40	0.43	0.076	0.028
14.0	1.80	0.57	0.11	0.041
15.0	2.25	0.72	0.14	0.056
15.7	2.70	0.89	0.17	0.073
16.0	2.90	1.10	0.22	0.093
17.0	3.20	1.30	0.25	0.120
18.0	3.70	1.50	0.31	0.140
19.0	4.50	1.65	0.36	0.170
20.0	5.15	1.85	0.41	0.195
20.5	5.75	2.20	0.47	0.225
21.0	6.20	2.40	0.53	0.255
22.0	6.85	2.60	0.59	0.290
22.5	7.30	2.90	0.65	0.320
23.0	7.80	3.10	0.71	0.360

Table 4.1 (Contd) : Photon attenuation through different thicknesses of aluminium absorber with 20.4 W applied to the filament

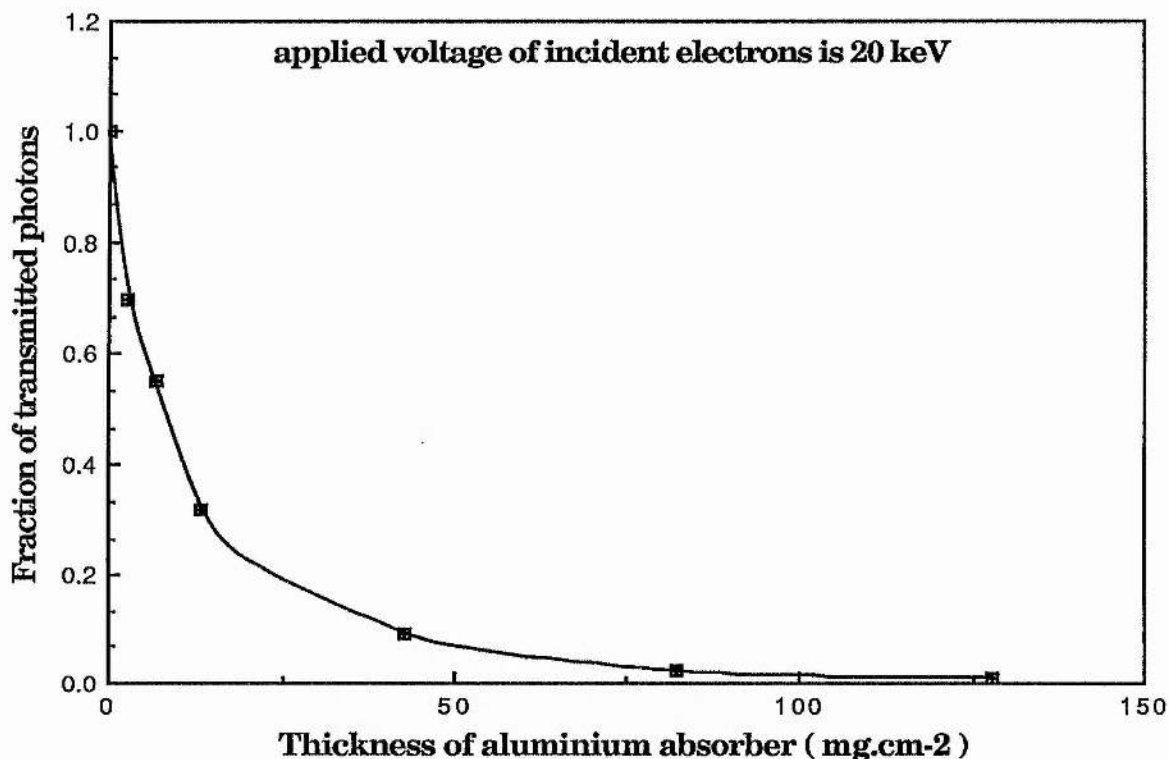


Figure 4.12: Fraction of transmitted Photons through aluminium absorber

4.3.3 Energy Calibration Curve and the Determination of Unknown Photon Energy

To investigate the energy of unknown photons emitted by a source (our X-ray machine), the photopeak energies of known sources are measured and an energy calibration curve drawn. From this, the unknown source energy can be determined.

A calibration curve is created by using the following procedure. Having set up the electronic equipment as in figure 4.13, determine a suitable detector for the appropriate energy range. (In our procedure NaI(Tl) was used.) Place the known source (Cs^{137} , which gives X-rays of energy $K\alpha_1 = 32.19$ keV and $K\alpha_2 = 31.82$ keV with yield $3.92 \text{ E-}2$ and $3.13 \text{ E-}2 \text{ (Bq-s)}^{-1}$ respectively; Am^{241} , $E_{\gamma 2} = 26.34$ keV and $E_{\gamma 14} = 59.54$ keV with yield $2.4 \text{ E-}2$ and $3.57 \text{ E-}1 \text{ (Bq-s)}^{-1}$ respectively) 2 cm in front of the detector window. Adjust the gain controls of the linear amplifier

and the gain output of the whole system, until a reasonable spectrum can be detected on the multichannel analyser, MCA. Accumulate the spectrum of the known source for a time period long enough to determine the peak position. Read the corresponding channel number for each peak. Repeat the procedure for all known sources.

Plot the known energy of the peaks against the corresponding channel numbers to give the calibration curve. The curves for our data are depicted in figure 4.14.

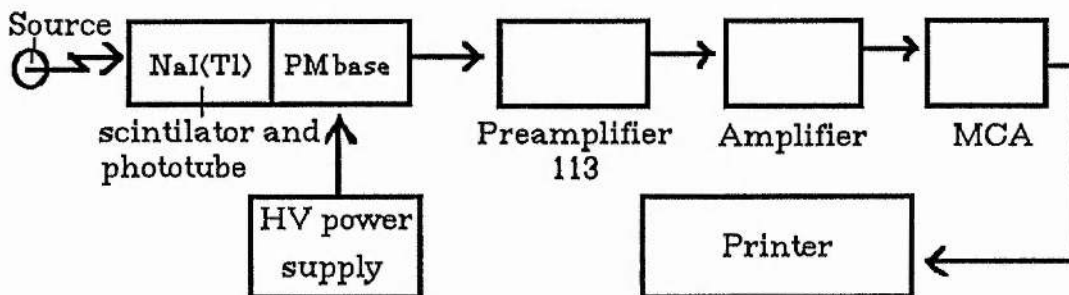


Figure 4.13: The electronic equipments set up for radiation source spectroscopy by using NaI(Tl) as spectrometer

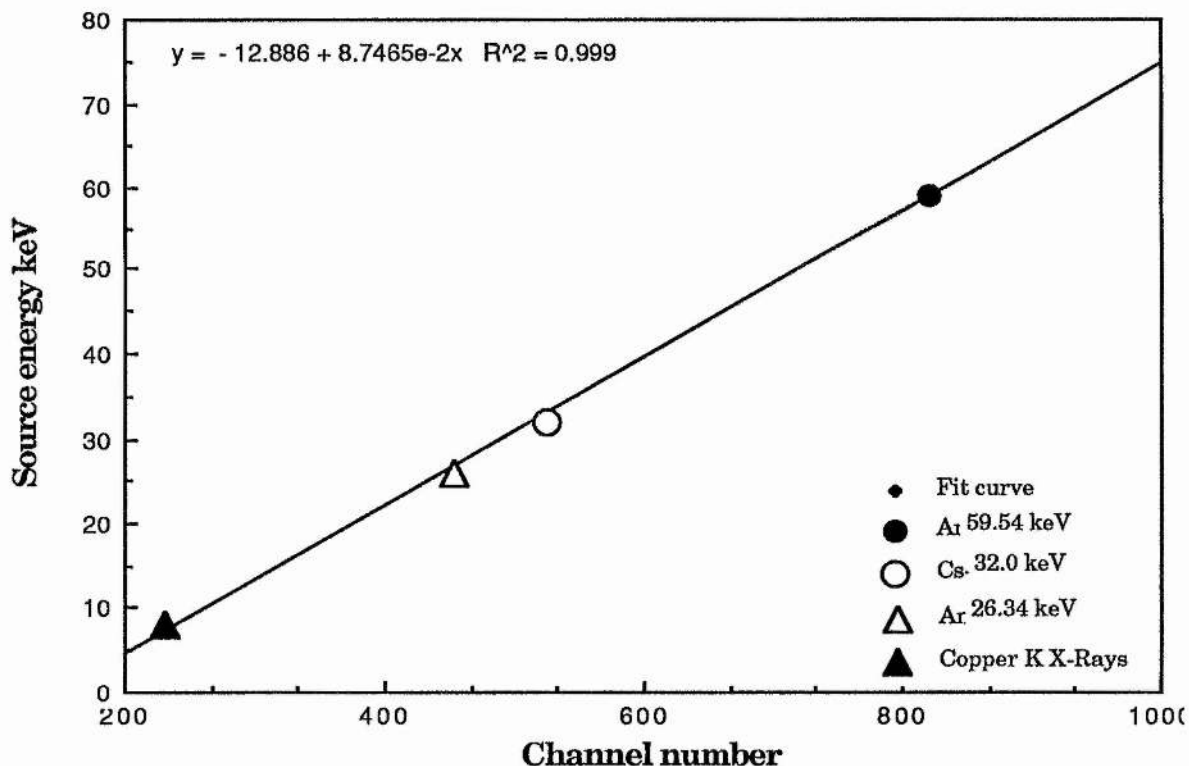


Figure 4.14 : Calibration curve of radiation sources.

To determine the energy of the unknown source, the same procedure is followed, ensuring that the electronic parameters remain constant, accumulation takes place over the same time period, and that the detector is placed at the same distance from the source exit window. From the resulting spectrum, the channel number corresponding to the peak is determined, and the energy of this peak read from the calibration curve. The spectra for the known sources and the X-rays are given in Appendix A.

4.4 Attenuation of the Photon Beam

The photon's fluence is attenuated on several occasions before it reaches the detecting material in the counter. In our experimental arrangement this occurs at:-

(i) The window of the exit of the X-ray machine, where the beam passes through 1.25×10^{-2} cm of Beryllium foil.

(ii) The flight column where it passes through 4.00 cm of air between the Beryllium foil and the detector's window.

(iii) The window of the detector be it air equivalent ionisation chamber, (3×10^{-3} g cm⁻² thick of polythene), calorimeter, or proportional counter, (both with window of aluminium foil 0.01 mm thick).

These three types of attenuation have been calculated and are presented in table 4.2.

There is another type of attenuation which occurs within the sample itself. This results from the distribution of the dose through the depth, with the lowest dose occurring at the bottom, and the highest at the top of the sample, providing that the beam is directed downwards.

The converse holds true if the beam is directed upwards. To allow for this, the mean dose has been used in all calculations.

Attenuating material	Thickness (cm)	Density (gm cm ⁻³)	μ/ρ * (mass attenuation coef.) (cm ² gm ⁻¹)	% Absorption of the original beam
Beryllium (window of X-ray machine)	1.25×10^{-2}	1.848	1.08	2.46
Air (flight column, dry air STP)	4.0	1.205×10^{-3}	9.72	4.6
Polyethylene (window of ionisation chamber)	3×10^{-3} gm cm ⁻²		3.84	1.15
Aluminium (window of calorimeter or proportional counter)	10^{-3}	2.699	49.55	12.52

[* Mass attenuation coefficient from Hubbell (1982)]

Table 4.2 : Attenuation Correction for K-X-ray from copper

4.5 Calorimetry

Calorimetry is an absolute method of measuring the dose absorbed by a substance in a radiation field (X-, γ -, electron, etc). The response of the calorimeter is a function of temperature change.

This method is a well established, and widely used technique (Gunn 1964, 1970, 1976, Domen 1987, and Meger *et al* 1987). Gunn

(1964, 1970, 1976) has given a comprehensive survey of the field. Greening *et al* (1968) described a calorimeter for the measurement of energy fluence in beams of low energy X-rays (≤ 30 keV) in which the beam is totally absorbed. Table 4.3 summarises the published work concerned with the calorimetric determination of X-ray energy fluence and intensity.

The total absorption technique is particularly suited to the measurement of very low energy X-rays. However, calorimeters have some disadvantages and limitations. Although their sensitivity is adequate for the radiation intensities and dose rates used in diagnostic, therapeutic and most industrial applications, it is insufficient for radiation protection purposes.

There are some processes which lead to the loss of some of the energy that should be measured by the calorimeter. These include scattering of radiation out of the calorimeter, photonuclear reactions resulting in a change in the rest mass of the nucleus, the emission of a penetrating neutron that carries energy out of the calorimeter, Bremsstrahlung production by secondary electrons, and exo- or endothermic chemical reactions.

The effect of these processes on a calorimetric measurement is dependent upon whether the energy fluence or the absorbed dose is the quantity being measured. The measurement of energy fluence requires that all of the energy in the radiation beam be converted to heat in the calorimeter. In this case, the calorimeter should be designed to minimise all of the above effects, and corrections should be applied to account for those effects which cannot be eliminated. The measurement of absorbed dose is dependent on the actual energy absorbed by the material.

Reference	Energy (KV)	Absorber	Intensity and accuracy $\mu\text{W cm}^{-2}$	Detector
Kulenkampff (1926)	6 - 22	Silver	$1 \pm 5\%$	Thermocoup.
Rump (1927)	43 - 150	Mercury	$100 \pm 1.6\%$	Capillary rise
Crowther & Bond (1929)	50	Oil	$200 \pm 2\%$	Thermocoup.
Laughlin <i>et al</i> (1953)	400	Lead	$100 \pm 1\%$	Thermistor
Pauly (1959)	25 - 45	Cu, Al, Ph Plexiglass	$50 - 50,000$ $\pm 2\%$	Thermocoup.
Coekelbergs <i>et al</i> (1965)	30-60	Gold	$100 - 1000 \pm 7\%$	Thermocoup.
Gomberg <i>et al</i> (1965)	5 - 10	Gold	$1 - 5 \pm 2.5\%$	Thermistor
Greening <i>et al</i> (1968)	≤ 30	Gold	$1.7 - 240$ $\pm 0.25\%$	Thermistor

Table 4.3 : Calorimetric determinations of energy fluence with different absorbers and temperature detectors (after Greening *et al*, 1968)

4.5.1 Principles of the Calorimeter

A calorimeter's design depends on the mechanisms of heat transfer, the relation between thermal energy and temperature changes, and temperature measurement and control.

4.5.1.1 Heat Transfer

The essential factor determining the design, and optimising the accuracy of a calorimetric system is the net rate of heat transfer between the absorber and its surroundings. The problem of transfer can be subdivided into three phenomena: convection, radiation and conduction.

The latter is the predominant mode of heat transfer, thus care must be taken to minimise the rate of heat loss through the connections.

According to Newton's law of cooling, the total heat transfer loss can be expressed (in Wm^{-2}) as:

$$\left(\frac{1}{A}\right) \left(\frac{dE}{dt}\right) = -\sum_i h_i (T - T_0) \quad \text{W/m}^2 \quad 4.9$$

where A is the area of the absorber, h_i represents the heat transfer coefficient, and T and T_0 denote the temperatures of the absorber and its surroundings respectively. (Laughlin and Genna, 1966).

(i) Convective Heat Transfer

Under normal atmospheric pressure conditions, the dominant mode of heat transfer through air is convection. Heat is transported by air movement.

Experimental investigation of natural convection between parallel plates, a distance, d , apart, at temperature difference, ΔT , (in $^{\circ}\text{C}$), was reported by Bosworth (1952) whose data were presented in terms of the dimensionless Raleigh number, R ,

$$R = m_c d^3 \Delta T \quad 4.10$$

where m_c is the convection modulus for air (in $\text{cm}^{-3} \text{ } ^{\circ}\text{C}^{-1}$).

No heat convection was observed when $R < 1620$. On the other hand, the convection modulus for air is a function of gravitational acceleration, and of the air density. It is proportional to the square of the density, which, in turn, is proportional to the pressure, P . Thus heat convection will not occur under the following condition:

$$P/760 < [16.2 / d^3 \Delta T]^{1/2} \quad 4.12$$

where P is the air pressure in torr (mm of Hg).

If d (separation between the absorber and its jacket) is less than 3 cm, ΔT is less than 10°C , and P is less than 10 torr, then the convection heat transfer coefficient (h_1) will be very small, and can be ignored.

(ii) Conductive Heat Transfer

Energy can be transported along thermal gradients, as a result of intermolecular collisions in the calorimeter from the absorber into its surrounding air or other substance. Heat flow can be described by equation 4.9.

The conduction heat transfer coefficient (h_2 or h_c) is proportional to the thermal conductivity, k . The proportionality constant depends on the geometrical shape and dimensions of the conducting path. (For parallel surfaces, $h_c = k/d$, for concentric spheres, $h_c = k [(r/d) + (d/r)]$, and for concentric cylindrical surfaces, $h_c = k / [r \ln(1 + d/r)]$, where r is the radius of the sphere or cylinder, and d is the separation between the surfaces.) Thus, for our design, (concentric cylindrical surfaces),

$$h_c = k / [r \ln(1 + d/r)] \quad 4.11$$

The thermal conductivity of air, k , is proportional to $\rho V \lambda C_v$, where ρ is the density of the air, V is the mean velocity of molecules, λ is the mean free path of molecules, and C_v is the thermal capacity at constant volume. In air, the mean free path, λ , is 4.5 cm at 10^{-3} mm Hg, and 45 m at 10^{-6} mm Hg. (At room temperature, λ is roughly equal to $5/p$ cm, where p is the pressure in m torr, ie 10^{-3} mm Hg.)

To lower the heat conduction rate transfer in a calorimeter, the pressure should be reduced as much as possible. Heat can be transferred by conduction through electrical connections or suspension

wires of the absorber, and other materials inside the jacket. The heat leakage rate (heat conduction rate) of these materials, L_c , is given by

$$L_c = \sum_i (k_i A_i) / l_i \quad 4.12$$

where k_i , A_i , and l_i are the thermal conductivity, cross-section, and length of material i respectively.

(iii) Radiative Heat Transfer

This mode of heat transfer involves the transport of electromagnetic energy from one body to another. This can occur even in space. For a surface that is not black, the energy current density radiated at an absolute temperature, T , can be expressed as

$$\left(\frac{1}{A}\right) \left(\frac{dE}{dt}\right) = \epsilon \sigma T^4 \quad 4.13$$

where σ is the Stefan-Boltzman constant ($5.67 \times 10^{-12} \text{ Wcm}^{-2} \text{ K}^{-4}$), and ϵ is the ratio of the energy emission of a surface to that which would be emitted by a black body at the same temperature.

A calculation of the net rate of radiative heat transfer between a suspended absorber and its surroundings involves consideration of that fraction of the radiation emitted by each body which is absorbed by the other, since the bodies concerned are not black. Thus many partial absorptions and reflections will occur. The final expression for the net heat flow between the absorber and its surroundings is

$$\frac{1}{A} \frac{dE}{dt} = \frac{\sigma F(T^4 - T_0^4)}{(T - T_0)} \quad 4.14$$

where F is a function of emissivities ϵ , ϵ_0 and areas A , A_0 of the radiative body (the absorber) and the jacket materials, and T, T_0 are the absolute temperatures of the inner body surface and the enclosure respectively.

From equations 4.9 and 4.14, the radiative heat transfer coefficient, h_3 , or h_r , may be given as

$$h_r = \frac{\sigma F(T^4 - T_0^4)}{(T - T_0)} \quad 4.15$$

McAdams (1942) has given a useful approximation for the factor, F , for an absorber suspended in an enclosure.

$$F^{-1} = \left(\frac{1}{\epsilon}\right) + \left(\frac{A}{A_0}\right) \left(\left(\frac{1}{\epsilon_0}\right) - 1\right)$$

If $A_0 \gg A$ (ie $A/A_0 \approx 0$), or if $\epsilon_0 = 1$, then $F = \epsilon$, and the area of the absorber, and the temperature difference between it and its enclosure, will determine the loss of radiative energy.

4.5.1.2 Methods of Calorimetry and Temperature Change Control

There are two methods of calorimetry, isothermal and non-isothermal. In the former it is difficult to establish a state of thermodynamic equilibrium (Laughlin and Genna, 1966). Thus it is easier to construct and use a non-isothermal calorimeter for which a constant environmental temperature is assumed, and the correction for heat leakage can be made.

There are two ways of measuring temperature change. These are by using either a thermocouple or a resistance thermometer.

A thermocouple, (or a thermopile which is composed of a number of thermocouples), consists of a pair of conductors of different metals, and measures, using a potentiometer, the electromagnetic force, emf, which is generated at the junction of the conductors.

A resistance thermometer gives a higher accuracy. It may be a semi-conductor thermometer or a platinum resistor. Both are called

thermistors. The resistance-temperature relationship of the former is approximately exponential.

$$R_T = R_0 \exp \beta (1/T - 1/T_0) \quad 4.16$$

where R_T and R_0 are the resistances at temperature T and T_0 respectively, and β is the characteristic temperature constant ($^{\circ}\text{K}$). β can be determined by plotting $\log R$ against $1/T$. (table 4.4 and figure 4.15). The temperature coefficient is defined by

$$\left(\frac{dR}{dT}\right) = \alpha_T R \quad \text{ie } \alpha_T = \left(\frac{1}{R}\right) \left(\frac{dR}{dT}\right).$$

By differentiating R with respect to T in equation 4.16,

$$\left(\frac{dR}{dT}\right) = \left(\frac{-\beta R_0}{T^2}\right) \exp \beta (1/T - 1/T_0)$$

By substituting for α_T we get

$$\alpha_T = -\left(\frac{\beta}{T^2}\right) \quad 4.17$$

Resistance, R (k Ω)	log R	Temperature, T ($^{\circ}$ K)	1/T ($\times 10^{-3}$)
10.33	1.014	297.2	3.364
9.7	0.987	298.0	3.356
9.33	0.970	299.0	3.344
8.8	0.944	301.0	3.322
8.36	0.922	302.0	3.311
7.67	0.884	304.0	3.289
6.36	0.823	308.0	3.247
6.38	0.805	309.0	3.236
5.94	0.774	312.0	3.205
5.44	0.736	313.0	3.195
5.24	0.719	314.0	3.185
5.02	0.701	315.0	3.175
4.84	0.685	316.0	3.165
4.52	0.655	318.0	3.145
4.34	0.637	319.0	3.135
4.16	0.619	320.0	3.125
3.85	0.585	322.0	3.105
3.69	0.567	323.0	3.096
3.43	0.535	325.0	3.077
3.20	0.505	327.0	3.058
3.05	0.484	328.0	3.049
2.57	0.410	333.0	3.003
2.37	0.375	335.0	2.985
2.16	0.334	338.0	2.959
1.93	0.286	341.0	2.933
1.86	0.270	342.0	2.924
1.77	0.248	343.0	2.915
1.71	0.233	345.0	2.899
1.67	0.223	346.0	2.890
1.60	0.204	347.0	2.882
1.55	0.190	348.0	2.874

Table 4.4 : Relationship between resistance and temperature of the thermistor

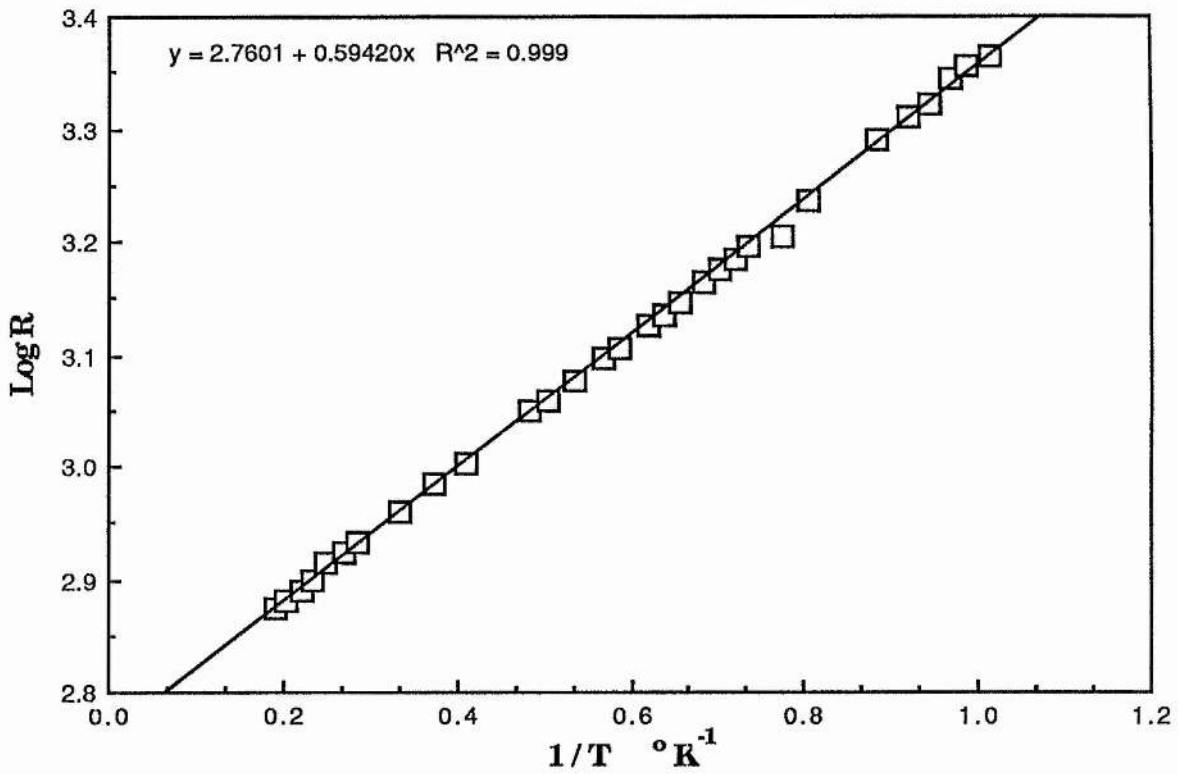


Figure 4.15: Characteristic temperature constant of the thermistor.

In order to get a very high accuracy in measuring a small temperature change, the semiconductor thermistor is preferred because its temperature coefficient is one order higher (negative) than for a platinum thermistor (α_T of platinum at 298° K is about 0.4). For further details see references of table 4.3.

For the best performance of the thermistor, the following characteristics have been considered:

(i) Self-heating

The rise in the temperature of the thermistor comes from the electrical current passing through it. This self-heating is described by the dissipation constant of the thermistor, H_D , which is the amount of power in mW which raises the temperature of the thermistor by one degree centigrade, and is given by

$$H_D = \frac{R I^2}{\Delta T} \times 10^3$$

4.18

where R is the thermistor resistance in ohms, I is the current passing through it in amps, and ΔT is the temperature difference in degrees centigrade. (table 4.5 and figure 4.16).

(ii) Thermal Time Constant

This constant measures the speed of the thermistor's response to the change in temperature, and is dependent on the characteristic temperature constant, β .

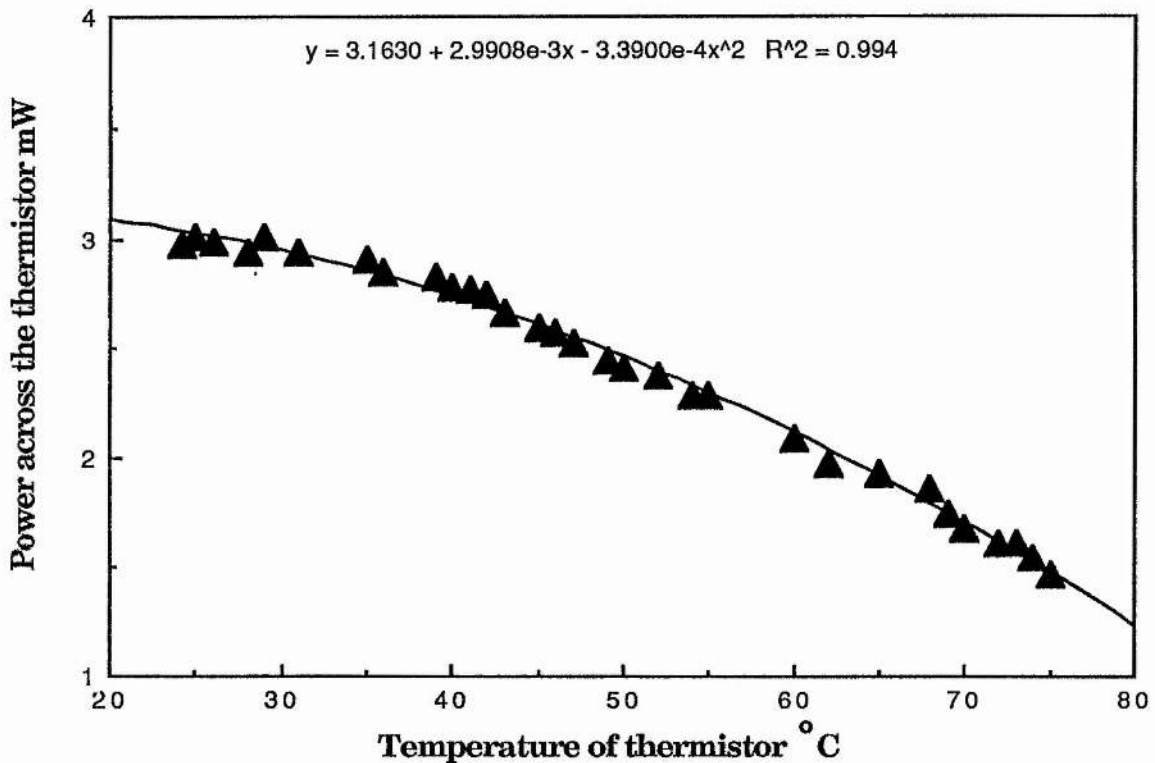


Figure 4.16 : relation between temperature rising and power dissipation.

Temperature °C	Resistance kΩ	Current mA	Voltage V	Power mW
24.2	10.33	0.450	6.6	2.97
25	9.70	0.470	6.4	3.01
26	9.33	0.475	6.3	2.99
28	8.80	0.490	6.0	2.94
29	8.36	0.510	5.9	3.01
31	7.67	0.525	5.6	2.94
35	6.66	0.560	5.2	2.91
36	6.38	0.570	5.0	2.85
39	5.94	0.590	4.8	2.83
40	5.44	0.605	4.6	2.78
41	5.24	0.615	4.5	2.77
42	5.02	0.625	4.4	2.75
43	4.84	0.635	4.2	2.67
45	4.52	0.650	4.0	2.60
46	4.34	0.660	3.9	2.57
47	4.16	0.665	3.8	2.53
49	3.85	0.680	3.6	2.45
50	3.69	0.690	3.5	2.42
52	3.43	0.700	3.4	2.38
54	3.20	0.715	3.2	2.29
55	3.05	0.725	3.0	2.29
60	2.57	0.750	2.8	2.10
62	2.37	0.760	2.6	1.98
65	2.16	0.770	2.5	1.93
68	1.93	0.780	2.4	1.87
69	1.86	0.795	2.2	1.75
70	1.77	0.800	2.1	1.68
72	1.71	0.810	2.0	1.62
73	1.67	0.815	2.0	1.62
74	1.60	0.820	1.9	1.55
75	1.55	0.820	1.8	1.47

(Initial battery voltage : 9.8 V)

Table 4.5 : Relationship between resistance, temperature and the power dissipated in the thermistor

(iii) Thermistor Tolerance

This is the stability and reproducibility of the thermistor resistance at any given time. It depends on the magnitude of the resistance tolerance. Thus the most suitable thermistor is one with a small tolerance.

4.5.1.3 Calorimeter design

The component parts of the calorimeter which has been designed to measure a high fluence of low energy photons produced in our characteristic X-ray machine are shown in figure 4.17. The design has taken into account the factors affecting heat loss measurement techniques as described in section 4.5.1.

(i) The Collimator

This is made of a disc of brass 12 cm in diameter and 0.6 cm thick, at the centre of which a hole of 3 mm diameter has been drilled to allow a parallel beam of photons to be directed towards the absorber (Faraday cup). The calorimeter is mounted on the linear motor drive in such a way that the hole in the collimator is directed towards the source. It is then easy to scan the whole beam to determine the distribution of the photons across the exit window.

(ii) The Entrance Window

To keep the internal components under low pressure in order to satisfy the best conditions of negligible energy transfer (see section 4.5.1.1), a disc of pure (99.8%) aluminium foil, of thickness 0.01 mm, is fitted over the entrance window. The photon beam intensity will be attenuated according to equation 4.7.

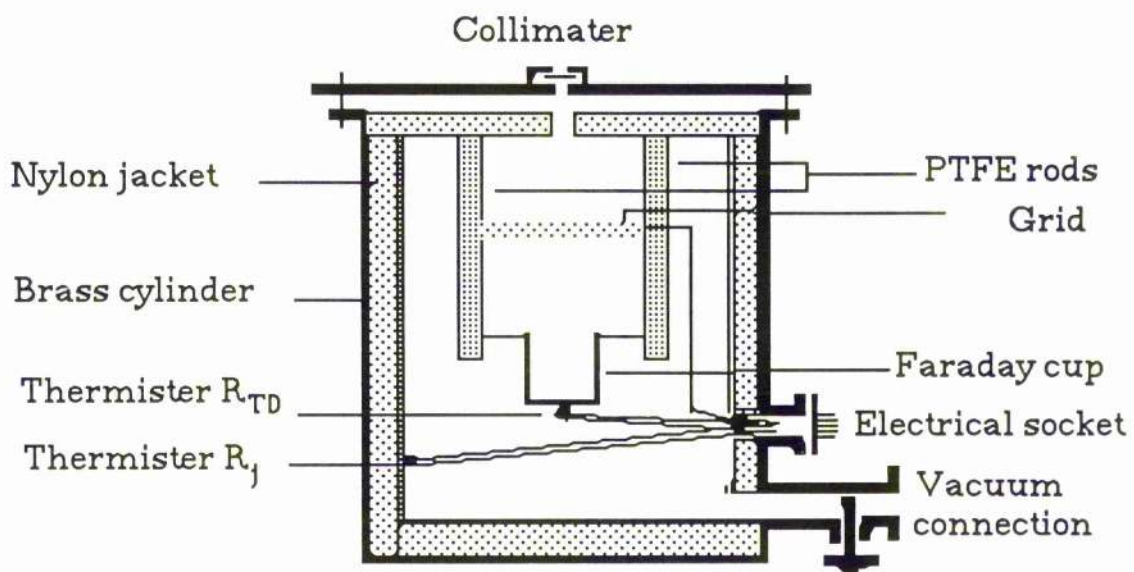


Figure 4.17: The component parts of the calorimeter

(iii) The Bias Grid

A copper micromesh disc (manufactured by EMI Components) with aperture size of 1125 μm , (90% transparency), is mounted on a copper ring and located above the Faraday cup. A negative voltage (100 V) was applied to the grid by means of a variable-power, stabilised high voltage source. This negative bias grid repels the emitted secondary electrons which scatter back into the Faraday cup to be absorbed there.

(iv) The Faraday Cup

There are several factors affecting the choice of the Faraday cup material. It should have a small thermal capacity whilst being sufficiently thick to absorb more than 99% of the incident radiation. A material with high atomic number and a large attenuation coefficient for low energy X-rays is the obvious choice, and by choosing a material with its L - absorption edge at an energy greater than the K-X-rays under investigation, then the fluorescence escape can be reduced.

The thermal conductivity should be high so that any energy deposited is rapidly distributed throughout the absorber. In this way, any spatial distribution of absorbed energy will produce a temperature rise at the thermistor, with minimum delay. To minimise heat transfer by radiation, the thermal emissivity of the material, ϵ , should be low (see section 4.5.1.1).

After consideration of these factors, a gold sheet of thickness 0.32 μm was chosen to make the Faraday cup, which is a cylinder of 1 cm in height, and 1 cm in diameter, opened at one end. The total weight is 1488 mg (including the thermistor weight of 50 mg which is embedded with a heat conductive glue weighing about 5 mg in the bottom of the cup). The heat capacity mc_p (mass of the cup material times the specific heat of gold, 128.93 J Kg⁻¹ K⁻¹), is 0.185 J K⁻¹.

(v) The Thermal and Electrostatic Shielding

The bias grid and Faraday cup were suspended separately by two rods of PTFE to provide electrical insulation for each part, and thermal insulation for the Faraday cup. These rods were fitted into the lower surface of a plastic disc of diameter 9.5 cm. The whole assembly (Faraday cup, bias grid, and the PTFE suspension rods) is enclosed in a plastic cylinder which damps down the effects of temperature fluctuation.

A thermistor, R_{TJ} , is embedded in the internal surface of the plastic cylinder to use as a thermal reference, and to find the absorption efficiency of the Faraday cup.

All the above components are fitted inside a brass cylinder of height 11 cm, and diameter 9.5 cm. This cylinder is provided with connections to the vacuum system and to the measuring circuit.

4.5.1.4 The Electronic Measurement of Temperature Differences

Since the absorbed dose in the calorimeter is a function of temperature changes, a conventional Wheatstone bridge is the preferred circuit for measuring the temperature changes. Figure 4.18 shows the practical circuit, where R_J or R_T , R_1 , R_2 , and R_p comprise the bridge circuit. It is convenient to choose R_J and R_T equal to R_1 and R_2 . In practice, R_p is a potentiometer which can be adjusted to be equal to R_T after irradiation time interval (the current temperature resistance).

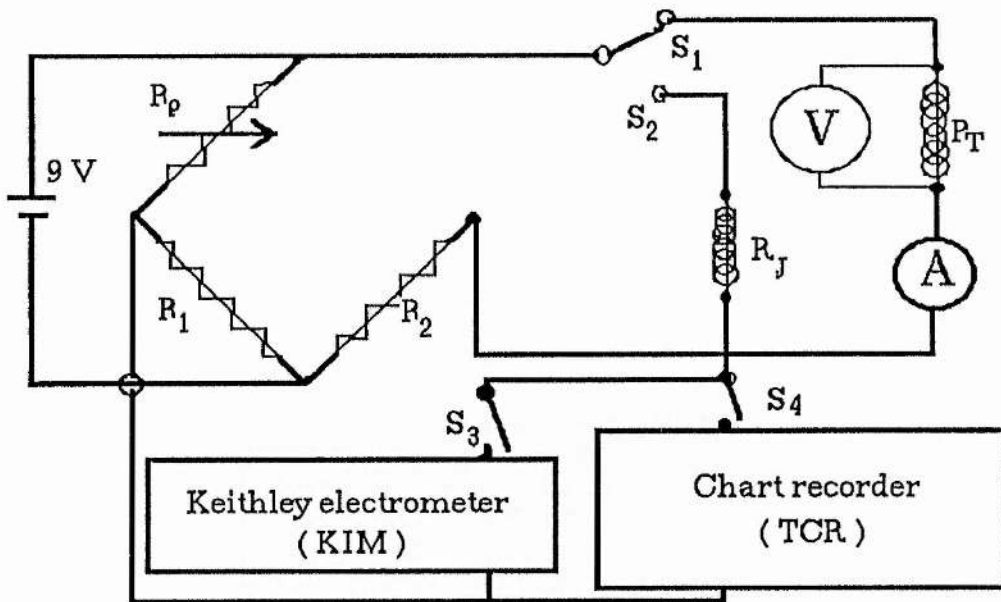


Figure 4.18 : Conventional Wheatstone bridge circuit for measuring the temperature changes in the thermistor of the calorimeter.

The total temperature increase, ΔT , is detected after a time interval Δt , of irradiation. In our arrangement, we assumed that there was a constant dose rate. Then

$$T - T_0 = \Delta T = \left(\frac{T T_0}{\beta} \right) \ln \left(\frac{R_T}{R_{T_0}} \right) \quad 4.19$$

From data which has been given by the manufacturer of the thermistor (RS Components), β is equal to 3795.29 which can be determined by applying equation 4.16, by plotting $\log R$ against $1/T$, (figure 4.15) and using the least squares method.

In figure 4.18, two thermistors, R_J and R_T , were used (see section 4.5.1.3). The output of R_T is connected via the switch S_1 and for R_J through S_2 to the Wheatstone Bridge circuit. R_J reflects the jacket temperature and hence can be used for calibration purposes, since at time $t=0$, $R_J = R_{T_0}$.

The resistance of the thermistor, R_{T_0} , before irradiation was commenced, is scaled via switch S_3 to a Keithley electrometer (KIM), of input impedance $>10^{14}$ Ohms, used as a voltmeter.

A Tekman chart recorder (TCR) of impedance $>10^6$ Ohms was used to display the voltage signal from the bridge through S_4 . The electrometer and the chart recorder were scaled to each other before use.

4.5.15 The Absorbed Dose and Energy Leakage

The actual energy absorbed by the calorimeter, E_D , is

$$E_D = E + E_d$$

where E is the energy which can be determined by practical measurement, and E_d is the energy which is converted into chemical energy in the absorber (energy defect).

From equation 4.9 and section 4.5.1.3 (iv), $dE = mc_p dT$. If we assume that $k = (A / mc_p) \sum h_i$, then the heat leakage rate, $\overset{\circ}{T}$ is

$$\overset{\circ}{T} = \frac{dT}{dt} = -k (T_A - T_j) \quad 4.20$$

where T_A and T_j denote the absorber and the jacket temperatures respectively.

The net constant rate of temperature rise of R_T corresponding to the constant rate of input dT_A/dt is the difference between the real rate, $\overset{\circ}{T}_r = (dE/dt) / (mc_p)$, which we want to measure, and the leakage rate.

Then

$$\frac{dT_A}{dt} = \overset{\circ}{T}_r - \left(\frac{dT}{dt} \right) \quad 4.21$$

Since T_j is considered to be constant, then equation 4.20 summed over T_i to T_f is

$$T_{Af} - T_{Ai} = \left(\frac{T_r^0}{k} \right) (1 - e^{-k\Delta t}) + (T_{Ai} - T_j) e^{-k\Delta t} \quad 4.22$$

where $\Delta t = t_f - t_i$.

The real rate of temperature difference, T_r^0 is given by

$$T_r^0 = \frac{k(T_{Af} - T_{Ai}) - k(T_{Ai}) e^{-k\Delta t}}{(1 - e^{-k\Delta t})} \quad 4.23$$

If $T_{Ai} = T_j$ and $T_m = T_{Af} - T_{Ai}$ then

$$T_m = T_r^0 (1 - e^{-k\Delta t}) / k \quad 4.24$$

$$\text{ie } \frac{dT_r^0}{dt} = T_m k / (1 - e^{-k\Delta t}) \quad 4.24 \text{ b}$$

The absorbed dose, D , is defined as the differential quotient dE_D/dm , where dE_D is the mean energy imparted by ionising radiation to a material of mass dm (ICRU 1980). Thus the dose rate, $\dot{D} = \frac{E_D}{dm} \frac{1}{dt}$.

Then

$$\dot{D} = \left(\frac{1}{m} \right) \left(\frac{dE}{dt} \right) = C_p \left(\frac{dT_r^0}{dt} \right)$$

$$\text{ie } \dot{D} = \frac{C_p k (T_{Af} - T_{Ai})}{(1 - e^{-k\Delta t})} \quad 4.25$$

4.6 Measurement of the Dose from Characteristic X-rays using an air-equivalent Ion Chamber

An air-filled ionisation chamber with air-equivalent walls (graphite/aluminium) for the measurement of exposure over the entire therapy range of photon energies has been manufactured. Chambers of different sizes between 0.03 cc and 0.6 cc in volume can be used to measure exposures. Applications include standardisation of radiation

output from radiation generators and isotropic sources, measuring dose distributions in photon beams, phantoms, and for clinical uses.

The instruments are available commercially, and can be fitted with various perspex build-up caps according to the application. The chamber which has been selected to measure the output of our low energy X-ray machine (~8.0 keV) is a low energy parallel plate ionisation chamber with a sensitive volume of 0.3 cc (low energy X-ray chamber type 2536/3 from Nuclear Enterprises Ltd) and of shallow cylindrical construction. It is fitted with a very thin polyethylene window, graphite-coated and with an acrylic body, located with its effective centre at the position of samples to be irradiated.

The ionisation current was measured with an electrometer. The circuit is shown in figure 4.19. Density of air, ρ_{air} , in the chamber has been corrected to the temperature, t , in $^{\circ}\text{C}$ and under pressure, H , in cm of mercury by using the relation.

$$\rho_{\text{air}} = \frac{0.001293}{1+0.00367 t} \frac{H}{76} \quad 4.26$$

Thus at 20°C and 76 cm Hg , $\rho_{\text{air}} = 1.205 \times 10^{-6}\text{ kg cm}^{-3}$ and the mass of air in the ion chamber (0.3 cm^3 volume) is $0.3615 \times 10^{-6}\text{ kg}$. Then the dose rate, $\overset{\circ}{D}_{\text{air}}$, in the cavity of the chamber is given by

$$\overset{\circ}{D}_{\text{air}} = \frac{I}{M_{\text{air}}} \frac{W_{\text{air}}}{e} \quad 4.27$$

where I is the measured electric current in Amps, M_{air} is the mass of the air in the cavity in kilograms corrected as above, W_{air} is the energy required to release an ion pair in air ($33.85 \pm 0.15\text{ eV}$ from ICRU 1979 a), and e is the electronic charge. Thus from equation 4.27,

$$\overset{\circ}{D}_{\text{air}} = 9.364 \times 10^7 I \quad (\text{Gray/sec.}) \quad 4.28$$

Conversion of the dose rate in the ionisation chamber into dose rate in the medium of the irradiated sample, the kerma ratio, K_m/K_{air} , is used.

$$\overset{\circ}{D}_m = \overset{\circ}{D}_{air} \frac{(\mu_{en}/\rho)_m}{(\mu_{en}/\rho)_{air}} \quad (\text{Gray/sec.}) \quad 4.29$$

where $\overset{\circ}{D}_m$ is the dose rate for the irradiated material, and $(\mu_{en}/\rho)_m$ and $(\mu_{en}/\rho)_{air}$ are the mass energy absorption coefficients for the irradiated material and air respectively.

Ionisation currents have been measured for different Voltages applied to accelerate the electrons and for different powers applied to the filament (Current x Voltage) of the cathode, and the dose rates to the air, have been calculated from equation 4.28 and arranged in table 4.6.

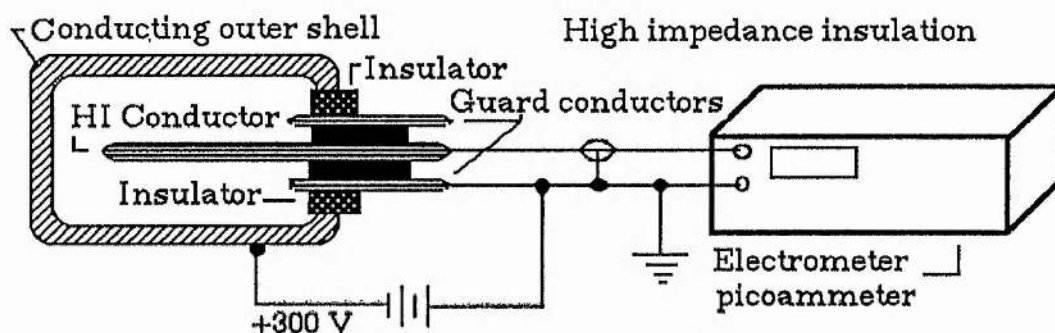


Figure 4.19: The most common circuitry for the ionisation chamber

Applied current and voltage to the filament	2.8 Amp. 3.8 volts		3.0 Amp. 4.0 volts	
Applied accelerated voltage (kV)	Ionisation current, I (Amp.)x10 ⁻¹⁰	Air dose rate, D _{air} (Gy/sec.x10 ⁻²)	Ionisation current, I (Amp.)x10 ⁻⁹	Air dose rate, D _{air} (Gy/sec.x10 ⁻¹)
10.0	0.69	0.646	0.185	0.017
11.0	0.83	0.777	0.225	0.021
12.0	1.00	0.936	0.270	0.025
12.5	1.20	1.124	0.315	0.029
13.0	1.40	1.310	0.360	0.034
14.0	1.55	1.451	0.410	0.038
15.0	1.75	1.639	0.460	0.043
15.5	1.95	1.826	0.510	0.048
16.0	2.10	1.966	0.560	0.052
17.0	2.25	2.107	0.620	0.058
18.0	2.50	2.341	0.680	0.064
19.0	2.70	2.528	0.730	0.068
20.0	2.90	2.716	0.79	0.074
20.5	3.10	2.903	0.85	0.080
21.0	3.35	3.137	0.90	0.084
22.0	3.55	3.324	0.96	0.090
22.5	3.80	3.558	1.10	0.103
23.0	4.00	3.746	1.50	0.140

Table 4.6 a:The relation between the applied power (current x voltage), the applied accelerated voltage and the exposure dose rate to the ionisation chamber from Cu-k X-rays

Applied current and voltage to the filament	3.2 Amp. 4.4 volts		3.5 Amp. 5.2 volts	
Applied accelerated voltage (kV)	Ionisation current, I (Amp.) $\times 10^{-9}$	Air dose rate, D_{air} (Gray/sec.)	Ionisation current, I (Amp.) $\times 10^{-8}$	Air dose rate, D_{air} (Gray/sec.)
10.0	0.55	0.052	0.18	0.169
11.0	0.68	0.064	0.22	0.206
12.0	0.81	0.076	0.24	0.225
12.5	0.95	0.089	0.28	0.262
13.0	1.10	0.103	0.33	0.309
14.0	1.25	0.117	0.36	0.337
15.0	1.40	0.131	0.41	0.384
15.5	1.50	0.140	0.46	0.407
16.0	1.70	0.159	0.51	0.478
17.0	1.90	0.178	0.56	0.524
18.0	2.10	0.197	0.61	0.571
19.0	2.30	0.215	0.67	0.627
20.0	2.50	0.234	0.71	0.665
20.5	2.70	0.253	0.78	0.730
21.0	2.90	0.272	0.84	0.787
22.0	3.10	0.290	0.90	0.843
22.5	3.30	0.309	0.96	0.899
23.0	3.50	0.328	1.05	0.983

Table 4.6 b:The relation between the applied power (current x voltage), the applied accelerated voltage and the exposure dose rate to the ionisation chamber from Cu-k X-rays

Applied current and voltage to the filament	3.7 Amp. 5.4 volts		3.9 Amp. 6.0 volts	
Applied accelerated voltage (kV)	Ionisation current, I (Amp.) $\times 10^{-8}$	Air dose rate, D_{air} (Gray/sec.)	Ionisation current, I (Amp.) $\times 10^{-8}$	Air dose rate, D_{air} (Gray/sec.)
10.0	0.35	0.328	0.66	0.618
11.0	0.42	0.393	0.80	0.749
12.0	0.51	0.478	0.97	0.908
12.5	0.59	0.552	1.20	1.124
13.0	0.68	0.637	1.40	1.311
14.0	0.78	0.730	1.55	1.451
15.0	0.88	0.824	1.70	1.592
15.5	0.98	0.918	2.00	1.873
16.0	1.10	1.030	2.20	2.060
17.0	1.20	1.124	2.40	2.247
18.0	1.35	1.264	2.70	2.528
19.0	1.45	1.358	3.00	2.809
20.0	1.55	1.451	3.20	2.996
20.5	1.70	1.592	3.50	3.277
21.0	1.80	1.686	3.70	3.465
22.0	1.90	1.778	4.00	3.746
22.5	2.10	1.966	4.20	3.933
23.0	2.20	2.060	4.50	4.214

Table 4.6 c: The relation between the applied power (current x voltage), the applied accelerated voltage and the exposure dose rate to the ionisation chamber from Cu-k X-rays

Chapter V

Experimental Aspects and Techniques Used to Study the Metaloenzyme (Dihydroorotate Dehydrogenase)

5.1 Characteristic of the Enzyme

In order to study the direct and the indirect actions of ionising radiation, the metaloenzyme dihydroorotate dehydrogenase, D.De-nase, was chosen since it is a biochemical molecule containing most of the atoms of soft tissues. The enzyme is membrane-bound, and linked with the electron transport systems of the cells (Taylor and Taylor, 1964). The metal in this enzyme (iron) plays an important role in the oxidation reduction processes in the catalytic cycle.

Evidence has previously been presented that the enzyme D. De-nase from *Zymobacterium oroticum* is a flavoprotein (Lieberman and Kornberg 1953, Friedmann and Vennessland 1958). The flavin content was determined by Friedmann and Vennessland (1960), Kondo et al (1960) and Miller and Massey (1965 a) both for the total flavin content and for the amount of flavin mononucleotide, FMN, and flavin adenine dinucleotide, FAD. It is of great interest that both FMN and FAD appear to be involved in the catalytic activities of the enzyme (Miller and Massey, 1965 b).

The crystalline enzyme has been shown to contain equal amounts of FMN and FAD, giving in total 32.2 μmole moles of flavin per mg of protein. This is equivalent to 1 mole of flavin per 31,000 gm of protein giving a combined weight of 62,000 gm. Analyses have also been done to determine the metal content of the enzyme. Samples which had not been recrystallized give an average value of 1.24 μmoles of iron per μmole of flavin, while other samples of recrystallized enzyme give an

average value of 0.91 μ mole of iron per μ mole of flavin (Friedmann and Vennesland, 1960). These results suggested that there was one atom of iron bound per flavin molecule and no significant amount of other metals were present in the crystalline enzyme.

It is not easy to work with enzymes since they are heat-sensitive, lose their catalytic function with time at elevated temperatures, their assay is pH-dependant and they display a high sensitivity to ultraviolet radiation.

The D.De-nase was supplied by Sigma Chemical Company as partially purified, lyophilized powder approximately 32% protein, the remainder buffered salts, and with an activity of 6.4 units per mg of protein. (1 unit will oxidise 1 μ mole of β -DPNH per minute at pH 6.5 at 25°C using orotic acid as substrate.)

Enzyme solutions of different concentrations (number of units or mg per ml) were prepared by dissolving the lyophilized enzyme powder in a 0.4M phosphate buffer of pH 6.5 just prior to irradiation. The manufacturer recommends that the enzyme is stable indefinitely when stored desiccated below 0 °C, and will retain most of its activity at room temperature for a week. Solutions of 1 unit per ml or more, may be stored frozen for several days.

5.2 Preparation of Chemical Solutions

As recommended in the method for testing the level of activity of the enzyme by the supplier (Sigma Chemical Co. procedures), it is necessary to prepare the following solutions.

(A) Phosphate buffer solutions

Two types of phosphate buffer solutions are prepared from sodium dihydrogen orthophosphate anhydrous, NaH_2PO_4 , (molecular weight

~119.977 gm) and di-sodium hydrogen orthophosphate anhydrous, Na_2HPO_4 , (molecular weight ~141.959 gm). From each of NaH_2PO_4 and Na_2HPO_4 anhydrous salts prepare two solutions of 0.4M and 0.1M.

(A.1) 0.4M sodium di-hydrogen orthophosphate buffer solution, pH 6.5

Disolve 4.799 gm of Sodium dihydrogen orthophosphate (NaH_2PO_4) in 80 ml of deionized H_2O . Adjust to pH 6.5 at 25 °C with NaOH. Dilute to a final volume of 100 ml with deionized H_2O .

(A.2) 0.4M Di-sodium hydrogen orthophosphate buffer solution, pH 6.5

Disolve 5.678 gm of Disodium hydrogen orthophosphate (Na_2HPO_4) in 80 ml of deionized H_2O . Adjust to pH 6.5 at 25 °C with NaOH. Dilute to a final volume of 100 ml with deionized H_2O .

(A.3) 0.1 M sodium di-hydrogen orthophosphate buffer solution, pH 7.5

Disolve 1.199 gm of sodium di-hydrogen orthophosphate (NaH_2PO_4) in 80 ml of deionized H_2O . Adjust to pH 7.5 at 25 °C with NaOH. Dilute to a final volume of 100 ml with deionized H_2O .

(A.4) 0.1 M di-sodium hydrogen orthophosphate buffer solution, pH 7.5

Disolve 1.419 gm of sodium di-hydrogen orthophosphate (Na_2HPO_4) in 80 ml of deionized H_2O . Adjust to pH 7.5 at 25 °C with NaOH. Dilute to a final volume of 100 ml with deionized H_2O .

(A.5) 0.4M phosphate buffer solution, pH 6.5

11 ml of 0.4M NaH_2PO_4 solution mixed with 8 ml of 0.4M Na_2HPO_4 solution, adjusted to pH 6.5 with NaOH.

(A.6) 0.1M phosphate buffer solution, pH 7.5

1.6 ml of 0.1M NaH_2PO_4 solution is mixed with 8.9 ml of 0.1M Na_2HPO_4 solution, adjusted to pH 7.5 with NaOH.

(B) L-Cysteine hydrochloride solutions

(B.1) 0.4 M L-Cysteine hydrochloride

Disolve 702 mg of L-Cysteine hydrochloride Hydrate, in 8 ml of deionized H_2O . Adjust to pH 6.5 with NaOH and dilute to a final volume of 10 ml with deionized H_2O . This solution is prepared fresh daily.

(B.2) 0.01 M L-Cysteine hydrochloride

Disolve 175.5 mg of L-Cysteine hydrochloride Hydrate, in 80 ml of deionized H_2O . Adjust to pH 6.5 with NaOH and dilute to a final volume of 100 ml with deionized H_2O . This solution is prepared fresh daily.

(C) 0.01M Orotic acid solution, pH 6.5

Dissolve 156.0 mg of orotic acid (6-Carboxy-2,4-dihydroxypyrimidine) in dilute NaOH and titrate to pH 6.5 with HCl. Dilute to a final volume of 100 ml with deionized H_2O . The solution must be kept at 4°C .

(D) 3 mM Flavin Adenine Dinucleotide solution

Disolve 2.5 mg of Flavin Adenine Dinucleotide Disodium salt in 1 ml of deionized H_2O . Protect from light.

**(E) 1.7mM β -NADH solution (β Nicotinamide Adenine Dinucleotide ,
Reduced form)**

This compound, $\text{C}_{21}\text{H}_{27}\text{O}_{14}\text{N}_7\text{P}_2\text{Na}_2$, (molecular weight \approx 709) has some other names (β -DBNH; Dihydrodiphosphopyridine Nucleotide;

β -Dihydro-Nicotinamide Adenine Dinucleotide, reduced form), and is prepared enzymatically from Grade III β -NAD (from yeast). Solution for the assay is prepared by dissolving 6.2 mg of β -NADH in 5 ml of (i) phosphate buffer of 0.1 M and pH 7.5 (solution A.6) for procedure 1 and 1n 5 ml of (ii)Sodium di-hydrogen orthophosphate buffer solution of pH 6.5 for procedure 2. These solutions must be prepared fresh for use the same day.

5.3 Enzymatic Assay

A- Procedure 1

The procedure which has been adopted to assay the irradiated enzyme, control, and blank samples was recommended by the manufacturer (Sigma Chemical Co. Lot No. 22C-6850) as follows.

Three test tubes labelled Blank, Control and test samples. To each test-tube add:

1. 1.0 ml 0.4M NaH_2PO_4 , pH 6.5 (solution A.1)
2. 0.5 ml 0.01M L-Cysteine hydrochloride (solution B.1)
3. 0.6 ml 0.01M Orotic acid, pH 6.5 (solution C)
4. 0.65 ml deionized H_2O
5. 0.05 ml irradiated enzyme solution for test samples, non-irradiated enzyme solution for control samples, and distilled water for blank samples.
6. Mix well by inversion and incubate for 5 minutes in a water bath at 25°C to activate the enzyme.
7. After incubation, add 0.2 ml β -NADH solution of pH 7.5 in phosphate buffer of 0.1M prepared fresh daily (solution E (i)).
8. Transfer the 3 ml of incubated solution to a cuvette of 1 cm light path and measure the absorbancy of each of test, control, and blank samples. (The optical density of the ultraviolet absorption at 340 nm is

measured in a Perkin-Elmer spectrophotometer, Coleman model 55, by using filter 1 of the system.) The optical density of deionized H₂O was set to zero in the spectrophotometer to be used as the reference density.

B- Procedure 2

Three test tubes labelled Blank, Control and test samples. To each test-tube add:

- 1- 1.0 ml 0.4 M sodium phosphate buffer (solution A.1)
- 2- 0.5 ml 0.4 M L-Cysteine HCl (solution B.1)
- 3- 0.6 ml 0.01 M Orotic acid (solution C)
- 4- 0.01 ml 3 mM Flavin Adenine Dinucleotide (solution D)
- 5- 0.64 ml deionized H₂O

Steps 6, 7, 8 and 9 as steps 5, 6, 7 and 8 in procedure 1

5.4 Reaction Rate and Calibration curve of enzyme

To measure the activity of the enzyme throughout the incubation time period a calibration curve has been drawn for control samples by plotting the optical density of (blank optical density - control optical density) against the incubation time with β -NADH at 25°C for each specified concentration, figure 5.1 . From these curves, the reaction rate for each enzyme concentration can be deduced which is equal to the slope of these curves. The curve of these slopes against the corresponding concentration can be used as a calibration curve for enzyme activity at different concentrations, figure 5.2. As we can see from the slopes of the reaction rate curves (figure 5.1), the reaction rates are approximately linear until the fifth minute. After that the reaction rates decrease dramatically, then the survival fractions of the

inactivated enzyme will be the average of the survival fractions over five minutes of incubation with β -NADH solution.

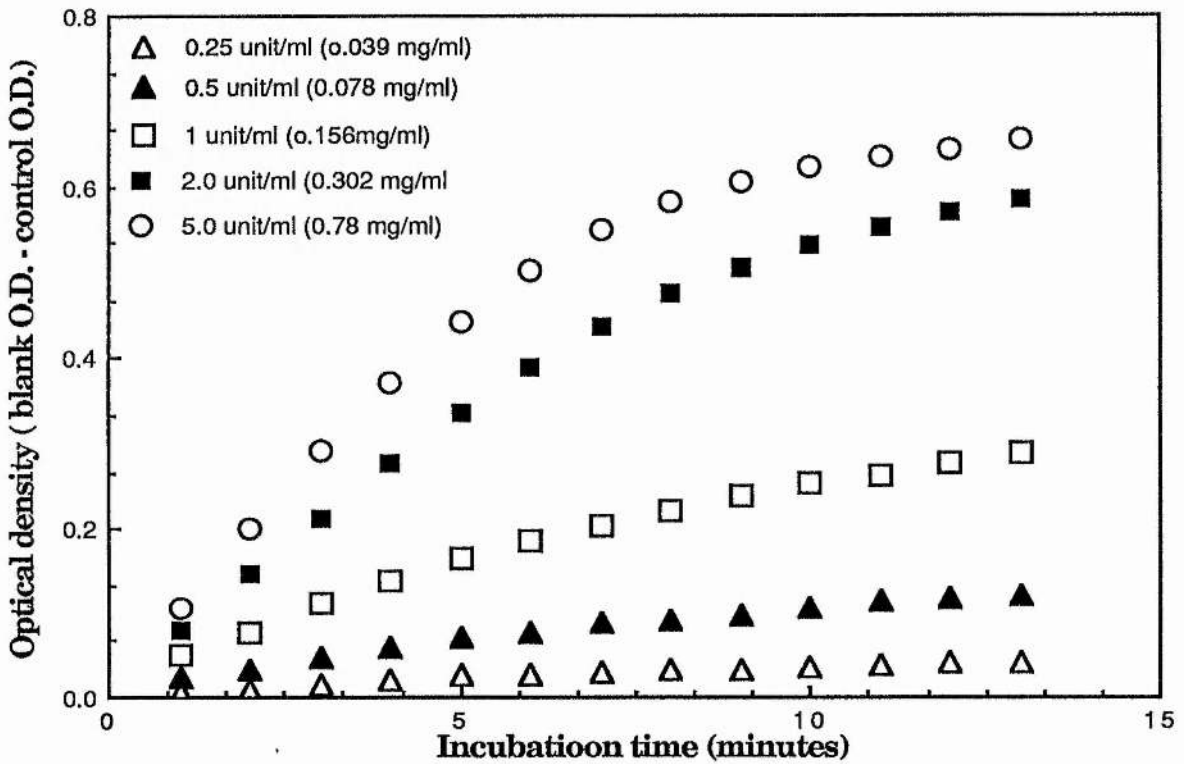


Figure 5.1: Curves of reaction rate for enzyme at different concentrations

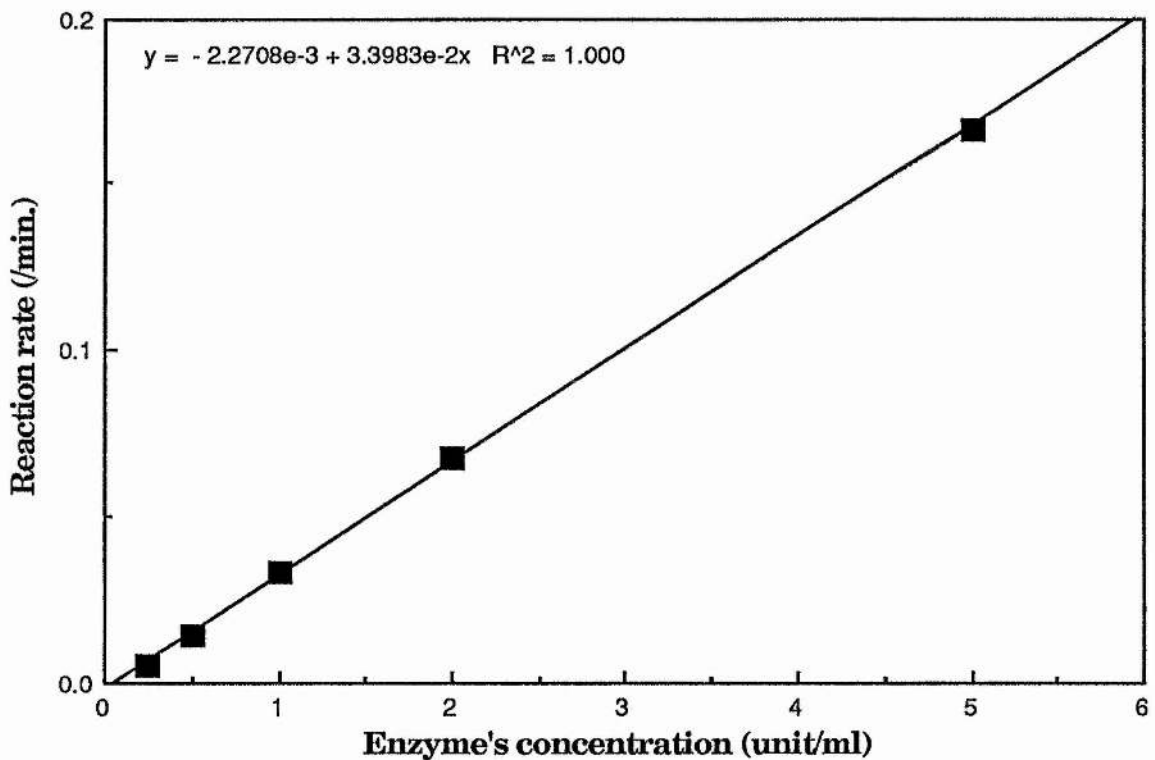


Figure 5.2: Calibration curve of enzyme's reaction.

5.5 Irradiation Procedure and Survival Fraction Determination for the Enzyme

Four different concentrations of enzyme solutions were used in this experiment (0.5, 1.0, 2.0 and 5.0 units per ml). 0.1 ml of the solution at a certain concentration was poured over the base of a perspex tube of cross-sectional area 1.768 cm^2 , and exposed to a photon beam from the X-ray machine (copper target of K X-ray 8.04 keV) at a distance of 4 cm from the exit window. For each concentration, three or four different doses were used to determine the survival fraction for each dose.

The experimental procedure was repeated three times and the average of the results is reported (tables B.1- B.11). Control samples are assayed in the same manner as the test samples except that the enzyme solution was not exposed to radiation, and for blank samples, distilled water was used instead of enzyme solution.

Survival fractions, SF, can be determined from the optical density readings, O.D., of test, control, and blank samples by using the following equation

$$\text{SF} = \frac{\text{Test O.D.} - \text{Blank O.D.}}{\text{Control O.D.} - \text{Blank O.D.}} \times 100 \%$$

Irradiation of the enzyme in dry state was carried out by taking 1 mg of lyophilized enzyme powder, spread over the base of a perspex tube of cross-sectional area of 2 cm in diameter. Irradiation took place 4 cm from the exit window. Four different doses were used. After irradiation, an enzyme solution of 1 unit per ml was prepared from the irradiated powder. The rest of the procedure for enzyme solution assay was followed. Control samples were created by putting 1 mg of the enzyme powder in a similar test tube and left in the same environment as the test samples, but without irradiation.

Chapter VI

Inactivation of Enzyme in Solid and in solution by CU-K X- rays

6.1 Radiation dosimetry

Radiation dosimetry was carried out mainly with a 0.3 cm³ low energy parallel plate ionisation chamber (section 4.6). It was positioned with its window parallel to the exit window of the x-ray machine. A bias voltage of 240 V was chosen from the best plateau on the characteristic curve.

The dose rate inside the chamber was calculated as in section 4.6 and multiplied by the following factors to obtain the average surface dose rate (i) the attenuation of the photon beam in the window of the ion chamber (table 4.2), (ii) a factor of 0.98 to allow for the photon beam density variation over an area of 2 cm diameter at 4 cm from the exit window. Dose rates were calculated before and after each irradiation, and the average used as the exposure dose rate. Each sample was irradiated for a predetermined exposure time to achieve the approximate dose required.

To calculate the actual dose rate to the irradiated samples, the mass energy absorption coefficient is needed (section 4.6), since the detailed composition of the irradiated materials (especially for soft tissues and other low atomic number materials) is of great importance for soft x-rays. In contrast the mass energy absorption coefficient is relatively unimportant for high energy x-rays, as for these, the coefficients are only slightly dependent on the detailed composition.

The mass energy absorption coefficient of the enzyme D. De-nase molecule (in dry state) can be calculated from measured values of mass energy absorption coefficients of the constituent atoms of the enzyme (Hubbell 1977 & 1982) and by using the mixture rule (section 3.4). Friedmann and Vennessland (1960) reported that the molecular weight of

the enzyme is 1.2×10^8 gm per mole, and that there is one flavin molecule for each 3.1×10^4 gm of protein but the detailed atomic structure is not fully known. Emmons (1959) reported the atomic composition of catalase enzyme which might have the same composition as the flavoprotein enzyme. Data for this composition and the corresponding mass energy absorption coefficient of atoms are listed in table 6.1. From these data and equation 3.5 the mass energy absorption coefficient of enzyme in the dry state was calculated to be $7.697 \text{ cm}^2 \text{ g}^{-1}$ for photons of energy 8.04 keV. The mass energy absorption coefficients for enzyme in solution can also be calculated in the same way since the enzyme was dissolved in a known solvent (The solvent was taken to be water regardless of the possible presence of small quantities of impurity, table 6.2).

The dose rates for the irradiated enzyme samples (dry or in solution), calculated using equations 4.28 and 4.29 and information from table 6.1 or table 6.2, are presented in table 6.3.

Element	Fraction in percentage by weight of atoms to the whole molecule	Mass energy absorption coeff. of the element * ($\text{cm}^2 \text{ g}^{-1}$)
C	49.9	4.056
O	25.0	10.907
N	16.0	6.926
H	7.0	1.158×10^{-2}
S	1.0	89.470
P	1.0	72.370
Fe	0.1	221.600

* Data from Hubbell 1982, for photons of energy 8.04 keV

Table 6.1: Elemental composition of the catalase enzyme (Emmons 1959).

Enzyme concentration in solution (unit/ml or mg/ml)		Enzyme % by weight	Water % by weight	Mass energy absor. coeff. (μ_{en}/ρ) ($\text{cm}^2 \text{g}^{-1}$)
0.5	0.417	0.0417	99.9583	9.719
1.0	0.833	0.0832	99.9168	9.718
2.0	1.667	0.166	99.834	9.717
5.0	4.167	0.415	99.585	9.712

* Mass energy absorption coefficient of water for 8.04 keV photons is $9.73 \text{ cm}^2 \text{g}^{-1}$

Table 6.2: Mass energy absorption coefficients for enzyme D. De-nase at different concentrations.

Irradiated Enzyme	Dose rate (gray/sec.)
0.5 unit/ml	$9.855 \times 10^7 \text{ I}^*$
1.0 unit/ml	$9.854 \times 10^7 \text{ I}^*$
2.0 unit/ml	$9.853 \times 10^7 \text{ I}^*$
5.0 unit/ml	$9.848 \times 10^7 \text{ I}^*$
Dry enzyme	$7.805 \times 10^7 \text{ I}^*$

* I is the actual ionisation current collected by the ionisation chamber

Table 6.3: The dose rates for enzyme in different concentration as calculated from equations 4.28 and 4.29 and tables 6.1 and 6.2.

6.2 Dose response curves

Samples of enzyme in solution and in dry state were irradiated as in section 6.1 and the survival fraction for each dose and for each dose rate was calculated as described in section 5.5. The experimental data are arranged in tables B.1-B-11.

From the results of these calculations, dose survival curves were drawn on semilogarithmic scales (figures 6.1 - 6.5) and the dose of 37%

survival for all these experiments have been extracted from these curves (table 6.4).

Enzyme conc. (unit/ml)	Dose rate (gray/sec.)	Dose 37% (gray)	1/concen.	1/Dose 37% (gray ⁻¹)
0.5	0.246	127.5	2.0	7.84×10^{-3}
	0.689	97.5		10.26×10^{-3}
	1.99	89.5		11.17×10^{-3}
1.0	0.246	172.5	1.0	5.797×10^{-3}
	0.689	147.0		6.803×10^{-3}
	1.99	131.5		7.605×10^{-3}
2.0	0.246	405.5	0.5	2.466×10^{-3}
	0.689	368.5		2.714×10^{-3}
	1.99	331.2		3.019×10^{-3}
5.0	1.99	1233.25	0.2	8.109×10^{-4}
Dry enzyme	1.99	1.31×10^4	0.0	7.633×10^{-5}

Table 6.4: Doses at 37% survival of enzyme in solution at different concentrations and in the dry state irradiated at different dose rates by photons of energy 8.04 keV.

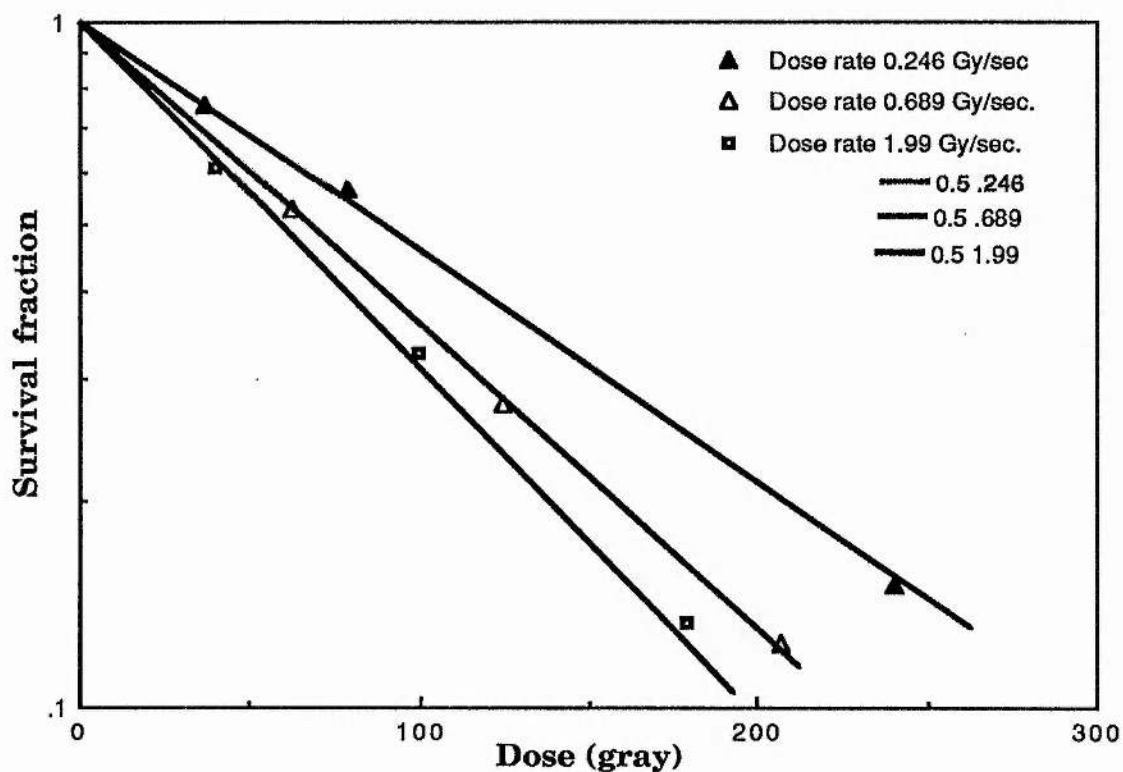


Figure 6.1: Dose survival curves of enzyme solution 0.5 unit/ml irradiated by photons of energy 8.04 keV at different dose rates.

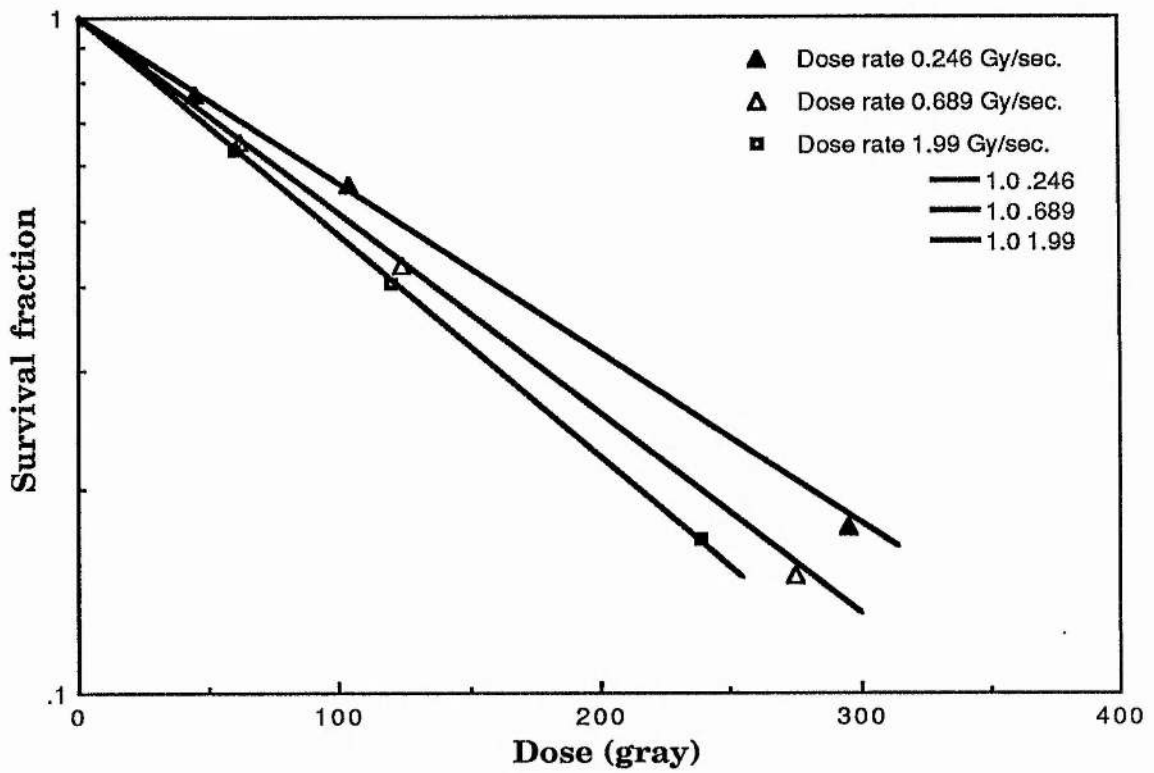


Figure 6.2: Dose survival curves of enzyme solution 1.0 unit/ml irradiated by photons of energy 8.04 keV at different dose rates.

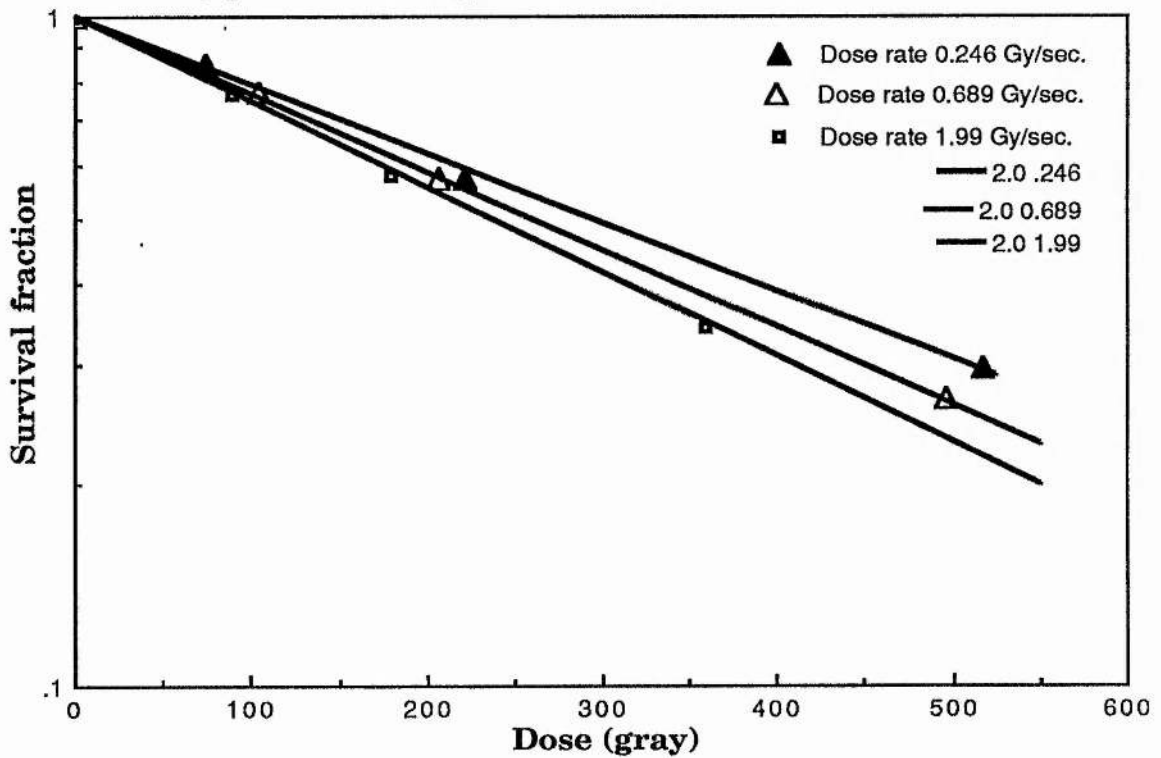


Figure 6.3: Dose survival curves of enzyme solution 2.0 unit/ml irradiated by photons of energy 8.04 keV at different dose rates.

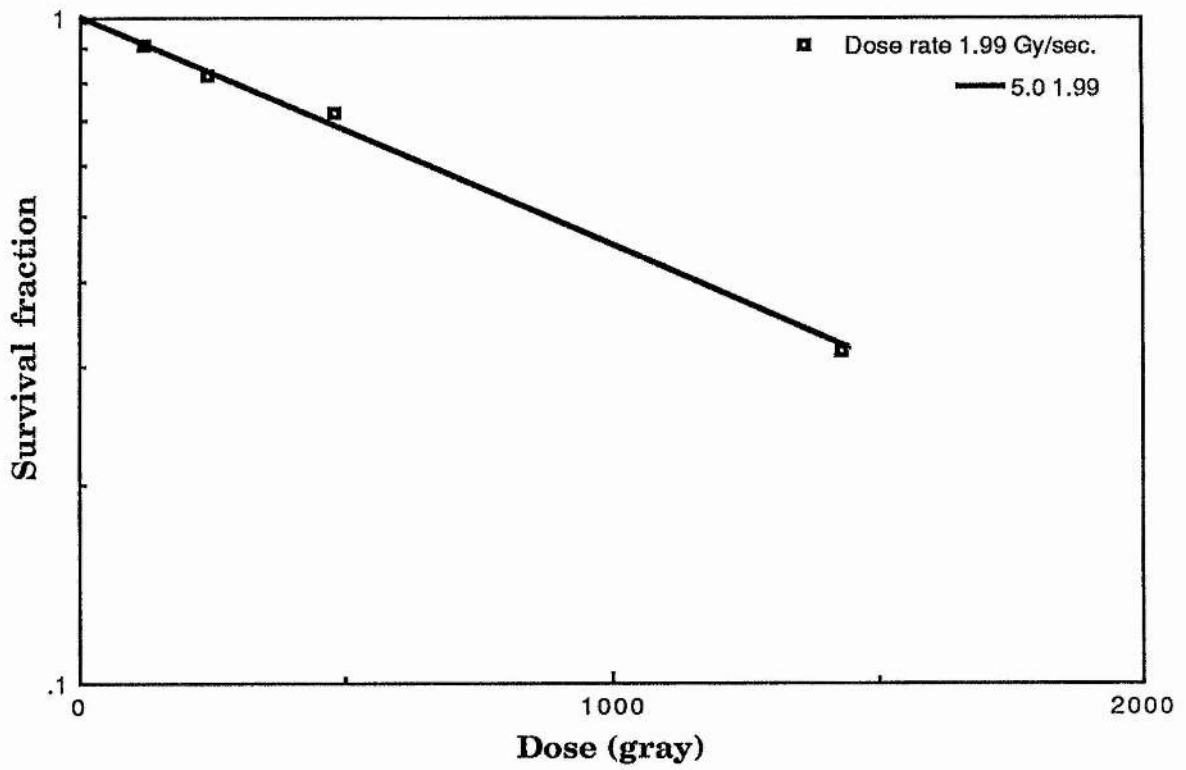


Figure 6.4: Dose survival curve of enzyme solution 5.0 unit/ml irradiated by photons of energy 8.04 keV at a dose rate 1.99 gray/sec.

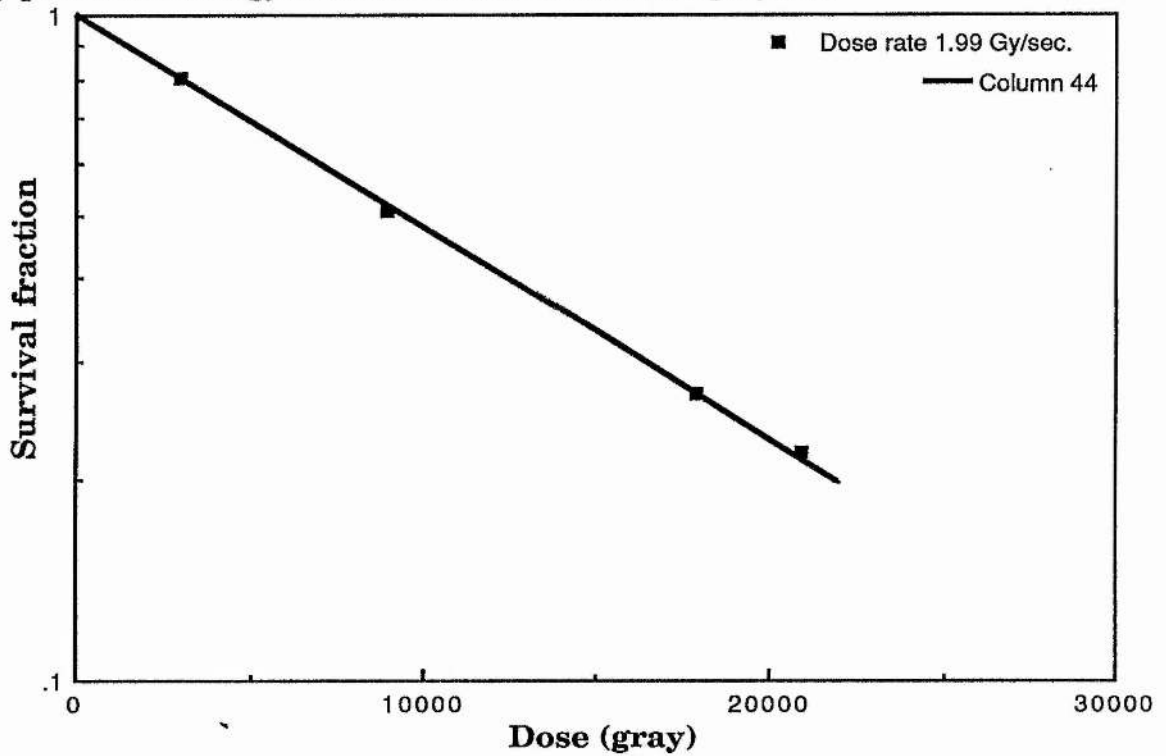


Figure 6.5: Dose survival curve of dry enzyme irradiated by photons of energy 8.04 keV at a dose rate 1.99 gray/sec.

6.3 Inactivation cross-sections of enzyme

To express the radiation action effect it is useful to explore the physical mechanism involved in terms of intrinsic efficiency, σ_R , given by the ratio of the effect cross-section, σ_{eff} , to the geometrical cross-sectional area of the target molecule, σ_g . This gives a measure of the net effectiveness of a single radiation track which is actually responsible for inactivation. Then the effectiveness of electrons can be tested in the equilibrium slowing down spectrum generated by the primary electron field (table 6.5) and given as an effect cross-section.

$$\sigma_{\text{eff}} = \frac{L_T(\text{keV}/\mu\text{m})}{D(\text{Gy}) \cdot \rho (\text{gm} \cdot \text{cm}^{-3})} 1.6 \times 10^{-9} \text{ cm}^2 \quad 6.1$$

Where L_T is the track average LET weighted for the equilibrium electron fluence spectrum, D is the dose of 37% survival and ρ is the density of the irradiated material.

The effect cross-sections of radiation action are divided by the geometrical cross-sectional area of enzyme which is $4.1 \times 10^{-13} \text{ cm}^2$. Results of these calculations are listed in table 6.6.

Electron spectrum	Average energy of electron (keV)	L_T (keV/ μm)	L_D (keV/ μm)	I_t (μm^{-1})
primary	7.16	3.31	3.32	48.4
secondary in equilib.	4.29	6.33	11.15	104.0

Table 6.5: electron spectrum generated by the interaction of 8.04 keV photons with water.

Enzyme sample concentration	Dose rate (gray/sec.)	σ_{eff} (cm^2) $\times 10^{-10}$	σ_{R}^* $\times 10^2$
0.5 unit/ml	0.25	0.79	1.94
	0.69	1.04	2.53
	1.99	1.13	2.76
1.0 unit/ml	0.25	0.59	1.43
	0.69	0.69	1.68
	1.99	0.77	1.88
2.0 unit/ml	0.25	0.25	0.61
	0.69	0.28	0.67
	1.99	0.31	0.74
5.0 unit/ml	1.99	0.08	0.20
Dry enzyme	1.99	0.01	0.02

* $\sigma_{\text{R}} = \sigma_{\text{eff}} / \sigma_{\text{g}}$ where $\sigma_{\text{g}} = 4.1 \times 10^{-13} \text{ cm}^2$

Table 6.6: Effect cross-sections and intrinsic efficiencies of the interactions of electrons in the slowing down spectrum for enzyme in solution and in the dry state

6.4 Model for inactivation of enzyme in solution and in solid state

Inactivation of enzyme in solution and in the solid state is known to be a single hit / single target process (figures 6.1-6.5). Two basic types of radiation interaction are thought to occur: direct and indirect action. For the inactivation of enzyme in solid state, direct radiation action is the only process expected. For inactivation of enzyme in solution both direct and indirect radiation actions may occur. These two processes are in competition depending on the concentration of the enzyme in the solution.

6.4.1 Direct action

Let the mean chord diameter through the enzyme molecule = d and let the mean free path for ionisation = λ . Then the mean number of ionisations per enzyme traversal by a track = d/λ . Hence the probability that one or more ionisations occur in the enzyme molecule, P_i , is

$$P_i = (1 - e^{-d/\lambda}) \quad 6.2$$

Let the charged particle fluence at equilibrium be Φ_s . Then the mean number of ionisations produced per target by direct radiation action, N_D , is

$$N_D = \sigma_D \Phi_s (1 - e^{-d/\lambda}) \quad 6.3$$

where σ_D is the direct interaction cross-section

6.4.2 Indirect action:

To find the mean number of ionisation per target, we need to find the concentration of radicals, C_R (cm^{-3}), growing in the medium during the irradiation time, t_i . It can be written as follows:

$$C_R = G \bar{L}_T \dot{\phi}_s t_c (1 - e^{-t_i/t_c}) \cdot 10^5 \quad (\text{cm}^{-3}) \quad 6.4$$

where G is the number of radicals liberated in the medium per 100 eV imparted by the charged particles, \bar{L}_T is the track average LET ($\text{keV}/\mu\text{m}$) of the charged particle equilibrium spectrum, $\dot{\phi}_s$ is the fluence rate of the latter and t_c is the radical reaction time constant in seconds.

The fluence rate of radicals, $\dot{\phi}_R$, is

$$\dot{\phi}_R = C_R v_R \quad (\text{cm}^{-2} \cdot \text{sec}^{-1}) \quad 6.5$$

where v_R is the mean velocity of the radicals in cm/sec .

But the mean number of interactions per second per target, N_i , due to indirect radiation action, is

$$N_i = \sigma_R \dot{\phi}_R \quad (\text{sec}^{-1}) \quad 6.6$$

where σ_R is the radical effect cross-section. Due to the finite diffusion length of a radical and the competition for interaction between radicals at high concentrations, this will be an asymptotic limiting value of the

cross-section, σ_R , as the enzyme concentration is diluted beyond a concentration, n_0 . Then σ_R , can be written as:

$$\sigma_R = \pi \bar{r}^2 \times \text{probability of radical interaction}$$

$$\text{ie. } \sigma_R = \pi \bar{r}^2 e^{-n_c/n_0} \quad 6.7$$

where \bar{r}^2 is the mean square distance that a radical can diffuse, n_c is the concentration of irradiated enzyme in solution and n_0 is the concentration of enzyme after which radiation action assumed to be constant

For solids $\sigma_R = \text{zero}$ as there is no indirect action (no radical diffusion). But for enzyme in solution there are two types of interaction: direct and indirect, In solution the indirect radiation action increases as the concentration of the enzyme decreases until it reaches a constant value of $\pi \bar{r}^2$ times an efficiency factor (e^{-n_c/n_0}). On the other hand the direct action per target is constant. Thus the direct and the indirect interaction cross-section can be written as follows:

$$\text{Direct inter. cross-section, } \sigma_D = \sigma_g (1 - e^{-d/\lambda}) \quad 6.8$$

$$\text{Indirect inter. cross-section, } \sigma_R = \pi \bar{r}^2 e^{-n_c/n_0} \quad 6.9$$

Hence in solution the mean number of interactions per target due to direct, N_D , and indirect, N_i , actions (total number of direct and indirect radiation interactions per target, N_T) is given as follow

$$N_T = \left\{ [\sigma_g \Phi_s (1 - e^{-d/\lambda})] + [\pi \bar{r}^2 e^{-n_c/n_0} v_R G \bar{L}_T \phi_s t_i t_c (1 - e^{-t_i/t_c}) \cdot 10^5] \right\} \quad 6.10$$

6.4.3 Enzyme's survival equations

As we know that inactivation of enzyme in solution and in solid state is of a single hit / single target process then, for solid enzyme

$$\ln(F) = - [\sigma_g (1 - e^{-d/\lambda})] \Phi_s \quad 6.11$$

and for enzyme in solution

$$\ln(F) = - \{ [\sigma_g (1 - e^{-d/\lambda})] + [\pi \bar{r}^2 e^{-n_c/n_0} v_R G \bar{L}_T t_c (1 - e^{-t_i/t_c}) \cdot 10^5] \} \Phi_s$$

$$\text{ie } \ln(F) = - \{ [\sigma_g (1 - e^{-d/\lambda})] + [K e^{-n_c/n_0}] \} \Phi_s \quad 6.12$$

Where $K = 10^5 \pi \bar{r}^2 v_R G \bar{L}_T t_c$, and t_i is the irradiation time. In our experiments $t_i \gg t_c$, then $(1 - e^{-t_i/t_c}) \rightarrow 1$.

6.4.4 Determination of damage Model parameters

From the experimental data of irradiated enzyme in solid state (table B.11 and equation 6.11) a graph can be drawn between $\ln(F)$ and Φ_s (figure 6.6), from which $\frac{\ln(F)}{\Phi_s} = \sigma_D$ and then σ_g can be determined. $\sigma_D = 9.4 \times 10^{-13} \text{ cm}^2$ and then, $\sigma_g = 1.3 \times 10^{-12} \text{ cm}^2$.

Other parameters, K and n_0 can also be determined by using equation 6.12 as follows.

$$\ln \left[\frac{[\ln(F)_{\text{exp}}]}{\Phi_s} - \sigma_D \right] = \ln(K) - n_c A$$

$$\text{i.e. } \ln(M) = \ln(K) - n_c A \quad 6.13$$

$$\text{Where } \sigma_D = 9.4 \times 10^{-13} \text{ cm}^2, M = \left[\frac{[\ln(F)_{\text{exp}}]}{\Phi_s} - \sigma_D \right] \text{ and } A = \frac{1}{n_0}$$

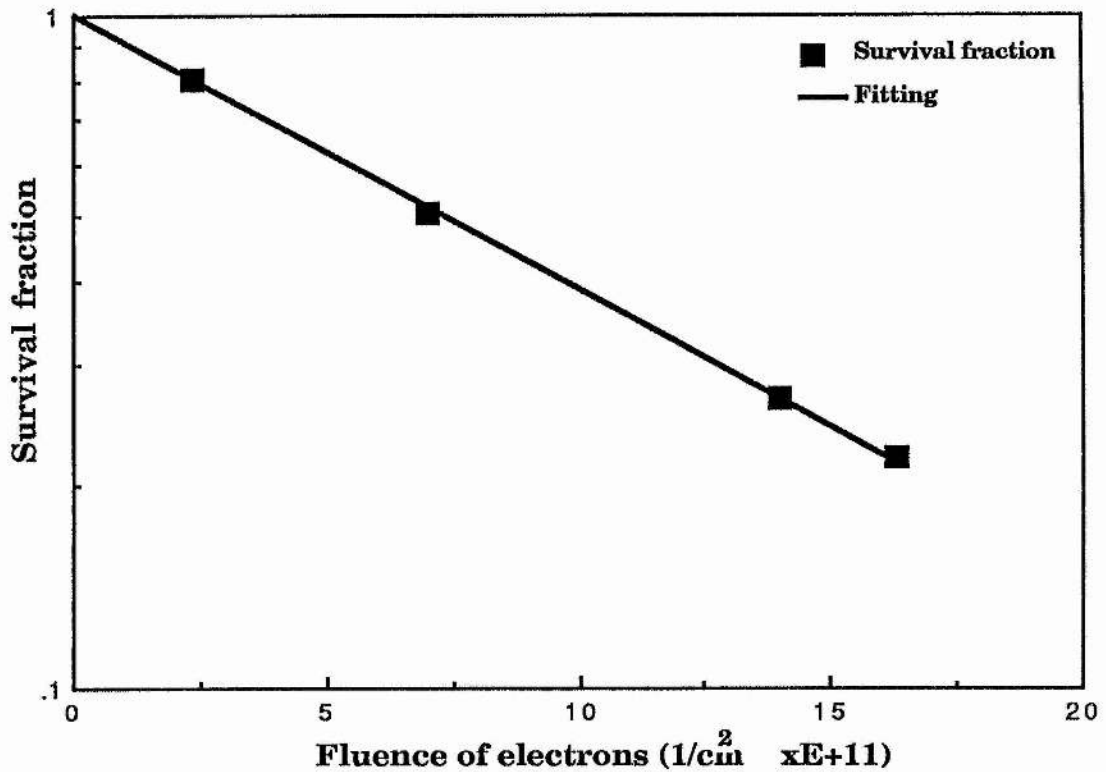


Figure 6.6: survival curve of dry enzyme drawn against the applied fluence of electrons.

By using the experimental data for irradiated enzyme in solution at different concentrations and at dose rate 1.99 Gy/sec (tables B.3, B.6, B.9 and B.10), a curve can be drawn between $\ln(M)$ and n_c , from which $\ln(K)$ is the intercept and $A = \frac{\ln(M/K)}{n_c}$ (equation 6.13). From figure 6.7, $\ln(K) = -22.751$, then $K = 1.32 \times 10^{-10} \text{ cm}^2$ and when the value of K is substituted in equation 6.12 we find that $\pi \bar{r}^2 v_R G \bar{L}_T t_c = 1.32 \times 10^{-15} \text{ cm}^2$.

Since $A = \frac{\ln(M/K)}{n_c}$ then from figure 6.7, $A = \frac{26.0 - 22.751}{5.5} = 0.59$ and $A = \frac{1}{n_o}$, $n_o = 1.69 \text{ unit/ml}$. It was given by the manufacturer that 1.2 unit is equal 1 mg of solid enzyme or 6.4 unit = 1 mg protein, then 1.69 unit/ml is equal to 1.4 mg of solid enzyme per ml or 0.26 mg protein/ml. The molecular weight of the flavoprotein enzyme is $\sim 1.2 \times 10^8 \text{ gm/mol}$. then 0.26 mg protein/ml is equal to $2.16 \times 10^{-12} \text{ mol/ml}$.

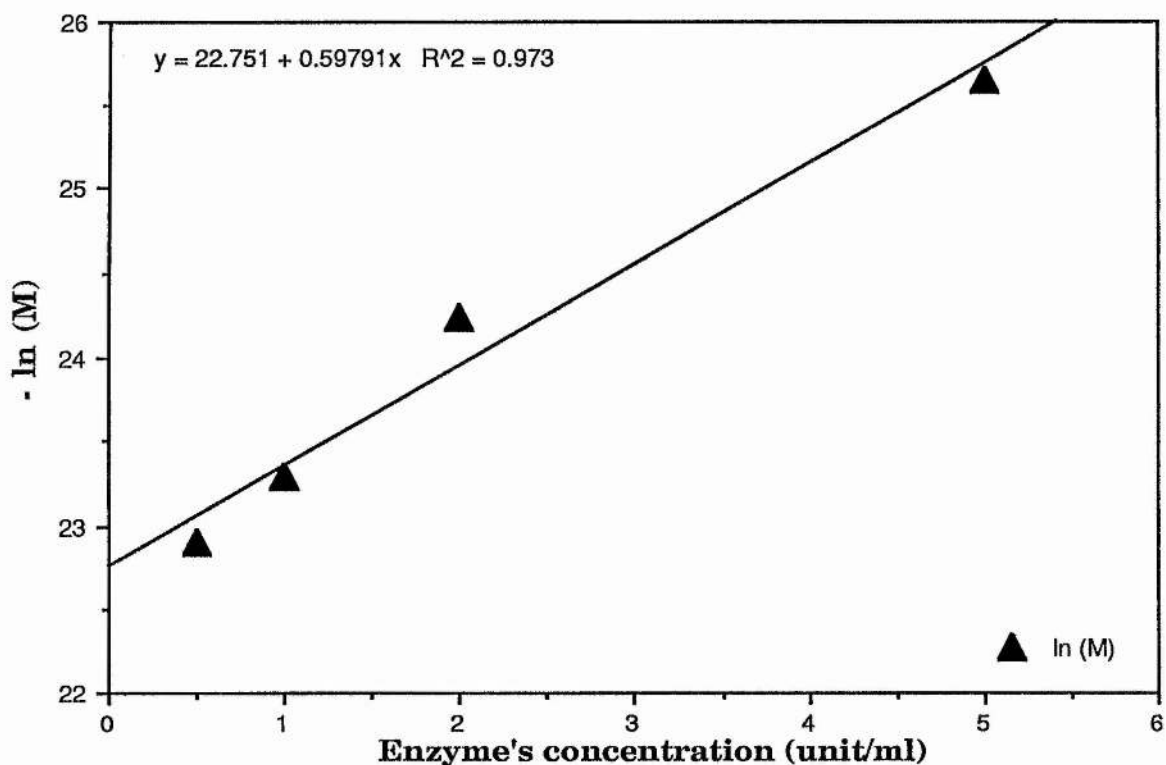


Figure 6.7: Calibration curve drawn from equation 6.13 by using experimental data of enzyme solution irradiated at different concentration.

To calculate the G value of radical production, we need the values of r^2 , v_R and t_c of radical species. Roots and Okada (1975) have used mammalian cells, irradiated by X-rays, to calculate both the life times and diffusion distances in DNA scissions and cell killing for the three main products of water radiolysis: OH, H and e_{aq}^- . Using various alcohols as radical scavengers, they reported that the average life time for OH is 4×10^{-9} sec. and the mean diffusion distance is 60 \AA (6×10^{-7} cm). For H atoms the life time varied from about 2×10^{-7} to 4×10^{-6} sec. and the diffusion distance was between 880 and 4040 \AA and for hydrated electrons the diffusion distance was between 9590 and 19810 \AA . In cell killing, OH radical life time was estimated to be about 8.7×10^{-9} sec. which gives an average diffusion distance for this radical of about 93 \AA . They reported also that OH is the radical species primarily responsible

for the indirect effect in radiation injury and that H and $e aq^-$ are not significantly involved. Other publications supported the premise that the hydroxyl radicals play the major role in inactivation processes in dissolved biomolecules (Collinson et al 1950, Okada 1957, Holmes *et al* 1967, Wright *et al* 1985 and Chatterjee and Magee 1985).

Chatterjee and Magee (1985) have reported G values for the radicals OH, $e aq^-$ and H, and mean life time and estimated diffusion distance for OH radicals. Their calculations have been made on DNA irradiated in dilute aqueous solutions including the extent of OH reaction with both sugar and the bases, their results gave the decay rates of hydrated electrons and OH radicals in pure water. For OH, which was assumed to be the major important product, these values were G value ~ 5.88 , mean life time $\sim 3 \times 10^{-8}$ sec. and estimated diffusion distance, $L \sim 40$ nm. Using Chatterjee and Magee's values for mean life time and diffusion distance in our damage model will provide a means of comparison.

From equation 6.7, $\sigma_R \rightarrow \pi \bar{r}^2$ as radical action reaches the saturation point, then from figure 6.10, $\pi \bar{r}^2 \sim 10^{-10} \text{ cm}^2$ or $\bar{r}^2 \approx 3.2 \times 10^{-11} \text{ cm}^2$, i.e. $\bar{r} = 56$ nm, but if we assume that $\sigma_R = \pi \bar{r}^2 e^{-n_c/n_0} = \pi \bar{r}^2 e^{-0.59 n_c}$, where $1/n_0 = 0.59$, then $\pi \bar{r}^2 e^{-0.59 n_c} \sim 10^{-10} \text{ cm}^2$, for $n_c = 0.5$ unit/ml, $\bar{r}^2 \approx 4.28 \times 10^{-11} \text{ cm}^2$, i.e. $\bar{r} = 65$ nm.

Consequently the mean diffusion distance, $L \approx \left[\left(\frac{\bar{r}^2}{6} \right)^{1/2} \right] \approx 27$ nm.

This (the mean diffusion distance of radical, L) seems to be more consistent with OH estimated diffusion distance calculated by Chatterjee and Magee (1985) ($L \sim 40$ nm).

We have $\pi \bar{r}^2 v_R G \bar{L}_T t_c = 1.32 \times 10^{-15} \text{ cm}^2$, then, $v_R G t_c = 1.6 \times 10^{-6}$ cm. Where \bar{L}_T from table 6.5 is $6.33 \text{ keV}/\mu\text{m}$, as $v_R t_c$ represents the mean distance travelled by the radical in its lifetime it should be larger than the diffusion distance and consequently G must be less than 0.6.

6.5 Interpretation of damage in metallo-enzyme

6.5.1 Radiation action in dry enzyme

The radiation action which takes place in dry molecules is direct and includes the direct action of photons with the constituent atoms of the molecule, the action by the subsequent photo-electrons, Compton electrons and associated electron cascades produced in the molecule and the multiple charging of the affected atoms. Certain molecules such as metallo-enzymes are composed almost entirely of light atoms and only a small fraction by weight of heavy atoms. It was reported by many authors (Emmons 1959, Gomberge 1964 and Diehn *et al* 1976) that there is an additional effect due to the response of such biomolecules to certain energy bands of photons, called "resonance response". Their evidence can be summarised as follows: as the energy of incident photons exceeds the K-absorption edge of the constituent heavy atoms, the observed effect will increase suddenly. They related this to additional consequences of Auger electron cascades and charge build up from the heavy atoms. Simple calculation proves that the excess absorbed energy in the enzyme due to the existence of the small fraction of iron atoms in the metallo-enzyme dihydroorotic dehydrogenase for 8.04 keV photons above the K edge of Fe (7.11 keV) is less than 1.5% (Jawad and Watt 1986 and Watt and Younis 1987).

Ratios of the D_{37} obtained for irradiation by photon energies below and above the K edge for the heavy atoms range from 1.0 to 1.6 and are approximately the same whether in solid or in solution (Emmons 1959, Diehn *et al* 1976, Jawad and Watt 1986). Our survey for metallo-enzyme irradiated in dry state summarised in table 6.7 and figure 6.8, shows that the ratio of the 37% survival dose from photons of energy below the K edge to that above the K edge of heavy atoms, D_r , is on average 1.38. The observed dose ratios for enzyme irradiated in solution or in dry state are

fully accounted for by the normal increase in photon energy in the energy band used. For example the ratio of the energy absorbed in water per photon of 7.0 keV to that of 8.0 keV is 1.46. In other words the damage per interacting X-rays is in effect the same above and below the K edge.

From table 6.7, D_{37} for inactivating the metallo-enzyme by monoenergetic photons from targets Mn ($K_{\alpha}=5.89$ keV) and Cu ($K_{\alpha}=8.04$ keV) are 1.82×10^4 and 1.31×10^4 Gy respectively this means that the ratio of D_{37} of photons below K edge to that above the K edge is 1.39, but if we take the actual energy absorbed across the K edge for both photons, we find that the mass energy absorption coefficients for the photons (5.89 and 8.04 keV) are 16.74 and $7.7 \text{ cm}^2 \text{ g}^{-1}$ respectively, then if we test the effectiveness of K_{α} X-rays undergoing direct interaction cross-section, the following relation can be used

$$\sigma_{\text{eff}} = \frac{E_{K_{\alpha}} (\mu_{\text{en}}/\rho)_{K_{\alpha}}}{D_{37}} 1.6 \times 10^{-13} \text{ cm}^2 \quad 6.14$$

Where $E_{K_{\alpha}}$ is the energy of K_{α} photons in keV, $(\mu_{\text{en}}/\rho)_{K_{\alpha}}$ is the mass energy absorption coefficient of enzyme to K_{α} photons in $\text{cm}^2 \text{ g}^{-1}$ and D_{37} is the 37% survival dose in Gy.

From this we found that the direct effect cross sections for the photons (5.89 and 8.04 keV) are 8.7×10^{-16} and $7.6 \times 10^{-16} \text{ cm}^2$ respectively, then the intrinsic efficiencies, σ_R ($\sigma_{\text{eff}}/\sigma_g$) are 2.1×10^{-3} and 1.84×10^{-3} , these results are approximately equal, within the experimental errors. Thus the use of intrinsic efficiencies for the interpretation of radiation effects is basically a very powerful method which avoids many of the anomalies that arise through the use of absorbed energy (Watt et al 1987 and Watt and Younis 1987). Direct effect cross-sections in metallo-enzyme irradiated in the dry state have been calculated and presented in

table 6.6 as $1.0 \times 10^{-12} \text{ cm}^2$, it is also determined by using the damage model and was $0.94 \times 10^{-12} \text{ cm}^2$ (section 6.5 and figures 6.10 and 6.11).

Source of mono-energetic photons	Photon's energy (keV)	37% dose (gray $\times 10^4$)	$D_R = D_{\text{below}}/D_{\text{above}}$
Cr ⁽¹⁾	5.40	1.48	
Mn ⁽¹⁾	5.89	1.82	
Fe ⁽¹⁾	6.40	1.82	
Ni ⁽¹⁾	7.47	1.48	1.23
Cu ⁽²⁾	8.04	1.31	1.39
Cu ⁽³⁾	8.14	dose %from ⁽³⁾	
Zn ⁽³⁾	8.74	-do-	
Ge ⁽³⁾	10.01	-do-	1.52
As ⁽³⁾	10.69	-do-	1.52

⁽¹⁾ after Emmons 1959 with catalase enzyme, ⁽²⁾ this work with D.Denase enzyme and ⁽³⁾ after Diehn et al (1976).

Table 6.7: Metallo-enzymes irradiated in dry state with different mono-energetic photons

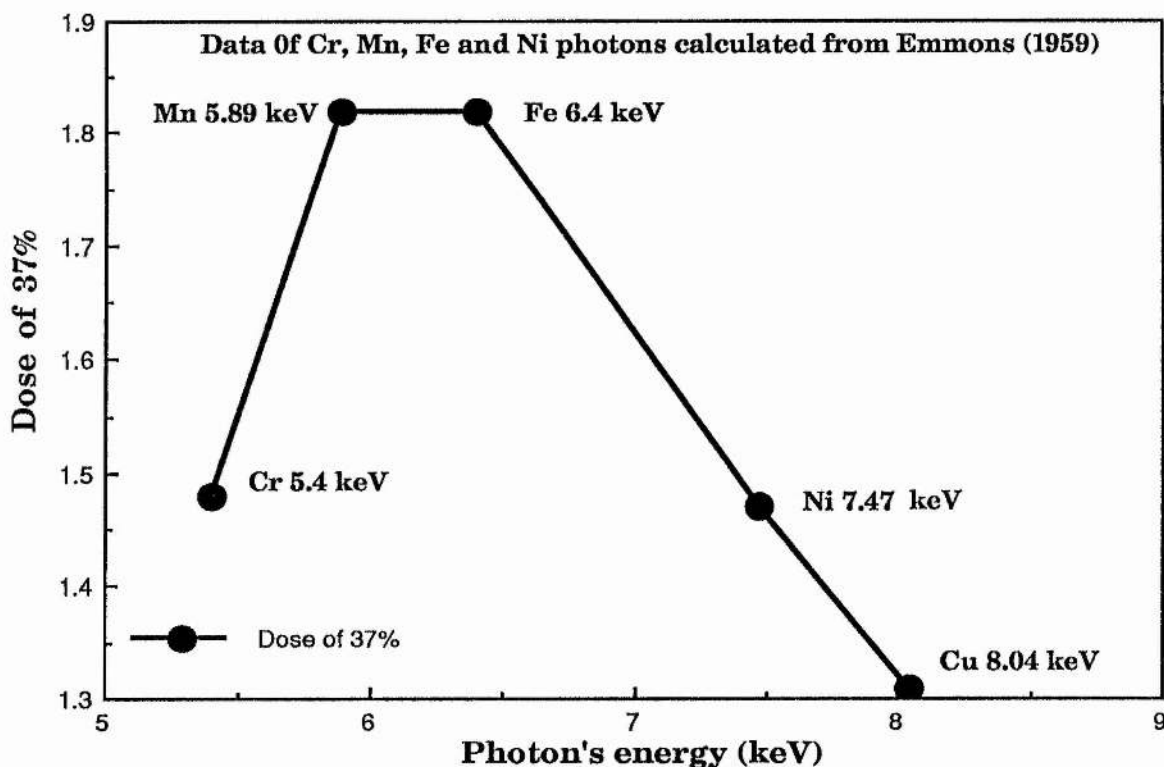


Figure 6.8: Dose of 37% survival of dry metallo-enzyme irradiated with different monoenergetic photons.

6.5.2 Interpretation of damage in enzyme's solution

Enzyme in solution is thought to be inactivated by X-rays through the following processes: (i) direct action of radiation as explained in section 6.5.1; (ii) indirect action of radiation through the interaction of photons and their secondary electrons with the solvent's molecules (water) to liberate radicals as products of water radiolysis. The main three products of water radiolysis are OH, H and e_{aq}^- . These free radicals can diffuse over distances varied from 60 to 19810 Å (Roots and Okada 1975) and react effectively with dissolved biological molecules. Although the exact site of inactivation is not fully known, it was found that the efficiency of radical inactivation is dose-rate-, target-molecule-concentration- and environmental-temperature-dependent. The behaviour of dose-rate and enzyme-molecule-concentration for metallo-enzyme was tested and studied. It was found that the inactivation of enzyme solution increased in proportion to dose-rate and in inverse

proportion to the enzyme's molecule concentration (figures 6.1-6.3). These findings are supported by other work by Dale 1942, Dale *et al* 1943, Okada 1957, Aldorie 1982 and Alwajidi 1984. Temperature dependence of indirect radiation action was reported by many authors for low LET ionising radiations interacting with different type of targets (mammalian cells, E.Coli, bacteriophages and enzyme solutions) (Okada 1957, Krisch 1970, 1972, Burki *et al* 1973 and Koch and Burki 1975). The dose rate dependence might be explained as follows: as the dose rate (energy per unit time) increases, then the number of radicals generated in the solvent will increase, and since we know that the interaction of radicals is time dependent (Roots and Okada 1975, Wright *et al* 1985 and Chatterjee and Magee 1985) the inactivation will be proportional to the applied dose rate. This proportionality is not linear, possibly as a result of the over saturation of radicals on the same inactivated sites (figure 6.9).

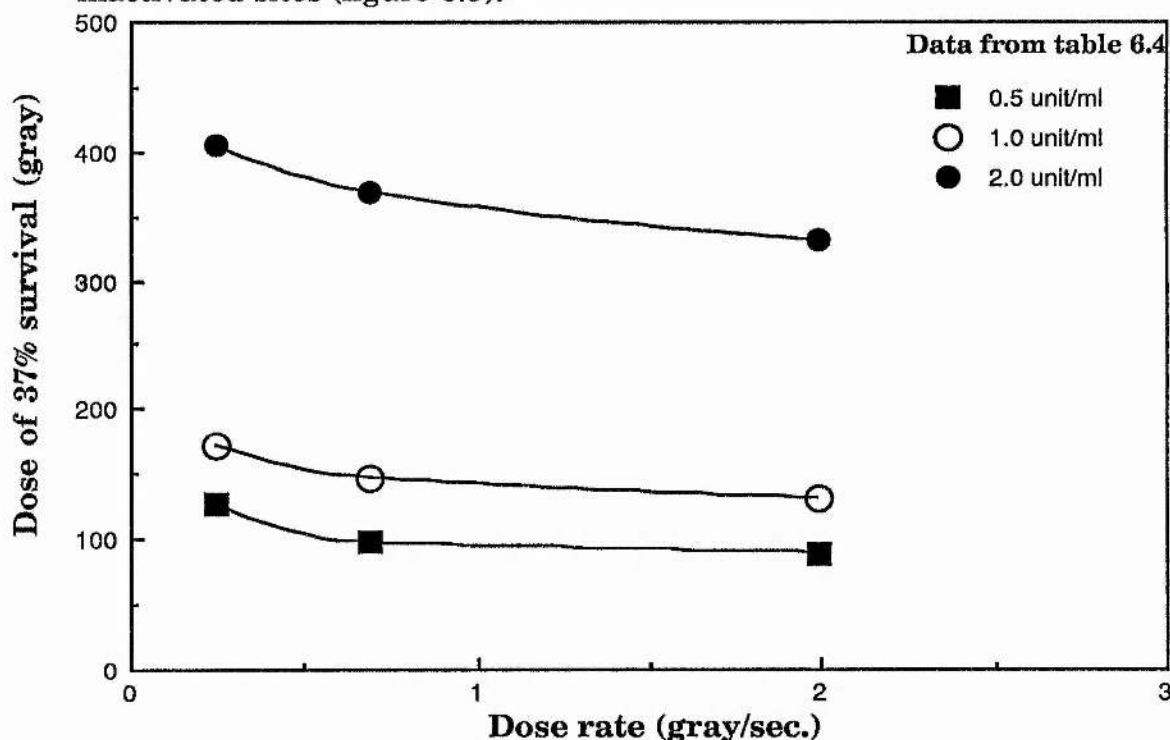


Figure 6.9: Enzyme in solution of different concentration inactivated by Cu-K-photons at different dose rates.

The dependence of the D_{37} on the enzyme concentration might be explained by the fact that, as the concentration of enzyme molecules increases then the probability that photons produce radical species decreases and in turn the number of inactivated sites decreases. As the concentration reaches the solid state, any indirect radiation action must be trivial. This dependence is clear in figure 6.10. Intrinsic efficiencies for the interpretation of radiation effects is basically important method which gives clear explanation for radiation quality, by which we avoid many problems that arise from using the absorbed dose, then the intrinsic efficiency of damage by $K\alpha$ photons (8.04 keV) for the metallo-enzyme irradiated in solution and in solid state and at different dose rates is drawn in figure 6.11 to summarise the radiation action of photons in enzyme

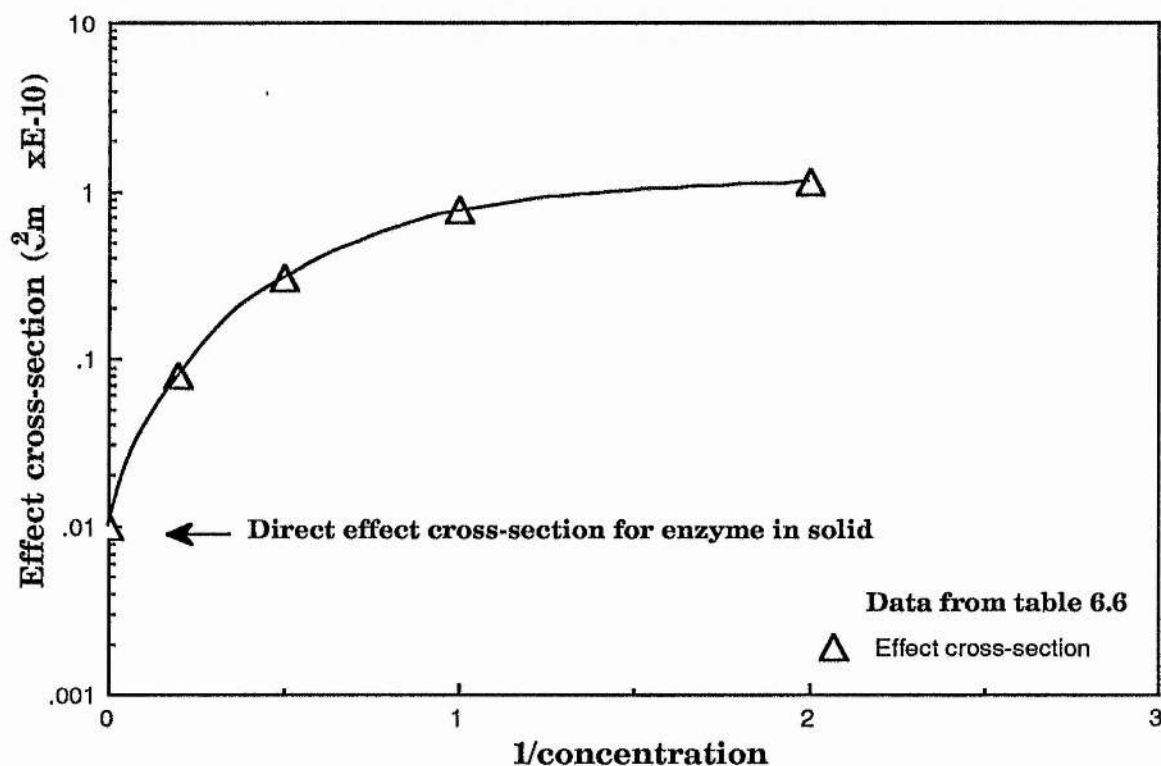


Figure 6.10: Effect cross section for dry enzyme and in solution of different concentrations irradiated by Cu-K x-rays at 1.99 gray/sec.

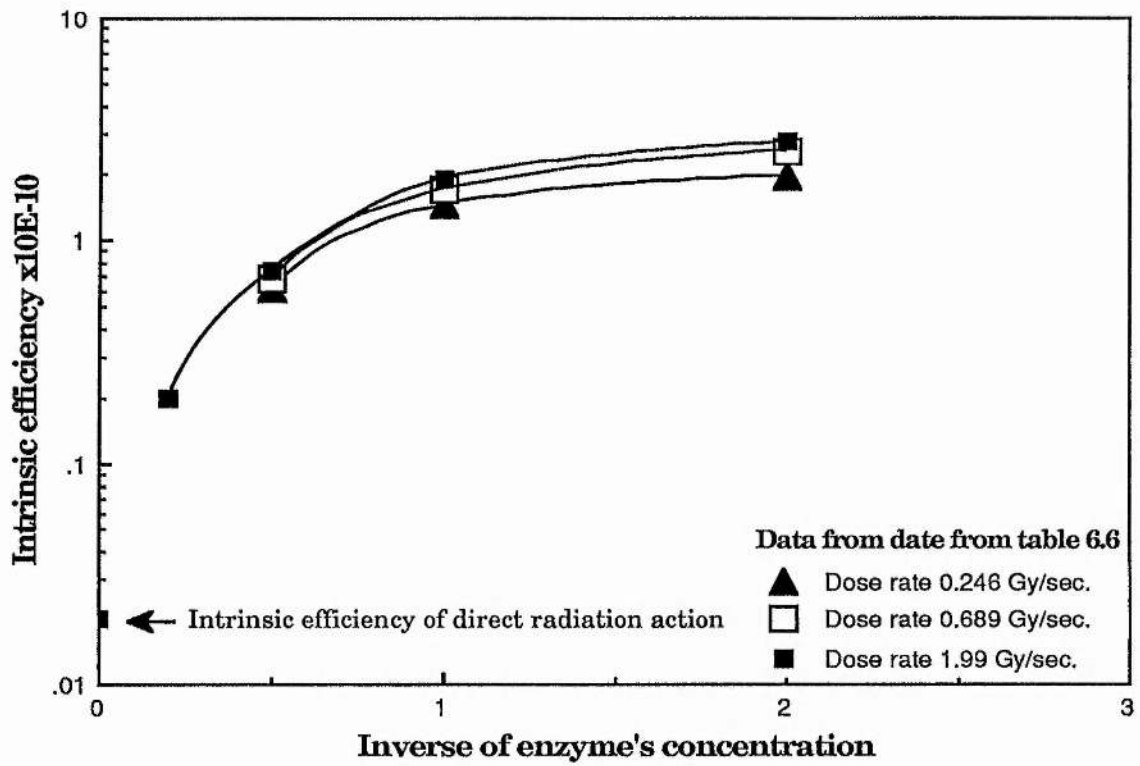


Figure 6.11: The intrinsic efficiency of damage by Cu-K x-rays for the metallo- enzyme in solution and in solid state at diferent dose rates.

Chapter VII

Conclusions and Recommendations

The quality of radiation from radionuclides incorporated into the DNA of the cell nucleus can be determined by the absolute biological effectiveness (the effect cross-section and the intrinsic efficiency) which may be used as a qualitative measure to categorize these nuclides, and to enable comparison with external irradiation. Such comparison is not obtainable using conventional dosimetry. The adoption of a new damage model enabled the interpretation of the mechanism responsible for the experimental results, and the attribution of the dominant cause of biological damage to three processes, namely direct, mixed and indirect effect.

Radionuclides may be divided into two groups, those whose radiation effect is absorbed completely inside the cell nucleus (^{125}I , ^{77}Br and ^3H) and those with long range radiation in which case the energy is absorbed outwith the sensitive targets (^{33}P , ^{131}I and ^{32}P).

For ^{125}I and ^{77}Br the action was predominantly direct and the effect was very great in the vicinity of the site of disintegration causing irreparable and irreversible damage. No temperature-dependence or dose-rate-dependence has been observed.

For ^3H only the indirect component of action appeared to be significant. Therefore the radiation action is expected to be both temperature - and dose-rate - dependent and is observed.

The inactivation probabilities of ^{33}P , ^{131}I and ^{32}P were found to be appreciably smaller than those for external irradiation. Since their projected range is very long, their energy is absorbed outwith the sensitive target. The action of these nuclides must have a significant

indirect component but their concentration is not sufficiently high to allow the build up of enough radicals around the sensitive targets, so these electrons have significant action only at the end of their tracks. Temperature-dependence was observed and dose-rate-dependence is expected.

If the dose-rate is sufficiently low that there is negligible indirect action, the quality as expressed by the effect cross-section is a function of the mean free path for ionisation. Otherwise the quality is represented by the general expression given in equation 2.8 or, in the special case where exposure is for a constant time period, by equation 2.10.

From analysis of the observed survival curves it is concluded that a consistent picture can be obtained if the dominant cause of damage is attributed to the electron tracks in the slowing down spectrum generated by the emitted primary electrons and if the secondary electron cascades interact directly or indirectly with sites in the DNA.

Since the effect cross-section is used to specify quality, a generalised scheme of dosimetry becomes possible for all ionising radiation in any irradiation situation. Then enough data from the experimental survival curves on the chemical reaction kinetics and on the time parameters determining the biological repair and the time of damage fixation needs to be known for different biological targets and for different ionising radiations. Therefore accurate experiments are required in which the exposure time is varied over a wide range at a constant dose-rate, and *vice versa*.

In an attempt to quantify the fundamental mechanism involved in direct and indirect action it was decided to irradiate a molecule of atomic composition similar to soft tissue but without a repair mechanism. Towards this objective, the metalloenzyme Dihydroorotic dehydrogenase

was irradiated in solution at different concentrations and in the dry state. The inactivation was found to be a single-hit single-target process. Two basic types of radiation interaction are thought to occur: direct and indirect action. For the inactivation of enzyme in solid state, direct radiation action is the only process expected. For inactivation of enzyme in solution both direct and indirect radiation actions may occur. These two processes are in competition depending on the concentration of the enzyme in the solution.

Another radiation action in metallo-enzymes has been called by some authors "resonance response" which they attribute to the additional consequences of Auger electron cascades, charge build up and radical species generated in the medium from the interaction of radiation with heavy atoms. Simple calculation proves that the excess absorbed energy in the enzyme due to the existence of the small fraction by weight of heavy atoms to the whole enzyme across the K-edge is very small (<1.5%). Hence the maximum radiation effectiveness for inducing damage associated with the iron atoms is less than 15%.

The ratio of 37% survival doses obtained for irradiation by photons energies below and above the K-edge for the heavy atoms is found to be a poor measure to specify the quality of radiation action. Ratios are found in the range from 1.0 to 1.6 and are approximately the same whether in solid or in solution, but if the actual energy absorbed across the K-edge has been taken into account, then the intrinsic efficiencies are approximately equal. Thus the use of intrinsic efficiency for the interpretation of radiation effects is basically a very useful method to quantify the radiation action which avoids many of the anomalies that arise through the use of absorbed dose.

A new damage model for the inactivation of the enzyme has been suggested and its parameters, namely direct and indirect effect cross-

sections, geometrical cross-section, saturated concentration constant, mean free path for radical absorption, root mean square diffusion constant, life time and G value for radical production, have been determined.

The direct and indirect effect cross-sections were calculated in two ways using firstly equation 6.1 and secondly the new damage model.

The direct effect cross-section was determined, using data from the survival curve of the enzyme irradiated in solid state, and equation 6.1, to be $1.0 \times 10^{-12} \text{ cm}^2$ while using the same data and the damage model it was determined to be $0.94 \times 10^{-12} \text{ cm}^2$. From the latter the geometrical cross-section was determined to be $1.3 \times 10^{-12} \text{ cm}^2$.

The indirect effect cross-section was determined using equation 6.1 and survival data from the enzyme irradiated in solutions of different concentrations and at different dose-rates. The resultant total effect cross-sections including both direct and indirect components can be seen in table 6.6 and figure 6.10, from the indirect effect cross-section for each enzyme concentration and for each dose rate can be determined, since the microscopic direct effect cross section is known (table 6.6). The root mean square of radical diffusion constant, \bar{r} , was calculated from equation 6.7, as the radical action reaches the saturation point (figure 6.10) and was between 56 - 65 nm. Consequently the mean diffusion distance of radicals, $L \sim 27 \text{ nm}$, this value is more consistent with the value for OH radicals reported by Chatterjee and Magee (1985). As the mean distance travelled by the radical in its life time ($t_c \sim 10^{-9} \text{ sec.}$) should be larger than the diffusion distance, then the G value must be less than 0.6. The saturated concentration constant for the enzyme solution was $2.2 \times 10^{-12} \text{ mol./ml.}$

It is concluded that the direct radiation action consists of the action of Compton electrons, photo-electrons, and the associated cascades of electrons produced in the molecule. Enzyme in solution is inactivated by direct action of radiation and by indirect action which appeared to be very important through the interaction of photons and their secondary electrons with the solvent's molecules (water) to liberate radicals. It was found that the efficiency of radical inactivation has an exponential dependence on dose-rate and is dependent on the inverse of the enzyme molecule concentration (figure 6.11 and section 6.3).

It is probable that the damage model can be generalised to suit other enzymes, so it is recommended that further study be undertaken using different ionising radiations and different enzymes to explore the generalisation. Temperature dependence should also be studied by irradiating enzyme in solution of different concentrations over a broad temperature range (-196 °C to 37 °C).

Appendix A

Spectra from Soft X-rays and Other Radiation Sources Obtained by Using a NaI(Tl) Scintillation Detector and a Proportional Counter

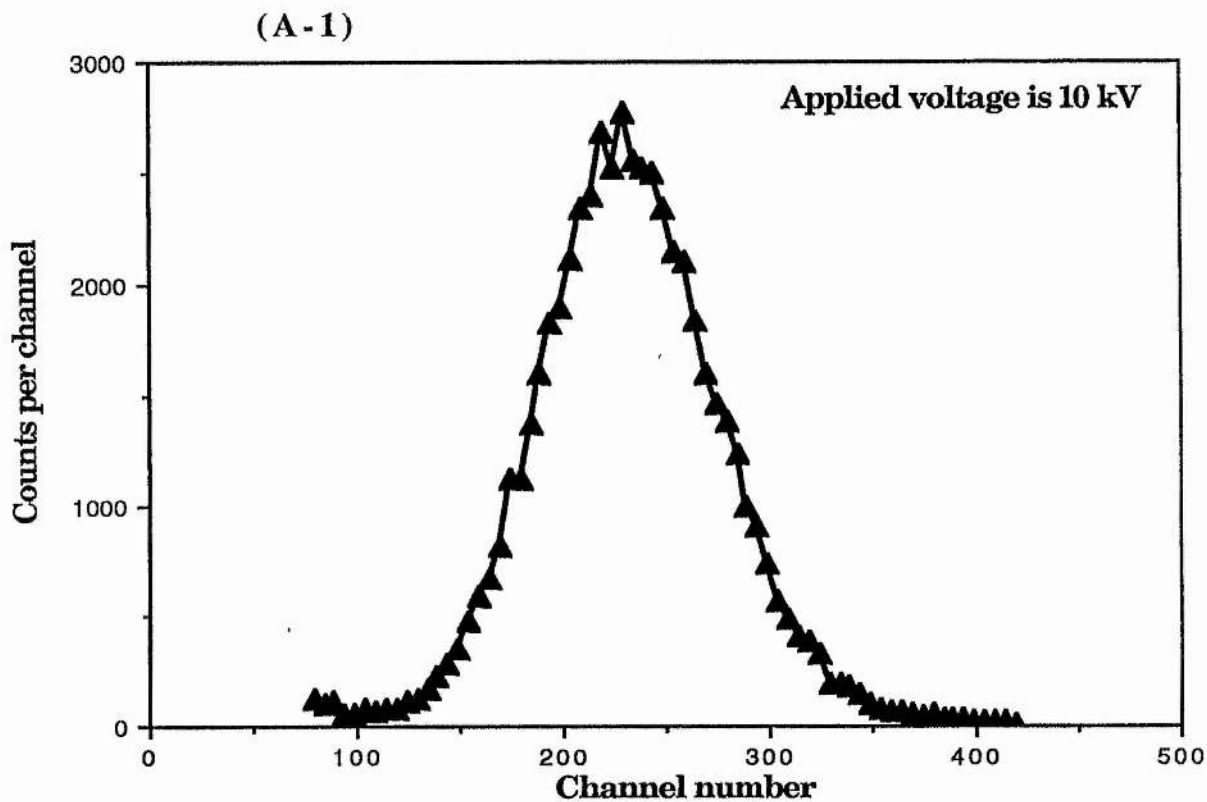
Radiation spectroscopy is the measurement of the energy distribution of the incident radiation, and the detector which is used to measure this distribution is called a spectrometer. To consider the qualities of this type of detector, its response to a monoenergetic source of the appropriate radiation is examined. The distribution of differential pulse heights produced by a detector illustrates its response function for the particular energy used.

The detector has good resolution if there is only one possible distribution around a mean pulse height, but has poor resolution if there are many such distributions, even if they are centred at the same average height. In this case the width of the spectrum will determine the type of resolution of the detector, the broader spectrum reflecting the poorer resolution. This width reflects the fact that a large amount of fluctuation is recorded from pulse to pulse even though the same energy is deposited in the detector for each event. If the amount of these fluctuations is decreased the width of the corresponding distribution will also decrease and the peak will approach a sharp spike.

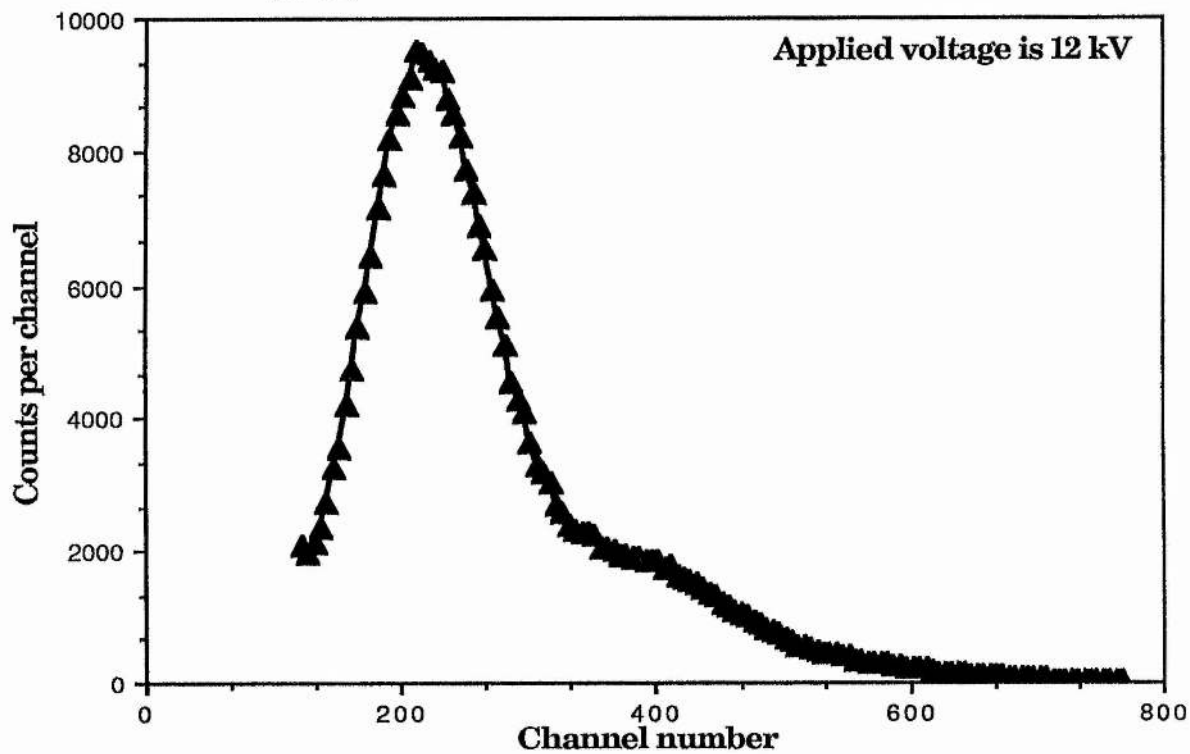
Energy resolution of the detector is defined as "the full width of the distribution at a level which is just half the maximum ordinate of the peak, FWHM, divided by the location of the peak centroid, H_0 . The energy resolution, R , is thus a dimensionless fraction expressed as a percentage

$$R = \frac{\text{FWHM}}{H_0} \times 100 \%$$

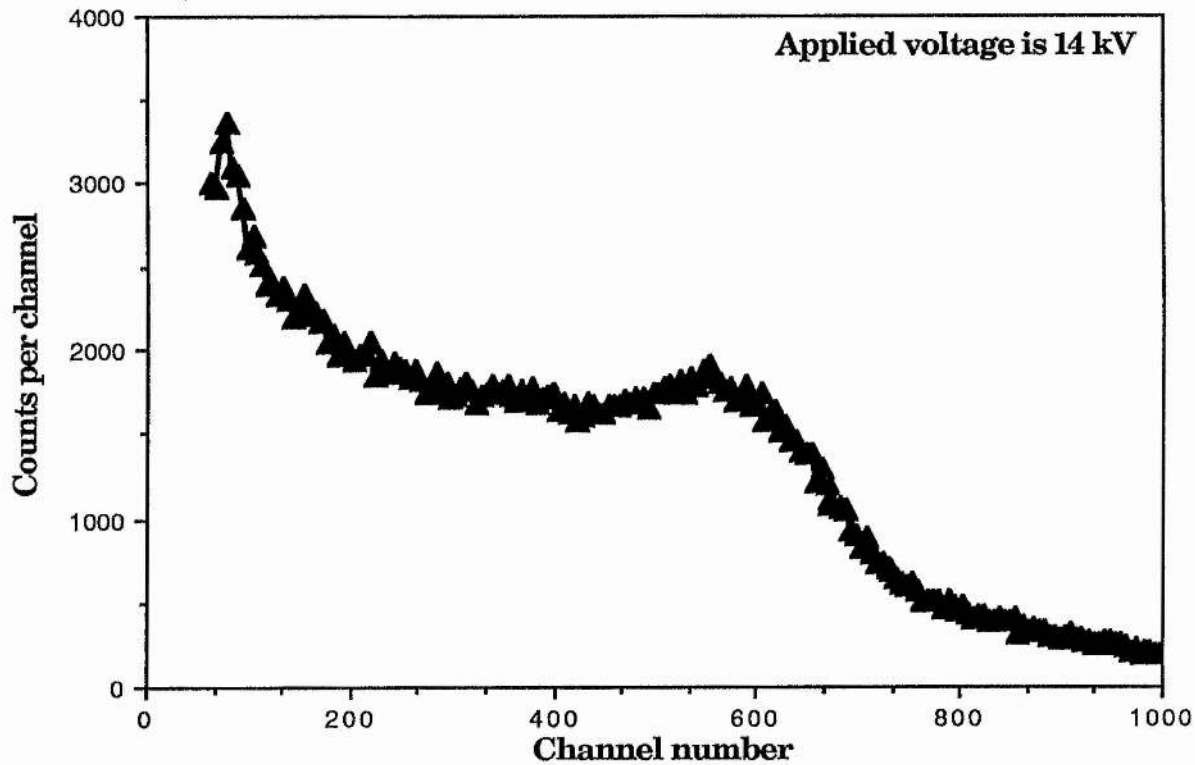
Spectra of soft X-rays and other radiation sources have been detected by using both a NaI(Tl) scintillation detector, as illustrated in A.1 - A.8, and a proportional counter, as illustrated in A.9 - A-12.

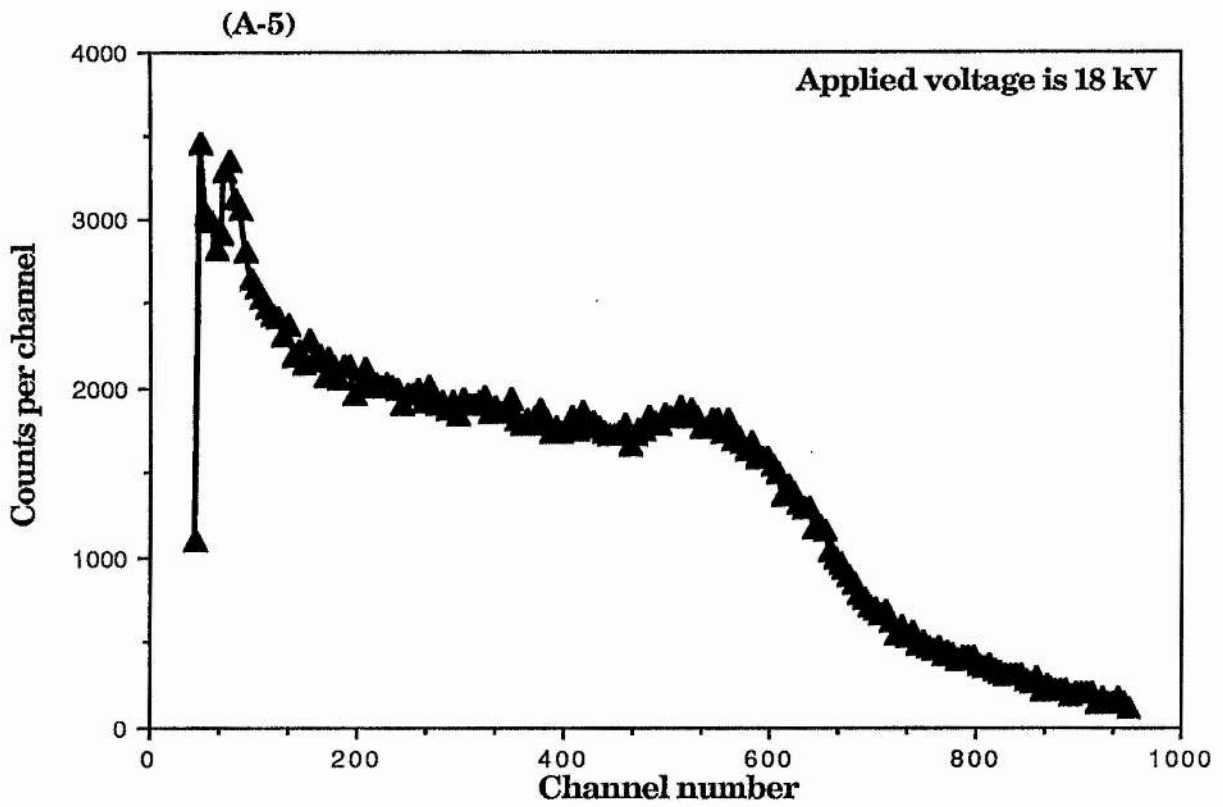
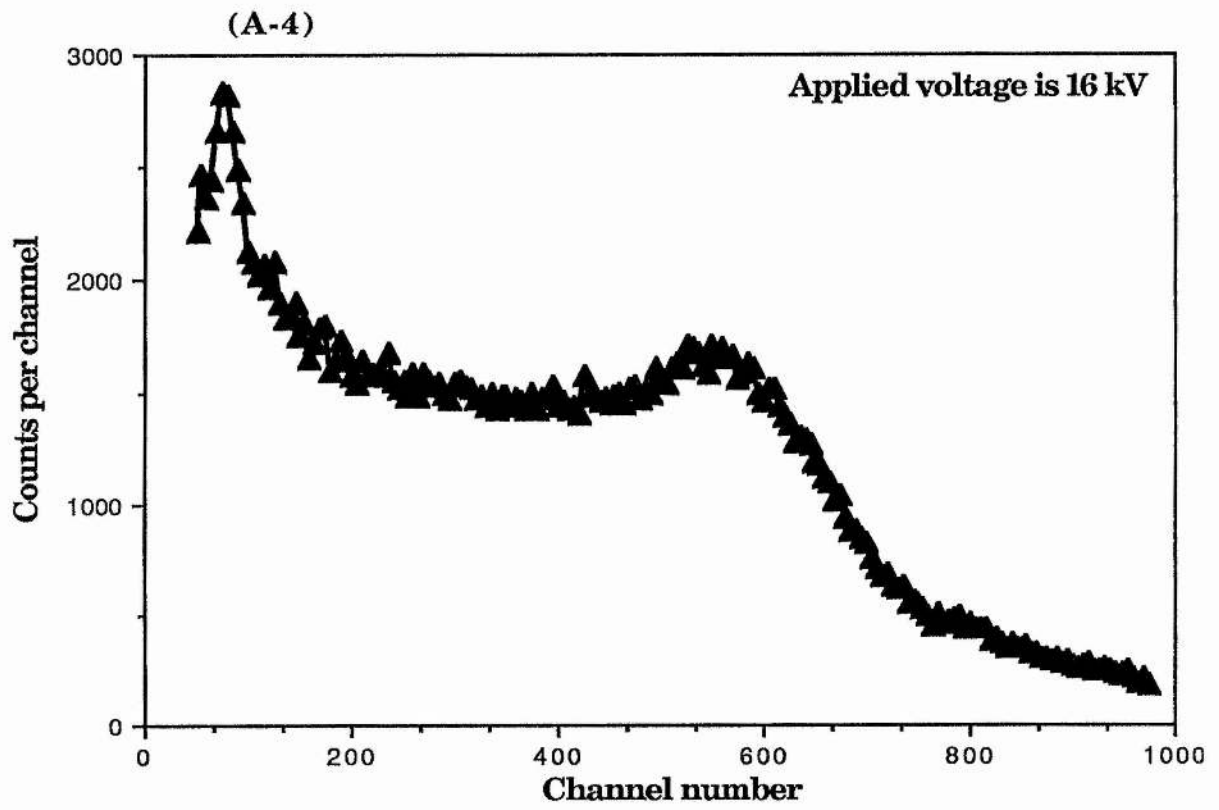


(A-2)

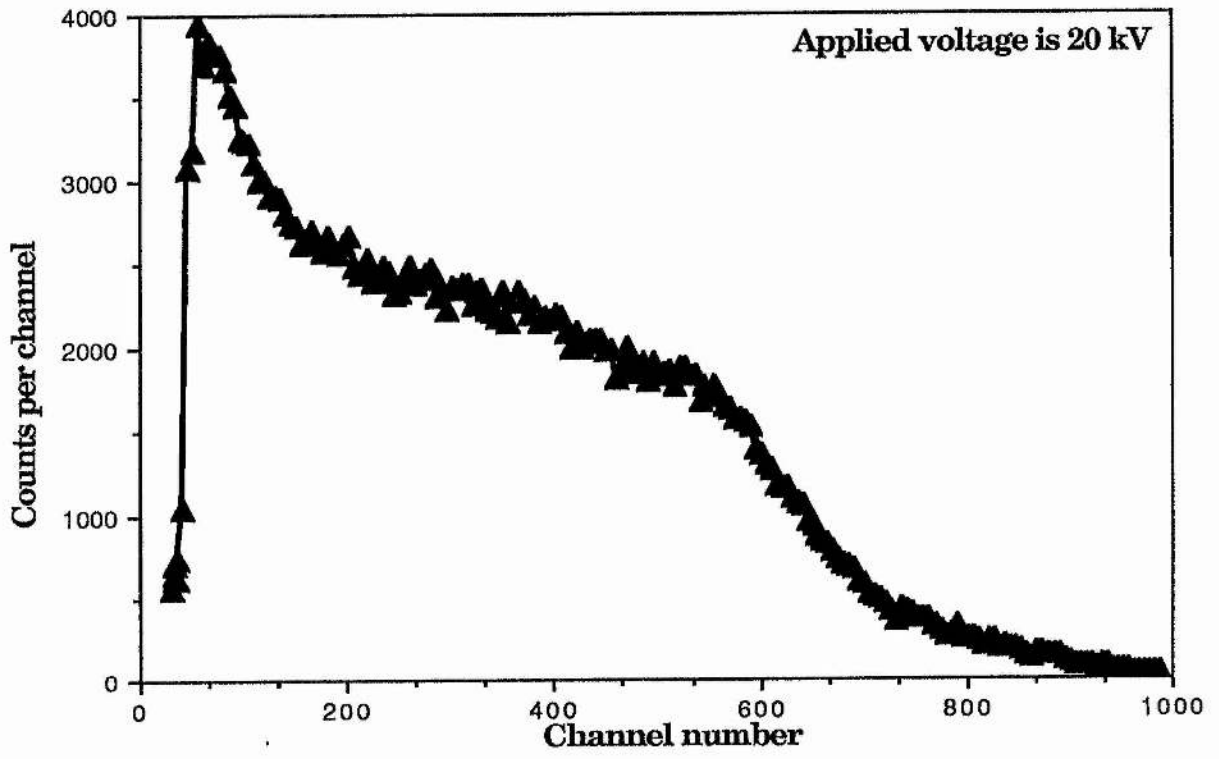


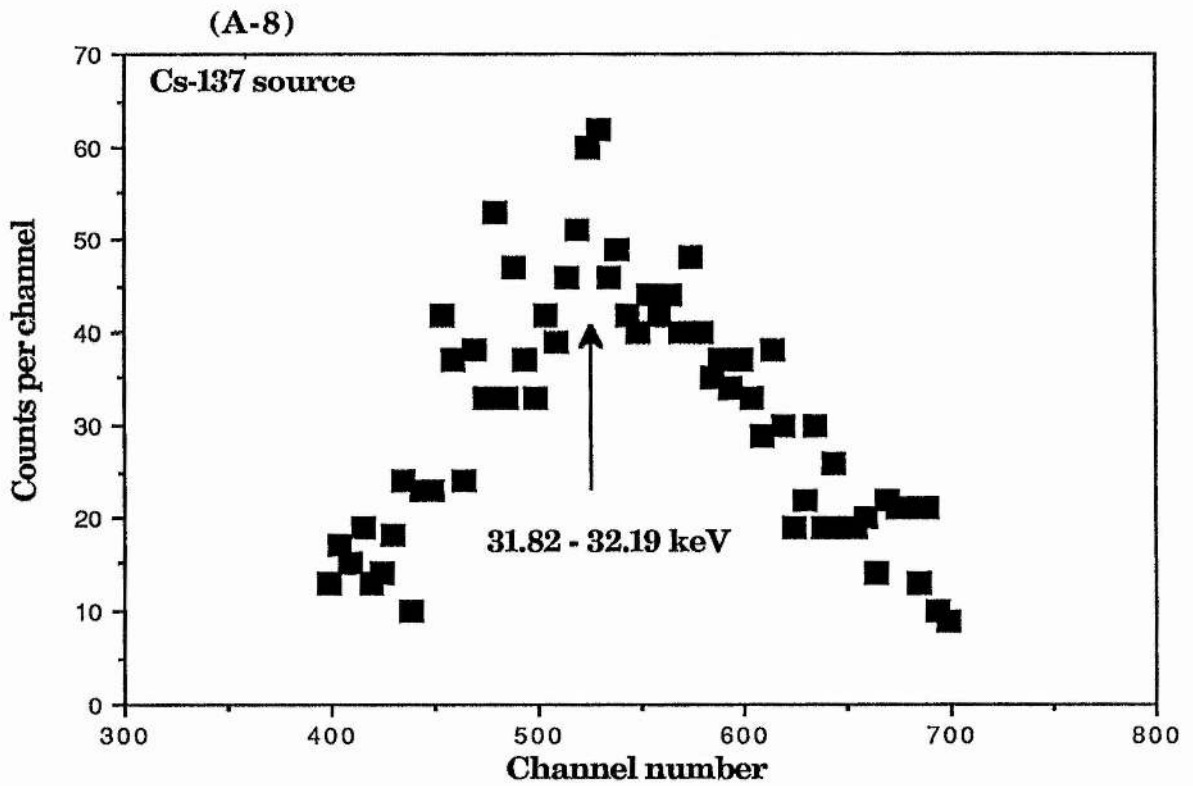
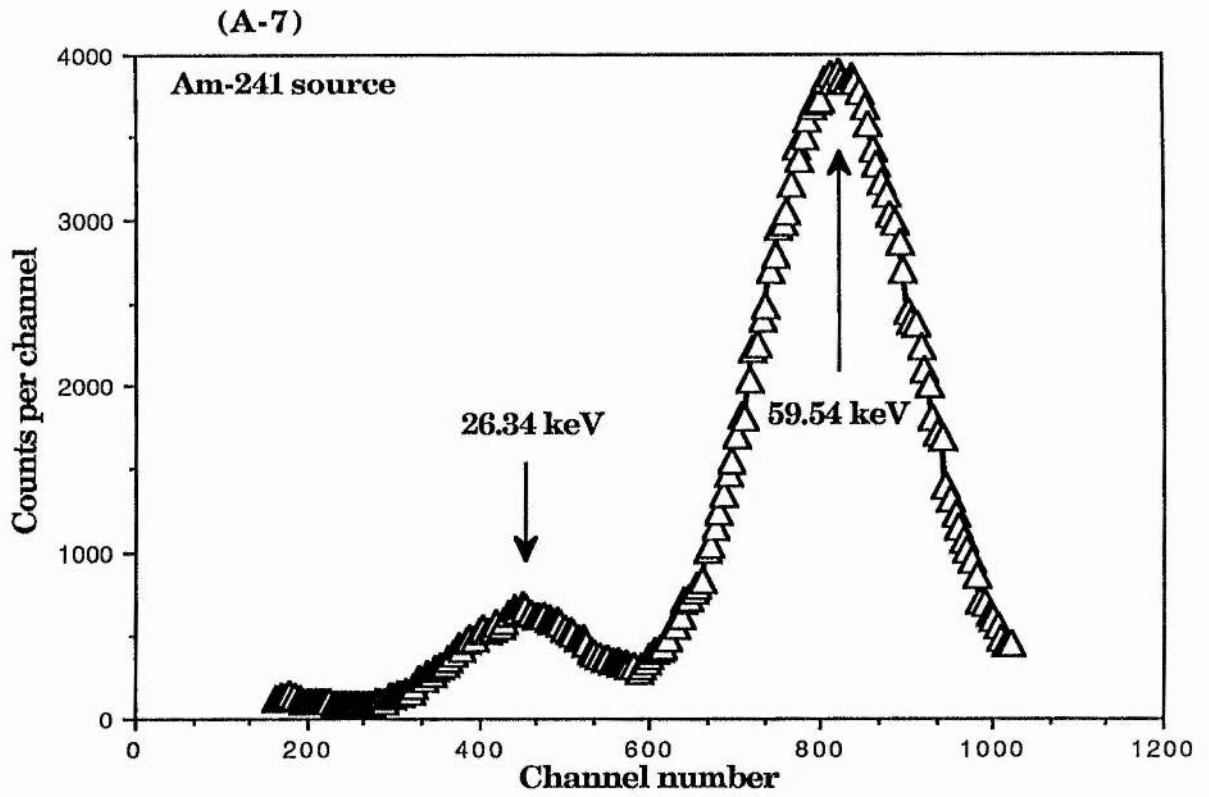
(A-3)

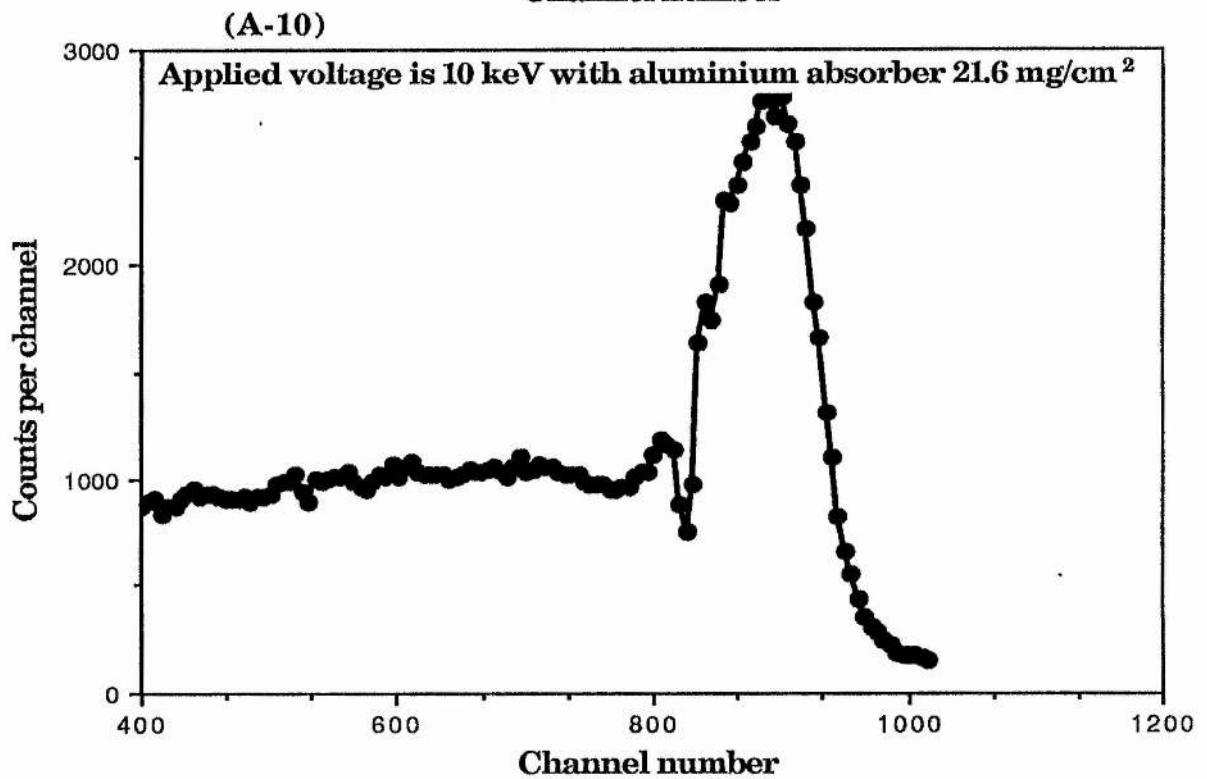
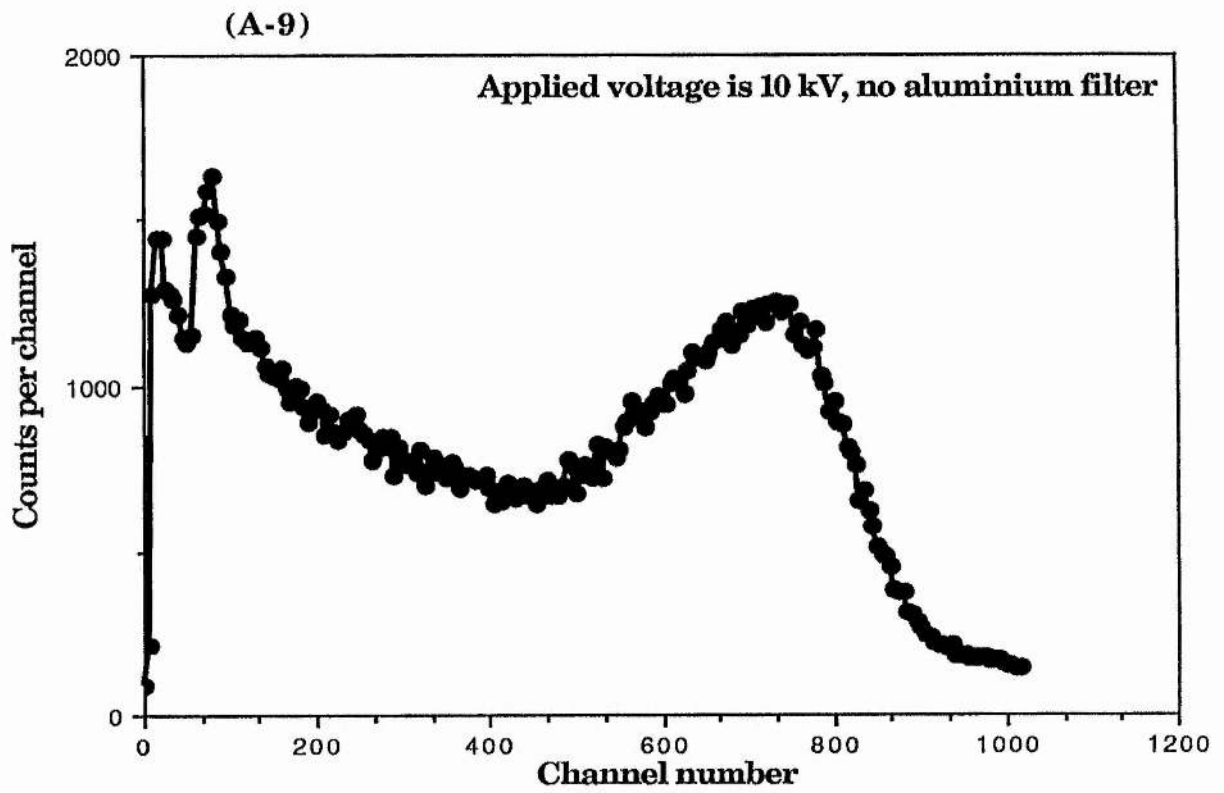




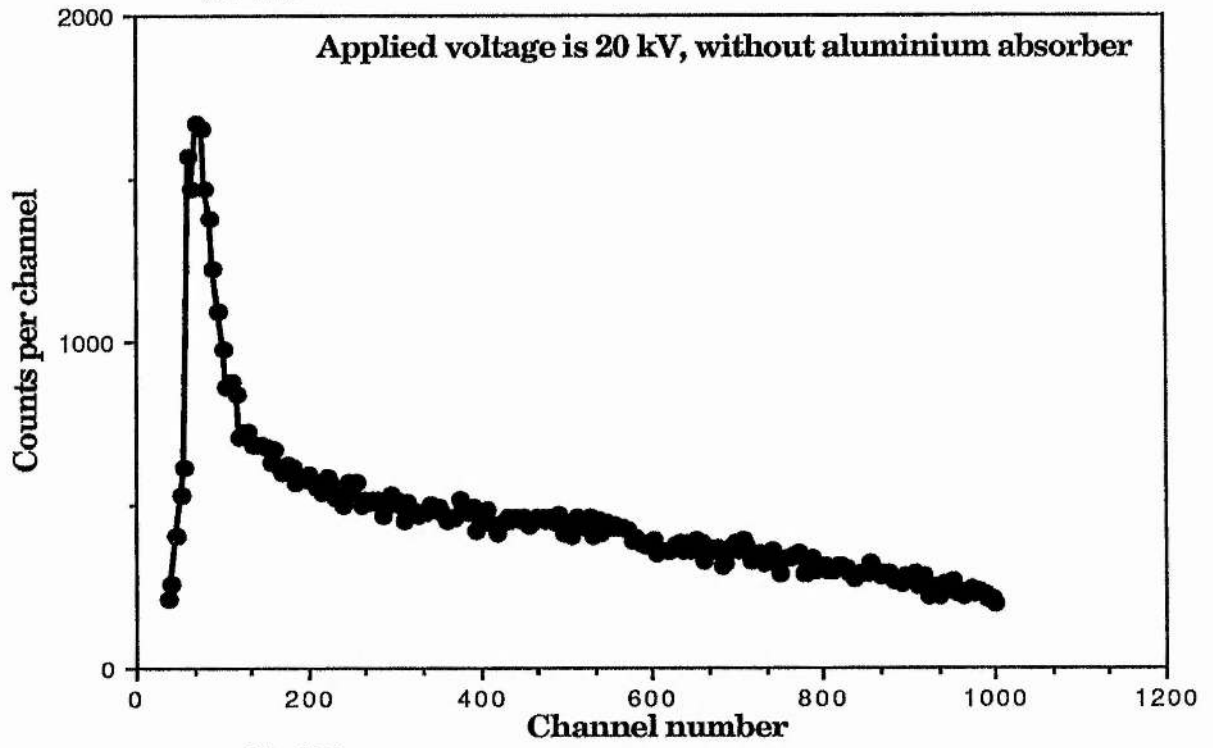
(A-6)



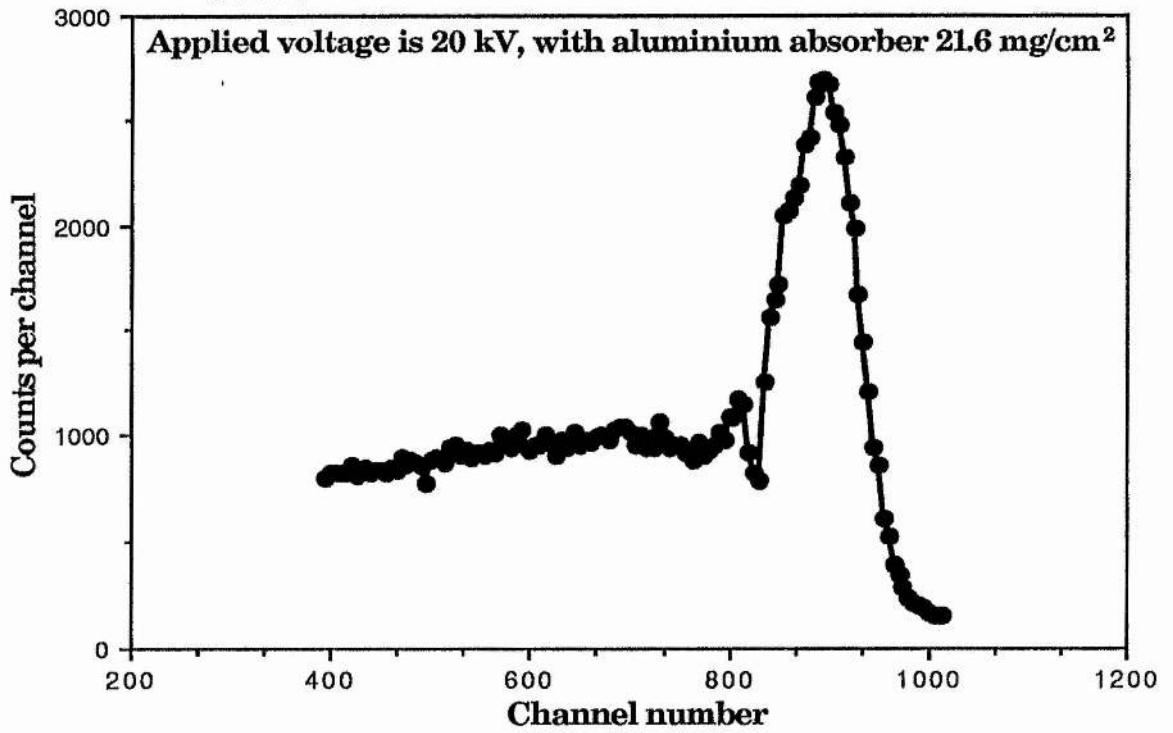




(A-11)



(A-12)



Appendix B
Experimental data of the Metallo-enzyme irradiated
by Cu-K x-rays in solution and in dry state

Table B.1: 0.5 unit/ml enzyme solution irradiated at dose rate 0.246 Gy/sec

Incubation time (min.)	Blank (O.D.) _B	Control (O.D.) _C	Test (O.D.) _T	$\frac{(O.D.)_B - (O.D.)_T}{(O.D.)_B - (O.D.)_C} \frac{N}{N_0}$
1	0.675	0.643	0.651	0.750
2	0.675	0.610	0.628	0.723
3	0.674	0.572	0.597	0.755
4	0.673	0.531	0.563	0.775
5	0.673	0.496	0.535	0.780
Dose rate = 0.246 Gray/sec. Irradiation time = 150 sec. Total dose = 36.9 Gray Enzyme concn. = 0.5 unit/ml			Average survival fraction	0.755 ± 0.02

Incubation time (min.)	Blank (O.D.) _B	Control (O.D.) _C	Test (O.D.) _T	$\frac{(O.D.)_B - (O.D.)_T}{(O.D.)_B - (O.D.)_C} \frac{N}{N_0}$
1	0.679	0.647	0.662	0.531
2	0.679	0.612	0.642	0.552
3	0.678	0.565	0.614	0.566
4	0.677	0.534	0.594	0.580
5	0.677	0.504	0.575	0.590
Dose rate = 0.246 Gray/sec. Irradiation time = 300 sec. Total dose = 73.8 Gray Enzyme concn. = 0.5 unit/ml			Average survival fraction	0.564 ± 0.015

Incubation time (min.)	Blank (O.D.) _B	Control (O.D.) _C	Test (O.D.) _T	$\frac{(O.D.)_B - (O.D.)_T}{(O.D.)_B - (O.D.)_C} \frac{N}{N_0}$
1	0.680	0.640	0.675	0.125
2	0.680	0.601	0.669	0.139
3	0.679	0.564	0.662	0.148
4	0.678	0.529	0.656	0.148
5	0.677	0.499	0.649	0.157
Dose rate = 0.246 Gray/sec. Irradiation time = 975 sec. Total dose = 239.85 Gray Enzyme concn. = 0.5 unit/ml			Average survival fraction	0.15 ± 0.007

Table B.2: 0.5 unit/ml enzyme solution irradiated at dose rate 0.689 Gy/sec

Incubation time (min.)	Blank (O.D.) _B	Control (O.D.) _C	Test (O.D.) _T	$\frac{(O.D.)_B - (O.D.)_T}{(O.D.)_B - (O.D.)_C} \frac{N}{N_0}$
1	0.856	0.817	0.836	0.513
2	0.855	0.778	0.815	0.519
3	0.855	0.748	0.799	0.523
4	0.853	0.718	0.781	0.533
5	0.851	0.688	0.763	0.540
Dose rate = 0.689 Gray/sec. Irradiation time = 90 sec. Total dose = 62.01 Gray Enzyme concn. = 0.5 unit/ml			Average survival fraction	0.528 ± 0.008

Incubation time (min.)	Blank (O.D.) _B	Control (O.D.) _C	Test (O.D.) _T	$\frac{(O.D.)_B - (O.D.)_T}{(O.D.)_B - (O.D.)_C} \frac{N}{N_0}$
1	0.853	0.816	0.844	0.240
2	0.852	0.780	0.833	0.270
3	0.850	0.744	0.822	0.270
4	0.849	0.711	0.810	0.280
5	0.849	0.675	0.800	0.280
Dose rate = 0.689 Gray/sec. Irradiation time = 180 sec. Total dose = 124.02 Gray Enzyme concn. = 0.5 unit/ml			Average survival fraction	0.275 ± 0.005

Incubation time (min.)	Blank (O.D.) _B	Control (O.D.) _C	Test (O.D.) _T	$\frac{(O.D.)_B - (O.D.)_T}{(O.D.)_B - (O.D.)_C} \frac{N}{N_0}$
1	0.850	0.816	0.846	0.118
2	0.849	0.779	0.841	0.114
3	0.849	0.744	0.836	0.124
4	0.848	0.709	0.829	0.136
5	0.847	0.675	0.825	0.128
Dose rate = 0.689 Gray/sec. Irradiation time = 300 sec. Total dose = 206.7 Gray Enzyme concn. = 0.5 unit/ml			Average survival fraction	0.124 ± 0.005

Table B.3: 0.5 unit/ml enzyme solution irradiated at dose rate 1.99 Gy/sec

Incubation time (min.)	Blank (O.D.) _B	Control (O.D.) _C	Test (O.D.) _T	$\frac{(O.D.)_B - (O.D.)_T}{(O.D.)_B - (O.D.)_C} N_0$
1	0.867	0.832	0.846	0.600
2	0.865	0.797	0.824	0.603
3	0.865	0.764	0.803	0.614
4	0.864	0.732	0.782	0.621
5	0.863	0.702	0.763	0.621
Dose rate = 1.99 Gray/sec. Irradiation time = 20 sec. Total dose = 39.8 Gray Enzyme concn. = 0.5 unit/ml			Average survival fraction	0.612 ± 0.008

Incubation time (min.)	Blank (O.D.) _B	Control (O.D.) _C	Test (O.D.) _T	$\frac{(O.D.)_B - (O.D.)_T}{(O.D.)_B - (O.D.)_C} N_0$
1	0.796	0.762	0.785	0.324
2	0.795	0.727	0.773	0.323
3	0.795	0.693	0.762	0.324
4	0.794	0.659	0.749	0.333
5	0.793	0.627	0.737	0.337
Dose rate = 1.99 Gray/sec. Irradiation time = 50 sec. Total dose = 99.5 Gray Enzyme concn. = 0.5 unit/ml			Average survival	0.328 ± 0.008

Incubation time (min.)	Blank (O.D.) _B	Control (O.D.) _C	Test (O.D.) _T	$\frac{(O.D.)_B - (O.D.)_T}{(O.D.)_B - (O.D.)_C} N_0$
1	0.781	0.750	0.777	0.129
2	0.780	0.717	0.772	0.127
3	0.780	0.685	0.767	0.137
4	0.779	0.651	0.763	0.125
5	0.777	0.620	0.754	0.146
Dose rate = 1.99 Gray/sec. Irradiation time = 90 sec. Total dose = 179.1 Gray Enzyme concn. = 0.5 unit/ml			Average survival	0.133 ± 0.008

Table B.4: 1.0 unit/ml enzyme solution irradiated at dose rate 0.246 Gy/sec

Incubation time (min.)	Blank (O.D.) _B	Control (O.D.) _C	Test (O.D.) _T	$\frac{(O.D.)_B - (O.D.)_T}{(O.D.)_B - (O.D.)_C} N_0$
1	0.831	0.752	0.772	0.747
2	0.830	0.670	0.708	0.763
3	0.830	0.593	0.648	0.768
4	0.829	0.518	0.590	0.768
5	0.828	0.444	0.532	0.771
Dose rate = 0.246 Gray/sec. Irradiation time = 180 sec. Total dose = 44.28 Gray Enzyme concn. = 1.0 unit/ml			Average survival fraction	0.764 ± 0.004

Incubation time (min.)	Blank (O.D.) _B	Control (O.D.) _C	Test (O.D.) _T	$\frac{(O.D.)_B - (O.D.)_T}{(O.D.)_B - (O.D.)_C} N_0$
1	0.885	0.815	0.846	0.557
2	0.884	0.744	0.806	0.557
3	0.884	0.675	0.765	0.569
4	0.882	0.607	0.727	0.564
5	0.881	0.541	0.691	0.559
Dose rate = 0.246 Gray/sec. Irradiation time = 420 sec. Total dose = 103.32 Gray Enzyme concn. = 1.0 unit/ml			Average survival	0.561 ± 0.004

Incubation time (min.)	Blank (O.D.) _B	Control (O.D.) _C	Test (O.D.) _T	$\frac{(O.D.)_B - (O.D.)_T}{(O.D.)_B - (O.D.)_C} N_0$
1	0.892	0.824	0.881	0.162
2	0.891	0.752	0.866	0.189
3	0.891	0.685	0.856	0.170
4	0.889	0.620	0.842	0.178
5	0.888	0.562	0.829	0.181
Dose rate = 0.246 Gray/sec. Irradiation time = 1200 sec. Total dose = 295.2 Gray Enzyme concn. = 1.0 unit/ml			Average survival fraction	0.176 ± 0.004

Table B.5: 1.0 unit/ml enzyme solution irradiated at dose rate 0.689 Gy/sec

Incubation time (min.)	Blank (O.D.) _B	Control (O.D.) _C	Test (O.D.) _T	$\frac{(O.D.)_B - (O.D.)_T}{(O.D.)_B - (O.D.)_C} N$ = $\frac{N}{N_0}$
1	0.891	0.830	0.852	0.639
2	0.890	0.771	0.812	0.655
3	0.889	0.714	0.775	0.651
4	0.889	0.658	0.739	0.649
5	0.887	0.602	0.699	0.660
Dose rate = 0.689 Gray/sec. Irradiation time = 90 sec. Total dose = 62.01 Gray Enzyme concn. = 1.0 unit/ml			Average survival fraction	0.651 ± 0.005

Incubation time (min.)	Blank (O.D.) _B	Control (O.D.) _C	Test (O.D.) _T	$\frac{(O.D.)_B - (O.D.)_T}{(O.D.)_B - (O.D.)_C} N$ = $\frac{N}{N_0}$
1	0.863	0.806	0.840	0.403
2	0.863	0.750	0.816	0.416
3	0.861	0.694	0.789	0.431
4	0.860	0.640	0.763	0.441
5	0.858	0.589	0.737	0.450
Dose rate = 0.689 Gray/sec. Irradiation time = 180 sec. Total dose = 124.02 Gray Enzyme concn. = 1.0 unit/ml			Average survival fraction	0.428 ± 0.01

Incubation time (min.)	Blank (O.D.) _B	Control (O.D.) _C	Test (O.D.) _T	$\frac{(O.D.)_B - (O.D.)_T}{(O.D.)_B - (O.D.)_C} N$ = $\frac{N}{N_0}$
1	0.850	0.791	0.842	0.136
2	0.849	0.732	0.832	0.145
3	0.849	0.673	0.823	0.148
4	0.848	0.617	0.811	0.160
5	0.846	0.563	0.801	0.159
Dose rate = 0.689 Gray/sec. Irradiation time = 400 sec. Total dose = 275.6 Gray Enzyme concn. = 1.0 unit/ml			Average survival fraction	0.150 ± 0.005

Table B.6: 1.0 unit/ml enzyme solution irradiated at dose rate 1.99 Gy/sec

Incubation time (min.)	Blank (O.D.) _B	Control (O.D.) _C	Test (O.D.) _T	$\frac{(O.D.)_B - (O.D.)_T}{(O.D.)_B - (O.D.)_C} N$ ----- = ---- _{N_0}
1	0.875	0.814	0.837	0.623
2	0.876	0.752	0.797	0.637
3	0.874	0.693	0.758	0.641
4	0.874	0.636	0.725	0.626
5	0.872	0.585	0.686	0.641
Dose rate = 1.99 Gray/sec. Irradiation time = 30 sec. Total dose = 59.7 Gray Enzyme concn. = 1.0 unit/ml			Average survival fraction	0.634 ± 0.004

Incubation time (min.)	Blank (O.D.) _B	Control (O.D.) _C	Test (O.D.) _T	$\frac{(O.D.)_B - (O.D.)_T}{(O.D.)_B - (O.D.)_C} N$ ----- = ---- _{N_0}
1	0.862	0.803	0.839	0.390
2	0.862	0.743	0.814	0.403
3	0.860	0.683	0.789	0.401
4	0.859	0.626	0.763	0.412
5	0.859	0.570	0.741	0.408
Dose rate = 1.99 Gray/sec. Irradiation time = 60 sec. Total dose = 119.4 Gray Enzyme concn. = 1.0 unit/ml			Average survival fraction	0.403 ± 0.005

Incubation time (min.)	Blank (O.D.) _B	Control (O.D.) _C	Test (O.D.) _T	$\frac{(O.D.)_B - (O.D.)_T}{(O.D.)_B - (O.D.)_C} N$ ----- = ---- _{N_0}
1	0.860	0.803	0.851	0.158
2	0.861	0.746	0.843	0.157
3	0.859	0.690	0.831	0.169
4	0.858	0.636	0.820	0.171
5	0.856	0.584	0.804	0.191
Dose rate = 1.99 Gray/sec. Irradiation time = 120 sec. Total dose = 238.8 Gray Enzyme concn. = 1.0 unit/ml			Average survival fraction	0.169 ± 0.01

Table B.7: 2.0 unit/ml enzyme solution irradiated at dose rate 0.246 Gy/sec

Incubation time (min.)	Blank (O.D.) _B	Control (O.D.) _C	Test (O.D.) _T	$\frac{(O.D.)_B - (O.D.)_T}{(O.D.)_B - (O.D.)_C} \frac{N}{N_0}$
1	0.792	0.721	0.731	0.859
2	0.791	0.656	0.678	0.837
3	0.791	0.596	0.627	0.841
4	0.789	0.540	0.577	0.851
5	0.788	0.489	0.534	0.849
Dose rate = 0.246 Gray/sec. Irradiation time = 5.0 min. Total dose = 73.8 Gray Enzyme concn. = 2.0 unit/ml			Average survival fraction	0.845 ± 0.005

Incubation time (min.)	Blank (O.D.) _B	Control (O.D.) _C	Test (O.D.) _T	$\frac{(O.D.)_B - (O.D.)_T}{(O.D.)_B - (O.D.)_C} \frac{N}{N_0}$
1	0.785	0.717	0.747	0.569
2	0.783	0.650	0.709	0.556
3	0.782	0.588	0.669	0.582
4	0.780	0.529	0.637	0.570
5	0.780	0.472	0.598	0.591
Dose rate = 0.246 Gray/sec. Irradiation time = 15.0 min. Total dose = 221.4 Gray Enzyme concn. = 2.0 unit/ml			Average survival fraction	0.575 ± 0.013

Incubation time (min.)	Blank (O.D.) _B	Control (O.D.) _C	Test (O.D.) _T	$\frac{(O.D.)_B - (O.D.)_T}{(O.D.)_B - (O.D.)_C} \frac{N}{N_0}$
1	0.771	0.708	0.753	0.296
2	0.769	0.650	0.733	0.302
3	0.768	0.594	0.718	0.287
4	0.765	0.541	0.698	0.299
5	0.763	0.489	0.681	0.299
Dose rate = 0.246 Gray/sec. Irradiation time = 35 min. Total dose = 516.6 Gray Enzyme concn. = 2.0 unit/ml			Average survival fraction	0.297 ± 0.005

Table B.8: 2.0 unit/ml enzyme solution irradiated at dose rate 0.689 Gy/sec

Incubation time (min.)	Blank (O.D.) _B	Control (O.D.) _C	Test (O.D.) _T	$\frac{(O.D.)_B - (O.D.)_T}{(O.D.)_B - (O.D.)_C} \frac{N}{N_0}$
1	0.697	0.638	0.652	0.763
2	0.696	0.581	0.609	0.757
3	0.693	0.530	0.568	0.767
4	0.690	0.480	0.528	0.771
5	0.687	0.431	0.487	0.781
Dose rate = 0.689 Gray/sec. Irradiation time = 150 sec. Total dose = 103.35 Gray Enzyme concn. = 2.0 unit/ml			Average survival fraction	0.769 ± 0.008

Incubation time (min.)	Blank (O.D.) _B	Control (O.D.) _C	Test (O.D.) _T	$\frac{(O.D.)_B - (O.D.)_T}{(O.D.)_B - (O.D.)_C} \frac{N}{N_0}$
1	0.687	0.630	0.655	0.561
2	0.687	0.576	0.623	0.577
3	0.685	0.524	0.593	0.571
4	0.683	0.471	0.562	0.571
5	0.682	0.419	0.530	0.578
Dose rate = 0.689 Gray/sec. Irradiation time = 5 min. Total dose = 206.7 Gray Enzyme concn. = 2.0 unit/ml			Average survival fraction	0.574 ± 0.003

Incubation time (min.)	Blank (O.D.) _B	Control (O.D.) _C	Test (O.D.) _T	$\frac{(O.D.)_B - (O.D.)_T}{(O.D.)_B - (O.D.)_C} \frac{N}{N_0}$
1	0.682	0.622	0.666	0.267
2	0.681	0.564	0.651	0.256
3	0.679	0.507	0.633	0.267
4	0.676	0.456	0.615	0.268
5	0.674	0.407	0.599	0.281
Dose rate = 0.689 Gray/sec. Irradiation time = 12 min. Total dose = 496.08 Gray Enzyme concn. = 2.0 unit/ml			Average survival fraction	0.268 ± 0.008

Table B.9: 2.0 unit/ml enzyme solution irradiated at dose rate 1.99 Gy/sec

Incubation time (min.)	Blank (O.D.) _B	Control (O.D.) _C	Test (O.D.) _T	$\frac{(O.D.)_B - (O.D.)_T}{(O.D.)_B - (O.D.)_C} N$
1	0.823	0.770	0.783	0.755
2	0.822	0.714	0.740	0.759
3	0.820	0.663	0.701	0.758
4	0.817	0.616	0.662	0.771
5	0.816	0.569	0.623	0.781
Dose rate = 1.99 Gray/sec. Irradiation time = 45 sec. Total dose = 89.55 Gray Enzyme concn. = 2.0 unit/ml			Average survival fraction	0.767 ± 0.009

Incubation time (min.)	Blank (O.D.) _B	Control (O.D.) _C	Test (O.D.) _T	$\frac{(O.D.)_B - (O.D.)_T}{(O.D.)_B - (O.D.)_C} N$
1	0.815	0.760	0.784	0.564
2	0.814	0.704	0.751	0.573
3	0.811	0.649	0.716	0.586
4	0.809	0.596	0.683	0.592
5	0.807	0.547	0.656	0.581
Dose rate = 1.99 Gray/sec. Irradiation time = 90 sec. Total dose = 179.1 Gray Enzyme concn. = 2.0 unit/ml			Average survival fraction	0.582 ± 0.006

Incubation time (min.)	Blank (O.D.) _B	Control (O.D.) _C	Test (O.D.) _T	$\frac{(O.D.)_B - (O.D.)_T}{(O.D.)_B - (O.D.)_C} N$
1	0.796	0.739	0.777	0.333
2	0.796	0.685	0.758	0.342
3	0.794	0.632	0.739	0.340
4	0.791	0.580	0.719	0.341
5	0.790	0.531	0.700	0.347
Dose rate = 1.99 Gray/sec. Irradiation time = 180 sec. Total dose = 358.2 Gray Enzyme concn. = 2.0 unit/ml			Average survival fraction	0.342 ± 0.003

Table B.10: 5 unit/ml enzyme solution irradiated at dose rate 1.99 Gy/sec

Incubation time (min.)	Blank (O.D.) _B	Control (O.D.) _C	Test (O.D.) _T	$\frac{(O.D.)_B - (O.D.)_T}{(O.D.)_B - (O.D.)_C} N$ ----- = ---- N_o
1	0.730	0.674	0.680	0.893
2	0.730	0.619	0.630	0.900
3	0.729	0.570	0.584	0.912
4	0.727	0.522	0.540	0.912
5	0.726	0.475	0.495	0.920
Dose rate = 1.99 Gray/sec. Irradiation time = 60 sec. Total dose = 119.4 Gray Enzyme concn. = 5.0 unit/ml			Average survival fraction	0.910 ± 0.007

Incubation time (min.)	Blank (O.D.) _B	Control (O.D.) _C	Test (O.D.) _T	$\frac{(O.D.)_B - (O.D.)_T}{(O.D.)_B - (O.D.)_C} N$ ----- = ---- N_o
1	0.722	0.673	0.683	0.796
2	0.721	0.623	0.642	0.806
3	0.721	0.575	0.601	0.822
4	0.720	0.527	0.562	0.819
5	0.720	0.480	0.526	0.808
Dose rate = 1.99 Gray/sec. Irradiation time = 120 sec. Total dose = 238.8 Gray Enzyme concn. = 5.0 unit/ml			Average survival fraction	0.815 ± 0.005

Incubation time (min.)	Blank (O.D.) _B	Control (O.D.) _C	Test (O.D.) _T	$\frac{(O.D.)_B - (O.D.)_T}{(O.D.)_B - (O.D.)_C} N$ ----- = ---- N_o
1	0.720	0.664	0.681	0.696
2	0.721	0.609	0.641	0.714
3	0.720	0.555	0.601	0.721
4	0.718	0.502	0.562	0.722
5	0.718	0.450	0.523	0.728
Dose rate = 1.99 Gray/sec. Irradiation time = 240 sec. Total dose = 477.6 Gray Enzyme concn. = 5.0 unit/ml			Average survival fraction	0.716 ± 0.007

continued.

Incubation time (min.)	Blank (O.D.) _B	Control (O.D.) _C	Test (O.D.) _T	$\frac{(O.D.)_B - (O.D.)_T}{(O.D.)_B - (O.D.)_C} N_0$
1	0.729	0.673	0.712	0.304
2	0.728	0.618	0.694	0.309
3	0.728	0.566	0.678	0.309
4	0.727	0.516	0.660	0.318
5	0.725	0.467	0.640	0.329
Dose rate = 1.99 Gray/sec. Irradiation time = 720 sec. Total dose = 1432.8 Gray Enzyme concn. = 5.0 unit/ml			Average survival fraction	0.317 ± 0.008

Table B.11: Dry enzyme irradiated at dose rate 1.99 Gy/sec

Incubation time (min.)	Blank (O.D.) _B	Control (O.D.) _C	Test (O.D.) _T	$\frac{(O.D.)_B - (O.D.)_T}{(O.D.)_B - (O.D.)_C} N_0$
1	0.695	0.648	0.657	0.808
2	0.693	0.604	0.622	0.798
3	0.693	0.563	0.588	0.808
4	0.691	0.524	0.555	0.814
5	0.689	0.489	0.527	0.810
Dose rate = 1.99 Gray/sec. Irradiation time = 25.0 min. Total dose = 2.985x10 ³ Gray Dry enzyme			Average survival fraction	0.807 ± 0.006

Incubation time (min.)	Blank (O.D.) _B	Control (O.D.) _C	Test (O.D.) _T	$\frac{(O.D.)_B - (O.D.)_T}{(O.D.)_B - (O.D.)_C} N_0$
1	0.683	0.640	0.661	0.512
2	0.683	0.599	0.641	0.500
3	0.681	0.561	0.620	0.508
4	0.678	0.524	0.599	0.513
5	0.676	0.489	0.581	0.508
Dose rate = 1.99 Gray/sec. Irradiation time = 75.0 min. Total dose = 8.955x10 ³ Gray Dry enzyme			Average survival fraction	0.507 ± 0.004

continued.

Incubation time (min.)	Blank (O.D.) _B	Control (O.D.) _C	Test (O.D.) _T	$\frac{(O.D.)_B - (O.D.)_T N}{(O.D.)_B - (O.D.)_C N_o}$
1	0.734	0.685	0.721	0.265
2	0.732	0.637	0.707	0.263
3	0.731	0.593	0.694	0.268
4	0.729	0.554	0.681	0.274
5	0.728	0.518	0.671	0.271
Dose rate = 1.99 Gray/sec. Irradiation time = 150 min. Total dose = 1.79×10^4 Gray Dry enzyme			Average survival fraction	0.269 ± 0.004

Incubation time (min.)	Blank (O.D.) _B	Control (O.D.) _C	Test (O.D.) _T	$\frac{(O.D.)_B - (O.D.)_T N}{(O.D.)_B - (O.D.)_C N_o}$
1	0.710	0.672	0.702	0.210
2	0.709	0.632	0.692	0.220
3	0.706	0.595	0.681	0.225
4	0.704	0.559	0.673	0.214
5	0.701	0.516	0.660	0.222
Dose rate = 1.99 Gray/sec. Irradiation time = 175 min. Total dose = 2.089×10^4 Gray Dry enzyme			Average survival fraction	0.220 ± 0.004

REFERENCES

- ACKERY D and BAVERSTOCK K (1987). Implications of Auger emitter microdosimetry in nuclear medicine. *In proceeding of the 8th international congress of radiation research, Edinburgh, July 1987, vol. 2.* Ed. Fielden E M, Fowler J F, Hendry J H and Scott D 357 - 362 (Taylor and Francis, London)
- ADDINK N W H (1965). Agreement between carcinoma experiments *in vivo* and low-energy X-ray irradiation of the metalloprotein carbonic anhydrase. Nature, **207**, 1271-1272
- AL-AHMAD K O and WATT D E (1984). Stopping powers for low energy electrons (<10 keV) in solid polyethylene. Journal of Physics D : Applied Physics, **17**, 1899-1904
- AL-DORIE F (1982). *Inactivation of enzymes in aqueous solution*, MSc Thesis University of Dundee
- AL-WAJIDI T A M (1984). *Cross-sections for inactivation of ribonuclease in solution by low energy X-rays (10 KeV to 70 KeV)*. PhD Thesis, University of Dundee
- ARCHARD G D (1961). Back scattering of electrons. Journal of Applied Physics, **32**, 1505-1509
- ARCHARD G D and MULVEY T (1963). The present state of quantitative x-ray microanalysis. II - Computational methods. British Journal of Applied Physics, **14**, 626-634
- BAMBYNEK W, CRASEMANN B, FINK R W , FREUND H-U, MARK H, SWIFT C D, PRICE R E and RAO P V (1972). X-ray fluorescence yields, Auger, and Coster-Kronig transition probabilities. Reviews of Modern Physics, **44**, 716-813
- BARENDSSEN G W, KOOT C J, van KERSEN R R, BEWLEY D K, FIELD S B and PARNELL C J (1967). The effect of oxygen on impairment of the proliferative capacity of human cells in culture by ionizing radiation of different LET. International Journal of Radiation Biology, **10**, 317-327
- BEDFORD J S, MITCHELL J B, GRIGGS H G and BENDER M A (1975). Cell killing by gamma-rays and beta particles from tritiated water and incorporated tritiated thymidine. Radiation Research, **63** , 531-543
- BETHE H A (1930). Theory of passage of swift corpuscular rays through matter. Annalen der Physik, **5 Folge**, **5**, 325-400
- BLOCHER D and POHLIT W (1982). DNA double strand breaks in Ehrlich ascites tumour cells at low doses of X-rays. II. Can cell death be attributed to double strand breaks?. International Journal of Radiation Biology, **42**, 329-338
- BOOZ J, HUMM J, CHARLTON D E, POMPLUN E and FEINENDEGEN L E (1982). Microdosimetry of the Auger effect : the biological

significance of Auger-electron cascades of phosphorus after low-energy photon interaction with DNA. 625-638 in BOOZ J and EBERT H G (1983) *Radiation protection : 8th symposium on microdosimetry, Julich, Federal Republic of Germany, 27 September - 1 October 1982.* (Luxembourg, Commission of the European Communities)

BOSWORTH R C L (1952). *Heat transfer phenomena.* New York, Wiley

BRYANT P E and BLOCHER D (1980). Measurement of the kinetics of DNA double strand break repair in Ehrlich ascites tumour cells using the unwinding method. International Journal of Radiation Biology, **38**, 335-347

BURHOP E H S (1940). Inner-shell ionisation of atoms by electron impact. Proceedings of the Cambridge Philosophical Society, **36**, 43

BURHOP E H S (1952). *The Auger effect and other radiationless transitions.* (London, Cambridge University Press)

BURKI H J and OKADA S (1970). Killing of cultured mammalian cells by radio-active decay of tritiated thymidine at -196°C . Radiation Research, **41**, 409-424

BURKI H J, ROOTS R, FEINENDEGEN L E, and BOND V P (1973). Inactivation of mammalian cells after disintegration of ^3H or ^{125}I in cell DNA at -196°C . International Journal of Radiation Biology, **24**, 363-375

CAMPION P J (1971). Some comments on the operation of proportional counters. 601-617 in EBERT H G (1972) *Third symposium on microdosimetry, Stresa (Italy), October 18-22, 1971.* Vol 2. (Luxembourg, Commission of the European Communities)

CAMPION P J and KINGHAM M W J (1971 a). Spurious pulses in Ar- CH_4 filled proportional counters. International Journal of Applied Radiation and Isotopes, **22**, 55-65

CAMPION P J and KINGHAM M W J (1971 b). The measurement of the gas multiplication in tissue equivalent gas. International Journal of Applied Radiation and Isotopes, **22**, 703-706

CANNELL R L and WATT D E (1985). Biophysical mechanisms of damage by fast ions to mammalian cells *in vitro*. Physics in Medicine and Biology, **30**, 255-258

CARLSON T A and WHITE R M (1966). Measurement of the relative abundances and recoil-energy spectra of fragment ions produced as the initial consequences of x-ray interaction with CH_3I , HI and DI. Journal of Chemical Physics, **44**, 4510-4520

CATCHSIDE D G and LEA D E (1943). The effect of ionisation distribution on chromosome breakage by x-rays. Journal of Genetics, **45**, 186-196

CHADWICK K H and LEENHOUTS H P (1973). A molecular theory of cell survival. Physics in Medicine and Biology, **18**, 78-87

- CHARLTON D E, BOOZ J, FIDORRA J, SMIT Th and FEINENDEGEN L.E. (1978). Microdosimetry of radioactive nuclei incorporated into the DNA of mammalian cells. In *6th symposium on microdosimetry, Brussels, Belgium, May 22-26, 1977*. Vol. 1. Ed. Booz J and Ebert H G 91-110 (Harwood Academic publ. Ltd. for the Commission of the European Communities, London).
- CHARLTON D E and BOOZ J (1981). A Monte Carlo treatment of the decay of ^{125}I . Radiation Research, **87**, 10-23
- CHARLTON D E, GOODHEAD D T, WILSON W E and PARETZKE H G (1985). *Energy deposition in cylindrical volume: (a) protons (b) alpha particles*. MRC Radiobiology Unit Monograph, 85/1. Chilton, UK, July 1985
- CHATTARJI D (1976). *The theory of Auger transitions*. (London, Academic Press)
- CHATTERJEE A and MAGEE J L (1985). Theoretical investigation of the production of strand breaks in DNA by water radicals. Radiation Protection Dosimetry, **13**, 137-140
- CHEN C Z (1987). *A study of the biophysical mechanisms of damage by ionizing radiation to mammalian cells in vitro*. PhD Thesis, University of St Andrews.
- CHEN C Z and WATT D E (1986). Biophysical mechanism of radiation damage to mammalian cells by x-ray and γ -ray. International Journal of Radiation Biology, **49**, 131-142
- COCKCROFT A L and CURRAN S C (1951). The elimination of end effects in counters. Review of Scientific Instruments, **22**, 37-42
- COLLINSON E, DALTON F S and HOLMES B E (1950). Inactivation by hydroxyl radicals. Nature, **165**, 267-269
- COMMERFORD S L, BOND V P and CRONKITE E P (1980). Radiotoxicity of intranuclear ^{125}I atoms not bound to DNA. International Journal of Radiation Biology, **37**, 547-554
- COTTRALL M F (1985). Medical research and Auger cascades. The Lancet, **26 Oct 1985**, 942-943
- COX R, THACKER J and GOODHEAD D T (1977). Inactivation and mutation of cultured mammalian cells by aluminium characteristic ultrasoft x-rays. II Dose-responses of Chinese hamster and human diploid cells to aluminium x-rays and radiations of different LET. International Journal of Radiation Biology, **31**, 561-576
- COX R and MASSON W K (1976). X-ray induced mutation to 6-thioguanine resistance in cultured human diploid fibroblasts. Mutation Research, **37**, 125
- DALE W M (1942). Effects of x-rays on aqueous solutions of biologically active compounds. British Journal of Radiology, **16**, 80

- DALE W M, MEREDITH W J and TWEEDIE M C K (1943). Mode of action of ionizing radiations on aqueous solutions. Nature, **151**, 280-281
- DIEFALLAH EI H M, STELTER L and DIEHN B (1970). Chemical consequences of the Auger effect : iodine yield from iodoamino acids as a function of x-ray dose and energy. Radiation Research, **44**, 273-281
- DIEHN B, HALPERN A and STOCKLIN G (1976). Specific inactivation of solid carbonic anhydrase upon x-ray resonance absorption in the constituent zinc atom. Journal of the American Chemical Society, **98**, 1077-1079
- DOMEN S R (1987). Advances in calorimetry for radiation dosimetry. 245-314 in KASE KR, BJARNGARD BE and ATTIX F H (1987) *The dosimetry of ionising radiation*. Vol 2. (London, Academic Press)
- DYSON N A (1959). The continuous x-ray spectrum from electron-opaque targets. Proceedings of the Physical Society, **73**, 924-936
- DYSON N A (1973). The production of characteristic x rays by proton bombardment, and the ratio of characteristic to continuous radiation. Journal of Physics. B : Atomic and Molecular Physics, **6**, 562-572
- DYSON N A (1987). X-ray physics - a review. Birmingham University and 2nd Nile Winter College. Department of Physics University of Khartoum lectures
- E G and G ORTEC Inc (1984). *Experiments in nuclear science. : AN34 Laboratory manual*. 3rd edition. (Oak Ridge, Ortec Inc) 15-24
- EMERY E W (1966). Geiger-Mueller and proportional counters. 73-122 in ATTIX F H and ROESCH W C (1966) *Radiation dosimetry* . Vol 2. 2nd edition. (New York, Academic Press)
- EMMONS A H (1959). *Resonance radiation effects of low energy monochromatic x-ray on catalase*. PhD Thesis, University of Michigan
- EVERHART T E (1960). Simple theory concerning the reflection of electrons from solids. Journal of Applied Physics, **31**, 1483-1490
- FANO U (1952). *Tables of the analysis of beta spectra*. (Washington, National Bureau of Standards)
- FEINENDEGEN L E (1977). Biological damage from radioactive nuclei incorporated into DNA of cells : implications for radiation biology and radiation protection. 3-37 in BOOZ J and EBERT H G (1978) *Sixth symposium on microdosimetry, Brussels, Belgium, May 22-26, 1977*. Vol 1. (London, Harwood Academic for the Commission of the European Communities)
- FEINENDEGEN L E, ERTLE H H and BOND V P (1970). Biological Toxicity Associated with the Auger effect 419-430 in Morgan K Z (1970) *Biophysical Aspects of Radiation Quality* proceeding of a symposium Lucas Heights 8-12 March, Held by ' The International Atomic Energy Agency, Vienna.

- FITTING H J (1974) Transmission, energy distribution, and SE excitation of fast electrons in thin solid films. Physica Status Solidi A, **26**, 525-535
- FRANKENBERG D, FRANKENBERG-SCHWAGER M, BLOCHER D and HARBICH R (1981). Evidence for DNA double-strand breaks as the critical lesions in Yeast cells irradiated with sparsely or desely ionizing radiation under oxic or anoxic conditions. Radiation Research, **87**, 524 - 532
- FRANKENBERG-SCHWAGER M, FRANKENBERG D and HARBICH R (1988). Exponential or shouldered survival curves result from repair of DNA double- strand breaks depending on postirradiation conditions. Radiation Research, **114**, 54-63
- FRIEDMANN H C and VENNESLAND B (1958). Purification and properties of Dihydroorotic Dehydrogenase. Journal of Biological Chemistry, **233**, 1398-1406
- FRIEDMANN H C and VENNESLAND B (1960). Crystalline dihydroorotic dehydro-genase. Journal of Biological Chemistry, **235**, 1526-1532
- FUJIWARA Y and MAYAZAKI N (1987). Lethal mutagenic and DNA-breaking effects of decays of ¹²⁵I unifilarly incorporated into the DNA of mammalian cells, 169 - 180 in BAVERSTOCK K F and CHARLTON D E (1988). *DNA damage by Auger emitters..* (Taylor and Francis, London)
- FUNK F, PERSON S and BOCKRATH R C (1968). The mechanism of inactivation of T4 bacteriophage by tritium decay. Biophysical Journal, **8**, 1037-1050
- GAULDEN M E (1983). "Biological dosimetry" of radionuclides and radiation hazards. Journal of Nuclear Medicine, **24**, 160-164
- GOMBERG H J (1964). *Resonance in radiation effects*. (Puerto Rico Nuclear Center. Technical report, 2)
- GOODHEAD D T (1987). Biophysical models of radiation action; introductory review. 306-311 in FIELDEN E M, FOWLER J F, HENDRY J H and SCOTT D (1987) *Radiation research : proceedings of the 8th international congress of radiation research, Edinburgh, July 1987*. 2 vols. (London, Taylor and Francis)
- GOODHEAD D T and THACKER J (1977). Inactivation and mutation of cultured mammalian cells by aluminium characteristic ultrasoft X-rays. I - Properties of aluminium X-rays and preliminary experiments with Chinese hamster cells. International Journal of Radiation Biology, **31**, 541-559
- GOODHEAD D T, THACKER J and COX R (1979). Effectiveness of 0.3keV carbon ultrasoft x-rays for the inactivation and mutation of cultured mammalian cells. International Journal of Radiation Biology, **36**, 101-114
- GREENING J R, RANDLE K J and REDPATH A T (1968). The measurement of low energy x-rays. II- Total absorption calorimetry. Physics in Medicine and Biology, **13**, 359-369

- GUNN S R (1964). Radiometric calorimetry : a review. Nuclear Instruments and Methods, **29**, 1-24
- GUNN S R (1970). Radiometric calorimetry : a review. Nuclear Instruments and Methods, **85**, 285-312
- GUNN S R (1976). Radiometric calorimetry : a review. Nuclear Instruments and Methods, **135**, 251-265
- HALL E J (1978). Radiology for the Radiologist. 2nd Edition (London, Harper & Row), 111 - 128
- HALPERN A, and STOCKLIN G (1974). A radiation chemical resonance effect in solid 5-bromodeoxyuridine : chemical consequences of the Auger effect. Radiation Research, **58**, 329-337
- HOFER K G and HUGHES W L (1971). Radiotoxicity of intranuclear tritium, ^{125}I and ^{131}I . Radiation Research, **47**, 94-109
- HOFER K G, HARRIS C R and SMITH J M (1975). Radiotoxicity of intracellular ^{67}Ga , ^{125}I and ^3H : nuclear versus cytoplasmic radiation effects in murine L1210 leukaemia. International Journal of Radiation Biology, **28**, 225-241
- HOLMES B E, NAVON G and STEIN G (1967) Action of atomic hydrogen on Ribonuclease in aqueous solution. Nature, **213**, 1087-1091
- HOWELL R W; SASTRY K S R, HILL H Z and RAO D V (1985). CIS-PLATINUM-193m : Its microdosimetry and potential for chemo-Auger combination therapy of cancer. (Private communication)
- HUBBELL J H (1977). Photon mass attenuation and mass energy-absorption coefficients for H, C, O, Ar, and seven mixtures from 0.1 keV to 20 MeV. Radiation Research, **70**, 58-81
- HUBBELL J H (1982). Photon mass attenuation and energy-absorption coefficients from 1 keV to 20 MeV. International Journal of Applied Radiation and Isotopes, **33**, 1269-1290
- HUMM J, POMPLUN E, BOOZ J and CHARLTON D E (1982). Energy and number distribution of electrons and photons emitted after photoelectric interaction of x-rays with phosphorus and DNA. 187-198 in BOOZ J and EBERT H G (1983) *Radiation protection : 8th symposium on microdosimetry, Julich, Federal Republic of Germany, 27 September - 1 October 1982*. (Luxembourg, Commission of the European Communities)
- HUMM J and CHARLTON D E (1987 a). Double Strand Breakage in DNA produced by the photoelectric interaction with incorporated 'cold' Bromine. In BAVERSTOCK K F and CHARLTON D E (1988). *DNA damage by Auger emitters..* (Taylor and Francis, London) 111-122

- HUMM J and CHARLTON D E (1987 b). Theoretical estimates of strand breakage resulting from the decay of ^{125}I appended to the DNA by intermediate molecules. In proceeding of the 8th international congress of radiation research, Edinburgh, July 1987, vol. 2. Ed. Fielden E M, Fowler J F, Hendry J H and Scott D 68 (Taylor and Francis, London)
- HUNGER H-J and KUCHLER L (1979). Measurements of the electron backscattering coefficient for quantitative EPMA in the energy range of 4 to 40 keV. Physica Status Solidi A, **56**, K45-48
- HUSSEY R G and THOMPSON W R (1923). The effect of radio-active radiations and x-rays on enzymes. Journal of General Physiology, **5**, 647-659
- HUSSEY R G and THOMPSON W R (1924). The effect of radioactive radiations and x-rays on enzymes. Journal of General Physiology, **6**, 1-5
- HUSSEY R G and THOMPSON W R (1925 a). The effect of radio-active radiation and x-rays on enzymes. Journal of General Physiology, **9**, 211-215
- HUSSEY R G and THOMPSON W R (1925 b). The effect of radio-active radiations and x-rays on enzymes. Journal of General Physiology, **9**, 309-313
- HUSSEY R G and THOMPSON W R (1925 c). The effect of radio-active radiations and x-rays on enzymes. Journal of General Physiology, **9**, 315-317
- ICRU (1971). *Radiation quantities and units*. ICRU Report, 19. (Washington, ICRU)
- ICRU (1979). *Quantitative Concepts and Dosimetry in Radiobiology* ICRU Report. 30.(Washington, ICRU)
- ICRU (1979 a). *Average energy required to produce an ion pair*. ICRU Report, 31. (Bethesda, ICRU)
- ICRU (1979 b). *Methods of assessment of absorbed dose in clinical use of radionuclides*. ICRU Report, 32 (Washington, ICRU)
- ICRU (1980). *Radiation quantities and units*. ICRU Report, 33. (Bethesda, ICRU)
- ISKEF H (1981). *Stopping power and range of low energy electrons (20 eV - 10 keV)*. PhD Thesis, University Of Dundee.
- ISKEF H, CUNNINGHAM J W and WATT D E (1983). Projected ranges and effective stopping power of electrons with energy between 20eV and 10 keV. Physics In Medicine And Biology, **28**, 535-545
- JACOB J H (1974). Penetration and energy deposition of electrons in thick targets. Journal of Applied Physics, **45**, 467-475.

- JAWAD H H and WATT D E (1986). Physical mechanism for inactivation of metall-enzymes by characteristic X-rays. International Journal of Radiation Biology, **50**, 665-674.
- KASSIS A I, ADELSTEIN S J, HAYDOCK C and SASTRY K S R (1980). Radio-toxicity of ^{75}Se and ^{35}S : Theory and application to a cellular model. Radiation Research, **84**, 407-425
- KASSIS A I, ADELSTEIN S J, HAYDOCK C, SASTRY K S R, McELVANY K D and WELCH M J (1982). Lethality of Auger electrons from the decay of Bromine-77 in the DNA of mammalian cells. Radiation Research, **90**, 362-373
- KASSIS A I, FAYED F, KINSEY B M, SASTRY K S R, TAUBE R A and ADELSTIEN S J (1987 a). Radiotoxicity of I-125 in Mammalian cells. Radiation Research, **111**, 305-318
- KASSIS A I, HOWELL R W, SASTRY K S R and ADELSTEIN S J (1987 b). Positional effects of Auger decays in mammalian cells in culture. In *DNA damage by Auger emitters..* Ed. Baverstock K F and Charlton D E , 1988, 1-13 (Taylor and Francis, London)
- KATZ R, ACKERSON B, HOMAYOONFAR M and SHARMA S C (1971). Inactiv-ation of cells by heavy ion bombardment. Radiation Research, **47**, 402-425
- KATZ R, SHARMA S C and HOMAYOONFAR M (1972). The structure of particle tracks. 317-383 in ATTIX F H (1972) *Topics in radiation dosimetry*. (London, Academic Press)
- KELLERER A M and ROSSI H H (1972). The theory of dual radiation action. Current Topics in Radiation Research Quarterly, **8**, 85-158
- KOCH C J and BURKI H J (1975). The oxygen-enhancement ratio for reproductive death induced by ^3H or ^{125}I damage in mammalian cells. International Journal of Radiation Biology, **28**, 417-425
- KONDO H, FRIEDMANN H C and VENNESLAND B (1960). Flavin changes accompanying adaptation of Zymobacterium Oroticum to Orotate. Journal of Biological Chemistry, **235**, 1533-1535
- KRISCH R E (1970). Comparison of the lethal effects of ^{32}P and ^{33}P decay in E. Coli and in bacteriophagees. International Journal of Radiation Biology, **18**, 259 - 266.
- KRISCH R E (1972). Lethal effects of Iodine - 125 decay by electron capture in Escherichia Coli and in bacteriophage T-1. International Journal of Radiation Biology, **21**, 167 - 189.
- LABERRIGUE-FROLOW J and RADVANYI P (1956). Measurement of the k-fluorescence yield and study of the k Auger rays of Tc^{99} (6.04 hr) and In^{115} (4.5 hr). Comptes Rendus de l'Academie de Sciences, **242**, 901-904

- LAUGHLIN J S and GENNA S (1966). Calorimetry. 389-441 in ATTIX F H and ROESCH W C (1966) *Radiation dosimetry*. Vol 2. 2nd edition. (New York, Academic Press)
- LEA D E and CATCHSIDE D G (1942). The mechanism of the induction by radiation of chromosome aberrations in *Tradescantia*. Journal of Genetics, **44**, 216-245
- LEA D E and SALMAN M H (1942). The inactivation of vaccinia virus by radiations. British Journal of Experimental Pathology, **23** (1): 27-37.
- LEDERER C M and SHIRLEY V S (1978). *Tables of isotopes*. 7th Ed. Eds: C M Lederer and V S Shirley. (John Wiley and sons, Lmi. New York)
- LEENHOUTS H P and CHADWICK K H (1975). Stopping power and the radio-biological effect of electrons, gamma rays and ions. 289-310 in BOOZ J, EBERT H G and SMITH B G R (1976) *Fifth symposium on microdosimetry, Verbania, Pallanza (Italy), 22 - 26 September 1975*. 2 vols. (Brussels, Commission of the European Communities)
- LEHNERT, S (1975). Changes in radiosensitivity of V-79 cells accompanying growth and cell division. Radiation Research, **63**, 326-335
- LIBER H L, LeMOTTE P K and LITTLE J B (1983). Toxicity and mutagenicity of X-rays and [¹²⁵I]dUrd or [³H]TdR incorporated in the DNA of human lymphoblast cells. Mutation Research, **111**, 387-404
- LIEBERMAN I and KORNBERG A (1953). Enzymic synthesis and breakdown of a pyrimidine, Orotic Acid. Biochimica et Biophysica Acta, **12**, 223-233
- McADAMS W H (1942). *Heat transmission*. New York, McGraw-Hill
- McGINNIES R T (1959). *Energy Spectrum Resulting from Electron Slowing Down*. Circular 597 (National Bureau of Standards, Washington, DC)
- MEGER C M, PEARSON D W, DeLUCA P M, WELLS G M, REDAELLI R and CERRINA F (1987). A simple total absorption calorimetry technique to measure soft X ray energy fluence. Radiation Protection Dosimetry, **21**, 219-222
- MILLER R W and MASSEY V (1965a). Dihydroorotic dehydrogenase. I - Some properties of the enzyme. Journal of Biological Chemistry, **240**, 1453-1465
- MILLER R W and MASSEY V (1965b). Dihydroorotic dehydrogenase. II - Oxidation and reduction of cytochrome. Journal of Biological Chemistry, **240**, 1466-1472
- MIYAZAKI N and FUJIWARA Y (1981). Mutagenic and lethal effects of [⁵⁻¹²⁵I] iodo-2'-deoxyuridine incorporated into DNA of mammalian cells, and their RBE'S. Radiation Research, **88**, 456-465
- MOLE R H (1986). Biological damage caused by Auger cascades. The Lancet, **11 Jan 1986**, 90-91

- MOTT N F and MASSEY H S W (1949). *The theory of atomic collisions*. (Oxford, Clarendon Press)
- MULLER A and KOHNLEIN W (1964). Quantitative ESR-measurements of radiation-induced radicals in nucleosides. International Journal of Radiation Biology, **8**, 121-130.
- NAKHODKIN N G, OSTROUHKOV A A and ROMANOVSKII V A (1962). Electron inelastic scattering in thin films. Soviet Physics : Solid State, **4**, 1112-1119
- NEARY G J, SAVAGE J R K and EVANS H J (1964). Chromatid aberrations in Tradescantia pollen tubes induced by monochromatic x-rays of quantum energy 3 and 1.5 keV. International Journal of Radiation Biology, **8**, 1-19
- NEARY G J, PRESTON R J and SAVAGE J R K (1967). Chromosome aberrations and the theory of RBE. III - Evidence from experiments with soft x-rays, and a consideration of the effects of hard x-rays. International Journal of Radiation Biology, **12**, 317-345
- NEARY G J, SIMPSON-GILDEMEISTER V F W and PEACOCKE A R (1970). The influence of radiation quality and oxygen on strand breakage in dry DNA. International Journal of Radiation Biology, **18**, 25-40
- NEUBERT G and ROGASCHEWSKI S (1980). Backscattering coefficient measurements of 15 to 60 keV electrons for solids at various angles of incidence. Physica Status Solidi A, **59**, 35-41
- OHARA H, SHINOHARA K, KOBAYASHI K and ITO T (1987). An Additional Enhancement in Brdu-Labelled cultured mammalian cells with monoenergetic Synchrotron Radiation at 0.09 nm: Auger effect in mammalian cells. In BAVERSTOCK K F and CHARLTON D E (1988). *DNA damage by Auger emitters..* (Taylor and Francis, London). 123-133
- OKADA S (1957). Inactivation of Deoxyribonuclease by X-Rays: I. The Mechanisms of inactivation in aqueous solution; II. The Kinetics of Inactivation in aqueous solution and III. Modification of the Effect of Radiation on the DNA-DNase System. Archives of Biochemistry and Biophysics, **67**, 95-120
- PANTER H C (1981). Cell inactivation by tritium decays at 37 and -196°C : some comparisons with X rays. Radiation Research, **87**, 79-89
- RAAPHORST G P and DEWEY W C (1979). Fixation of potentially lethal radiation damage by post-irradiation exposure of chinese hamster cells to 0.5 M or 1.5 M NaCl solutions. International Journal of Radiation Biology, **36**, 303-315
- RAO D V, GOVELITZ G F and SASTRY K S R (1983). Radiotoxicity of Thallium-201 in mouse testes : inadequacy of conventional dosimetry. Journal of Nuclear Medicine, **24**, 145-153
- RAO D V, SASTRY K S R, GOVELITZ G F, GRIMMOND, H E and HILL H Z (1985 a). Radiobiological effects of Auger electrons emitters *in vivo* :

spermatogenesis in mice as an experimental model. Radiation Protection Dosimetry, **13**, 245-248

RAO D V, SASTRY K S R, GOVELITZ G F, GRIMMOND H E and HILL H Z (1985 b). In vivo effects of iron-55 and iron-59 on mouse testes : biophysical dosimetry of Auger electrons. Journal of Nuclear Medicine, **26**, 1456-1465

REITZ J R (1950). The effect of screening on beta-ray spectra and internal conversion. Physical Review, **77**, 10-18

ROTH R A, SHARMA S C and KATZ R (1976). Systematic evaluation of cellular radiosensitivity parameters. Physics in Medicine and Biology, **21**, 491-503

ROTI ROTI J L, KRISTY M S and HIGASHIKUBO R (1986). Nuclear protein content and cell progression kinetics following X irradiation. Radiation Research, **108**, 52-61

ROOTS R and OKADA S (1975) Estimation of Life Time and Diffusion Distances of Radicals Involved in X-Rays-Induced DNA Strand Breaks or Killing of Mammalian Cells. Radiation Research, **64**, 306-320

SASTRY K S R, HAYDOCK C, BASHA A M and RAO D V (1985). Electron dosimetry for radioimmunotherapy : optimal electron energy. Radiation Protection Dosimetry, **13**, 249-252

SKARSGARD L D, KIHLMAN D A, PARKER L, PIJARA C M and RICHARDSON S (1967). Survival chromosome abnormalities and recovery in heavy ion and x-irradiated mammalian cells. Radiation Research, **Suppl. 7**, 208-221

TAYLOR W H and TAYLOR M L (1964). Enzymes of the pyrimidine pathway in *Escherichia coli*. II Intracellular localization and properties of Dihydroorotic Dehydrogenase. Journal of Bacteriology, **88**, 105-110

THACKER J and COX R (1975). Mutation induction and inactivation in mammalian cells exposed to ionising radiation. Nature, **258**, 429-431

THACKER J, STRETCH A and STEPHENS M A (1977). The induction of thio-guanine-resistant mutants of chinese hamster cells by γ -rays. Mutation Research, **42**, 313-326

TODD P W (1967). Heavy ion irradiation of cultured human cells. Radiation Research, **7**, 196-207

TODD P W (1975). Heavy ion irradiation of human and Chinese hamster cells *in vivo* . Radiation Research, **61**, 288-297

UTSUMI H and ELKIND M M (1979). Potentially lethal damage versus sublethal damage : Independent repair processes in actively growing Chinese hamster cells. Radiation Research, **77**, 346-360

WAPSTRA A H, NIJGH G J and von LIESHOUT R (1959). *Nuclear spectroscopy tables*. (Amsterdam, North Holland), 42-44

- WATT D E (1967). Proportional counter design : Radiocarbon dating. Nuclear Instruments and Methods, **50**, 353-354
- WATT D E (1989 a). On Absolute Biological Effectiveness and Unified Dosimetry. Journal of Radiological protection, **9**, 33-49.
- WATT D E (1989 b). An Approach Towards a Unified Theory of Damage to Mammalian cells by ionising Radiation. Submitted to Radiation Protection Dosimetry, in press.
- WATT D E, AL-AFFAN I A M, CHEN C-Z and THOMAS G E (1985). Identification of biophysical mechanisms of damage by ionising radiation. Radiation Protection Dosimetry, **13**, 285-294.
- WATT D E and YOUNIS A-R S (1987). Physical mechanism for inactivation of metallo-enzymes: Response to correspondence from Goodhead and Nikjoo. International Journal of Radiation Biology, **52**, 657-658.
- WATT D E, CHEN C Z, KADIRI L A and YOUNIS A-R S (1987) Towards a unified system for expression of biological damage by ionising radiation. 37-41 in "*Health effects of low dose ionising radiation*" recent advances, and their implications". Proceedings of an international conference organised by British Nuclear Energy Society. London 11 - 14 may, 1987.
- WERNER U (1979). THEORETISCHE UND EXPERIMENTELLE UNTERSUCHUNCEN ZUR ELEKTRONEN-RUCKSTREUUNG AM FESTKORPER (Theoretical and experimental investigations on electrons-Backscattering in solids). PhD Thesis, University of Martin- Luther, Halle-Wittenberg.
- WORTHINGTON C R and TOMLIN S G (1956). The intensity of emission of characteristic x-radiation. Proceedings of the Physical Society. Series A, **69**, 401-412
- WRIGHT H A, MAGEE J L, HAMM R N, CHATTERJEE A, TURNER J E and KLOTS C E (1985). Calculations of physical and chemical reactions produced in irradiated water containing DNA. Radiation Protection Dosimetry, **13**, 133-136.
- YASUI L S, HOFER K G and WARTERS R L (1985). Inhomogeneity of the nucleus to ^{125}I UDR cytotoxicity. Radiation Research, **102**, 106-118
- YASUI L S and HOFER K G (1986). Role of mitochondrial DNA in cell death induced by ^{125}I decay. International Journal of Radiation Biology, **49**, 601-610
- YASUI L S, PASCHOA A S, WARTERS R L and HOFER K G (1987). Cytotoxicity of ^{125}I decay produced lesions in chromatin, 181 - 189 in BAVERSTOCK K F and CHARLTON D E (1988). *DNA damage by Auger emitters..* (Taylor and Francis, London).

Selective bibliography

- ALPER T (1977). Elkind recovery and "sub-lethal damage": a misleading association. British Journal of Radiology, **50**, 459-467
- ASHLEY J C, TUNG C J AND RITCHIE R H (1978). Inelastic of electron with polystyrene : calculation of mean free paths, stopping powers and csda ranges. Transactions on Nuclear Science, **NS 25**, 1566-1570
- ATTIX F H (1972). *Topics in radiation dosimetry*. (London, Academic Press)
- ATTIX F H (1986). *Introduction to radiological physics and radiation dosimetry*. (New York, Wiley)
- BLAKELEY E A, TOBIAS C A, YANG T C H, SMITH K C and LYMAN J T, (1979). Inactivation of human kidney cells by high energy monoenergetic heavy ion beams. Radiation Research, **80**, 122-160
- BLOHM R and HARDER D (1985). Restricted LET : still a good parameter of radiation quality for electrons and photons. Radiation Protection Dosimetry, **13**, 377-381
- BRAGG W H (1912). *Studies in radioactivity*. (New York, Macmillan), 95
- BURKI H J, KOCH C J, and WOLFF S (1977). Molecular suicide studies of I-125 and H-3 disintegration in the DNA of Chinese hamster. Current Topics In Radiation Research Quarterly, **12**, 408 - 425
- BURLIN T E (1966) A general theory of cavity ionization. British Journal of Radiology, **39**, 727-734
- CARLSSON G A (1985). Theoretical basis for dosimetry. 2-71 in KASE K R, BJARNGARD BE and ATTIX F H (1985) *The dosimetry of ionising radiation*. Vol 1. (London, Academic Press)
- CHAPMAN J D, REUVERS A P, BORSA J and GREENSTOCK C L (1973). Chemical radioprotection and radiosensitization of mammalian cells growing *in vitro*. Radiation Research, **56**, 291-306
- CHAPMAN J D, GILLESPIE C J, REUVERS A P and DUGLE D L (1975). The inactivation of Chinese hamster cells by X-rays : the effects of chemical modifiers on single and double-events. Radiation Research, **64**, 365-375
- COOK P R and BRAZELL I A (1976). Detection and repair of single-strand breaks in nuclear DNA. Nature, **263**, 679-682
- DATTA R, COLE A and ROBINSON S (1976). Use of track-end alpha particles from ^{241}Am to study radiosensitive sites in CHO cells. Radiation Research, **65**, 139-151
- DUTREIX A and BRIDIER A (1985). Dosimetry for external beams of photon and electron radiation. 164-223 in KASE KR, BJARNGARD BE and ATTIX F H (1985) *The dosimetry of ionising radiation*. Vol 1. (London, Academic Press)

- FANO U (1954). Note on the Bragg-Gray cavity principle for measuring energy dissipation. Radiation Research, **1**, 237-240
- GOODHEAD D T (1982). An assessment of the role of microdosimetry in radiobiology. Radiation Research, **91**, 45-76
- GRAY L H (1929). The absorption of penetrating radiation. Proceedings of the Royal Society of London, Series A, **122**, 647-668
- GRAY L H (1936). An ionization method for the absolute measurement of γ -ray energy. Proceedings of the Royal Society of London, Series A, **156**, 578-596
- GREEN M (1963). A Monte Carlo calculation of the spatial distribution of characteristic x-ray production in a solid target. Proceedings of the Physical Society, **82**, 204-215
- GREEN M (1964). The angular distribution of characteristic x radiation and its origin within a solid target. Proceedings of the Physical Society, **83**, 435-451
- GREEN M and COSSLETT V E (1963). The efficiency of production of characteristic x-radiation in thick targets of a pure element. Proceedings of the Physical Society, **78**, 1206-1214
- GREENING J R (1950). The determination of x-ray wavelength distribution from absorption data.
- GREENING J R (1964). Saturation characteristics of parallel-plate ionization chambers. Physics in Medicine and Biology, **9**, 143-154
- GREENING J R (1965). Saturation characteristics of parallel-plate ionization chambers. (Correction) Physics in Medicine and Biology, **10**, 566
- GREENING J R (1985). *Fundamentals of radiation dosimetry*. 2nd ed. (Bristol, Hilger)
- GREENING J R and RANDLE K J (1968). The measurement of low energy x-rays. I- General considerations. Physics in Medicine and Biology, **13**, 159-168
- HALL E J (1978). *Radiology for the Radiologist*. 2nd Edition (London, Harper & Row), 111 - 128
- HARDER D (1973). Fano's theorem and the multiple scattering correction. 677-689 in BOOZ J, EBERT H G, EICKEL R and WAKER A (1974) *Fourth symposium on microdosimetry, Verbania, Pallanza (Italy), 24 - 28 September 1973*. (Brussels, Commission of the European Communities)
- HARRIS J W, POWER J A and KOCH C J (1975). Radiosensitization of hypoxic mammalian cells by diamide. I-Effects of experimental conditions on survival. Radiation Research, **64**, 270-280

- HELD K D, BREN G D and MELDER D C (1986). Interactions of radioprotectors and oxygen in cellular mammalian cells. II-Effects of dithiothreitol on radiation-induced DNA damage and comparison with cell survival. Radiation Research, **108**, 296-306
- HEUSSEN C, NACKERDIEN Z, SMIT B J and BOHM L (1987). Irradiation damage in chromatin isolated from V-79 Chinese hamster lung fibroblasts. Radiation Research, **110**, 84-94
- HOFER K G and KEOUGH G (1977). Biological toxicity of Auger emitters : molecular fragmentation versus electron irradiation. Current Topics In Radiation Research Quarterly, **12**, 335-354
- ILKIAKIS G, BRYANT P E and NGO F Q H (1985). Independent forms of potentially lethal damage fixed in plateau-phase chinese hamster cells by postirradiation treatment in hypertonic salt solution or ara A. Radiation Research, **104**, 329-345
- KARIBIAN D (1978). Dihydroorotate dehydrogenase (Escherichia Coli). Methods in Enzymology, **1**, 58-63
- KASSIS A I, SASTRY K S R and ADELSTEIN S J (1985). Intracellular distribution and radiotoxicity of Chromium-51 in mammalian cells : Auger-electron dosimetry. Journal of Nuclear Medicine, **26** , 59-67
- KELLERER A M and ROSSI H H (1978). A generalized formulation of dual radiation action. Radiation Research, **75**, 471-488
- KIRKPATRICK P and BAEZ A V (1947). Absolute energies of K_{α} -radiation from thick targets of silver. Physical Review, **71**, 521-529
- KRUSE P F and PATTERSON M K (1973). *Tissue culture methods and applications*. (New York, Academic Press)
- LAW J and REDPATH A T (1968). The measurement of low energy x-rays. III - Ferrous sulphate G-values. Physics in Medicine and Biology, **13**, 371-382
- LITTLE J B and HAHN G M (1973). Life-cycle dependence of repair of potentially-lethal radiation damage. International Journal of Radiation Biology, **23**, 401-407
- MANTEL J (1972). The beta ray spectrum and the average beta energy of several isotopes of interest in medicine and biology. International Journal of Applied Radiation and Isotopes, **23**, 407-413
- MITCHELL J B, BEDFORD J S and BAILEY S M (1979). Dose rate effects on the cell cycle and survival of S_3 HeLa and V79 cells. Radiation Research, **79**, 520-536
- OKADA S (1970). *Radiation biochemistry. Vol1 - Cells*. (New York, Academic Press)
- POCKMAN L T, WEBSTER D L, KIRKPATRICK P and HARWORTH K (1947). The probability of K ionisation of nickel by electrons as a function of their energy. Physical Review, **71**, 330-338

- POHLIT W and HEYDER I R (1981). The shape of dose-survival curves for mammalian cells and repair of potentially lethal damage analyzed by hypertonic treatment. Radiation Research, **87**, 613-634
- POLLACK A, MOULIS H, GREENSTEIN D B, BLOCK N L and IRNIN G L (1985). III, Cell kinetic effects of incorporated 3H-thymidine on proliferating human lymphocytes: Flow cytometric analysis using the DNA/nuclear protein method. Cytometry, **6**, 428 - 436
- ROESCH W C (1968). Basic concepts of dosimetry. 1-41 in ATTIX F H and ROESCH W C (1968) *Radiation dosimetry*. Vol 1. 2nd edition. (New York, Academic Press)
- SCDOC D and OBELIC B (1975). Measurement of W at very low photon energy. 1007-1021 in BOOZ J, EBERT H G and SMITH B G R (1976) *Fifth symposium on microdosimetry, Verbania, Pallanza (Italy), 22 - 26 September 1975*. 2 vols. (Brussels, Commission of the European Communities)
- SINCLAIR W K and MORTON R A (1966). X-ray sensitivity during the cell generation cycle of cultured Chinese hamster cells. Radiation Research, **29**, 450-474
- SPENCER L V and ATTIX F H (1955). A theory of cavity ionization. Radiation Research, **3**, 239-254
- STERNGLOSS E J (1954). Backscattering of kilovolt electrons from solids. Physical Review, **95**, 345-358
- SZECHTER A and SCHWARZ D (1977). Dose-rate effects, fractionation and cell survival at lowered temperatures. Radiation Research, **71**, 593-619.
- WATT D E, CANNELL R J, and THOMAS G E (1984). Ion beams in quality determination for radiation protection. 267-282 in MAZZOLI P and MOSCHINI G (1984) *Proceedings of the international symposium on three-day in depth review on the nuclear accelerator impact in the interdisciplinary field May 30th - June 1st, 1984, Padova Italy*. (Padova, Laboratori Nazionali di Legnaro)
- WEBSTER D L, HANSEN W W and DUVENECK F B (1933) X-ray line intensities and cathode-ray retardation in thick targets of silver. Physical Review, **44**, 258-264
- WEICHSELBAUM R, DAHLBERG W, LITTLE J B, ERVIN T J, MILLER D, HELLMAN S and RHEINWALD J G (1984). Cellular x-ray repair parameters of early passage suamous cell carcinoma lines derived from patients with known responses to radiotherapy. British Journal of Cancer, **49**, 595-601
- WHIDDINGTON R (1912). The transmission of cathode rays through matter. Proceedings of the Royal Society of London, Series A, **86**, 360-370
- ZERMENO A and COLE A (1969). Radiosensitive structure of metaphase and interphase hamster cells as studied by low-voltage electron beam irradiation. Radiation Research, **39**, 669-684